PNNL-14618, Rev. 0

Pacific Northwest
National Laboratory
Operated by Battelle for the
U.S. Department of Energy

A Geostatistical Analysis of Historical Field Data on Tritium, Technetium-99, Iodine-129, and Uranium

C. J. Murray
Y.-J. Chien
P. D. Thorne

April 2004

Prepared for the U.S. Department of Energy
under Contract DE-AC06-76RL01830

PACIFIC NORTHWEST NATIONAL LABORATORY
operated by
BATTELLE
for the
UNITED STATES DEPARTMENT OF ENERGY
under Contract DE-AC06-76RL01830

Printed in the United States of America

Available to DOE and DOE contractors from the
Office of Scientific and Technical Information,
P.O. Box 62, Oak Ridge, TN 37831-0062;
ph: (865) 576-8401
fax: (865) 576-5728
email: reports@adonis.osti.gov

Available to the public from the National Technical Information Service,
U.S. Department of Commerce, 5285 Port Royal Rd., Springfield, VA 22161
ph: (800) 553-6847
fax: (703) 605-6900
email: orders@ntis.fedworld.gov
online ordering: http://www.ntis.gov/ordering.htm


This document was printed on recycled paper.

A Geostatistical Analysis of Historical Field Data on Tritium, Technetium-99, Iodine-129, and Uranium

C. J. Murray
Y.-J. Chien
P. D. Thorne

April 2004

Prepared for
the U.S. Department of Energy
under Contract DE-AC06-76RL01830

Pacific Northwest National Laboratory
Richland, Washington 99352

Executive Summary

Pacific Northwest National Laboratory performed a geostatistical study for the Groundwater Remediation Project (formerly the Groundwater Protection Program) managed by Fluor Hanford, Inc., and the U.S. Department of Energy (DOE). The objective of the study was to generate history matching data needed to test the performance of the System Assessment Capability (SAC) model that forms the basis for the Hanford Site 2004 Composite Analysis for low-level radioactive waste disposal in the Central Plateau at the Hanford Site. The SAC model is a stochastic model that uses probabilistic descriptions of inventory and transport parameters from the Hanford Site to generate predictions of the expected movement of contaminant plumes at the site. The history matching data generated by the study are based on geostatistical analysis of historical measurement of radionuclide concentrations in groundwater samples at Hanford.

The history matching study focused on concentration data for two points in time, fiscal year (FY) 1992 and FY 2001, and considered four radionuclides: tritium, technetium-99, iodine-129, and uranium. Geostatistical methods were used to analyze and model the spatial distribution of each radionuclide and then use that model to generate a suite of stochastic simulations of the concentrations. The simulations covered the entire Hanford Site in a series of regional grids that had similar properties in aquifer geology and contaminant transport. Each simulation would reproduce the data at the known measuring points; between those points the simulated values would reproduce the global probability distribution and the spatial correlation of the radionuclide data identified in the geostatistical model. The simulated concentrations were used together with estimates of the subsurface geology and the probability distributions for the porosity of each geologic unit to generate Monte Carlo realizations of the mass or activity of each contaminant. The suite of Monte Carlo realizations were used to estimate several metrics for the radionuclides that could be tested against the SAC model. Those metrics included the total mass or activity, the location of the center of mass, the area above the drinking water standard (DWS) for each contaminant, and, where relevant, the length of the Columbia River shoreline above the DWS. These metrics were calculated for several individual plume areas at the Hanford Site for FY 1992 and FY 2001. Each metric was calculated over the suite of realizations so that the average value for the metric could be provided along with a measure of uncertainty for the metric.

The history matching data generated by this study can be used to evaluate the ability of the SAC Rev. 1 model to produce simulated concentration histories over time that match the historical data. In addition, the study provides measures of the uncertainty in each of those metrics that can be used to determine if the predictions from the SAC model fall within the uncertainty bands expected due to spatial uncertainty in the historical contaminant concentration data.

This report also discusses several areas of uncertainty in the data and the modeling process that were not addressed by the current study. Several possible improvements or extensions of the approach are recommended for future study. These include:

- Generate results for additional time points beyond the two points in time considered in the present study. History matching data should be generated for earlier points in time, although the areas covered might need to be restricted due to the sparse distribution of data for earlier time periods.

- Examine the effect of vertical contaminant distribution assumptions on uncertainty bounds for history matching data.

- Perform an uncertainty analysis to examine the effect on uncertainty bounds for the various metrics that might arise from uncertainty in geologic structure. This should be done by using the results of work being performed in FY 2004 for the sitewide Groundwater Modeling task to develop stochastic alternative conceptual models of the geologic structure.

- Examine the sensitivity of history matching metrics to variation in parameters of the variogram models fit to the experimental variograms.

- Produce a set of metrics based on the SAC model runs that accounts for the sparseness of the concentration data available for geostatistical modeling. The suggested approach includes sampling concentration fields from the SAC model runs at historical well locations and over screened intervals that were used to sample groundwater. Geostatistical analysis of the sampled model runs would then be used to generate a set of metrics using the same methods described in this report. The metrics calculated from historical groundwater data and sampled SAC model runs would then be compared to evaluate the ability of the SAC model to reproduce historical groundwater concentration data.

Contents

Figures

Tables

1.0 Introduction

A composite analysis is required by U.S. Department of Energy (DOE) to ensure public health and safety through the management of low-level radioactive waste disposal facilities associated with the Hanford Site (DOE Order 435.1). A major component of the Hanford Site 2004 Composite Analysis (Kincaid et al. 2004) will be the use of the System Assessment Capability (SAC). The SAC is a stochastic risk assessment program consisting of several modules that address contaminant inventory, contaminant release, atmospheric transport, vadose zone flow and transport, groundwater flow and transport, the Columbia River shore environment, Columbia River flow and transport, and risk and impact assessment. During application of SAC to the composite analysis, predictions of the concentrations of radioactive contaminants in groundwater will be generated as a function of time. These predictions are based on an assumed release of inventory, and then simulates the migration of contaminants through the various transport modules. The results of these predictions will be evaluated by matching (comparing) them against historical groundwater contaminant data.

There is a large amount of historical data on the concentration of contaminants in groundwater at the Hanford Site. The most recent annual report, summarizing the groundwater data collected in 2002, can be found in Hartman et al. (2004) with background information on the purposes and methods for the groundwater monitoring effort given in Hartman (2000).

The purpose of the study described in this report was to generate maps and statistics that quantify contamination in groundwater, based on historical groundwater concentration data for multiple points in time. The maps and statistics could then be compared to predictions from the SAC model, and used for verification of SAC results that will be incorporated in the 2004 Composite Analysis. The results generated from this study include several quantitative summaries of contaminant distributions (e.g., the location of the center of mass of contaminant plumes and the total mass of contaminants in the plume) and are collectively referred to as history matching data. A primary goal of this study was to use geostatistical and Monte Carlo methods that allow one to provide an estimate of uncertainty in the history matching data generated.

This work was conducted as part of the Characterization of Systems Task of the Groundwater Remediation Project (formerly the Groundwater Protection Program) managed by Fluor Hanford, Inc. The scope of the study focused on four radioactive contaminants with a wide distribution at Hanford: tritium, technetium-99, iodine-129, and uranium. All four are current contaminants of concern at Hanford that will be examined in detail by the 2004 Composite Analysis (Kincaid et al. 2004, Table A.4). Results were generated for two time periods, fiscal year (FY) 2001 and FY 1992. To support the geographic scope of the 2004 Composite Analysis, the scope of this study covered the entire Hanford Site including the 200 West and East Areas in the Central Plateau, and the 100 Areas and 300 Area in the Columbia River corridor. Figure 1.1 shows the major features at the Hanford Site.

The purpose of this report is to document the source of the groundwater concentration data employed in the history matching data analysis, the geostatistical approach used for analyzing the spatial distribution of the contaminants, the Monte Carlo methods used to convert stochastic simulations of concentration to mass or activity, the approach used to calculate the metrics reported by the study, and the results generated for each of the four contaminants.

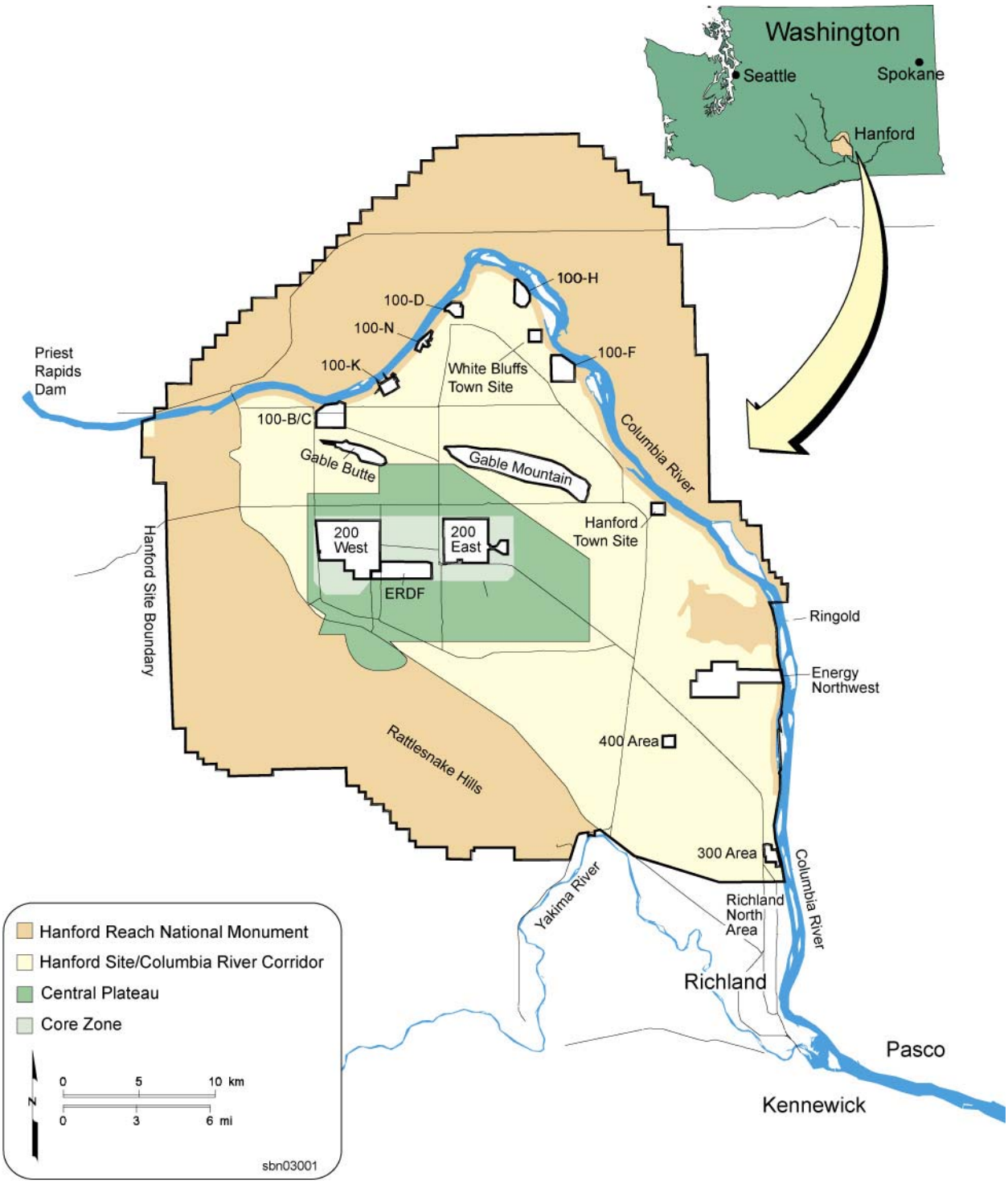

Figure 1.1. Major Areas at the Hanford Site (from Kincaid et al. 2004)

2.0 Approach

This study used a Monte Carlo approach to generate suites of realizations of mass or activity for four radioactive contaminants at the Hanford Site. These realizations were generated on a series of regular grids covering the Hanford Site. The foundation for the approach was geostatistical modeling and simulation of the spatial distribution of the concentrations of contaminants. Mass or activity estimates based on the geostatistical simulations were generated for several plume thickness assumptions using Monte Carlo sampling of porosity distributions for each hydrogeologic unit present in a grid cell. Aggregate metrics were computed for a series of sub-areas of the Hanford Site associated with major contaminant plumes. This section of the report provides detail on the data used in the study and the methods employed.

2.1 Data Compilation

Data for each contaminant were retrieved from the Hanford Environmental Information System (HEIS). All measurements of tritium, technetium-99, and iodine-129 data available at the Hanford Site were retrieved from the database (in pCi/L), along with all measurements of uranium concentration (μg/L). Data were included in this study in accordance with selection criteria generally employed for the Hanford Site Groundwater Monitoring Reports (e.g., Hartman et al. 2004). The data were reviewed for data quality, and only data meeting the qualifications generally accepted for inclusion in the annual monitoring reports[(a)] were included. This involved exclusion of data with "Y" or "R" review qualifiers, which indicate that the data quality review indicated that the data were invalid, or that the results were suspect with insufficient evidence to show if the results were valid or invalid, respectively. The hydrogeologic zone from which the samples were taken was also examined, and samples were retained that were from the upper portions of the unconfined aquifer, again in accord with criteria used to select groundwater concentration data for inclusion in the annual monitoring reports.[(a)] The selection criteria for the well zone included samples designated "TU" (Top Unconfined), "UU" (Upper Unconfined), and "U" (Undifferentiated Unconfined), together with samples for which the zone was not recorded on the assumption that wells that test the lower portions of the unconfined aquifer and/or the confined aquifers have been identified by scientists working for the Groundwater Performance Assessment Project.[(a)] This selection provides a two-dimensional dataset for the concentrations in the upper portion of the unconfined aquifer. While it would be preferable to map the concentrations in three dimensions, there is insufficient data available with discrete measurements of concentration with depth in the aquifer to make that feasible. As discussed in the following sections, the amount of three dimensional data in the aquifer are insufficient to determine the total thickness of the contaminant plumes, let alone to map the plumes in three dimensions.

Data for each contaminant were summarized on a fiscal year basis, averaging all observations for each well for each fiscal year for which data were available. Because a number of wells at the Hanford Site are not sampled on an annual basis, an algorithm was used to select data from the most recent year in order to represent the concentration at a well for a given fiscal year. The algorithm selects the annual average for a given fiscal year, or if this is not available, the most recent of the annual averages from the

(a) Personal communication from J Rieger to the authors, 2002.

two preceding fiscal years. This algorithm is also used to select the annual fiscal year average data for inclusion in the annual groundwater monitoring reports.[(a)]

Once the fiscal year annual average concentration data were calculated for each contaminant, the distribution of the number of data points with time was examined to select years for which history matching data would be generated. Figure 2.1 plots the number of wells for which an annual average is available for each fiscal year for the four contaminants. Two years were selected to generate history matching data, FY 1992 and FY 2001, which are highlighted in Figure 2.1. At the time this study was initiated, FY 2002 data were not yet available, and FY 2001 was the most recent year with available data. FY 1992 was selected because it represented the earliest date for which a high number of tritium observations (~700) were available. In addition, that year has among the highest number of observations ever recorded for both technetium-99 and uranium (Figure 2.1).

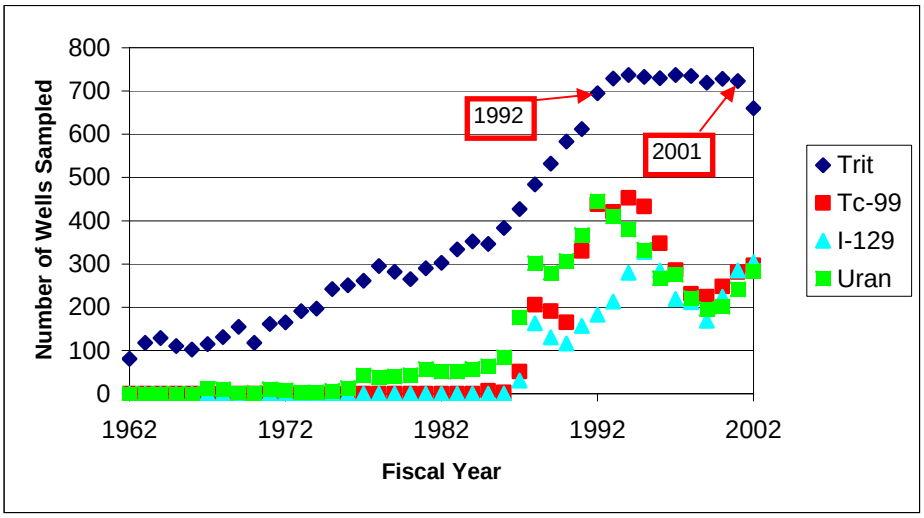

Figure 2.1. Number of Wells in Each Fiscal Year for Each Contaminant for Which An Annual Average is Available

2.2 Geostatistical Simulation Method for Concentration Distributions

The geostatistical analysis of the contaminant plume included variogram analysis and modeling to define a mathematical model of the spatial continuity of the contaminant concentration data. The most commonly used tool for describing the spatial continuity of geologic properties is the experimental variogram (Isaaks and Srivastava 1989; Davis 1986; Goovaerts 1997), which is a measure of the average dissimilarity between pairs of points separated by a given vector distance, as a function of that distance. The variogram is calculated as:

$$\gamma(\mathrm{h}) = \frac{1}{2N(\mathrm{h})} \sum_{\alpha=1}^{N(\mathrm{h})} \left[z(\mathrm{u}_\alpha) - z(\mathrm{u}_\alpha + \mathrm{h}) \right]^2 \qquad (2.1)$$

(a) Personal communication from J Rieger to the authors, 2002.

where γ(h) is the variogram value for a lag distance of h, and *N*(h) is the number of pairs of concentration values (z) separated by a lag distance of h. Variables that result from the operation of geologic processes that vary spatially (e.g., contaminant transport by groundwater) often display spatial continuity that can be identified by variogram analysis. If a variable exhibits spatial continuity, then points that are close to one another will have smaller differences, and, therefore, lower variogram values than pairs of points that are separated by greater distances. In variogram analysis, models are fit to the experimental variograms that quantify the spatial continuity of the variable. Variogram models are required for geostatistical estimation (i.e., kriging) or simulation algorithms because it is rare that experimental variogram values will be available for all lag distances for which estimates or simulations may be desired (Isaaks and Srivastava 1989). Figure 2.2 explains some of the important features of a variogram model. All but one of the variograms in this study were fit using a spherical model (Isaaks and Srivastava 1989), which is defined as follows:

$$\gamma(h) = \begin{cases} 1.5\frac{h}{a} - 0.5\left(\frac{h}{a}\right)^3 & \text{if } h \le a \\ 1 & \text{otherwise} \end{cases} \tag{2.2}$$

where h is the lag distance and a is the range of the spherical variogram model. The other model used was the Gaussian variogram (Isaaks and Srivastava 1989), which has the following form:

$$\gamma(\mathrm{h}) = 1 - \exp\left(-\frac{3h^2}{a^2}\right) \tag{2.3}$$

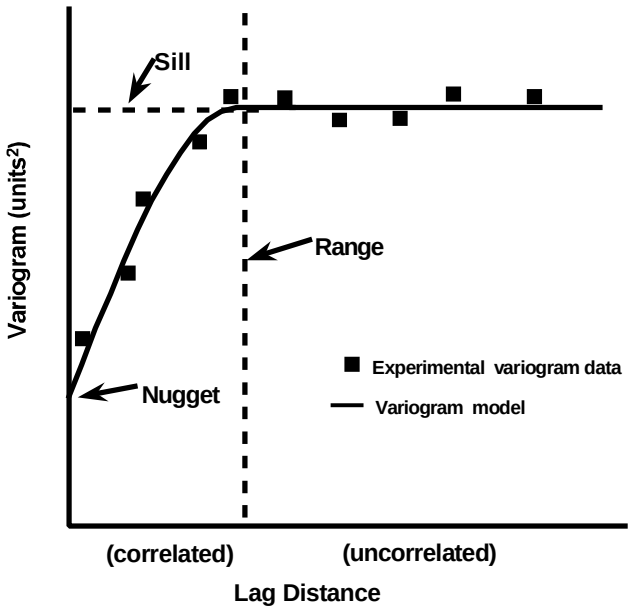

Figure 2.2. The Variogram is a Geostatistical Tool to Measures Average Squared Difference Between Pairs of Data Values Separated by a Given Lag Distance. At distances less than the range, the variogram is a function of distance related to the degree of spatial correlation. Points separated by distances greater than the range are uncorrelated.

The variogram analysis for each contaminant at the Hanford Site was performed for three separate areas. The three areas were 200 West Area (designated Grid 1), 100 Areas (Grid 2), and 200 East Area and the plumes that traveled northwest and southeast from it (Grid 3). Figure 2.3 shows the three grid areas for tritium in 2001. These areas were chosen because of differences in their hydrogeological properties. For example, Figure 2.3 is a map of the geological units exposed at the water table. The map shows that the area of Grid 1, which includes 200 West Area, is predominantly Ringold Formation at the

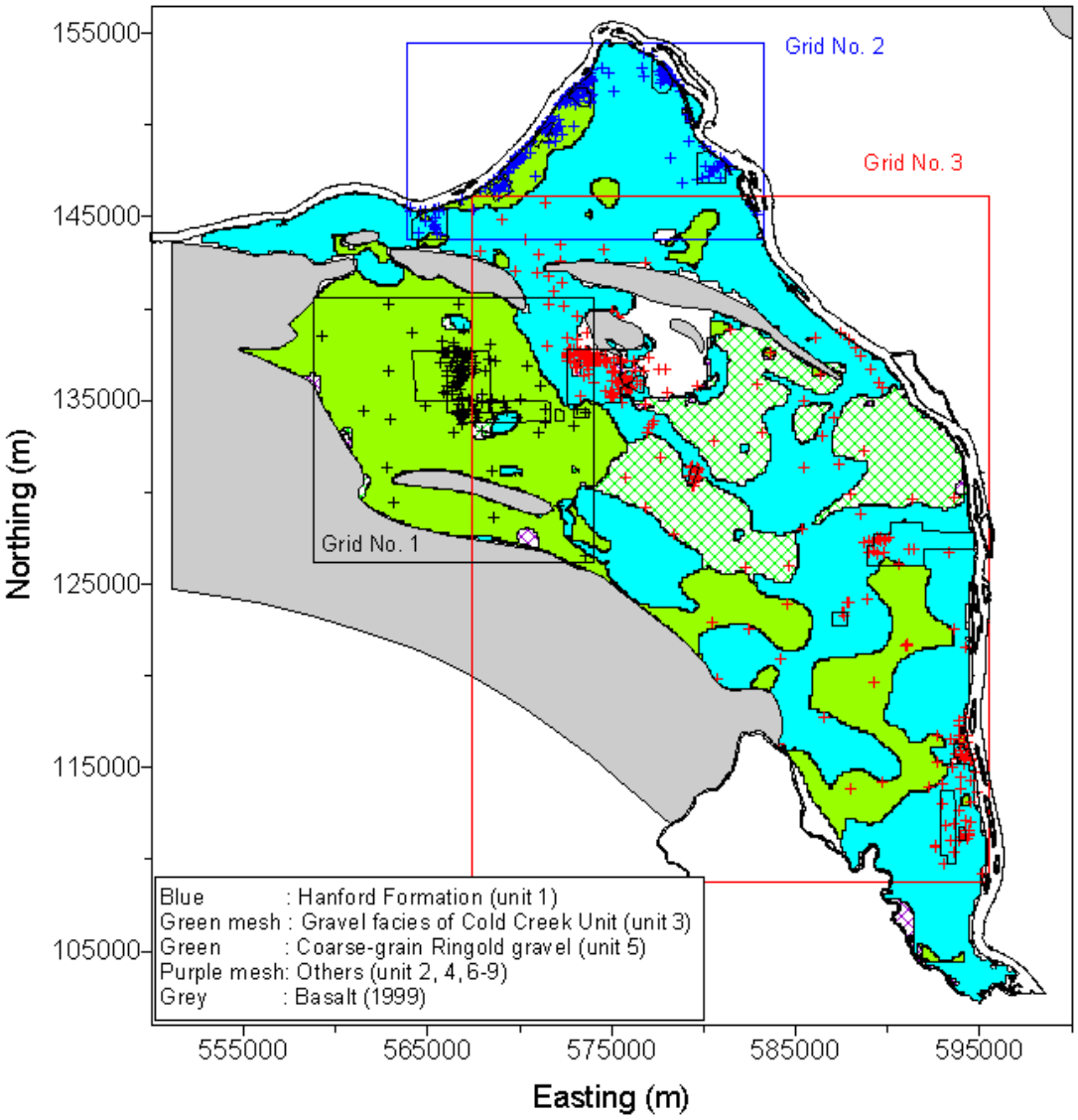

Figure 2.3. Subcrop Formation Units at FY 2001 Water Table

water table, while Grid 3 is predominantly Hanford formation. The hydraulic conductivity of the Ringold Formation is much lower than that of the Hanford formation, so the plumes in 200 West Area tend to be smaller and move more slowly than those emanating from 200 East Area. This difference in the plumes was expected to be reflected in the spatial continuity of the plumes measured by variogram analysis.

A multi-Gaussian sequential simulation (Gomez-Hernandez and Journel 1993; Goovaerts 1997) approach was used to simulate the distribution of contaminants at the Hanford Site. Because of the large number of separate geostatistical studies and large numbers of simulations generated for each study, Gaussian simulation was used as the default modeling approach because of the simplicity of the modeling approach and computational speed of the simulation algorithm relative to indicator geostatistical methods. All simulations were performed on square grids with a grid resolution of 50 meters. The multi-Gaussian simulation approach requires that the data exhibit a Gaussian distribution. Because the contaminant data are not normally distributed, the variogram modeling described above and the subsequent simulations were performed on a normal-score transformation of the contaminant data (Goovaerts 1997, p. 268), which transforms the variable so that it fits a univariate normal distribution. The normal score transform is a more general transformation than the lognormal transform often used in hydrogeologic studies and it has the advantage that it avoids most problems associated with back-transformation from the logarithmic space to the original data space (see Goovaerts 1997, p. 17, for a discussion of those problems).

Sequential Gaussian simulation is a stochastic simulation method that allows one to generate equally probable realizations of the spatial distribution of a variable that honor both the data and the variogram model fit to the data. The simulations are generated by taking a random path through the grid cells that are to be simulated (Figure 2.4). At each grid cell in the simulation domain, the surrounding data and the variogram model are used to estimate the conditional cumulative distribution function (CDF) of the variable at that cell (Figure 2.4) by estimating the conditional mean and variance of the distribution. The estimation of the conditional mean and variance are performed by kriging. Although simple kriging is theoretically the preferred form of kriging to estimate the conditional mean and variance, ordinary kriging can be used when sufficient data are available for local re-estimation of the mean (Deutsch and Journel 1998, p. 174). Ordinary kriging can be used to re-estimate the local mean when a spatial trend is present in the data (Journel and Rossi 1989), rather than using a single unchanging mean as occurs in simple kriging. In the simulations generated for this study, the mean and variance of the conditional distribution at each grid cell was estimated by ordinary kriging, with the conditional mean equal to

$$Z^*_{OK}(u) = \sum_{\alpha=1}^{n(u)} \lambda_\alpha^{OK}(u) Z(u_\alpha) \text{ with } \sum_{\alpha=1}^{n(u)} \lambda_\alpha^{OK}(u) = 1 \qquad (2.4)$$

where Z^*_{OK} is the ordinary kriging mean at location u. Thus, the ordinary kriging mean at each location u is a weighted linear combination of the nearby data ($Z(u_\alpha)$), with the ordinary kriging weights ($\lambda_\alpha^{OK}(u)$) constrained to sum to 1 and found by minimization of the error variance. The variance of the conditional distribution of the simulated cell was estimated by the ordinary kriging variance σ^2_{OK}:

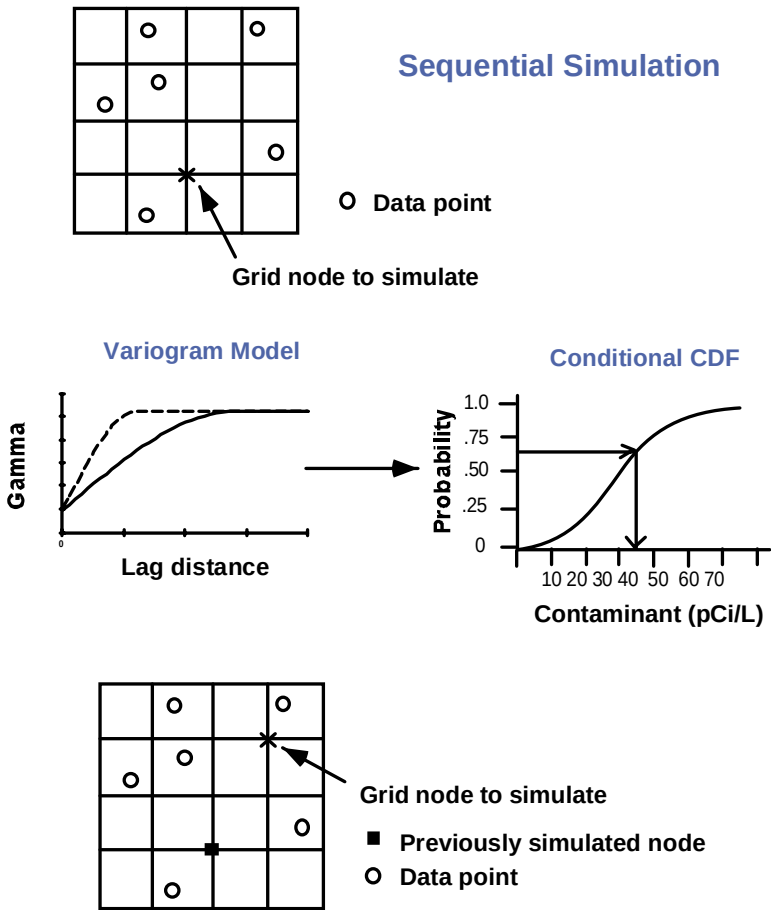

Figure 2.4. Diagram of Basic Elements of the Sequential Simulation Algorithm

$$\sigma^2_{OK} = C(0) - \sum_{\alpha=1}^{n(u)} \lambda_\alpha^{OK}(u) C(u_\alpha - u) - \mu_{OK}(u) \tag{2.5}$$

where C(0) is the covariance at zero separation distance, $C(u_\alpha - u)$ is the covariance between the data point at location α and the cell being simulated and $\mu_{OK}(u)$ is a Lagrange parameter that accounts for the constraint on the weights in ordinary kriging (see Goovaerts 1997, p. 133 for further detail on ordinary kriging). A uniform random number between 0 and 1 is then used to draw a value from the conditional distribution, which has been estimated by the ordinary kriging mean and variance (Figure 2.4). The simulated value then becomes a data point for the simulation of the remaining grid cells, and the process is repeated, moving to each cell in the domain until all cells in the grid have been evaluated. The sequential algorithm ensures reproduction of the variogram and histogram of the data through a recursive application of Bayes theorem. Additional simulations can be generated by taking different random paths through the simulation grid. A more detailed discussion of the sequential Gaussian simulation algorithm can be found in Goovaerts (1997, p. 376).

During the geostatistical modeling of the contaminant distributions, the results for the Gaussian simulations of technetium-99 in 200 East Area for FY 2001 did not agree with those provided by previous geostatistical modeling of that plume. Previous study of the technetium-99 distribution in that area for FY 2001 had been performed using sequential indicator simulation rather than sequential Gaussian simulation (DOE 2003). To be consistent with the results, which were felt to be more representative of the concentrations in the plume, sequential indicator simulation (Goovaerts 1997) was used for geostatistical simulations of technetium-99 in 200 East Area for FY 2001.

2.2.1 Post-Processing of Contaminant Concentration Simulations

The set of simulated values of the contaminant concentration for each 50 meters by 50 meters grid cell can be used as a model of the conditional probability distribution of the concentration in that cell (Journel 1987, 1989). The conditional probability distributions can be summarized in several ways. For example, they can be used to estimate the mean or median concentration at each grid cell and the uncertainty in that estimate, e.g., by calculating the variance of the simulated values or the 5th and 95th percentiles of the simulated concentration values. The suite of simulations can also be used to estimate the probability that the concentration exceeds some cutoff value, e.g., the drinking water standard (DWS) for a contaminant, by calculating the frequency with which the simulated values at each location exceed that cutoff. Each of these statistics of the local conditional distributions can be mapped, and they provide valuable information about the spatial distribution of the contaminant plume.

A large number of simulations, at least several hundred, were generated for each contaminant/grid/year combination. The number of realizations generated for each variable/year combination was determined by plotting the results for one of the metrics as a function of the number of simulations generated to determine if there was an obvious break in the curve that would indicate that the space of uncertainty was well-sampled. For example, Figure 2.5 shows a plot of the average of one of the metrics calculated

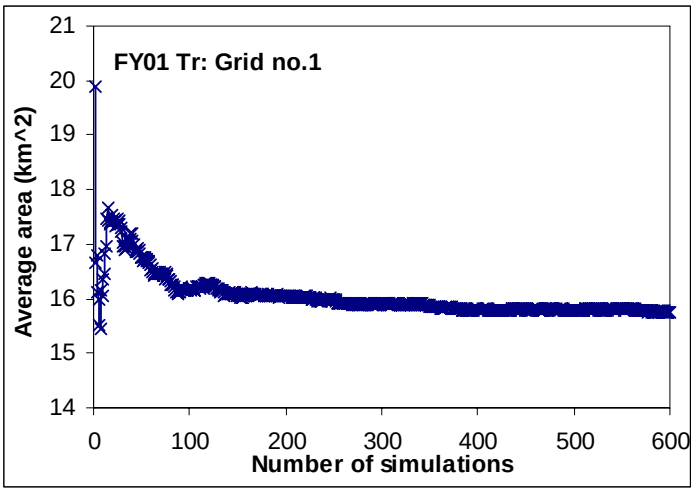

Figure 2.5. Plot of the Average Area Above the Tritium Drinking Water Standard as a Function of the Number of Simulations Generated for One of the FY 2001 Tritium Simulation Grids

for FY 2001 tritium (the area above the drinking water standard, see Section 2.2.3 for information on the procedure used to calculate that metric). The average area is relatively unstable early in the process with a large amount of variability, especially for less than 100 simulations, but appears to have stabilized after about 300 simulations have been generated.

2.3 Monte Carlo Simulation Method for Mass and Activity

The simulations of contaminant concentration generated using sequential Gaussian simulation were used as the basis to develop simulations of the mass and activity of contaminants in the study areas for FY 1992 and FY 2001.

To convert concentration values to mass or activity estimates, several factors need to be determined, including the thickness of the plume, vertical distribution of contaminant concentration within the plume, and porosity of the sediment.

2.3.1 Plume Thickness Scenarios

Information on the thickness of contaminant plumes at the Hanford Site is limited. One relatively simple way to address both the plume thickness and vertical distribution of contaminants is to examine the distribution of contaminant concentrations for samples taken from different hydrogeological zones. The hydrogeological zones used in this study were those identified by scientists working for the Groundwater Performance Assessment Project.[(a)] Table 2.1 gives the definitions of the hydrogeological zone in the unconfined aquifer that are plotted in Figure 2.6. Figure 2.6 is a plot of the median and average tritium concentration during FY 2001 for all samples at the Hanford Site taken within four hydrogeological zones in the unconfined aquifer. Thus, Figure 2.6 gives a rough idea of the distribution of tritium with depth in the unconfined aquifer for FY 2001. The median concentration falls off rapidly with depth in the aquifer, with median UU concentrations that are about one-third of those in the TU. However, the high average concentration for MU samples indicates that there are still some high concentration samples that occur at depths greater than 15.2 meters below the water table.

Table 2.1. Definitions of Aquifer Hydrogeological Zones

Zone	Definition
TU (Top Unconfined)	Screened across the water table with less than 9.1 m of the open interval extending below the water table.
UU (Upper Unconfined)	Screened across the water table for which the open interval is between 9.1 and 15.2 m below the water table.
	Screened below the water table for which the open interval extends less than 15.2 m below the water table.
MU (Middle Unconfined)	Open interval begins at greater than 15.2 m below the water table and does not extend below the middle coarse of the Ringold Formation (unit 7) or to within 15.2 m of the top of basalt.
LU (Lower Unconfined)	Open interval begins at greater than 15.2 m below the water table and below the middle coarse unit of the Ringold Formation (unit 7) or within 15.2 m of the top of basalt and does not extend more than 3 m below the top of basalt.

(a) Personal communication from J Rieger to the authors, 2002.

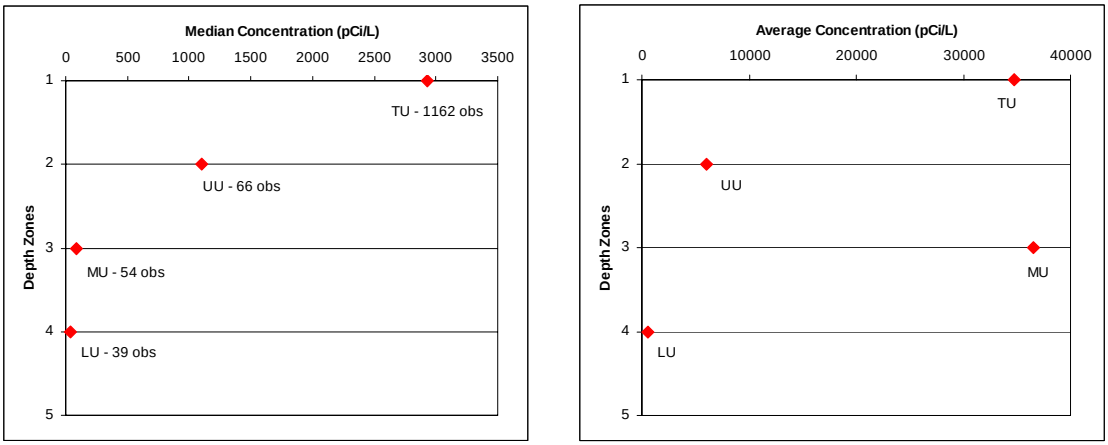

Figure 2.6. FY 2001 Tritium Distribution by Hydrogeological Zones

Other data compiled for this study provided insight into the thickness and concentration variations with depth of the contaminant plumes. Data from the tritium plume near the PUREX facility indicate the thickness of the tritium plume is at least 8 meters, but concentrations tend to be low for samples more than 10 meters below the water table:

- Data from well 299-E25-28 indicate some tritium at 18 meters, but the concentration is low at that depth and also at the water table.
- Data from well 299-E25-29 show the plume is more than 8 meters thick.
- Data from wells 699-24-1S and 699-24-1T show concentration at 10 meters below the water table of 15 to 30% of concentration at water table and none at 30 meters below the water table (note that well 699-24-1P, Q and R go to basalt).
- Data from well 699-28-40 P show a few sporadic high results, but generally does not show any peak in the late 1980s corresponding to that in the earlier well 699-28-40 data. It appears that plume thickness at that location is less than 50 meters.
- Data from well 699-26-34B show the plume thickness is greater than 8 meters.

Indications from discrete depth sampling conducted in FY 1999 at Waste Management Area S-SX suggest that the maximum concentrations of contaminants occur within the upper 2.5 to 7 meters of the aquifer (Johnson and Chou 2000). Some contaminants were found up to 30 meters deep and even below the Ringold lower mud unit (an aquitard deep in the unconfined aquifer); however, concentrations at these greater depths were low.

However, data from well 699-48-77C show that the tritium plume from the State-Approved Land Disposal Site (SALDS, north of 200 West) has gone to depths greater than 25 meters with peak concentrations at depth of about 1 million pCi/L compared to 2 million pCi/L near the water table. There is a large downward driving force from the discharge at the disposal site and the Ringold mud units are

missing in this location, which may contribute to the high concentrations with depth. Williams et al. (2002) discuss additional evidence from 200 West Area suggesting that significant concentrations of contaminants may be present at depth within the aquifer, with greater concentrations found at depth than occur at the water table in some locations.

The following approach was adopted for this study, based on the available data and the approach used in the history matching study performed for SAC Rev. 0 (Bryce et al. 2002). The concentration within a contaminant plume was assumed to be constant with depth over a finite plume thickness. In mass calculations, the mass of a contaminant within a plume was calculated for four different plume thickness scenarios of 5, 10, 15, and 20 meters. Although all four cases will be presented, the major focus will be on the results generated for the 5 meters plume thickness, because the limited data that are available tend to suggest the majority of contaminant mass is within 5 meters of the top of the aquifer (e.g., Eddy et al. 1978; Johnson and Chou 2000), although Williams et al. (2002) make a case for a deeper distribution of contaminants in the aquifer. Work will be performed within the characterization of systems groundwater task during FY 2004 to examine the vertical contaminant distribution in more detail; the assumptions about the distribution used to generate the history matching data should be revisited when the results of the characterization of systems study are available.

2.3.2 Probability Distributions of the Porosity of Sedimentary Units

The major factors that control the mass of contaminants present within the contaminant plume are contaminant concentrations, which were simulated using the methods discussed in Section 2.1 (and then assumed to be constant with depth over a specified plume thickness), and sediment porosity. The sediment porosity varies between the different geological units and also varies within each unit. The identification of the unit thicknesses that are present in the aquifer were taken from the current sitewide groundwater model (Vermeul et al. 2003). A grid of the thickness of each unit at each grid location was generated from the model using EarthVision and then downloaded as a text table. The table identified the thickness of each hydrogeologic unit below the elevation of the water table that was present in FY 1992 and FY 2001.

Using information from several sources, including data from Freeman et al. (2002) and Thorne and Newcomer (2002), a probability distribution was developed for the porosity of each hydrogeologic unit. Table 2.2 shows the probability distributions for each unit, which were assumed to be normal for each unit, with mean and standard deviation as specified. The data on which each probability distribution is based are provided in the last column of the table. No data were available for Unit 3, and the assumption was that the pre-Missoula gravels in that unit (now part of the Cold Creek unit) would have a porosity distribution similar to that of the coarse-grained units of the Ringold Formation (5, 7, and 9). No porosity or specific yield data were available for the fine-grained units of the Ringold Formation (4, 6, and 8), and the porosity of those units was assumed to be similar to that of the fine-grained portions of Unit 2.

Although porosity occurs in the fine-grained units of the sequence, the majority of that porosity was assumed to not be effective porosity. That implies only small amounts of contaminants would be transported into and out of the mud units. Therefore, for this study, it was assumed that there would be no mass or activity of contaminants contained within the mud units, so that the thickness of the mud units in

Table 2.2. Probability Distributions Assumed for Each Unit in the Unconfined Aquifer

Unit	Mean	Std Dev	Source
1	0.27	0.087	Pump tests (3)
2	0.42	0.081	Khaleel and Freeman (1995)
3	0.13	0.033	Assume Ringold porosity
4	0.42	0.081	Assume similar to Unit 2
5	0.13	0.033	Pump tests (10)
6	0.42	0.081	Assume similar to Unit 2
7	0.13	0.033	Pump tests (10)
8	0.42	0.081	Assume similar to Unit 2
9	0.13	0.033	Pump tests (10)

a grid cell would have zero concentration. This approach follows that developed for the earlier history matching studies that supported SAC Rev. 0 (Bryce et al. 2002).

2.3.3 Monte Carlo Calculations of Contaminant Mass

Monte Carlo simulations of contaminant mass or activity were produced as follows for each simulation of the concentration of a contaminant generated by the stochastic sequential algorithm described in Section 2.1. For each concentration simulation, porosity values were drawn from the porosity distributions for each of the non-mud sedimentary units present in the sitewide Groundwater Model (see Section 2.2.2) and were assumed to be constant for that sedimentary unit for all cells in that simulation. For each cell in the grid, the thickness of each unit present below the water table would be retrieved from the table of unit thicknesses described in Section 2.2.2. The total volume of pores within the cell would be determined by adding the products of the unit porosity times the unit thickness for each non-mud unit below the water table and above the base of the assumed plume thickness, then multiplying that sum by the area of the cell (2500 m^2). The total mass or activity in the cell would then be the product of the simulated concentration in the cell and the total porous volume. For each cell, four estimates of the mass or activity would be generated, one for each assumed plume thickness (i.e., 5, 10, 15, or 20 meters). This procedure was followed for each cell in each simulation, yielding a suite of simulated contaminant mass or activity values for each cell.

2.3.4 Calculation of Metrics

Several metrics were identified for use in the history matching effort, each of which would allow a quantitative assessment of the agreement between the SAC model and historical groundwater contamination data. The metrics included:

1. Total mass/activity
2. Location of center of mass
3. Area above DWS
4. Length of shoreline above DWS

The metrics were calculated for specific plume areas within the individual simulation grids. For example, Figure 2.7 shows the location of two plume-areas for which separate calculations were made within Grid 1, which covers 200 West Area.

An estimate of the spatial moments of a concentration field is found by numerical approximations to integral equations of the form (Rajaram and Gelhar 1991):

$$M_{ijk} = \iiint_{-\infty}^{+\infty} nC(x,y,z)\, x^i y^j z^k \, dx\, dy\, dz \tag{2.6}$$

where M_{ijk} = the ijk^{th} moment
n = the porosity
$C(x,y,z)$ = the concentration for the cell with coordinates x, y, and z

The moments calculated for the current study were the zero order moment, which is the total mass and first order moments, which corresponds to the center of mass. The total mass or activity was calculated as the sum of the mass in each cell in the grid area for a given simulation, with the mass calculated according to the scheme discussed in Section 2.2.3. By calculating the total mass for each simulation of contaminant concentration, a range of total mass values were calculated that provided information on the uncertainty in the total mass. Standard univariate statistics were then reported on that distribution,

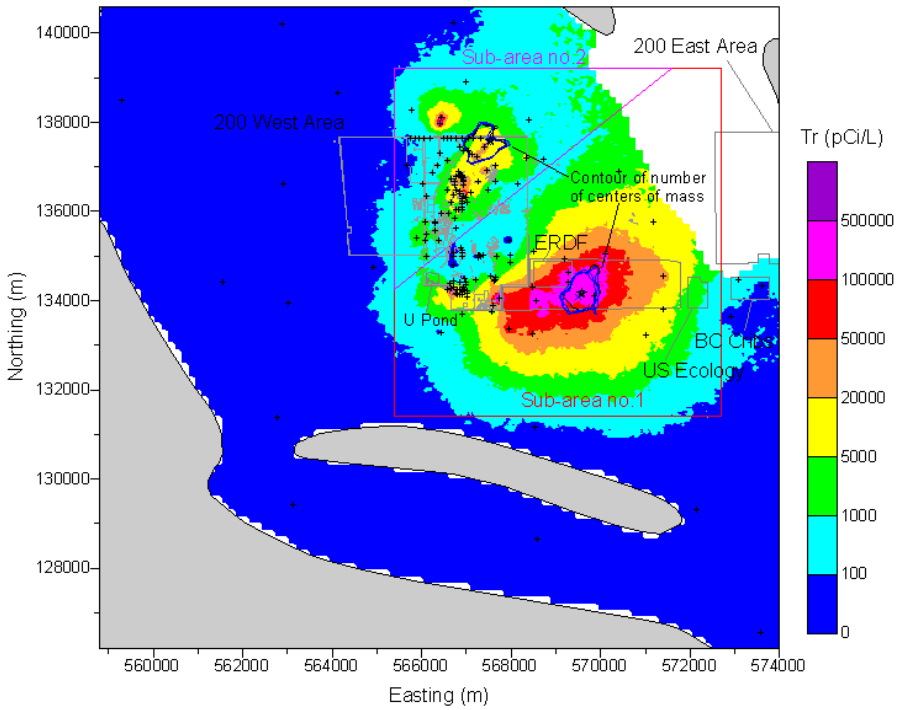

Figure 2.7. Median of Simulations of FY 2001 Tritium in Grid 1 (200 West Area) and Contour of Number of Centers of Mass within the Sub-Areas with the Average Centers of Mass Denoted by Black Stars

including the mean and median of the total mass and several uncertainty measures, including the standard deviation and 2.5th and 95th percentiles of the distribution.

The center of mass calculations were based on the cell mass estimates calculated assuming that the plume thickness is 5 meters. Given the two dimensional nature of the grid of mass values calculated in Section 2.2.3, the location of the center of mass of each simulation was calculated using the following approximation to equation 1:

$$xcmass = \sum_i x_i M_i / \sum_i M_i$$

$$ycmass = \sum_i y_i M_i / \sum_i M_i \qquad (2.7)$$

where *xcmass* and *ycmass* = the x and y coordinates of the center of mass, respectively
I = the cell number
x_i = the x coordinate of cell i
y_i = the y coordinate of cell i
M_i = the mass of cell i

Similar to the approach used for the total mass, the center of mass was calculated for each simulation in the suite of geostatistical simulations that were generated, providing a measure of the uncertainty in the location of the center of mass. This uncertainty was captured in two forms, graphically and in tabular form. Graphically, the mean center of mass was represented by a star, and the uncertainty is captured by contouring the number of times the center of mass occurred in each cell of a coarser grid covering the area of interest. The coarse grid for Grid 1 (200 West Area) and Grid 2 (100 Areas) was 200 meters by 200 meters, and for Grid 3 (200 East Area) the coarse grid was 400 meters by 400 meters. Figure 2.7 shows the average center of mass and the contours of the center of mass for two sub-areas of 200 West Area. In addition to the graphical display, the tabular information included the average x and y coordinates of the center of mass and confidence intervals for the location of those coordinates.

The remaining two metrics addressed the probability that the concentration within local areas exceeded the DWS. The DWS values used for this study are listed in Table 2.3, which is based on information listed in Hartman et al. (2004). One metric was the area above the DWS for each simulation, calculated by summing the area of the cells within each realization that exceeded the DWS, with each grid cell having an area of 2,500 m^2. This calculation was performed separately for each sub-area of a grid,

Table 2.3. Drinking Water Standards Used for Radionuclides

Constituent	Drinking Water Standard
Tritium	20,000 pCi/L
Technetium-99	900 pCi/L
Iodine-129	1 pCi/L
Uranium	30 µg/L

where sub-areas were defined. Statistical summaries of the mean and variability of the area above the DWS were reported for the suite of stochastic simulations. Another metric reported for Grid 2 (100 Areas) and Grid 3 (200 East Area plume) was the length of the Columbia River shoreline that exceeded the DWS. For each simulation of a grid that was bounded by the Columbia River, the number of grid cells intersecting the river that had concentrations exceeding the DWS were counted and multiplied by the average length of a cell intersected by the river. The average cell length is assumed to be the average of the edge (50 meters) and diagonal (70.7 meters) lengths of a cell, or 60.4 meters. As with the other metrics, the statistics for the distribution of shoreline lengths above the DWS were reported for the suite of simulations that were generated, providing an estimate of the most likely value as well as a measure of the uncertainty in the length.

The procedures used to compare the metrics generated in this study from the historical data and the predictions from the SAC model, as well as the results of the comparison, will be reported by the SAC project in the 2004 Composite Analysis.

3.0 History Matching Data for SAC/CA

A large number of maps, figures, and tables were prepared for this history matching data package. This chapter presents the results for tritium concentrations as an example of the results provided, focusing in particular on the results obtained for FY 2001. Section 3.6 identifies the appendices containing the results for other years and contaminants.

3.1 Definition of Grid Areas for Tritium Analysis

The Hanford Site was divided into three grids for the geostatistical analysis, with the primary basis for the grids being the differences in the type of sediment present at the top of the water table (Figure 3.1). Grid 1 occupied the area in the western portion of the Hanford Site where Ringold Formation sediment occurs at the FY 2001 water table, and the grid includes 200 West Area. Because the Ringold Formation

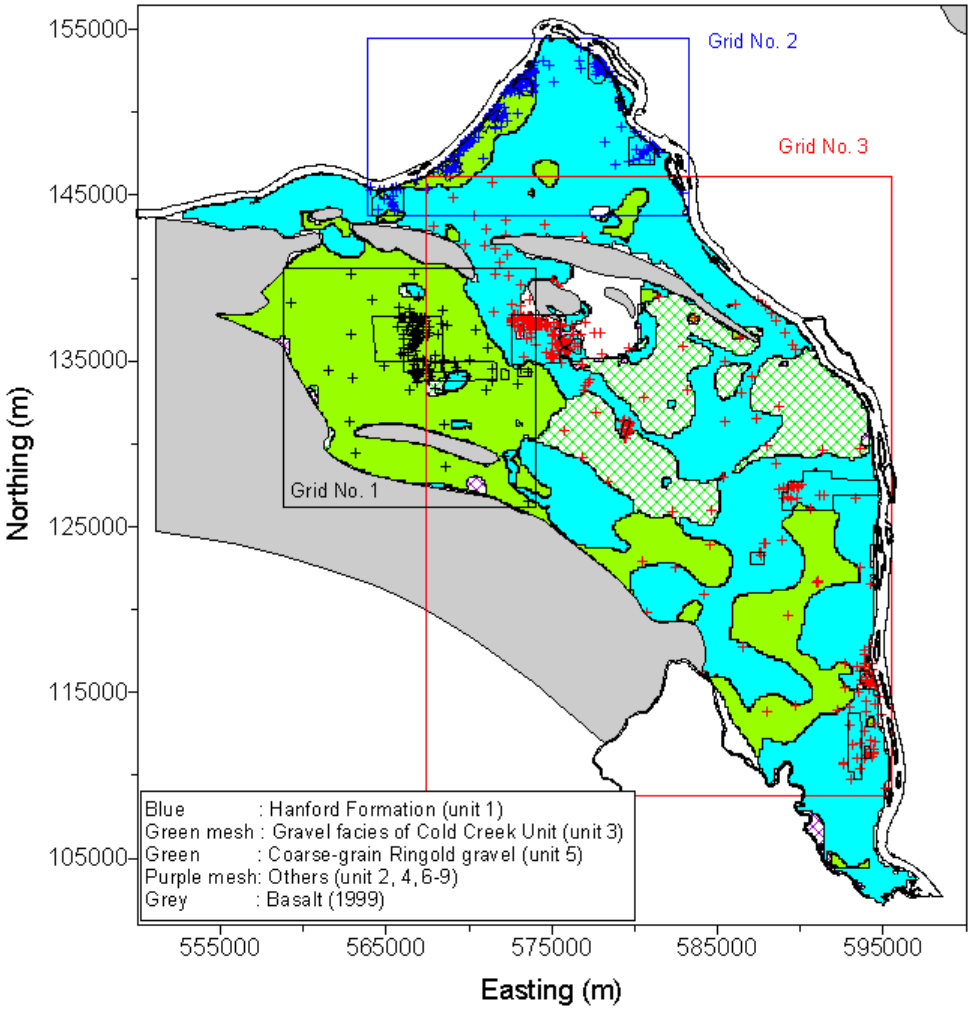

Figure 3.1. Subsets of FY 2001 Tritium Data and the Subcrop Formation Units at the FY 2001 Water Table

has relatively low hydraulic conductivity, plumes that occur within Grid 1 are spreading relatively slowly and tend to remain small. Grid 2 contains the contaminated areas along the Columbia River associated with the former nuclear reactors in the 100 Areas. Grid 2 has both Ringold and Hanford formations present at the water table. The plumes in this grid also tend to be small, in large part because they are constrained by their proximity to the Columbia River. In contrast to the first two grids, Grid 3 is dominated by high hydraulic conductivity sediment of the Hanford formation, which allows relatively rapid migration of contaminants and the development of larger plumes. For example the tritium plume in Grid 3 has migrated from its source in 200 East Area to the Columbia River. The differences in plume size in the three grid areas lead to differences in the ranges of the variograms, so the areas were treated separately for the geostatistical analysis. Figure 3.1 shows that there was overlap between the three grids. However, the boundary between Grids 1 and 3 was irregular, so that the areas on the eastern portion of Grid 1 where Hanford formation sediment was present were excluded from Grid 1, and the area at the western edge of Grid 3 where Ringold Formation sediment was present was excluded from Grid 3.

Similar decisions were made for analysis of FY 1992 tritium concentrations. Figure 3.2 shows the subcrop of different geologic units for the FY 1992 water table, which was at a higher elevation than the FY 2001 water table used to construct the subcrop map in Figure 3.1. The grid areas that were used for geostatistical analysis of the 1992 concentration data are shown in Figure 3.2. The three grid areas that were used for analysis in FY 1992 are similar to those used in FY 2001, but they are not identical, principally because of differences between the elevation of the water table in the two different years.

3.2 Variogram Analysis and Geostatistical Simulations of Tritium Concentration Data

The results of the variogram analysis of tritium concentrations for each of the three grid areas in FY 2001 are shown in Figure 3.3. As expected from the previous discussion, the variogram models fit to the experimental variograms are very different for the three areas. The total sill of the models fit to all three variograms are constrained to equal 1.0, as required for the sequential Gaussian simulation algorithm (Deutsch and Journel 1998). The variogram fit to the tritium concentration in Grid 2 has the shortest range, less than 1,000 meters. Grid 1, which contains the 200 West Area plumes, has a longer range of 2,000 meters but also has a short range structure of 200 meters that accounts for 40% of the total variance, indicating significant patchiness or variability of the plume at short distances. The variogram model fit to the data from Grid 3 is more continuous at short distances and has a longer total range of 6,000 meters. Although not explicitly modeled, a hole effect can be seen in Figures 3.3a and 3.3c, which results in lower variogram values for intermediate distances (e.g., at distances of about 2,500 meters in Figure 3.3a). This occurs in part because most variogram pairs for those distances tend to match low values on either side of the large central plumes emanating from facilities in 200 West and 200 East Areas. The hole effect and other differences between the long- and short-range variogram structure may also be caused by different variogram structures close to the source versus farther away from the source. This may have occurred because many local recharge areas associated with discrete waste facilities in the source area probably create complex local groundwater flow directions that affect the short-range variogram structure, whereas farther away from the source, the contaminant distribution and variogram structure associated with it was affected only by the regional groundwater flow.

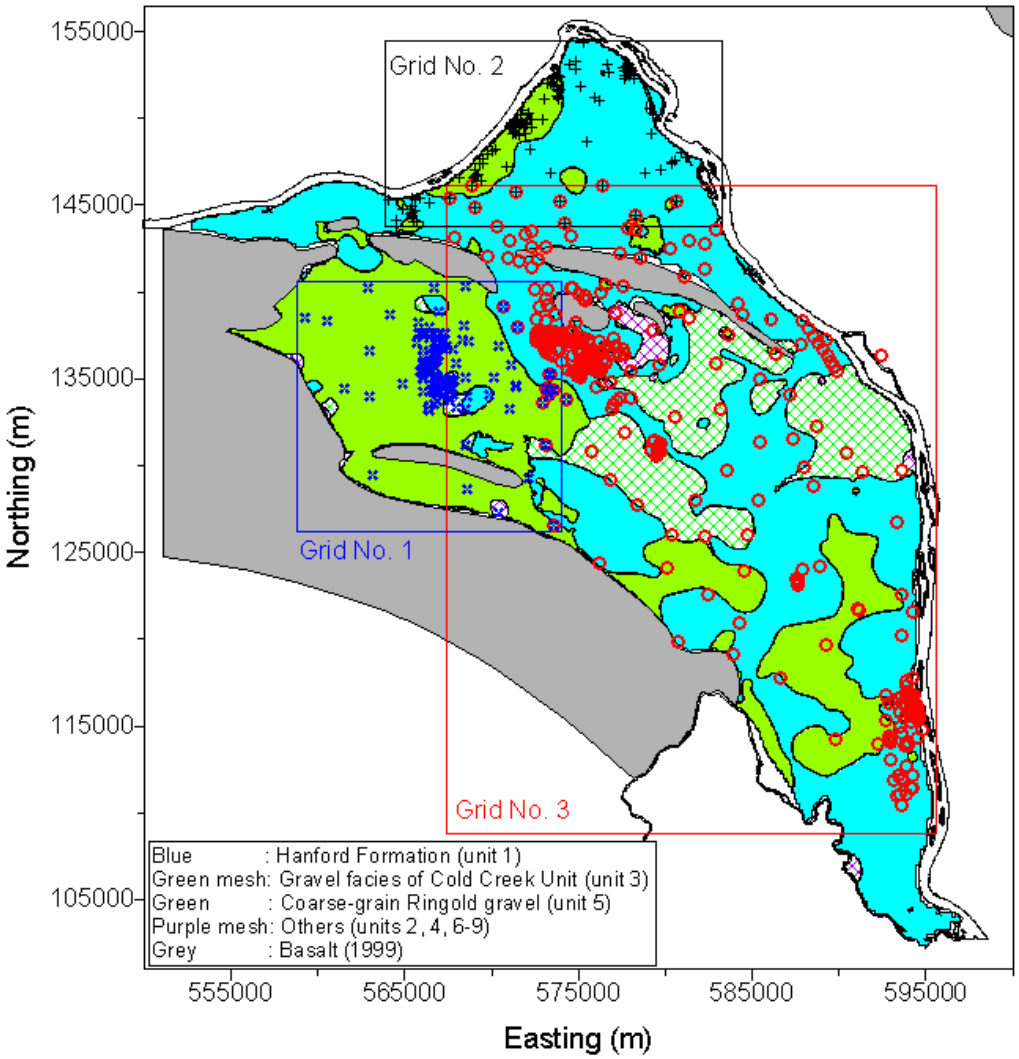

Figure 3.2. Subsets of FY 1992 Tritium Data and the Subcrop Formation Units at the FY 1992 Water Table

The variogram models shown in Figure 3.3 were used as input to sequential Gaussian simulations of the FY 2001 tritium concentrations. Figure 3.4 shows the median simulated values for all three grids, which were based on 300 simulations for Grid 1, and 400 simulations each for Grids 2 and 3. For comparison, Figure 3.5 shows the map of median simulated tritium concentration for FY 1992. Note the higher median tritium concentrations found in that map, especially in the plume emanating from 200 East Area in Grid 3. The decrease in tritium concentrations from FY 1992 to FY 2001 is primarily caused by radioactive decay of the tritium, which has a half-life of 12.35 years (Hartman et al. 2004).

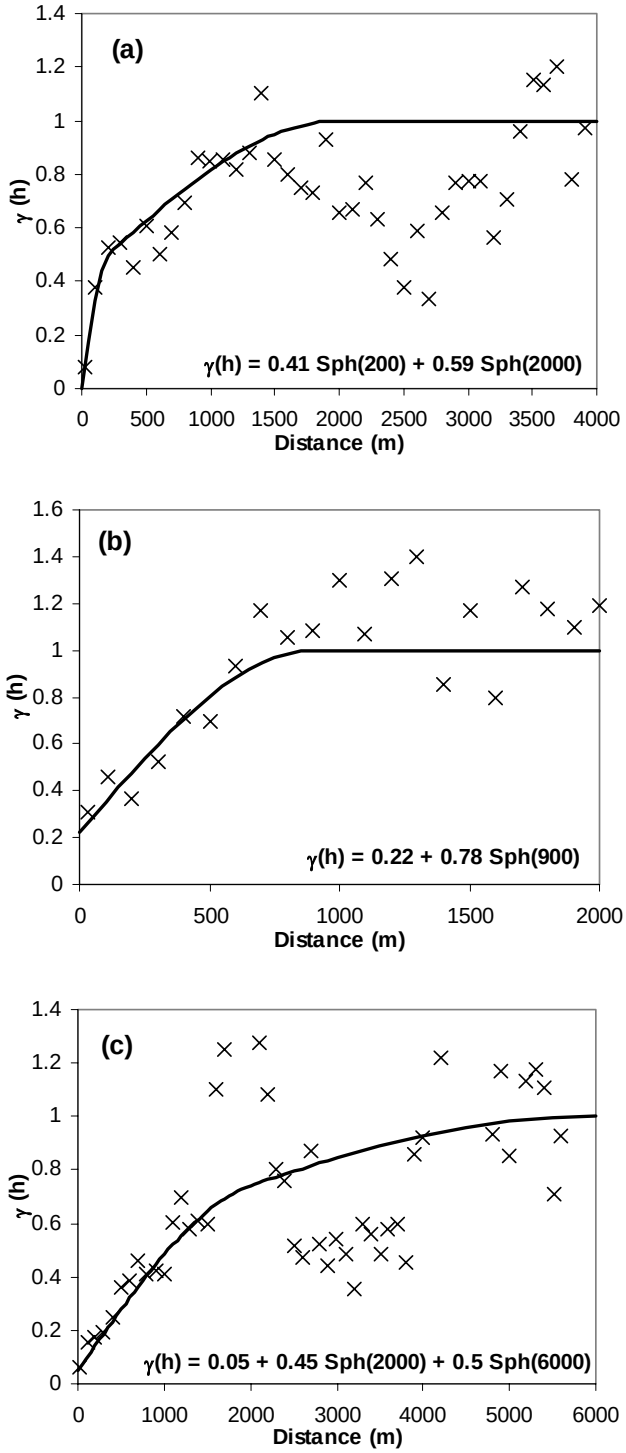

Figure 3.3. Variograms and Models of Normal Scores of the Subsets of FY 2001 Tritium Data in the Local Grids 1 (a), 2 (b), and 3 (c). Experimental variogram values designated by x, with the models fit to data denoted by solid black lines.

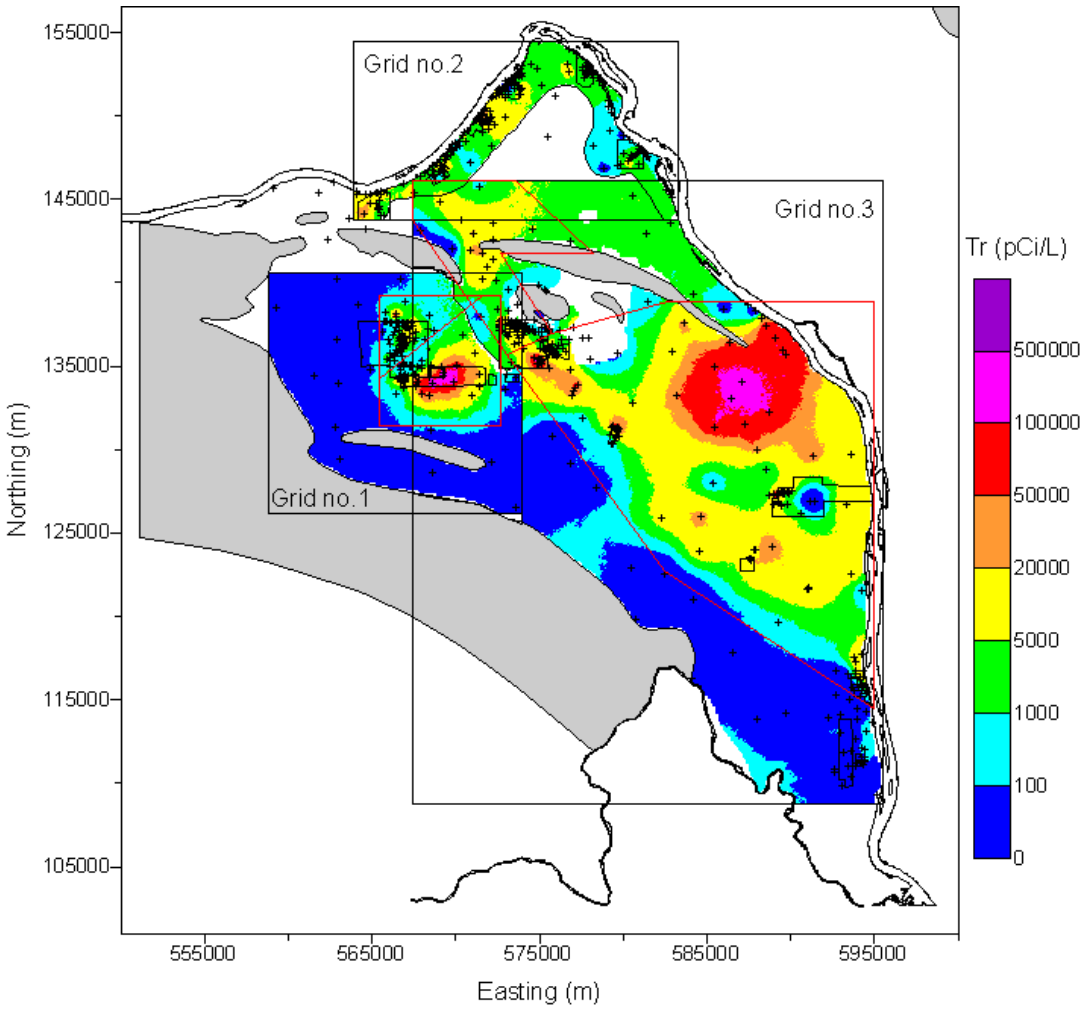

Figure 3.4. Median of Simulations of FY 2001 Tritium Concentrations for Grids 1, 2, and 3

3.3 Metrics for Tritium Concentration and Activity in Grid 1

Three hundred simulations of the FY 2001 tritium concentration were used as the basis for calculation of metrics for Grid 1. Grid 1 contains two distinct tritium plumes associated with 200 West Area (Figure 3.6), one to the southeast located near the REDOX plant and associated facilities and one to the northwest in the area of Waste Management Areas T-TX-TY. The areas containing those plumes are labeled sub-areas 1 and 2, respectively (Figure 3.6), and metrics were calculated separately for each sub-area. The XY coordinates of the digitized outlines of sub-areas 1 and 2 are contained as tables in Appendix A. All XY coordinates are Washington State Plane Coordinates (South, UTM Zone 11), in meters.

Figure 3.6 contains a map of the median simulated value for each grid cell, while Table 3.1 presents detailed statistics about the locations of the centers of mass that are contoured in Figure 3.6 for the 300 simulations of tritium for FY 2001. The statistics in Table 3.1 assume that the thickness of the tritium

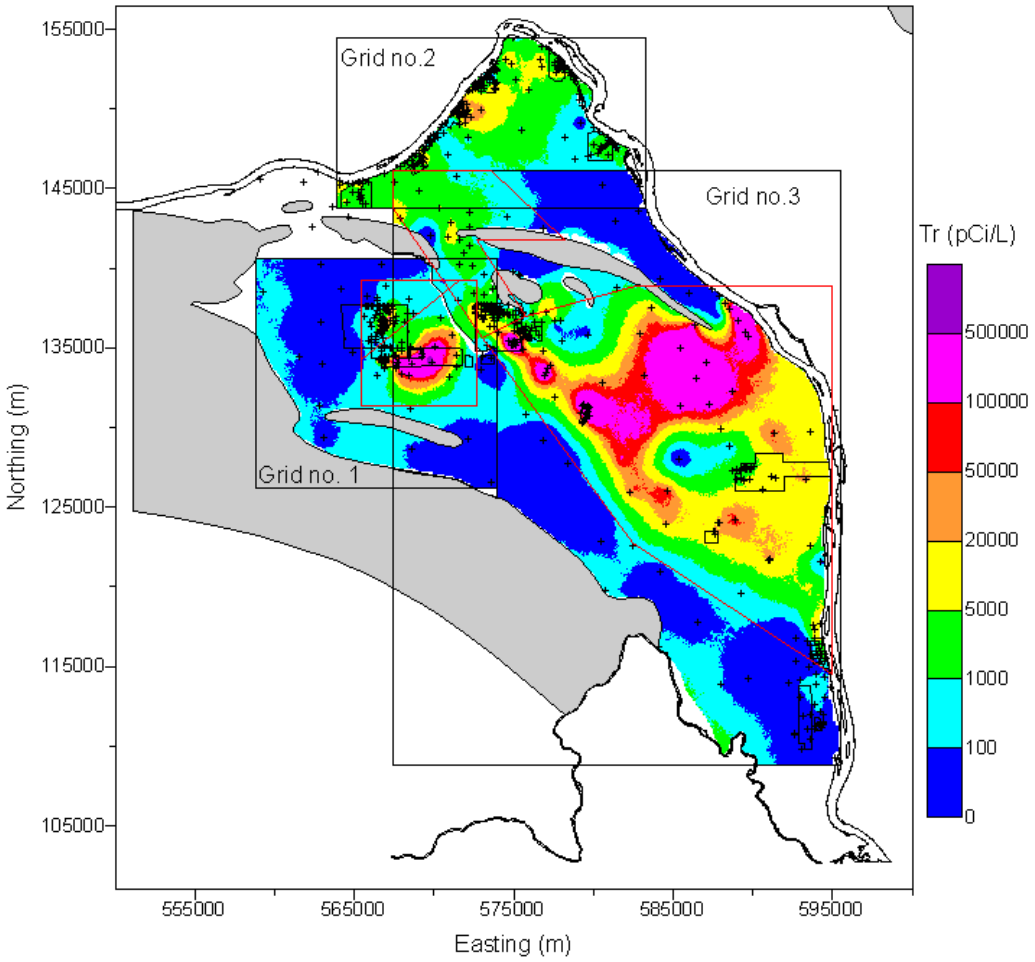

Figure 3.5. Median of Simulations of FY 1992 Tritium for Grids 1, 2, and 3

plume is 5 meters. Figure 3.7 shows a map of the probability that the tritium concentration exceeds the DWS within the grid area, based on the proportion of simulated values that exceeded the DWS for each grid cell. Table 3.2 shows statistics for the area exceeding the DWS of 20,000 pCi/L for FY 2001 tritium for each simulation within the two sub-areas of Grid 1 (200 West Area).

Figures 3.8 and 3.9 present histograms that show the total activity of tritium in FY 2001 for each simulation in sub-areas 1 and 2, respectively. There are four histograms for each sub-area, showing the results for each of four different depth assumptions, with thickness varying from 5 to 20 meters. Tables 3.3 and 3.4 show the corresponding statistics for the total activity for the four thickness assumptions for the two sub-areas of Grid 1. For example, Table 3.3 indicates that a 95 percent probability interval for the total activity of tritium in sub-area 1 of Grid 1 for FY 2001 is 1,104.6 Ci to 4,720.7 Ci, assuming that the tritium plume is 5 meters thick. Predicted total activity from the SAC model, either a single estimate or a range of values from a series of realizations, will be compared with the probability interval based on geostatistical modeling of the historical concentration data to determine if the simulated

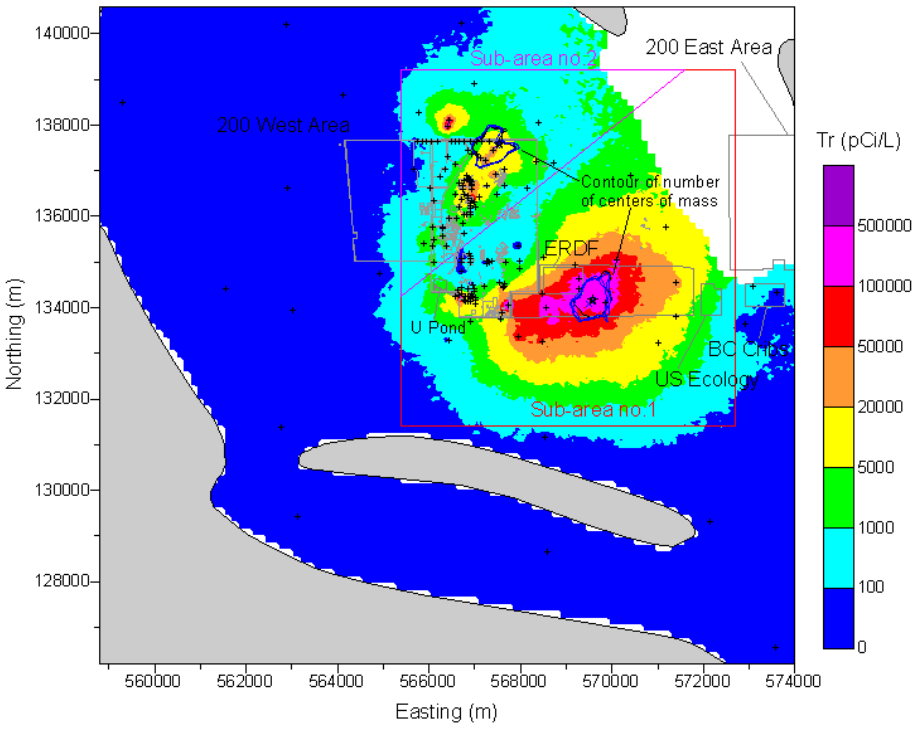

Figure 3.6. **Median of Simulated FY 2001 Tritium Concentrations in Grid 1 (200 West Area). Contours of the number of times that the center of mass within the sub-areas occurred within each cell of a coarser grid are shown. The average centers of mass are shown by black stars in each sub-area.**

Table 3.1. **Statistics of Locations of Centers of Mass of Individual Simulations of FY 2001 Tritium Calculated for a Depth of 5 m for Each Sub-Area of Grid 1 (200 West Area)**

Coordinate (m)	Sub-Area 1		Sub-Area 2	
	Easting	Northing	Easting	Northing
Mean	569569.5	134151.3	567542.4	137594.2
Standard Error	17.0	19.7	29.3	18.6
Median	569575.0	134137.5	567424.4	137555.8
Standard Deviation	294.0	340.4	507.8	322.4
Kurtosis	0.31	0.12	0.58	-0.28
Skewness	-0.37	0.10	0.97	0.12
Range	1776.3	1967.1	2590.7	1724.7
Minimum	568533.4	133216.6	566662.4	136752.1
Maximum	570309.6	135183.7	569253.1	138476.8
Count	300	300	300	300
97.5^{th} Percentile	570079.0	134815.7	568741.2	138207.9
2.5^{th} Percentile	568917.6	133430.9	566812.3	136980.6
Confidence Level of Mean (95.0%)	33.4	38.7	57.7	36.6

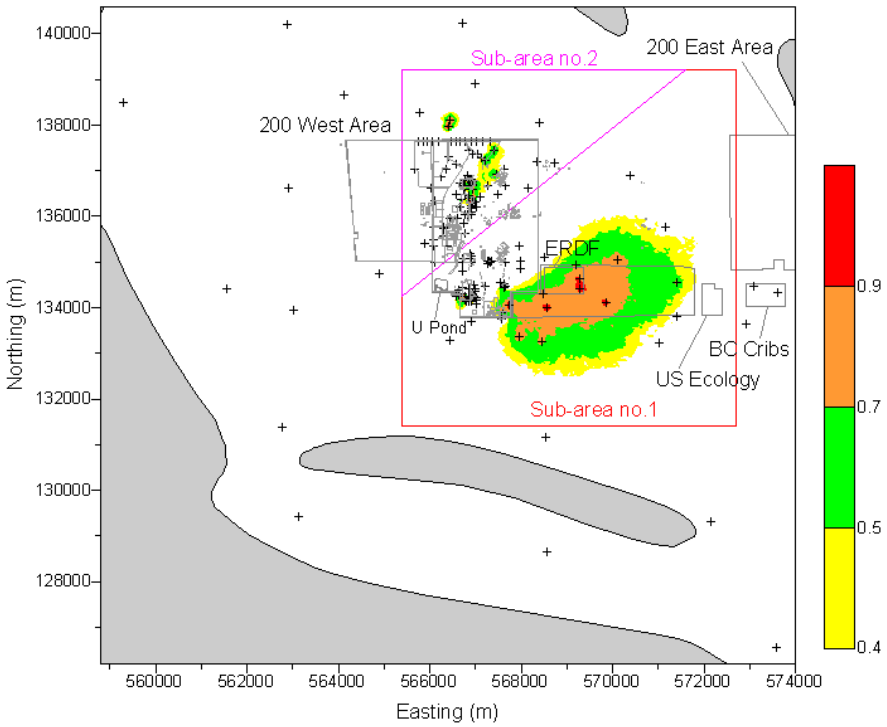

Figure 3.7. Probability of Exceeding 20,000 pCi/L Based on Simulations of FY 2001 Tritium in Grid 1 (200 West Area)

Table 3.2. Area Exceeding 20,000 pCi/L for FY 2001 Tritium for Each Simulation Within Two Sub-Areas of Grid 1 (200 West Area)

Area (km^2)	Sub-Area 1	Sub-Area 2	Grid 1
Mean	10.62	2.13	15.91
Standard Error	0.11	0.03	0.15
Median	10.62	2.01	15.87
Standard Deviation	1.94	0.60	2.67
Kurtosis	-0.04	1.12	0.39
Skewness	0.25	1.01	0.41
Range	10.39	3.14	16.50
Minimum	6.20	1.06	9.75
Maximum	16.59	4.21	26.25
Count	300	300	300
97.5^{th} Percentile	14.42	3.58	21.60
2.5^{th} Percentile	7.07	1.26	11.05
Confidence Level of Mean (95.0%)	0.22	0.07	0.30

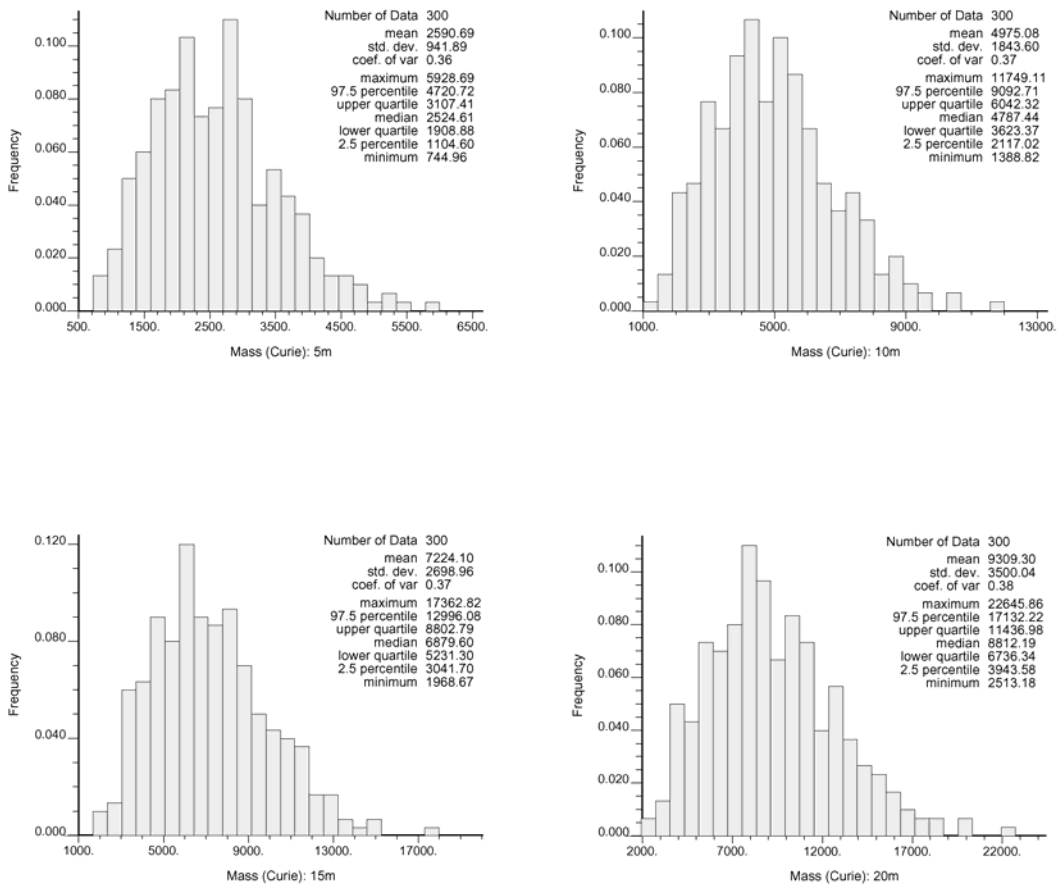

Figure 3.8. Histograms of Total Activity in Simulations of FY 2001 Tritium Within Sub-Area 1 of Grid 1 (200 West Area), Four Thickness Assumptions

Table 3.3. Statistics of Total Activity of Simulations of FY 2001 Tritium Within Sub-Area 1 of Grid 1 (200 West Area), Four Thickness Assumptions

Mass (Ci) in Depth	5 m	10 m	15 m	20 m
Mean	2,590.69	4,975.09	7,224.10	9,309.30
Standard Error	54.47	106.62	156.08	202.41
Median	2,524.61	4,787.44	6,879.59	8,812.19
Standard Deviation	943.46	1,846.68	2,703.47	3,505.88
Kurtosis	0.18	0.18	0.24	0.33
Skewness	0.57	0.57	0.59	0.61
Range	5,183.72	10,360.29	15,394.15	20,132.69
Minimum	744.96	1,388.82	1,968.67	2,513.18
Maximum	5,928.69	11,749.11	17,362.82	22,645.86
Count	300	300	300	300
97.5^{th} Percentile	4,720.72	9,092.70	12,996.05	17,132.18
2.5^{th} Percentile	1,104.60	2,117.02	3,041.70	3,943.58
Confidence Level of Mean (95.0%)	107.19	209.82	307.16	398.33

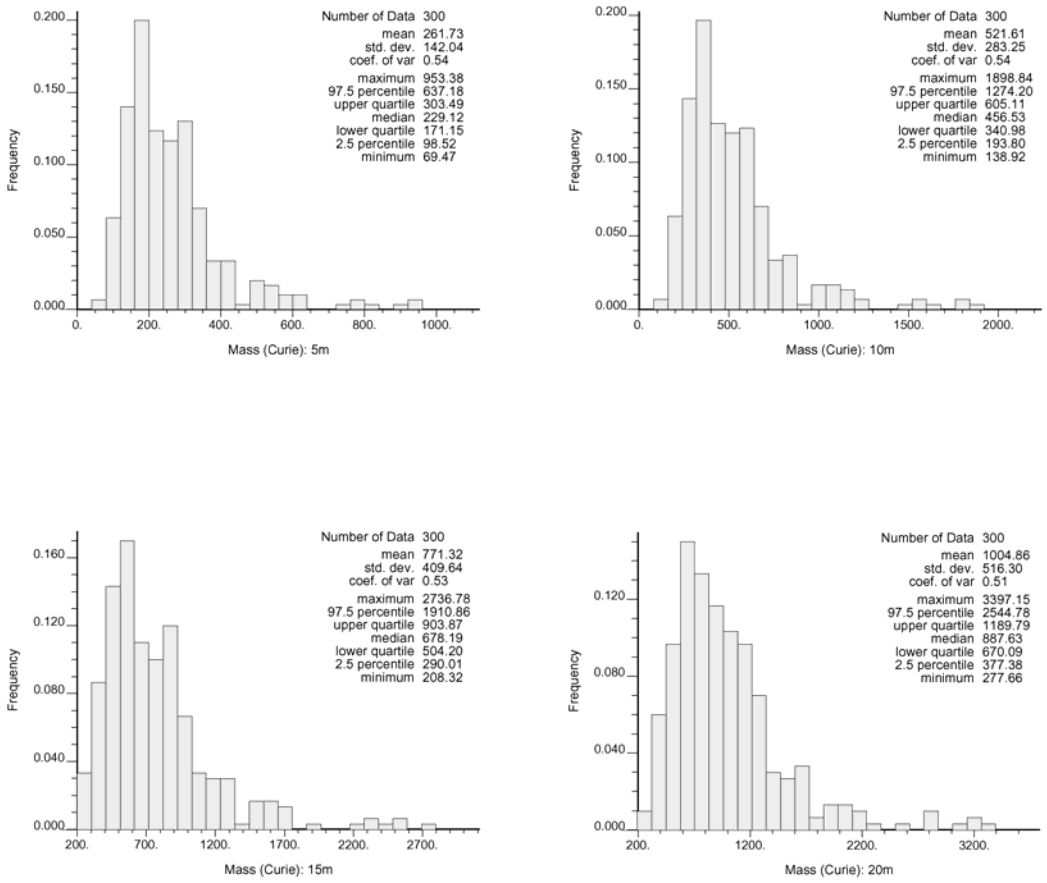

Figure 3.9. Histograms of Mass of Simulations of FY 2001 Tritium Within Sub-Area 2 of Grid 1 (200 West Area), Four Depth Assumptions

Table 3.4. Mass of Simulations of FY 2001 Tritium Within the Sub-Area 2 of Grid 1 (200 West Area), Four Depth Assumptions

Mass (Ci) in Depth	5 m	10, m	15 m	20 m
Mean	261.73	521.61	771.32	1,004.86
Standard Error	8.21	16.38	23.69	29.86
Median	229.11	456.53	678.19	887.63
Standard Deviation	142.28	283.72	410.33	517.16
Kurtosis	5.81	5.78	5.15	4.58
Skewness	2.05	2.05	1.94	1.83
Range	883.91	1,759.92	2,528.46	3,119.49
Minimum	69.47	138.92	208.32	277.66
Maximum	953.38	1,898.84	2,736.78	3,397.15
Count	300	300	300	300
97.5^{th} Percentile	637.15	1,274.15	1,910.79	2,544.70
2.5^{th} Percentile	98.52	193.80	290.01	377.38
Confidence Level of Mean (95.0%)	16.17	32.24	46.62	58.76

values from the SAC model fall within the 95 percent probability interval from the geostatistical study. Comparison of Tables 3.3 and 3.4 indicates that there is approximately an order of magnitude more tritium in sub-area 1 than there is in sub-area 2.

Figure 3.10 shows smooth curves fit to the histograms for the four thickness assumptions for each sub-area of Grid 1. The figure shows that in addition to the increase in mean total activity for greater thickness, there is also a large increase in the variability in the simulated total activity for increasing thickness assumptions of the plume.

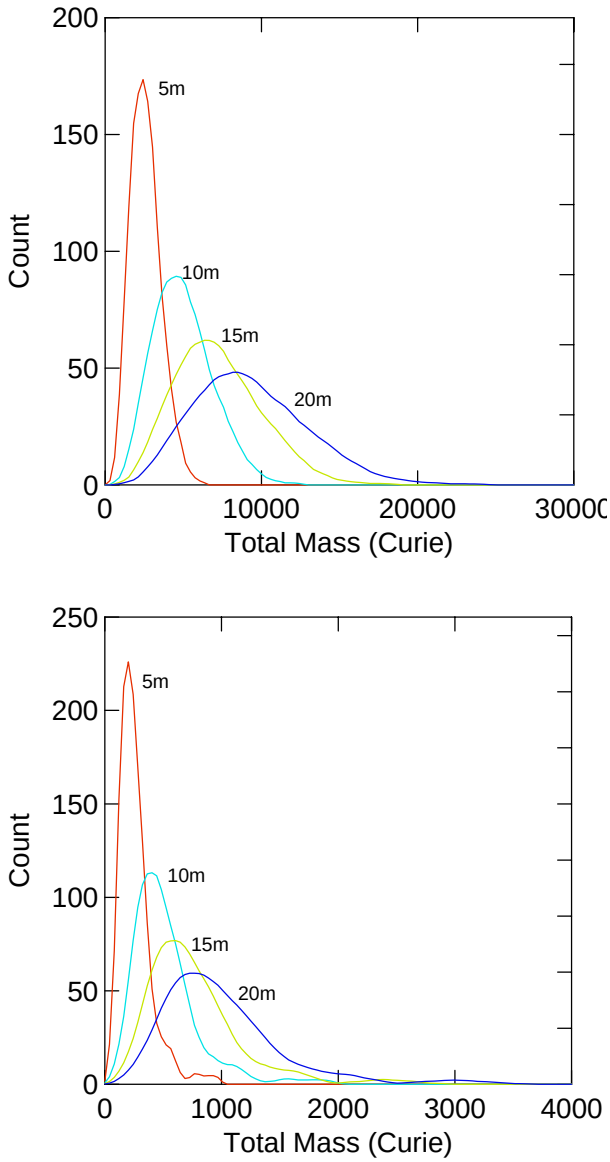

Figure 3.10. Curves Fit to Histograms of the Mass of FY 2001 Tritium at Four Depths within Sub-Areas 1 (upper) and 2 (lower) of Grid 1 (200 West Area)

3.4 Metrics for Tritium Concentration and Activity in Grid 2

The tritium concentration and activity were also simulated for Grid 2, and metrics were calculated for the entire area together. Sub-areas within Grid 2 were not identified during the study; however, if those areas are identified in the future it would be possible to calculate metrics for them (e.g., the area around one of the reactors). Figure 3.11 shows the median simulated tritium value within the simulation grid based on 400 simulations of the tritium concentration. The central portion of the grid was blanked after simulation because of the sparse data coverage in that area. Figure 3.12 shows the probability that tritium concentration in FY 2001 exceeded the DWS. Table 3.5 contains the statistics for the area exceeding the DWS and the locations of the center of mass based on the suite of simulations generated in Grid 2. Because the simulation grid is bounded on one side by the Columbia River, an additional metric was generated for Grid 2 that was not relevant for Grid 1. That metric is the length of the shoreline for which the tritium concentration exceeded the DWS for each simulation; a histogram and statistics of the distribution of results is given in Figure 3.13. Figure 3.14 and Table 3.6 provide the histograms and statistical summaries of the total tritium activity in the simulation grid for plume thicknesses of 5, 10, 15, and 20 meters.

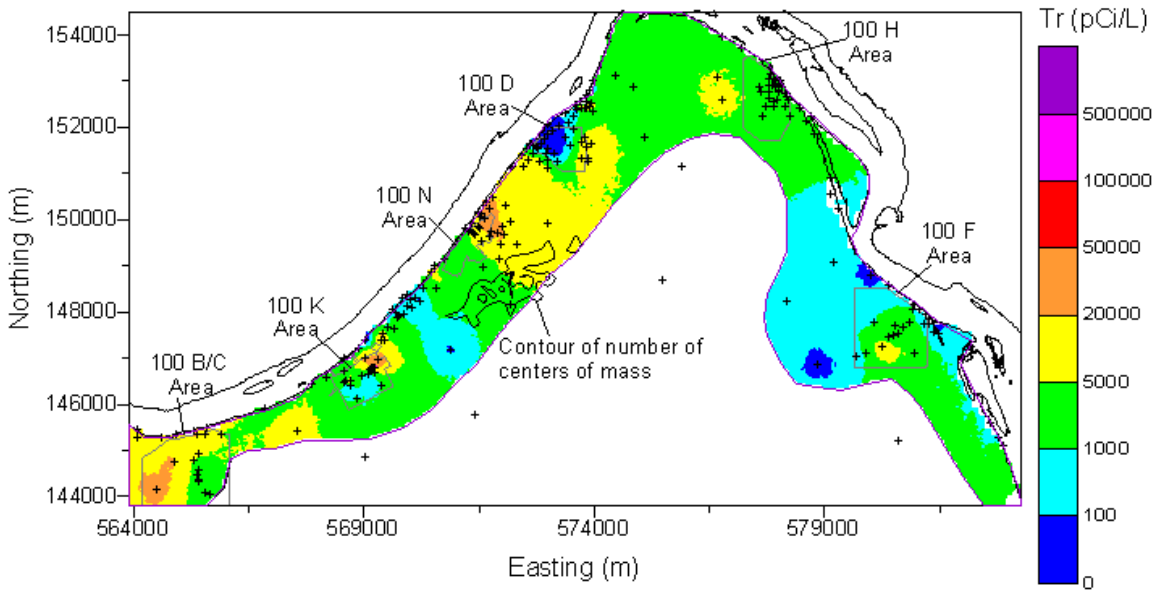

Figure 3.11. Median of Simulated FY 2001 Tritium Concentrations in Grid 2 (100 Areas). Contours of the number of times that the center of mass occurred within cells of an upscaled grid are shown with the average center of mass shown by a black star.

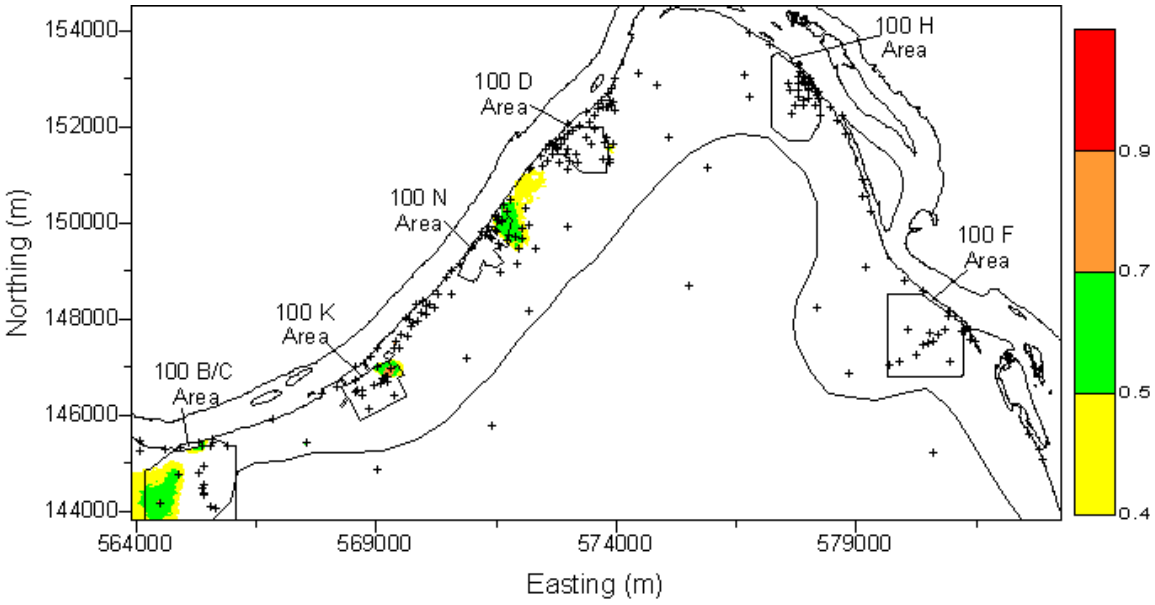

Figure 3.12. Probability of Exceeding 20,000 pCi/L Based on Simulations of FY 2001 Tritium in Grid 2 (100 Areas)

Table 3.5. Statistics of the Area Exceeding 20,000 pCi/L and Locations of Centers of Mass for Simulations of FY 2001 Tritium Within Grid 2 (100 Areas)

	Area (km^2)	Center of Mass (unit: m)	
		Easting	Northing
Mean	6.43	572143.8	148421.2
Standard Error	0.06	73.3	45.9
Median	6.40	572245.4	148399.7
Standard Deviation	1.19	1466.4	917.1
Kurtosis	-0.12	0.74	0.71
Skewness	0.16	-0.25	0.30
Range	6.75	9448.0	5894.6
Minimum	3.07	567631.9	145907.6
Maximum	9.82	577079.9	151802.2
Count	400	400	400
97.5^{th} Percentile	8.92	575177.7	150316.4
2.5^{th} Percentile	4.14	568673.3	146620.1
Confidence Level (95.0%)	0.12	144.1	90.2

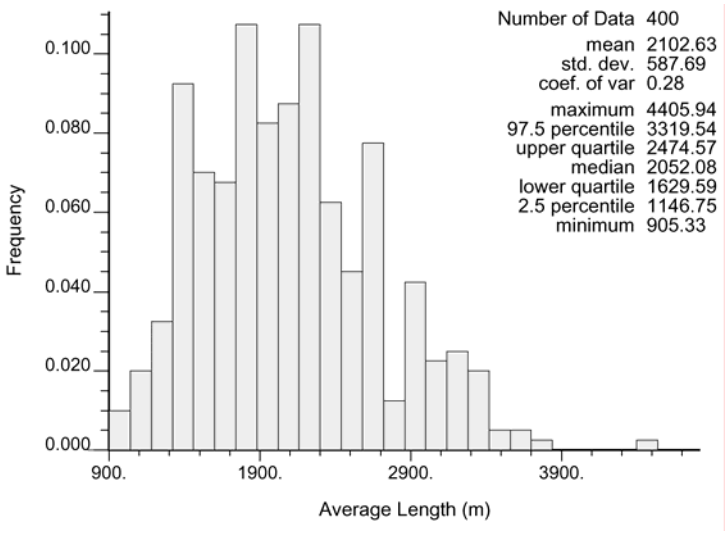

Figure 3.13. Histogram of the Average Length of Columbia River Shoreline Exceeding 20,000 pCi/L for FY 2001 Tritium in Grid 2 (100 Areas)

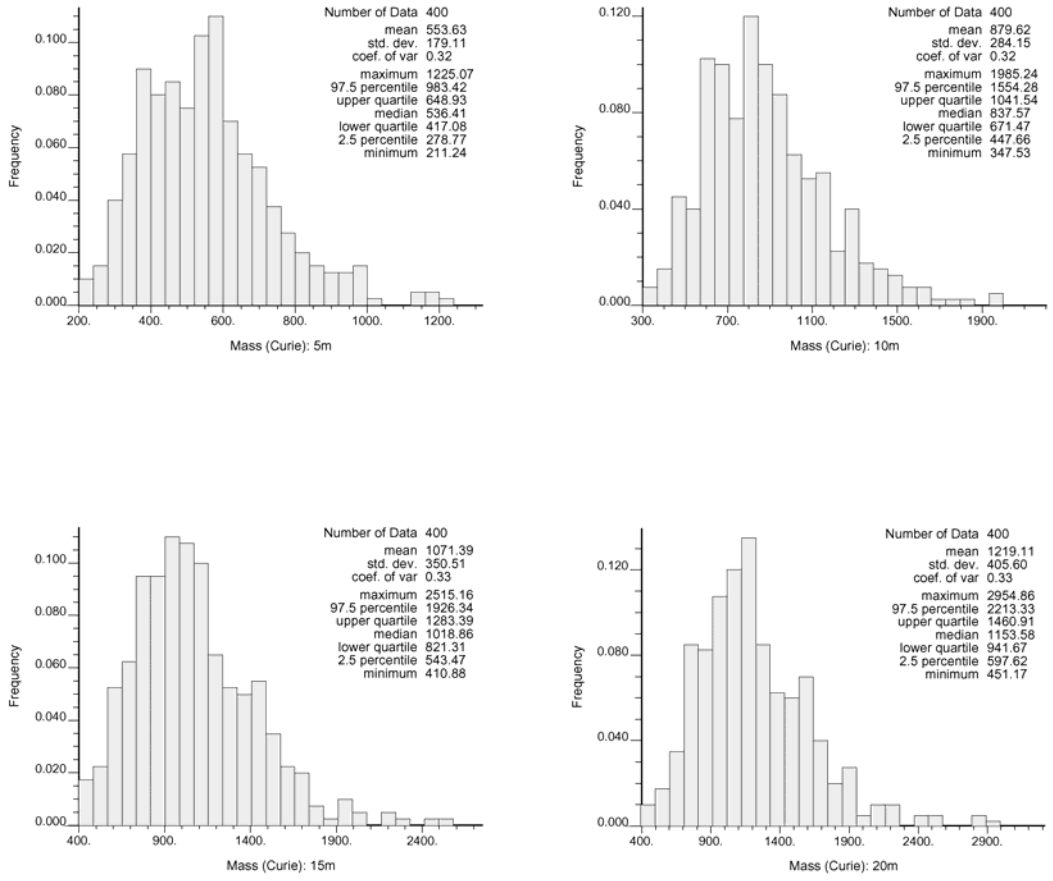

Figure 3.14. Histograms of Total Activity in Simulations of FY 2001 Tritium Within Grid 2 (100 Areas), Four Thickness Assumptions

Table 3.6. Statistics of Total Activity of Simulations of FY 2001 Tritium Within Grid 2 (100 Areas), Four Thickness Assumptions

Mass (Ci) in Depth	5 m	10 m	15 m	20 m
Mean	553.63	879.62	1,071.39	1,219.11
Standard Error	8.97	14.23	17.55	20.31
Median	536.41	837.57	1,018.86	1,153.58
Standard Deviation	179.33	284.51	350.94	406.11
Kurtosis	0.88	0.87	1.33	1.83
Skewness	0.81	0.81	0.92	1.03
Range	1,013.83	1,637.72	2,104.27	2,503.70
Minimum	211.24	347.53	410.88	451.17
Maximum	1,225.07	1,985.24	2,515.16	2,954.86
Count	400	400	400	400
97.5^{th} Percentile	984.96	1,562.88	1,935.89	2,218.85
2.5^{th} Percentile	276.74	444.00	543.39	594.34
Confidence Level of Mean (95.0%)	17.63	27.97	34.50	39.92

3.5 Metrics for Tritium Concentration and Activity in Grid 3

The tritium plumes emanating from 200 East Area and other sources occurring within the main plume were simulated as a single unit in Grid 3. Metrics were calculated for two sub-areas based on 400 simulations of the tritium concentration. Sub-area 1 (Figure 3.15) encompassed the plume that moved southeast from 200 East Area, while sub-area 2 included the northern portion of 200 East Area and portions of the tritium plume that moved to the north. The digitized boundaries for sub-areas 1 and 2 are found in a table within Appendix A. Figure 3.15 also shows the average center of mass for each of the sub-areas and contours around the center of mass that indicate the variability in the location of the center of mass for the suite of simulations. Table 3.7 provides detailed statistics for the distribution of the center of mass locations for the two sub-areas. Figure 3.16 illustrates the probability that the tritium concentration exceeded the DWS within Grid 3, while Table 3.8 provides detailed statistics for the distribution of the area exceeding the DWS for each simulation in the two sub-areas. Sub-area 1 is bounded on the east by the Columbia River, and the southeastern tritium plume had an impact on a significant length of the shoreline. Figure 3.17 contains a histogram of the distribution of the length of shoreline above the DWS for the suite of simulations, indicating that about 10 km of river shoreline were above the DWS in FY 2001 for sub-area 1. Figures 3.18 and 3.19 present histograms that show the total activity of tritium in FY 2001 for each simulation in sub-areas 1 and 2, respectively. There are four histograms for each sub-area, showing the results for each of four different depth assumptions, with thickness varying from 5 to 20 meters. Tables 3.9 and 3.10 show the corresponding statistics for the total activity for the four thickness assumptions for the two sub-areas of Grid 3.

Figure 3.15 shows the presence of low median concentrations mapped in the area between 200 East Area and the Central Landfill and stretching to the northeast and southeast from the Central Landfill. The 20,000-pCi/L contour is not as continuous or extensive in those areas as it is in the hand-contoured maps of tritium concentration presented in the Hanford Site groundwater monitoring report for the FY 2001 data (see Figure S-3, Hartman et al. 2002). The low concentrations could lead to under estimating the

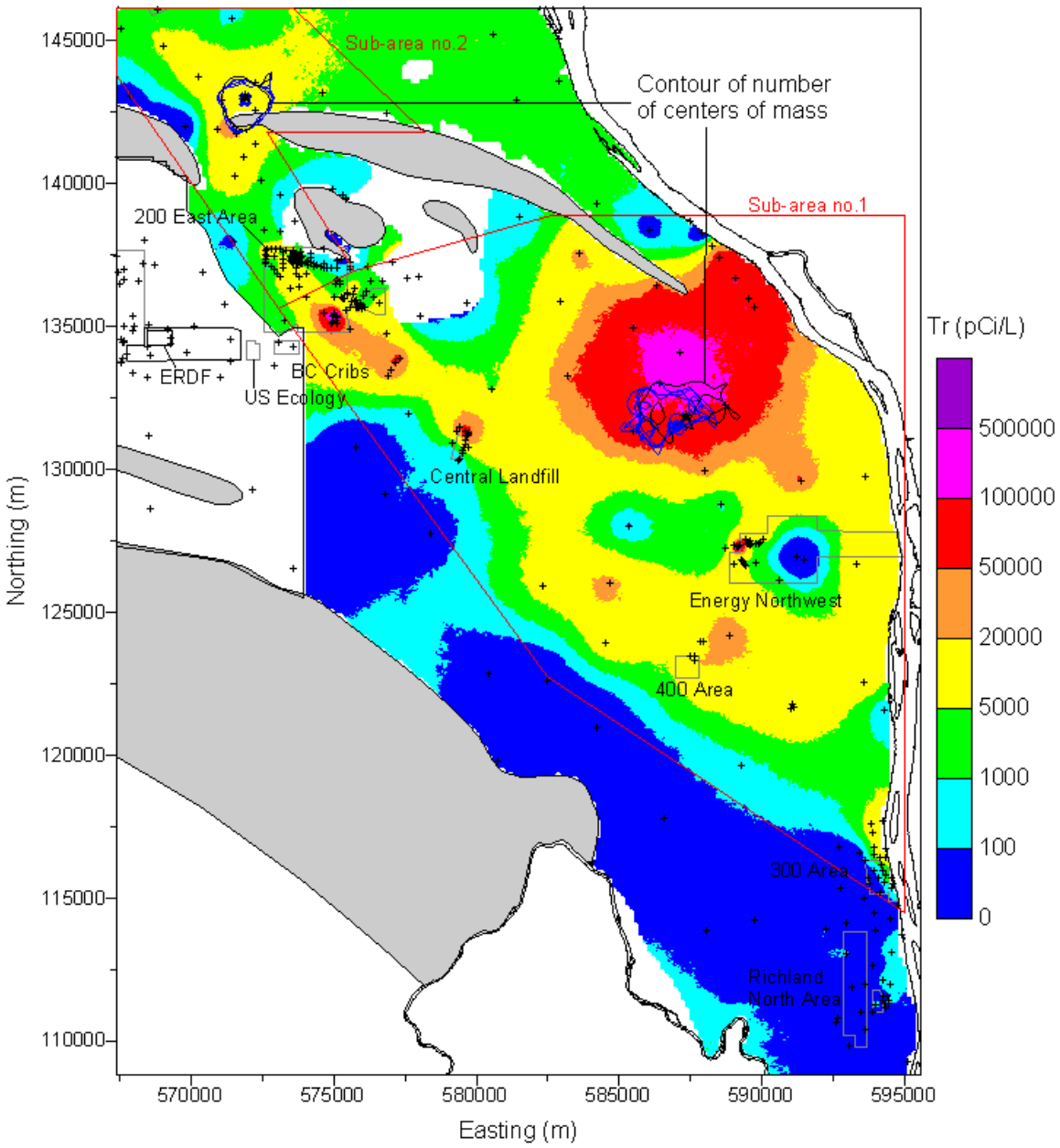

Figure 3.15. Median of Simulated FY 2001 Tritium Concentrations in Grid 3 (200 East Area Plumes). Contours of the number of times that the center of mass within the sub-areas occurred within cells of an upscaled grid are shown with the average centers of mass shown by blue stars in each sub-area.

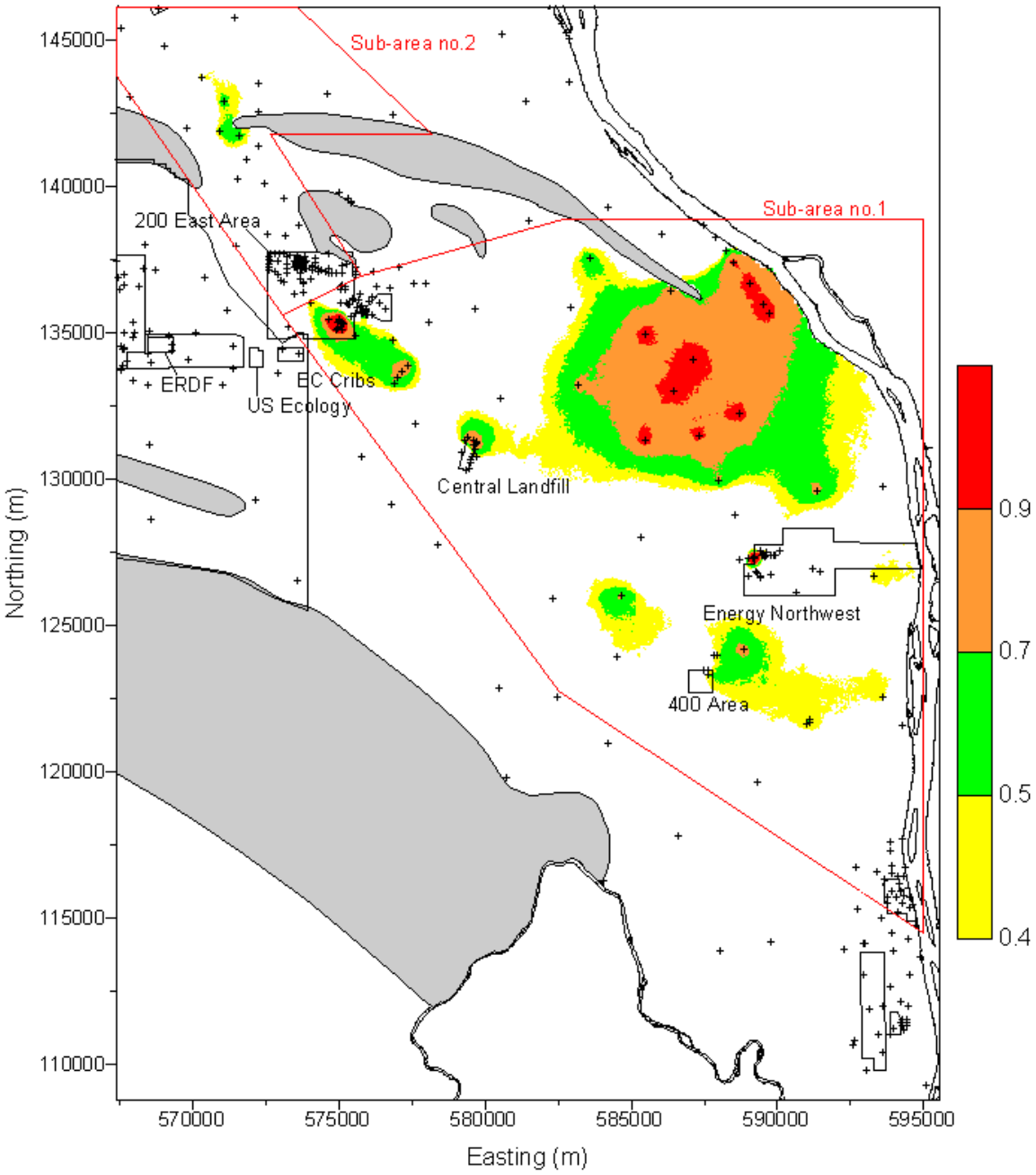

Figure 3.16. Probability of Exceeding 20,000 pCi/L Based on Simulations of FY 2001 Tritium in Grid 3 (200 East Area Plumes)

Table 3.7. Statistics of Locations of Center of Mass for Simulations of FY 2001 Tritium Calculated for a Depth of 5 m for Each Sub-Area of Grid 3 (200 East Area Plumes)

Coordinate (m)	Sub-Area 1		Sub-Area 2	
	Easting	Northing	Easting	Northing
Mean	587120.4	131577.5	571954.7	142941.6
Standard Error	59.0	62.0	39.8	37.5
Median	587055.7	131770.2	571923.2	142870.2
Standard Deviation	1180.4	1240.6	795.4	749.3
Kurtosis	-0.01	4.85	2.08	0.88
Skewness	0.34	-1.53	-0.25	0.26
Range	7598.6	10098.6	5817.5	4999.4
Minimum	584089.1	123933.2	568765.0	140385.3
Maximum	591687.7	134031.8	574582.5	145384.7
Count	400	400	400	400
97.5^{th} Percentile	589608.7	133434.5	573526.7	144634.3
2.5^{th} Percentile	585064.8	128621.8	570222.7	141542.2
Confidence Level of Mean (95.0%)	116.0	121.9	78.2	73.7

Table 3.8. Area Exceeding 20,000 pCi/L for FY 2001 Tritium for Each Simulation Within Two Sub-Areas of Grid 3 (200 East Area Plumes)

Area (km^2)	Sub-Area 1	Sub-Area 2	Grid 3
Mean	89.12	6.48	105.48
Standard Error	0.53	0.11	0.63
Median	88.22	6.15	105.02
Standard Deviation	10.60	2.27	12.60
Kurtosis	1.16	0.71	0.09
Skewness	0.57	0.77	0.32
Range	76.36	13.81	74.84
Minimum	60.74	1.97	74.34
Maximum	137.09	15.77	149.18
Count	400	400	400
97.5^{th} Percentile	112.55	11.79	132.39
2.5^{th} Percentile	70.66	2.93	83.11
Confidence Level of Mean (95.0%)	1.04	0.22	1.24

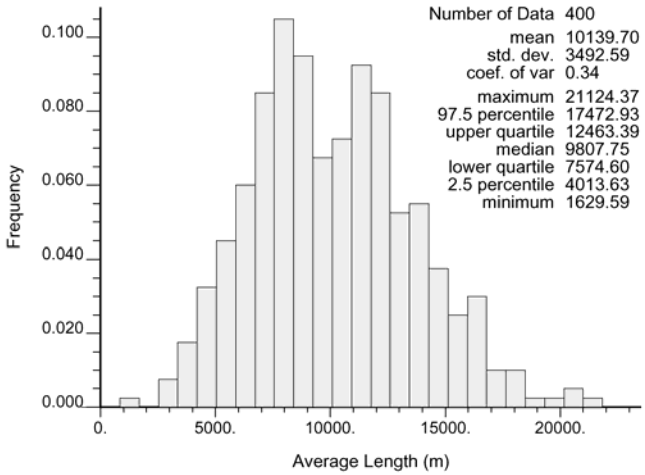

Figure 3.17. Histogram of the Average Length of Columbia River Shoreline Exceeding 20,000 pCi/L for FY 2001 Tritium in Grid 3

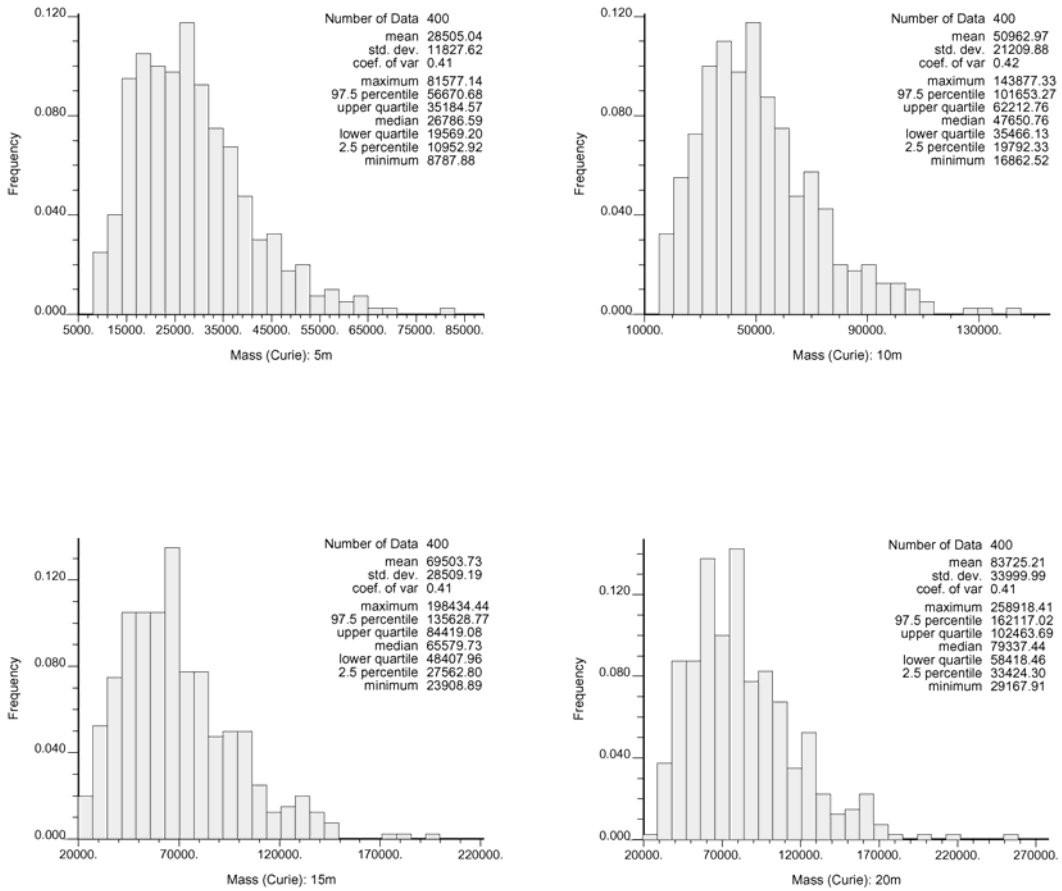

Figure 3.18. Histograms of Total Activity in Simulations of FY 2001 Tritium Within Sub-Area 1 of Grid 3 (200 East Area Plumes), Four Thickness Assumptions

Table 3.9. Statistics of Total Activity of Simulations of FY 2001 Tritium Within Sub-Area 1 of Grid 3 (200 East Area Plumes), Four Thickness Assumptions

Mass (Ci) in Depth	5 m	10 m	15 m	20 m
Mean	28,505.03	50,962.96	69,503.75	83,725.17
Standard Error	592.12	1,061.82	1,427.24	1,702.13
Median	26,786.58	47,650.75	65,579.73	79,337.43
Standard Deviation	11,842.43	21,236.44	28,544.90	34,042.57
Kurtosis	1.22	1.33	1.45	1.97
Skewness	0.96	1.00	1.01	1.08
Range	72,789.27	127,014.81	174,525.53	229,750.50
Minimum	8,787.88	16,862.52	23,908.89	29,167.91
Maximum	81,577.14	143,877.33	198,434.43	258,918.41
Count	400	400	400	400
97.5th Percentile	56,805.41	102,342.08	135,976.27	162,852.93
2.5th Percentile	10,900.02	19,731.24	27,472.34	33,391.60
Confidence Level of Mean (95.0%)	1,164.07	2,087.47	2,805.86	3,346.26

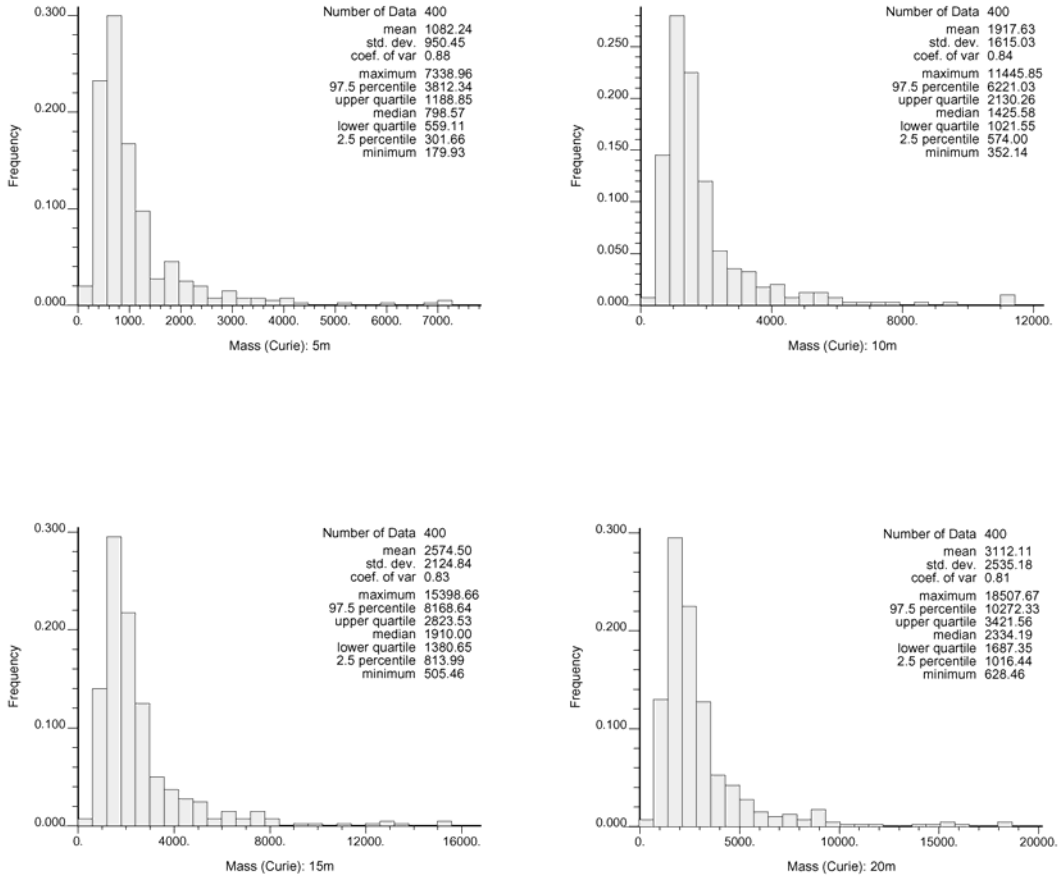

Figure 3.19. Histograms of Total Activity in Simulations of FY 2001 Tritium Within Sub-Area 2 of Grid 3 (200 East Area Plumes), Four Thickness Assumptions

Table 3.10. Statistics of Total Activity of Simulations of FY 2001 Tritium Within Sub-Area 2 of Grid 3 (200 East Area Plumes), Four Thickness Assumptions

Mass (Ci) in Depth	5 m	10 m	15 m	20 m
Mean	1,082.24	1,917.64	2,574.50	3,112.11
Standard Error	47.58	80.85	106.38	126.92
Median	798.56	1,425.58	1,910.00	2,334.19
Standard Deviation	951.64	1,617.06	2,127.50	2,538.36
Kurtosis	14.50	12.82	12.06	12.04
Skewness	3.29	3.15	3.09	3.10
Range	7,159.03	11,093.71	14,893.20	17,879.21
Minimum	179.93	352.14	505.46	628.46
Maximum	7,338.96	11,445.85	15,398.66	18,507.67
Count	400	400	400	400
97.5^{th} Percentile	3,877.40	6,370.49	8,203.01	10,638.91
2.5^{th} Percentile	294.30	563.60	810.07	1,004.63
Confidence Level of Mean (95.0%)	93.54	158.95	209.13	249.51

metrics calculated for sub-area 1 of Grid 3 for this study (e.g., total activity in the plume and the area above the DWS). The primary reason for this discrepancy is the sparseness of data distribution in those areas, where the distance between adjacent wells can be several kilometers. In hand-contouring the data, hydrogeologists cover those gaps using their understanding of groundwater flow patterns in the region. This is more difficult to do using a geostatistical model, which is constrained by the variogram model fit to the experimental variogram values calculated from the sparse concentration data. The effects of this problem appear to be greatest for the large 200 East groundwater plume that migrates to the southeast, because of the large area and the sparse distribution of monitoring wells in the down gradient portions of that plume. Several methods are being examined to reduce the impact of this effect on history matching the geostatistical results and the results from the SAC model, as detailed in Section 4.5.

3.6 Discussion of Additional Results

Sections 3.1 through 3.5 present the history matching data generated for tritium using FY 2001 data as an example of the data generated for this project. The results provide a number of metrics that can be used to evaluate the performance of the SAC model. These include estimates of the total activity of tritium within defined areas (e.g., plumes associated with facilities), the center of mass of the tritium activity within those areas, the area above the tritium DWS within the defined boundary, and the length of the Columbia River shoreline above the DWS (where appropriate). Each of those results are based on geostatistical analysis of historical groundwater concentrations. By calculating the metrics on a suite of geostatistical simulations it was also possible to provide uncertainty intervals for each of the metrics.

History matching data for other time periods and contaminants are contained in Appendices B through H. Each appendix contains the results for a single contaminant and sampling period. Table 3.11 gives the appendices and their contents. The XY coordinates for the sub-areas for which mass calculations were made are in Appendices A through H. All coordinates are Washington State Plane Coordinates (South, UTM Zone 11), in meters.

Table 3.11. Appendices and Content for Additional Contaminants

Appendix	Year	Contaminant
B	1992	Tritium
C	2001	Technetium-99
D	1992	Technetium-99
E	2001	Iodine-129
F	1992	Iodine-129
G	2001	Uranium
H	1992	Uranium

The procedures used to generate the geostatistical simulations and metrics for those other contaminants are the same as those used for tritium in FY 2001 with the exception of the FY 2001 technetium-99 plume for 200 East Area. As discussed in Section 2.1, that plume was simulated using sequential indicator simulation, with calculation of the metrics performed using the same methods as those applied to all other contaminant plumes.

4.0 Parameter Uncertainties and Data Gaps

The approach taken for the current study provides quantitative methods for providing history matching data, including estimates of uncertainty in the metrics that can be used to evaluate the SAC model. However, the approach does not address all possible sources of uncertainty in those metrics. Uncertainty in several factors could lead to additional variability in the range of data presented in this study. Those factors include the true concentration for a contaminant at a given point in time, the thickness of contaminant plumes and vertical distribution of contaminants within them, the geologic structure, the porosity of the geologic units, and assumptions made in the geostatistical modeling used as the basis to calculate the metrics.

A brief discussion of each of those sources of uncertainty follows. It might be useful in the future to assess the relative importance of those additional sources of uncertainty and determine the potential effect on the uncertainty bounds provided for the metrics. The width of those uncertainty bounds could have an impact on whether the results of the SAC model are deemed to be acceptable, i.e., the SAC results fall within the range of values estimated from the historical contaminant concentration data.

4.1 Concentration Uncertainty

The contaminant concentration data used for the current study were selected and processed in the same way as the data used for the Hanford Site groundwater monitoring reports (e.g., Hartman et al. 2004). The average annual concentration was calculated for each well for each fiscal year. A number of wells in areas where concentrations do not change rapidly are not sampled every fiscal year, but are only sampled every second or third year. For that reason, if data were not available for the desired fiscal year for a well, in this case FY 2001 and FY 1992, then the average annual concentration from the most recent of the two previous fiscal years was used.

The use of an annual average masks two sources of uncertainty. One source is the measurement error associated with each concentration measurement. The second source of additional uncertainty is the variability in the suite of concentration measurements taken within a fiscal year that are used to calculate an annual average.

Although both sources of additional variability exist, it is difficult to quantify their magnitude. For most concentration measurements, the total analytical error is reported in HEIS, which should provide an estimate of the measurement error that may have been introduced into the analysis at the laboratory. However, it has recently been discovered that in some instances the laboratories reporting the total analytical error have actually been calculating the analytical error for concentrations near the minimum detection limit and then scaling that error to other concentrations[(a)] (so the analytical error value reported in HEIS cannot be used to estimate the uncertainty associated with an individual measurement, especially for higher concentrations.

(a) Personal communication from PE Dresel (Pacific Northwest National Laboratory) to the authors, January 2004.

The reduction in uncertainty caused by the use of an annual average cannot be assessed either, because wells have widely varying sampling schedules. During fiscal years when wells are being sampled, they are usually sampled monthly, quarterly, semi-annually, or annually. The variability between samples within a fiscal year cannot be assessed for wells that are only sampled annually or semi-annually. Although the frequency of well sampling for some wells may be determined by regulatory requirements, if there is no regulatory driver, then wells tend to be sampled more frequently when there is reason to suspect greater temporal variability. Thus, the variability found for wells measured monthly cannot be assumed to be representative of the variability that should be expected for wells that are sampled less frequently.

Given the inability to estimate the measurement error or temporal variability in concentration measurements, it does not appear to be possible to quantify the additional uncertainty in estimated contaminant concentrations resulting from measurement error or between sample variability, relative to the uncertainty estimated using data averaged over a fiscal year.

There are additional sources of uncertainty in contaminant concentrations that arise due to the varying lengths of the open intervals of the well bore from which samples are drawn and variations in hydraulic conductivity within the open interval. For example, if two wells sample areas of a plume with the same concentration and one has a relatively short open interval that only covers the high concentration zone at the top of the aquifer while the second has a longer open interval that includes deeper zones in the aquifer with high hydraulic conductivity and low concentrations, then the second well would appear to have lower concentrations than the first well due to the effects of well bore mixing, even though the mass of contaminant within a unit area of the aquifer might be identical. Given the lack of detailed data on the vertical distribution of contaminant concentrations and hydraulic conductivity in the aquifer, the uncertainty arising from varying lengths of the open interval and well bore mixing cannot be quantified at this time.

4.2 Vertical Distribution of Contaminants

As discussed in Section 2.2.1, considerable uncertainty exists in the vertical distribution of contaminants in the aquifer. This leads to uncertainty in the thickness of the plume that should be assumed in converting the simulations of contaminant concentration at the top of the aquifer to mass or activity estimates, which greatly increases the uncertainty in several of the metrics (especially the total mass or activity in a plume). The uncertainty related to the differing thickness assumptions modeled in this study can be seen for several of the FY 2001 tritium plumes (e.g., Figures 3.18 and 3.19).

If the plume is assumed to be approximately 5 meters thick, as some of the data seem to suggest, then the vertical gradient of concentrations within that interval can probably be ignored. However, there are data that suggest the plumes may be considerably thicker than 5 meters, at least locally. For thicker plumes, the vertical concentration gradient within the plume would be much more important in assessing the total mass or activity of contaminant present. There appears to be data indicating that concentration decreases rapidly with depth even in the thicker plumes, so the assumption of constant concentration with depth that was made earlier in the history matching performed for SAC Rev. 0 and in the present study should be revisited, especially for the 15- and 20-meter plume-thickness assumptions.

A study to further examine the vertical distribution of contaminants is planned for FY 2004 by the groundwater task of the characterization of systems project. The results of that study might be used to re-examine the assumptions made for this study regarding the thickness of the contaminant plumes and distribution of concentration within those plumes, and to guide the design of any future efforts to estimate the mass and activity of contaminants within the plumes.

4.3 Geologic Structure Uncertainty

Considerable uncertainty exists in the geologic structure of the Hanford Site. The identification of geologic formations from borehole data can be difficult, especially in drill cuttings, because of the variability that exists in formations at the site, the inability to observe sedimentary structures that might be diagnostic, and the tendency for Ringold Formation sediments to be eroded and then redeposited in the Hanford formation (Xie et al. 2003). Although Xie et al. (2003) found that mineralogy and geochemistry data can be useful in discriminating between Hanford and Ringold formation sediment, those data are rarely available. Together, these factors cause difficulties in identifying geologic units, and especially in distinguishing between coarse-grained units that have similarities (e.g., gravels belonging to the Hanford, Cold Creek, and Ringold units). Therefore, the identification of the geologic unit present can be highly uncertain, even at the borehole locations.

Additional uncertainty in the geologic structure exists between the boreholes where data are not available. To calculate the mass or activity of contaminant present beneath a given grid cell, it was necessary to know the geologic units that were present beneath the water table and its thicknesses. In that way, the thickness of a plume associated with a particular thickness assumption (e.g., 5, 10, 15, or 20 meters), could be partitioned between the different geologic units, and a porosity value assigned. The data on formation thicknesses used in the study were based on the geologic model incorporated in the sitewide groundwater model. That geologic model is based on interpolation of geologic formation surfaces between the boreholes using EarthVision. This provides continuous surfaces for the top and bottom of each geologic unit in the model, but one that does not take into account the uncertainty between the boreholes. Currently, the sitewide groundwater modeling group is producing a series of stochastic alternative conceptual models of the geologic structure of the aquifer using geostatistical methods. An early version of this approach can be found in Vermeul et al. (2003). That approach will be used to generate alternative simulations of the aquifer geology that honor the tops at the well bores and capture the spatial uncertainty between the boreholes. In future studies, those alternative realizations could be used to determine the sensitivity of the mass and activity estimates and other metrics of uncertainty in the geologic structure.

One major element of the geologic uncertainty described in the preceding paragraph is the spatial distribution of mud units in the Ringold Formation. As discussed in Section 2.2.2, the current study assumed that the mud units would not contribute to the mass and activity of the contaminants. Therefore, improved models of the spatial distribution of the mud units would be an important aspect of any future mass and activity simulations for history matching. An additional aspect that could be examined is the potential for contaminants in the mud units to contribute to the total contaminant load. Based on data from the literature on contaminant transport into and out of mud units, different scenarios for the role of

the mud units at Hanford could be developed and a sensitivity analysis could be used to assess the potential effects of those scenarios on the uncertainty bounds for history matching metrics.

4.4 Uncertainty in Porosity Distributions

An additional element of geologic uncertainty that could contribute to increased uncertainty in history matching metrics is the porosity distribution within different units. For the current study, a single porosity value was sampled from the probability distributions given for each geologic unit in Table 2.1 and applied throughout the Hanford Site for a given simulation of concentration. This approach does not capture the spatial variability that might be expected in porosity within each of the geologic units caused by spatial variations in grain size, sorting, and cementation. Additional uncertainty could be introduced into the new model in two ways. One would be to simply draw a separate porosity value from the relevant probability distribution for each occurrence of a geologic unit. This would produce independent values of porosity for each unit and would not account for any spatial correlation that might be expected in the porosity within nearby cells. In order to account for spatial correlation, an alternative approach would be to use geostatistics to generate a series of simulations of the porosity of each geologic unit. However, this approach would be problematic because there are insufficient porosity data for inference of variogram models, so the variogram models would need to be developed from other data that are available for a large number of samples, e.g., grain size.

4.5 Uncertainty in Geostatistical Modeling

There are two major elements of uncertainty in the geostatistical modeling that have not been quantified. One is the impact that modifications in the variogram model might have on simulated concentration values, and thereby on the metrics that were developed for history matching. The fitting of variogram models to experimental variogram values is not a well-constrained process, and there is variation possible in the range, nugget, and other parameters selected in fitting the model, especially in cases where the data are few and highly clustered or spatially noisy (i.e., the concentration does not appear to vary smoothly in space). To determine the potential impact of uncertainty in variogram modeling, it would be possible to do sensitivity studies, vary model parameters and then generate alternative sets of stochastic simulations of the concentration that could be used to calculate alternative sets of metrics for a particular plume.

Also, as discussed in Section 3.5, metrics calculated from the geostatistical simulations, including the total activity in a plume and the area above the DWS, may underestimate the true values of metrics in areas with sparse data. In the current study, this situation appears to occur in the larger plumes associated with 200 East Area that have undergone rapid transport due to the presence of permeable Hanford formation gravels at the water table. In those areas, the spacing between wells is often beyond the range of the variogram model, and there are only a few high concentration data points within the plume that tend to be overshadowed by a larger number of low values located beyond the edge of the plume. Thus, high concentrations tend to be simulated within limited areas near high concentration data points within the plume, and the plume is not as well connected as it might be in a hand-drawn contour map.

Several avenues could be investigated to deal with this situation. One would be to split the plume within sub-area 1 of Grid 3 into near-field and far-field zones and model the experimental variograms

separately. As mentioned in Section 3.2, there may be differences between the long- and short-range variogram structures because many local recharge areas associated with discrete waste facilities in the near-field areas create complex local groundwater flow directions that affect the short-range variogram structure, whereas farther away from the source, the contaminant distribution and variogram structure associated with it are affected only by the regional groundwater flow. This suggests that there might be longer variogram ranges in far-field areas of the plume, though it remains to be seen if there is sufficient data to calculate reliable variograms in those areas.

An additional complexity is that the direction of maximum continuity varies in the far-field flow system. For example in Figure 3.15, the direction of maximum continuity of tritium concentration data is roughly northwest-southeast between 200 East Area and the Central Landfill. However, the plume bifurcates east of that area, apparently due to the distribution of relatively low permeability sediment of the Cold Creek unit and Ringold Formation in that area. A segment of the plume continues to the south-east, past the 400 Area toward the Columbia River, while a sizeable portion of the contamination has moved toward the northeast. Thus, the maximum continuity of the concentration data changes in that area from northwest-southeast to northeast-southwest. Because of the variability in anisotropy direction, it was necessary to model the variogram with an isotropic model. It might be possible to achieve greater continuity of the contaminant plumes in areas of sparse data if variations in the anisotropy field could be captured. It might be possible to do this by using the groundwater velocity field in Grid 3 to provide an estimate of local variations in the directions of maximum continuity. This would require modification of the sequential Gaussian simulation code used to simulate concentration data.

There is a simpler approach that would allow direct comparison of the metrics generated from geostatistical simulations of concentration data and SAC model runs. This would involve sampling the concentration output from the SAC model at locations, and over the same depth intervals, where historical concentration measurements were made by the Groundwater Performance Assessment Project. The data sampled from SAC model runs would then be analyzed geostatistically, using methods developed in this report, and the same metrics would be calculated from geostatistical simulations of concentration. Both sets of geostatistical simulations would be performed using the same set of sparse locations, so differences due to the sparse distribution of data would be eliminated.

5.0 Summary and Recommendations

The approach taken in this study has developed a set of metrics that quantify the spatial distribution of four radionuclide contaminants for two points in time FY 2001 and FY 1992, based on historical groundwater concentration measurements. Approximately 24 separate geostatistical studies were completed for that effort, with metrics developed for numerous individual plume areas. That information can be used to evaluate the ability of the SAC Rev. 1 model to produce simulated concentration histories over time that match historical data. In addition, this study provides measures of the uncertainty in each of those metrics that can be used to determine if predictions from the SAC model fall within the uncertainty bands expected due to spatial uncertainty in historical contaminant concentration data. The approach developed for this study appears to represent a significant improvement over the approach used for history matching evaluation of SAC Rev. 0.

Several possible improvements or extensions of the approach appear to be worth consideration and are recommended for future study. These include:

- Extend this approach to other contaminants. This is currently underway, with extension of the approach to several chemical contaminants for the same time periods. The contaminants that will be completed in FY 2004 are chromium, nitrate, and carbon tetrachloride.

- Generate results for additional time points beyond the two points in time considered in the present study. History matching data should be generated for earlier points in time, although the areas covered might need to be restricted due to the sparse distribution of data for earlier time periods (see Figure 2.1).

- Examine the effect of vertical contaminant distribution assumptions on uncertainty bounds for history matching data. As mentioned in Section 4.2, a characterization of systems study will be conducted in FY 2004 to examine the vertical distribution of contaminants. The results of that study should be used to guide a sensitivity or uncertainty analysis of the effect on uncertainty bounds of history matching data related to uncertainty in plume thickness and the vertical distribution of contaminants within the plume. For example, one could examine the difference in uncertainty bounds caused by using an assumption of constant concentration with depth versus models that assume the highest concentration occurs at the water table and then use simple mathematical models to decrease the concentration with increasing depth in the aquifer.

- Perform an uncertainty analysis to examine the effect on uncertainty bounds for various metrics that might arise from uncertainty in the geologic structure and porosity distribution. This should be done by using the results of work being performed in FY 2004 for the sitewide groundwater modeling task to develop stochastic alternative conceptual models of the geologic structure. In addition, it might be useful to examine how sensitive the metrics are to the assumption that the mud units do not store appreciable quantities of contaminants that will later become available to the aquifer again.

- Examine the sensitivity of history matching metrics to variation in the parameters of the variogram models fit to experimental variograms. This might include examining smaller grid areas more

representative of individual plumes, especially in the large plume associated with 200 East Area to examine the relationship between near source and far-field variograms.

- Produce a set of metrics based on the SAC model runs that accounts for the sparseness of concentration data available for geostatistical modeling. That set of metrics is more likely to match the metrics presented in this study. The suggested approach includes sampling the concentration fields from the SAC model runs at historical well locations and over the screened intervals that were employed in sampling groundwater. Geostatistical analysis of the sampled model runs would then be used to generate a set of metrics using the same methods described in this report. The metrics calculated from historical groundwater data and sampled SAC model runs would then be compared to evaluate the ability of the SAC model to reproduce historical groundwater concentration data.

6.0 References

Bryce RW, CT Kincaid, PW Eslinger, and LF Morasch. 2002. *An Initial Assessment of Hanford Impact Performed with the System Assessment Capability*. PNNL-14027, Pacific Northwest National Laboratory, Richland, Washington.

Davis, JC. 1986. *Statistics and Data Analysis in Geology*. New York, John Wiley & Sons, Inc.

Deutsch CV and AG Journel. 1998. *GSLIB: Geostatistical Software Library and User's Guide*. New York, Oxford University Press.

DOE Order 435.1. 1999. *Radioactive Waste Management*. U.S. Department of Energy, Washington, D.C. Available on the Internet at http://www.hanford.gov/wastemgt/doe/psg/pdf/doeo435.1.pdf

DOE. 2003. *Groundwater Sampling and Analysis Plan for the 200-BP-5 Operable Unit*. DOE/RL-2001-49, U.S. Department of Energy, Richland Operations Office, Richland, Washington.

Eddy PA, DA Myers, and JR Raymond. 1978. *Vertical Contamination in the Unconfined Groundwater at the Hanford Site, Washington*. PNL-2724, Pacific Northwest Laboratory, Richland, Washington.

Freeman EJ, R Khaleel, and PR Heller. September 2002. *A Catalog of Vadose Zone Hydraulic Properties for the Hanford Site*. PNNL-13672, Rev. 1, Pacific Northwest National Laboratory, Richland, Washington.

Gomez-Hernandez JJ and AG Journel. 1993. "Joint Sequential Simulation of MultiGaussian Fields." In *Geostatistics Troia '92*, A. Soares (ed.). Dordrecht, Kluwer Academic Publishers, 1:85-94.

Goovaerts P. 1997. *Geostatistics for Natural Resources Evaluation*. New York, Oxford University Press.

Hartman MJ (ed.). 2000. *Hanford Site Groundwater Monitoring: Setting, Sources, and Methods*. PNNL-13080, Pacific Northwest National Laboratory, Richland, Washington.

Hartman MJ, LF Morasch, and WD Webber (eds.). 2002. *Hanford Site Groundwater Monitoring for Fiscal Year 2001*. PNNL-13788, Pacific Northwest National Laboratory, Richland, Washington.

Hartman MJ, LF Morasch, and WD Webber (eds.). 2004. *Hanford Site Groundwater Monitoring for Fiscal Year 2003*. PNNL-14548, Pacific Northwest National Laboratory, Richland, Washington.

Isaaks EH and RM Srivastava. 1989. *An Introduction to Applied Geostatistics*. New York, Oxford University Press.

Johnson VG and CJ Chou. 2000. *RCRA Groundwater Quality Assessment Report for Waste Management Area S-SX (November 1997 through April 2000*). PNNL-13441, Pacific Northwest National Laboratory, Richland, Washington.

Journel AG. 1987. *Geostatistics for the Environmental Sciences*. CR 811893, U.S. Environmental Protection Agency, Environmental Monitoring Systems Laboratory, Las Vegas, Nevada.

Journel AG. 1989. *Fundamentals of Geostatistics in Five Lessons*. Volume 8, Short Courses in Geology, American Geophysical Union, Washington, D.C.

Journel AG and M Rossi. 1989. "When do we need a trend model in kriging?" *Mathematical Geology* 21,715-739.

Khaleel R and EJ Freeman. 1995. *Variability and Scaling of Hydraulic Properties for 200 Area Soils, Hanford Sit*e. WHC-EP-0883, Westinghouse Hanford Company, Richland, Washington.

Kincaid CT, RW Bryce, and JW Buck. 2004. *Technical Scope and Approach for the 2004 Composite Analysis of Low Level Waste Disposal at the Hanford Site*. PNNL-14372 Draft, Pacific Northwest National Laboratory, Richland, Washington.

Rajaram H and LW Gelhar. 1991. *Three-Dimensional Spatial Moments Analysis of the Borden Tracer Test.* Water Resources Research, 27(6), 1239-1251.

Thorne PD and DR Newcomer. 2002. *Prototype Database and User's Guide of Saturated Zone Hydraulic Properties for the Hanford Site*. PNNL-14058, Pacific Northwest National Laboratory, Richland, Washington.

Vermeul VR, MP Bergeron, CR Cole, CJ Murray, WE Nichols, TD Scheibe, PD Thorne, SR Waichler, and Y Xie. 2003. *Transient Inverse Calibration of the Site-Wide Groundwater Flow Model (ACM-2): FY03 Progress Report*. PNNL-14398, Pacific Northwest National Laboratory, Richland, Washington.

Williams BA, BN Bjornstad, R Schalla, and WD Webber. 2002. *Revised Hydrogeology for the Suprabasalt Aquifer System, 200-West Area and Vicinity, Hanford Site, Washington*. PNNL-13858, Pacific Northwest National Laboratory, Richland, Washington.

Xie Y, CJ Murray, GV Last, and R Mackley. 2003. *Mineralogical and Bulk-Rock Geochemical Signatures of Ringold and Hanford Formation Sediments*. PNNL-14202, Pacific Northwest National Laboratory, Richland, Washington.

Appendix A

Sub-Area Boundary Coordinates for FY 2001 Tritium

Appendix A

Sub-Area Boundary Coordinates for FY 2001 Tritium

Table A.1. Coordinates for Sub-Area Boundaries for Grid 1 (200 West Area) of FY 2001 Tritium

Sub-Area 1		Sub-Area 2	
Easting (m)	Northing (m)	Easting (m)	Northing (m)
565400	131400	565400	139200
565400	134250	569868	139200
570515	138320	570515	138320
571060	137034	565400	134250
571364	136328	565400	139200
572138	135554		
572405	134779		
572700	134629		
572700	131400		
565400	131400		

Table A.2. Coordinates for Sub-Area Boundary for Grid 2 (100 Areas) of FY 2001 Tritium

Easting (m)	Northing (m)	Easting (m)	Northing (m)
563900	143800	581522	145250
563900	145566	581309	145590
564206	145277	581053	145975
564778	145277	580882	146188
565610	145502	580455	146531
566373	145754	579944	146444
566915	145882	579390	146318
567588	146172	578834	146360
567905	146522	578407	146444
568736	147033	578067	146871
569056	147447	577766	147469
569597	147959	577682	147893
570361	148692	577766	148408
570967	149392	577980	148789
572118	150987	578193	149304
572754	151785	578193	149815
573070	152199	578193	150410
573965	152744	577938	151051
573996	153030	577511	151436
574315	153828	577171	151775
574379	154144	576573	151863
574635	154500	576061	151733
575910	154500	575508	151436
577761	153410	575123	151093
578239	152710	574441	150326
579740	151371	573971	149728
579962	150987	573544	149216
579962	150573	573033	148789
579706	149806	572606	148236
579582	149614	572179	147809
579706	149200	571839	147382
580124	148787	571454	146871
580985	148211	571027	146486
581463	147764	570474	145891
582227	147350	569876	145506
581941	146902	569109	145250
582516	145724	568426	145208
582897	145118	567702	145208
583216	144129	567061	145036
583250	143800	566508	144994
582450	143800	566123	144823
582205	144140	565951	144182
581992	144441	565600	143800
581736	144910	563900	143800

Table A.3. Coordinates for Sub-Area Boundaries for Grid 3 (200 East Area) of FY 2001 Tritium

Sub-Area 1		Sub-Area 2	
Easting (m)	Northing (m)	Easting (m)	Northing (m)
573050	135650	573050	135650
575750	136950	575750	136950
576319	137080	574816	137442
576946	136478	574009	137599
577308	135180	573749	138015
579183	135415	573568	137809
579805	135567	573230	137858
580221	136037	573230	139004
580246	138196	573827	139939
582650	138900	572657	141966
582909	138876	572501	142068
583780	138441	571487	142019
584838	137633	571409	142279
585773	137011	571722	142460
587393	136135	573593	142538
586272	137197	574557	142563
583966	138876	576868	142538
587109	138925	577416	142093
589685	137285	577910	142122
590620	136169	573600	146150
591192	134999	567400	146150
593273	133570	567400	143800
594184	131797	568291	142460
594497	130319	569250	142044
594521	128733	570263	140693
594732	127822	570498	139782
594913	126990	570239	139758
594575	124704	573050	135650
594521	123950		
594521	121947		
594472	118956		
594262	117605		
594340	116694		
594810	114643		
582500	122750		
573050	135650		

Appendix B

Figures and Data Tables for FY 1992 Tritium

Appendix B

Figures and Data Tables for FY 1992 Tritium

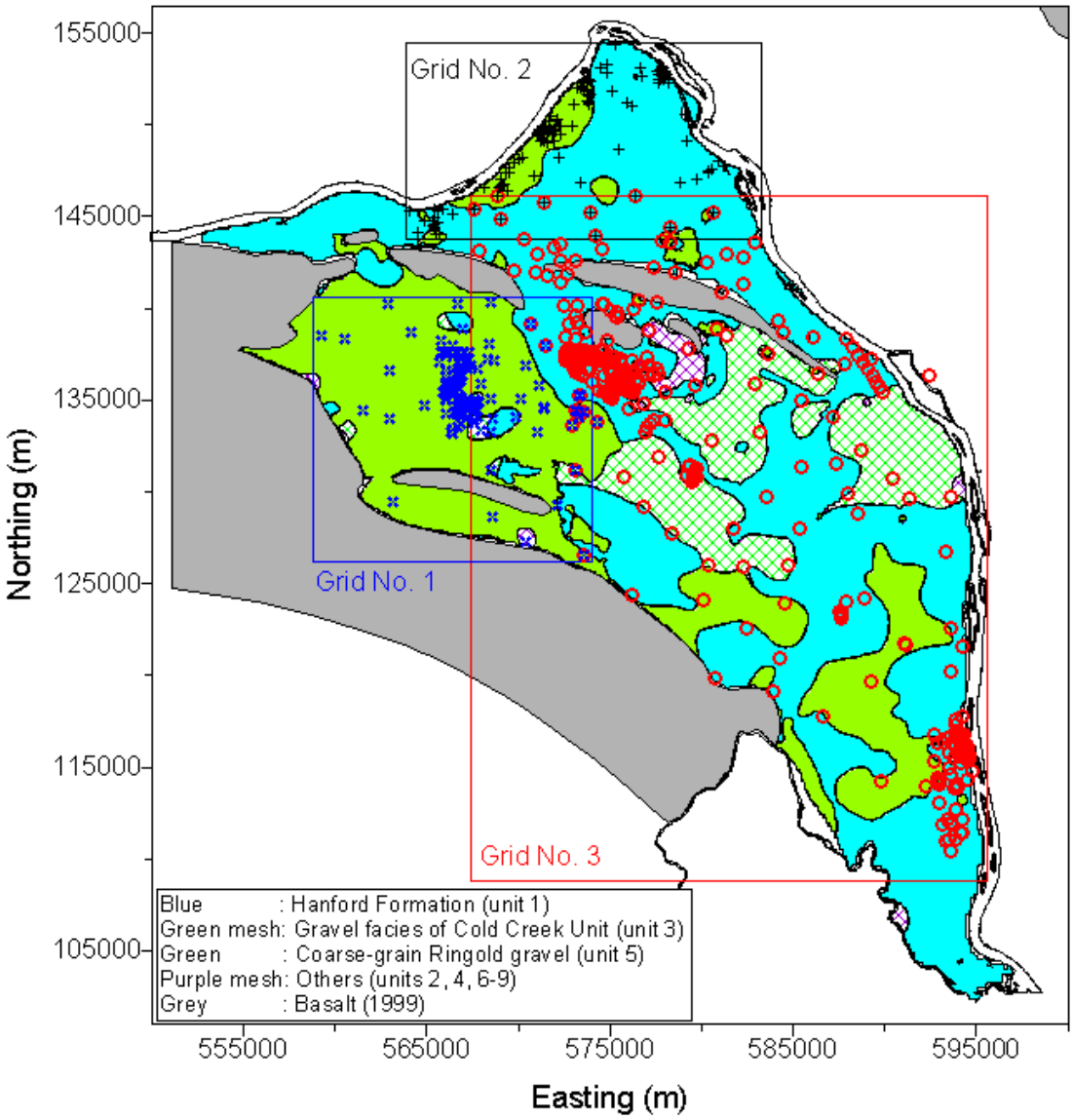

Figure B.1. Subsets of FY 1992 Tritium Data and Subcrop Formation Units at the FY 1992 Water Table

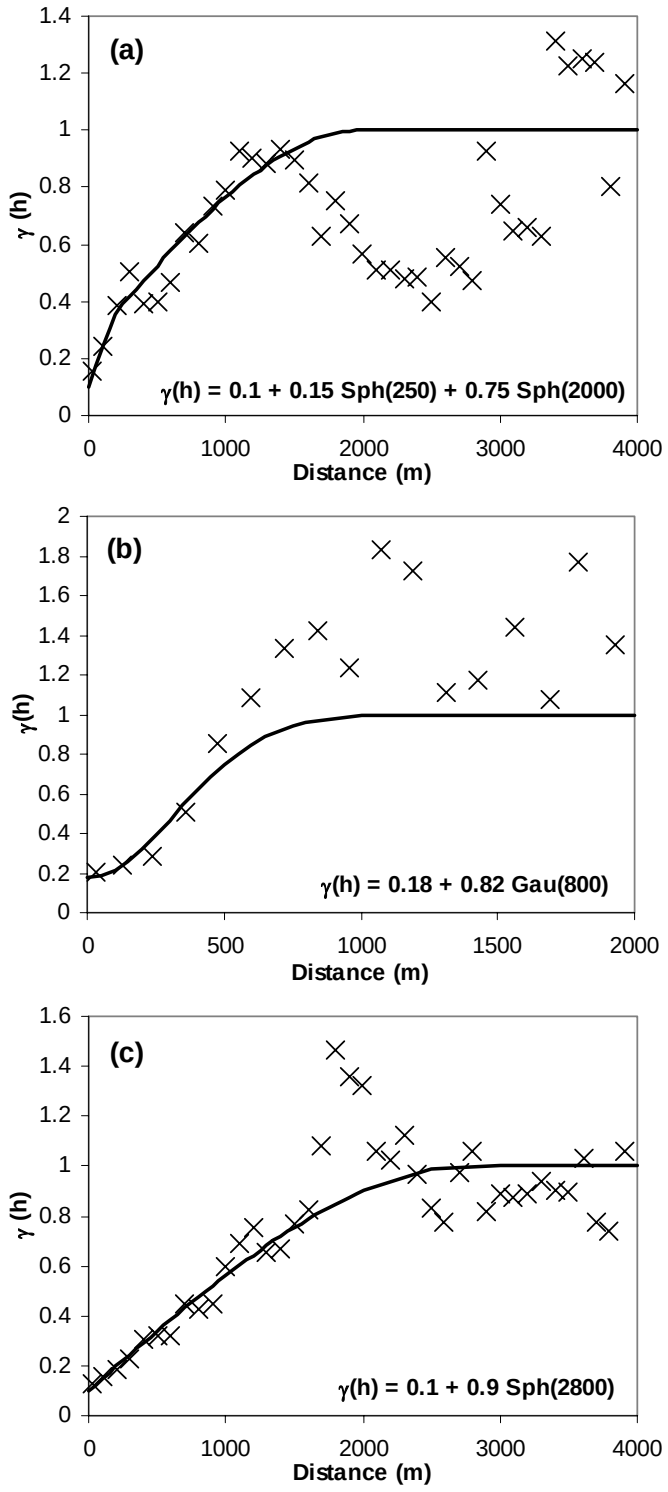

Figure B.2. Variograms and Models of Normal Scores of FY 1992 Tritium Data in Local Grid 1 (a), Grid 2 (b), and Grid 3 (c). Experimental variogram values designated by X, with the models fit to the data denoted by solid black lines.

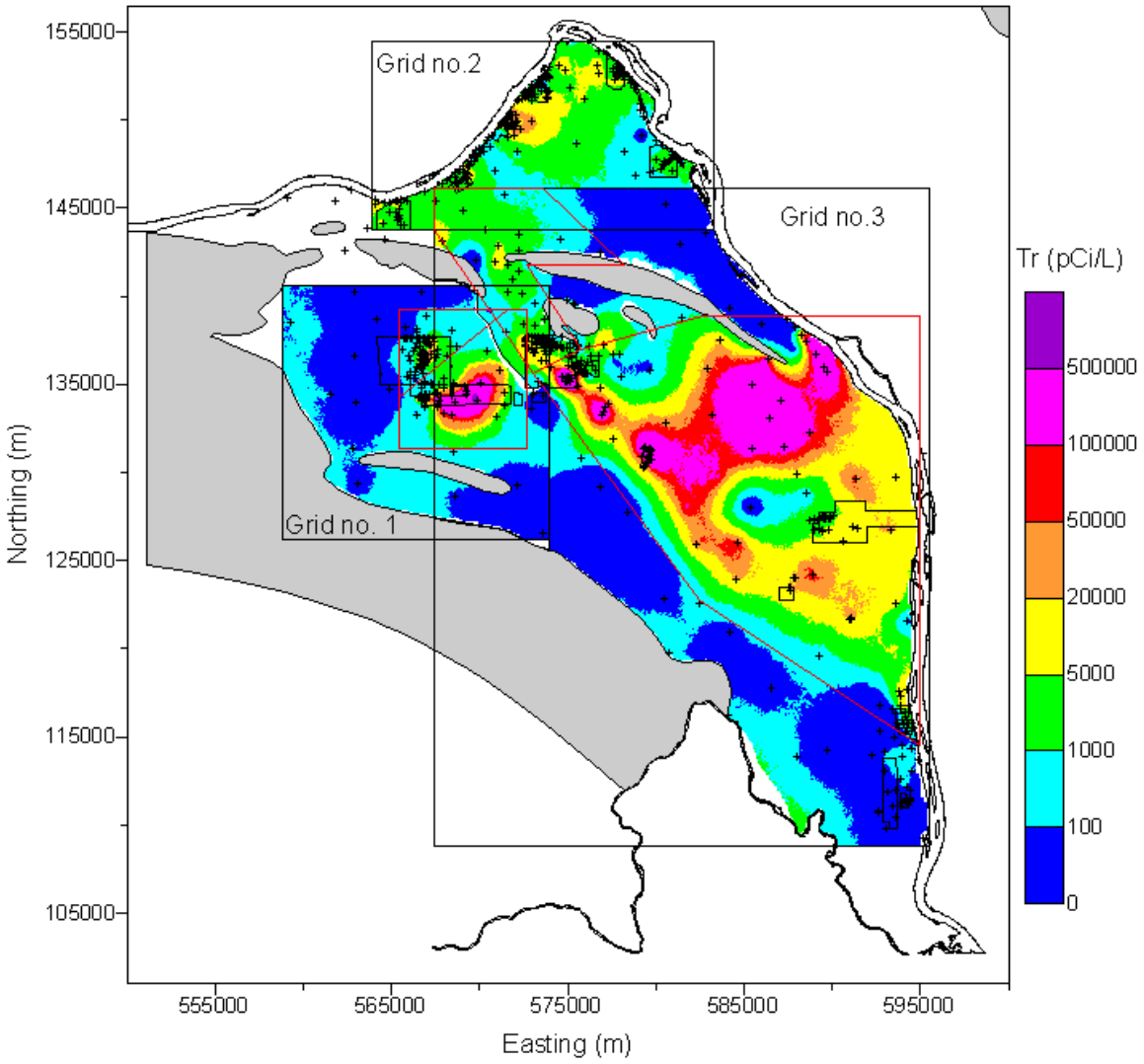

Figure B.3. Median of Simulations of FY 1992 Tritium Concentrations for Grids 1, 2, and 3

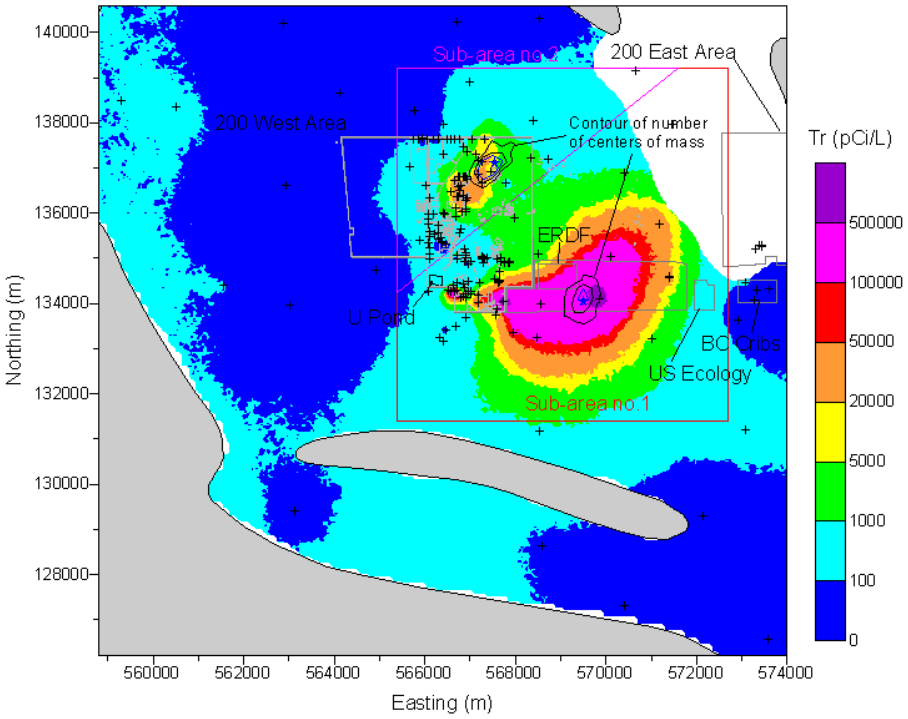

Figure B.4. **Median of Simulated FY 1992 Tritium Concentrations in Grid 1 (200 West Area). Contours of the number of times that the center of mass within the sub-areas occurred within cells of an upscaled grid are shown with the average centers of mass shown by blue stars in each sub-area.**

Table B.1. **Coordinates for Sub-Area Boundaries for Grid 1 (200 West Area) of FY 1992 Tritium**

Sub-Area 1		Sub-Area 2	
Easting (m)	Northing (m)	Easting (m)	Northing (m)
565400	131400	565400	139200
565400	134250	569786	139200
570473	138274	570473	138274
571023	136892	565400	134250
571274	136289	565400	139200
571940	135549		
572405	134779		
572700	134629		
572700	131400		
565400	131400		

Table B.2. Statistics of Centers of Mass of Individual Simulations of FY 1992 Tritium Calculated for a Depth of 5 m for Each Sub-Area of Grid 1 (200 West Area)

Coordinate (m)	Sub-Area 1		Sub-Area 2	
	Easting	Northing	Easting	Northing
Mean	569460.4	134018.9	567523.2	137113.7
Standard Error	12.5	15.4	15.3	14.3
Median	569466.3	134011.0	567458.0	137061.0
Standard Deviation	279.4	344.0	342.1	318.8
Kurtosis	1.09	0.03	3.37	0.89
Skewness	-0.32	0.02	1.42	0.88
Range	2069.4	1905.6	2403.6	1844.6
Minimum	568277.0	133041.8	566760.1	136499.3
Maximum	570346.3	134947.3	569163.7	138343.9
Count	500	500	500	500
97.5^{th} Percentile	570007.3	134746.7	568485.9	137876.5
2.5^{th} Percentile	568913.0	133317.2	567007.1	136620.6
Confidence Level of Mean (95.0%)	24.5	30.2	30.1	28.0

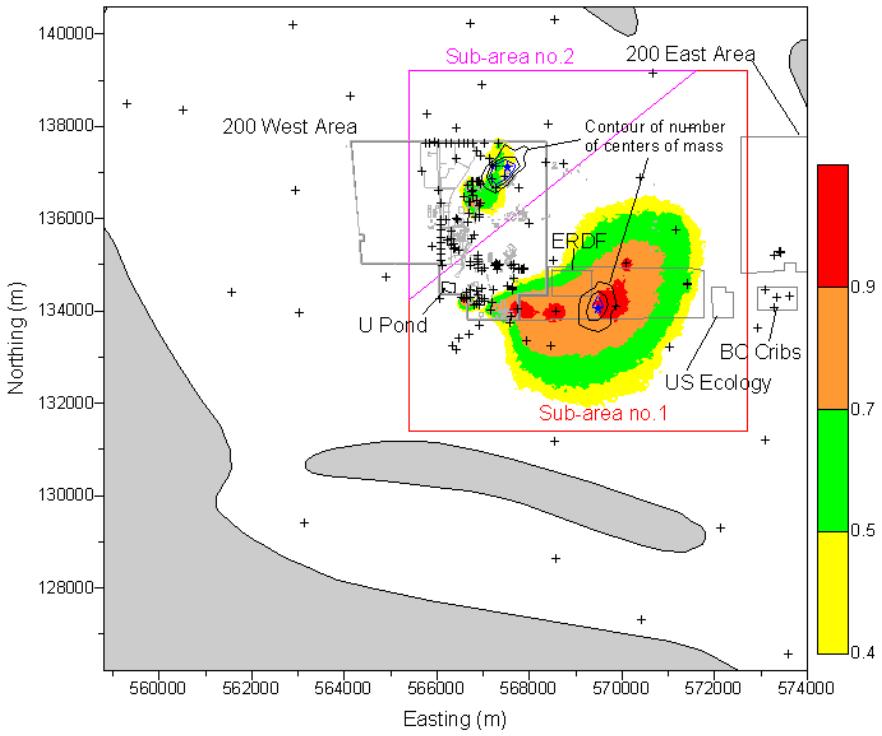

Figure B.5. Probability of Exceeding 20,000 pCi/L Based on Simulations of FY 1992 Tritium in Grid 1 (200 West Area)

Table B.3. Area Exceeding 20,000 pCi/L for FY 1992 Tritium for Each Simulation within Two Sub-Areas of Grid 1 (200 West Area)

Area (km^2)	Sub-Area 1	Sub-Area 2	Grid 1
Mean	13.16	1.83	20.13
Standard Error	0.10	0.02	0.17
Median	12.99	1.76	19.85
Standard Deviation	2.25	0.50	3.76
Kurtosis	0.02	3.21	0.30
Skewness	0.17	1.30	0.46
Range	13.86	3.43	22.48
Minimum	6.75	0.82	11.40
Maximum	20.61	4.25	33.88
Count	500	500	500
97.5^{th} Percentile	17.76	3.13	27.98
2.5^{th} Percentile	9.01	1.07	13.62
Confidence Level of Mean (95.0%)	0.20	0.04	0.33

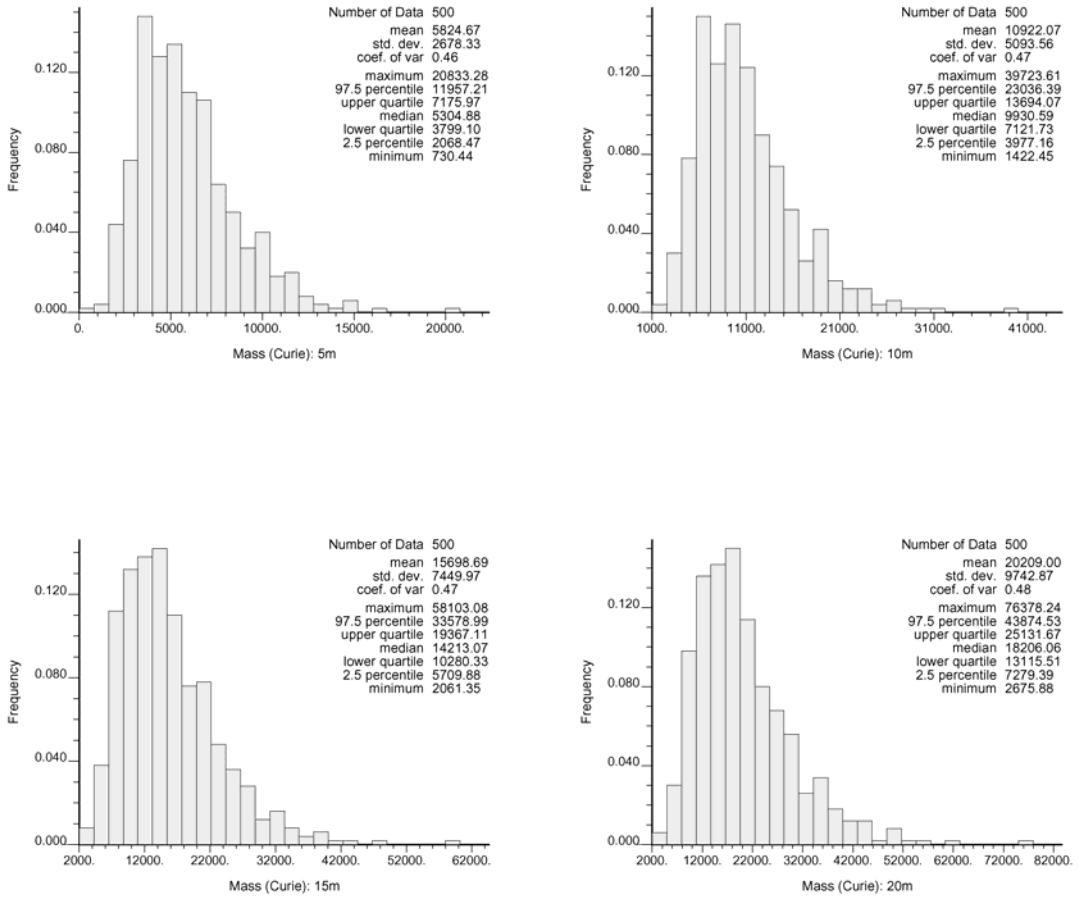

Figure B.6. Histograms of Total Activity in Simulations of FY 1992 Tritium within Sub-Area 1 of Grid 1 (200 West Area), Four Thickness Assumptions

Table B.4. Statistics of Total Activity of Simulations of FY 1992 Tritium within Sub-Area 1 of Grid 1 (200 West Area), Four Thickness Assumptions

Mass (Ci) in Depth	5 m	10 m	15 m	20 m
Mean	5,824.67	10,922.07	15,698.69	20,208.99
Standard Error	119.90	228.02	333.51	436.15
Median	5,304.89	9,930.60	14,213.08	18,206.07
Standard Deviation	2,681.01	5,098.66	7,457.43	9,752.63
Kurtosis	2.40	2.75	2.95	3.13
Skewness	1.17	1.26	1.31	1.36
Range	20,102.83	38,301.17	56,041.73	73,702.36
Minimum	730.44	1,422.45	2,061.35	2,675.88
Maximum	20,833.28	39,723.61	58,103.08	76,378.24
Count	500	500	500	500
97.5th Percentile	11,956.96	23,036.35	33,578.76	43,873.50
2.5th Percentile	2,068.47	3,977.16	5,709.88	7,279.39
Confidence Level of Mean (95.0%)	235.57	448.00	655.25	856.92

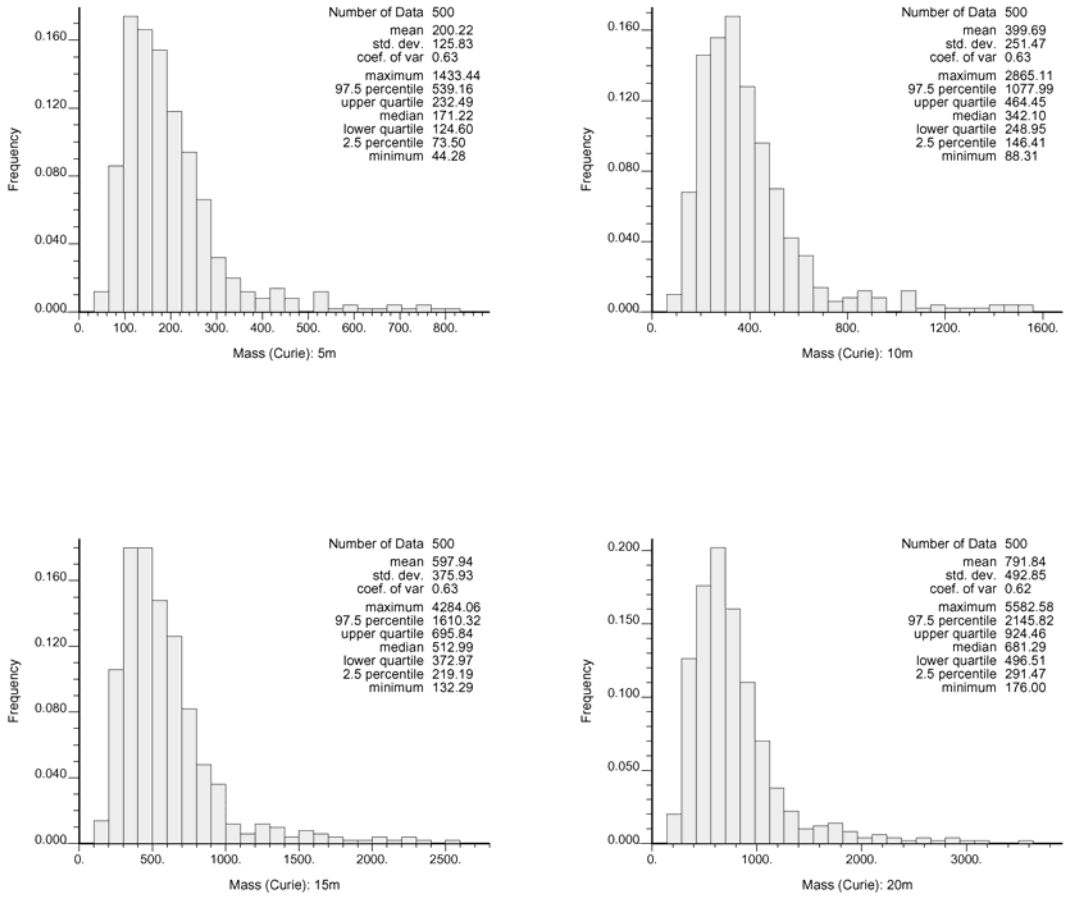

Figure B.7. Histograms of Mass of Simulations of FY 1992 Tritium within Sub-Area 2 of Grid 1 (200 West Area), Four Depth Assumptions

Table B.5. Mass of Simulations of FY 1992 Tritium within Sub-Area 2 of Grid 1 (200 West Area), Four Depth Assumptions

Mass (Ci) in Depth	5 m	10 m	15 m	20 m
Mean	200.22	399.69	597.94	791.84
Standard Error	5.63	11.26	16.83	22.06
Median	171.22	342.11	512.99	681.29
Standard Deviation	125.96	251.72	376.31	493.34
Kurtosis	21.73	21.75	21.77	21.22
Skewness	3.44	3.44	3.44	3.40
Range	1,389.16	2,776.79	4,151.77	5,406.58
Minimum	44.28	88.31	132.29	176.00
Maximum	1,433.44	2,865.11	4,284.06	5,582.58
Count	500	500	500	500
97.5^{th} Percentile	539.10	1,077.87	1,610.13	2,145.59
2.5^{th} Percentile	73.50	146.41	219.19	291.47
Confidence Level of Mean (95.0%)	11.07	22.12	33.06	43.35

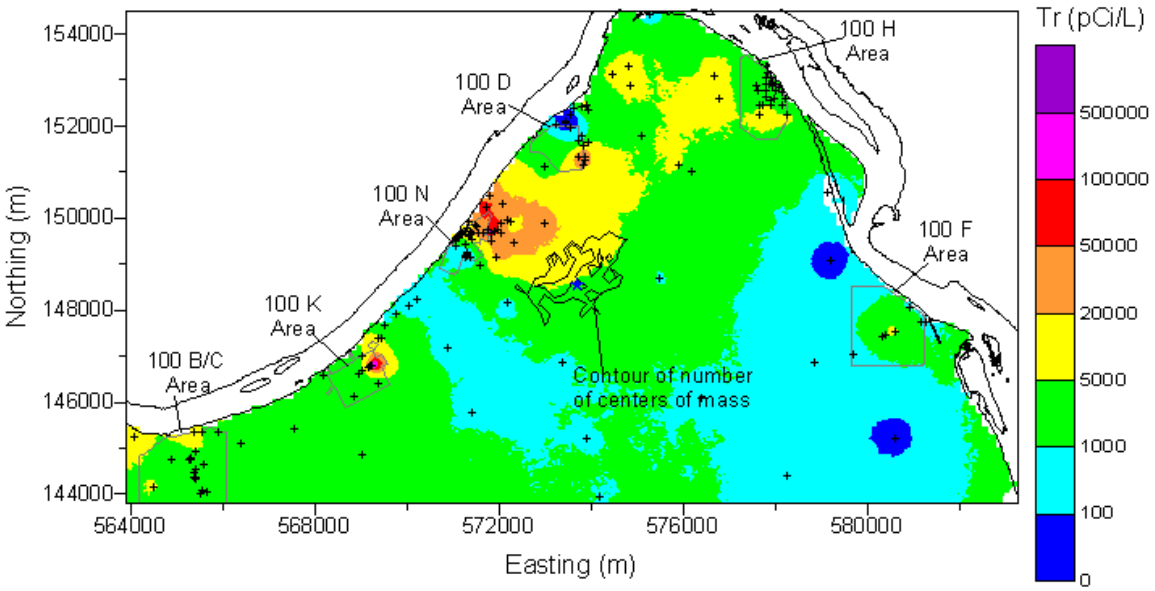

Figure B.8. Median of Simulated FY 1992 Tritium Concentrations in Grid 2 (100 Areas). Contours of the number of times that the center of mass occurred within cells of an upscaled grid are shown with the average center of mass shown by a blue star.

Table B.6. Coordinates for Sub-Area Boundary for Grid 2 (100 Areas) of FY 1992 Tritium

Easting (m)	Northing (m)	Easting (m)	Northing (m)
563900	143800	574635	154500
563900	145566	575910	154500
564206	145277	577761	153410
564778	145277	578239	152710
565610	145502	579740	151371
566373	145754	579962	150987
566915	145882	579962	150573
567588	146172	579706	149806
567905	146522	579582	149614
568736	147033	579706	149200
569056	147447	580124	148787
569597	147959	580985	148211
570361	148692	581463	147764
570967	149392	582227	147350
572118	150987	581941	146902
572754	151785	582516	145724
573070	152199	582897	145118
573965	152744	583216	144129
573996	153030	583250	143800
574315	153828	563900	143800
574379	154144		

Table B.7. Statistics of the Area Exceeding 20,000 pCi/L and Locations of Centers of Mass for Simulations of FY 1992 Tritium within Grid 2 (100 Areas)

	Area (km^2)	Center of Mass (m)	
		Easting	Northing
Mean	15.05	573710.1	148368.1
Standard Error	0.11	35.7	29.2
Median	14.69	573716.3	148370.0
Standard Deviation	2.86	944.9	773.7
Kurtosis	-0.24	0.90	-0.33
Skewness	0.35	0.00	-0.06
Range	16.38	7716.2	4549.5
Minimum	8.18	570248.0	145859.0
Maximum	24.56	577964.2	150408.5
Count	700	700	700
97.5^{th} Percentile	21.20	575466.8	149789.9
2.5^{th} Percentile	10.22	571800.9	146891.0
Confidence Level (95.0%)	0.21	70.1	57.4

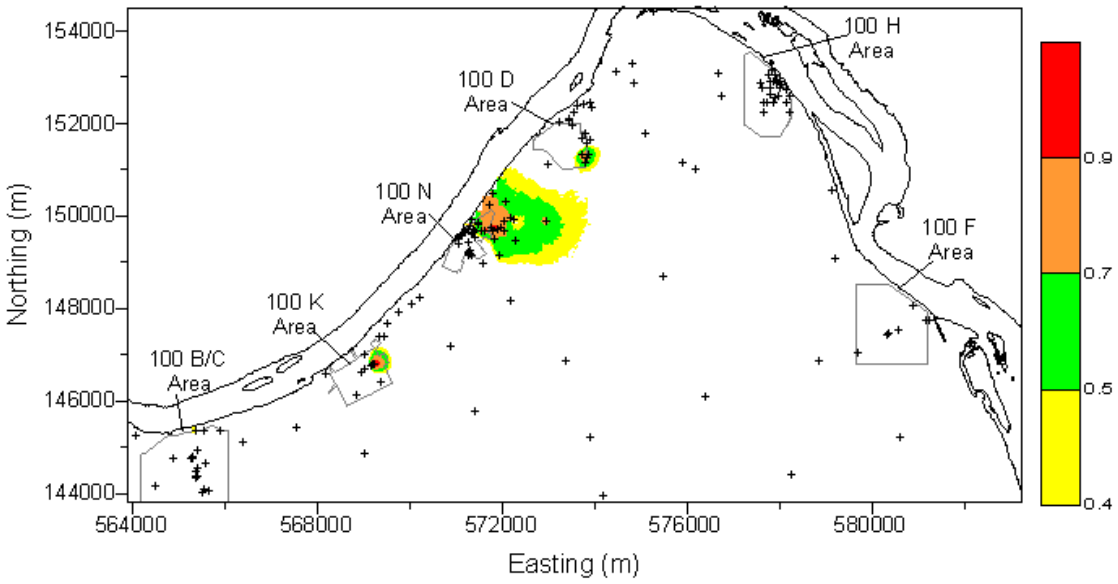

Figure B.9. Probability of Exceeding 20,000 pCi/L Based on Simulations of FY 1992 Tritium in Grid 2 (100 Areas)

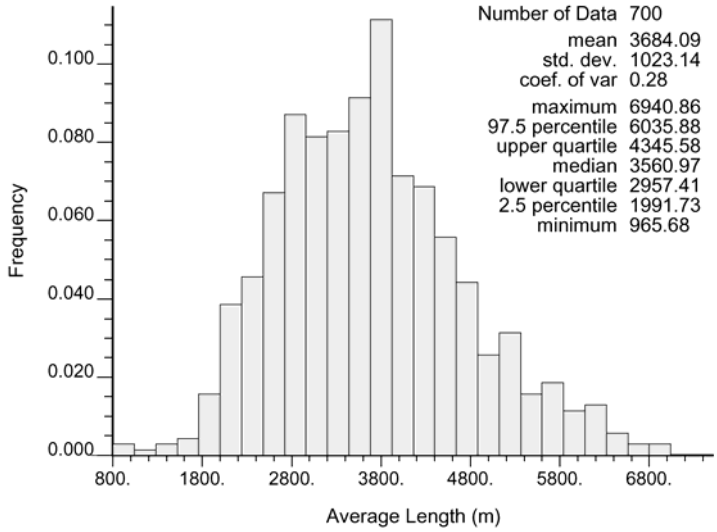

Figure B.10. Histogram of the Average Length of Columbia River Shoreline Exceeding 20,000 pCi/L for FY 1992 Tritium in Grid 2 (100 Areas)

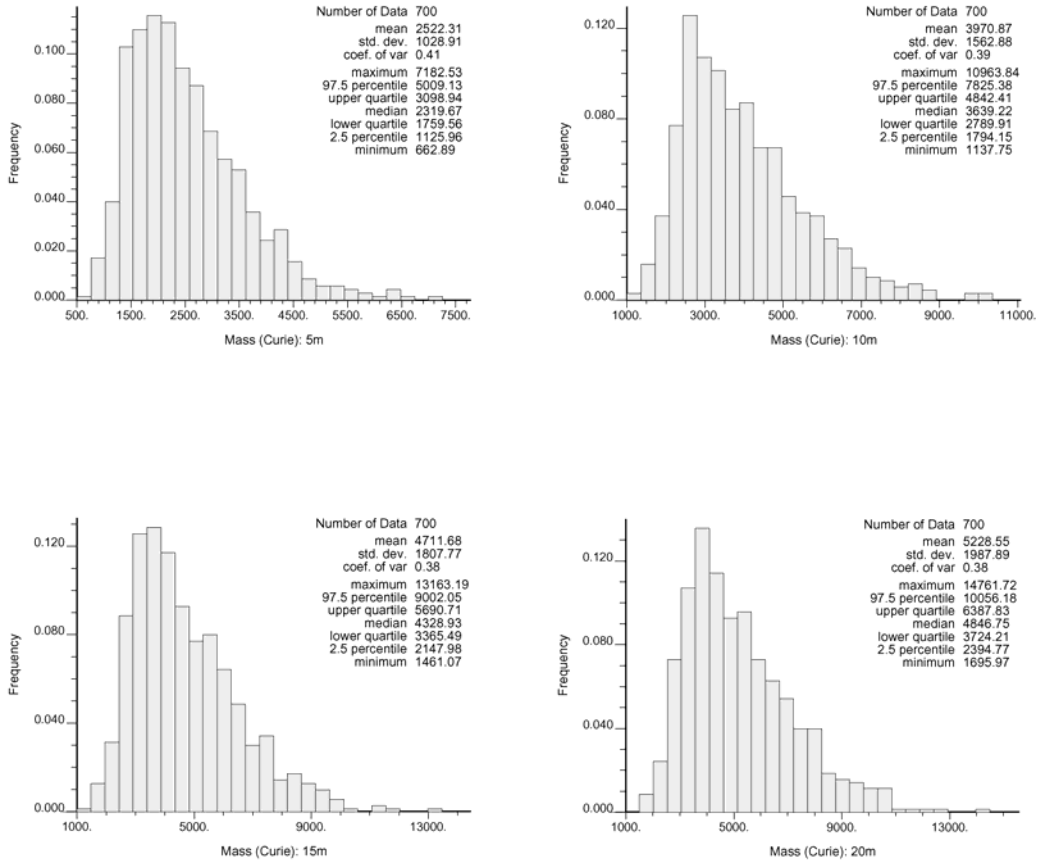

Figure B.11. Histograms of Total Activity in Simulations of FY 1992 Tritium within Grid 2 (100 Areas), Four Thickness Assumptions

Table B.8. Statistics of Total Activity of Simulations of FY 1992 Tritium within Grid 2 (100 Areas), Four Thickness Assumptions

Mass (Ci) in Depth	5 m	10 m	15 m	20 m
Mean	2,522.31	3,970.87	4,711.68	5,228.55
Standard Error	38.92	59.11	68.38	75.19
Median	2,319.67	3,639.23	4,328.94	4,846.75
Standard Deviation	1,029.65	1,564.00	1,809.06	1,989.31
Kurtosis	1.47	1.29	1.09	1.02
Skewness	1.08	1.04	0.98	0.96
Range	6,519.65	9,826.09	11,702.11	13,065.74
Minimum	662.89	1,137.75	1,461.07	1,695.97
Maximum	7,182.53	10,963.84	13,163.19	14,761.72
Count	700	700	700	700
97.5^{th} Percentile	5,008.89	7,825.31	9,001.98	10,055.47
2.5^{th} Percentile	1,125.96	1,794.15	2,147.98	2,394.77
Confidence Level of Mean (95.0%)	76.41	116.06	134.25	147.62

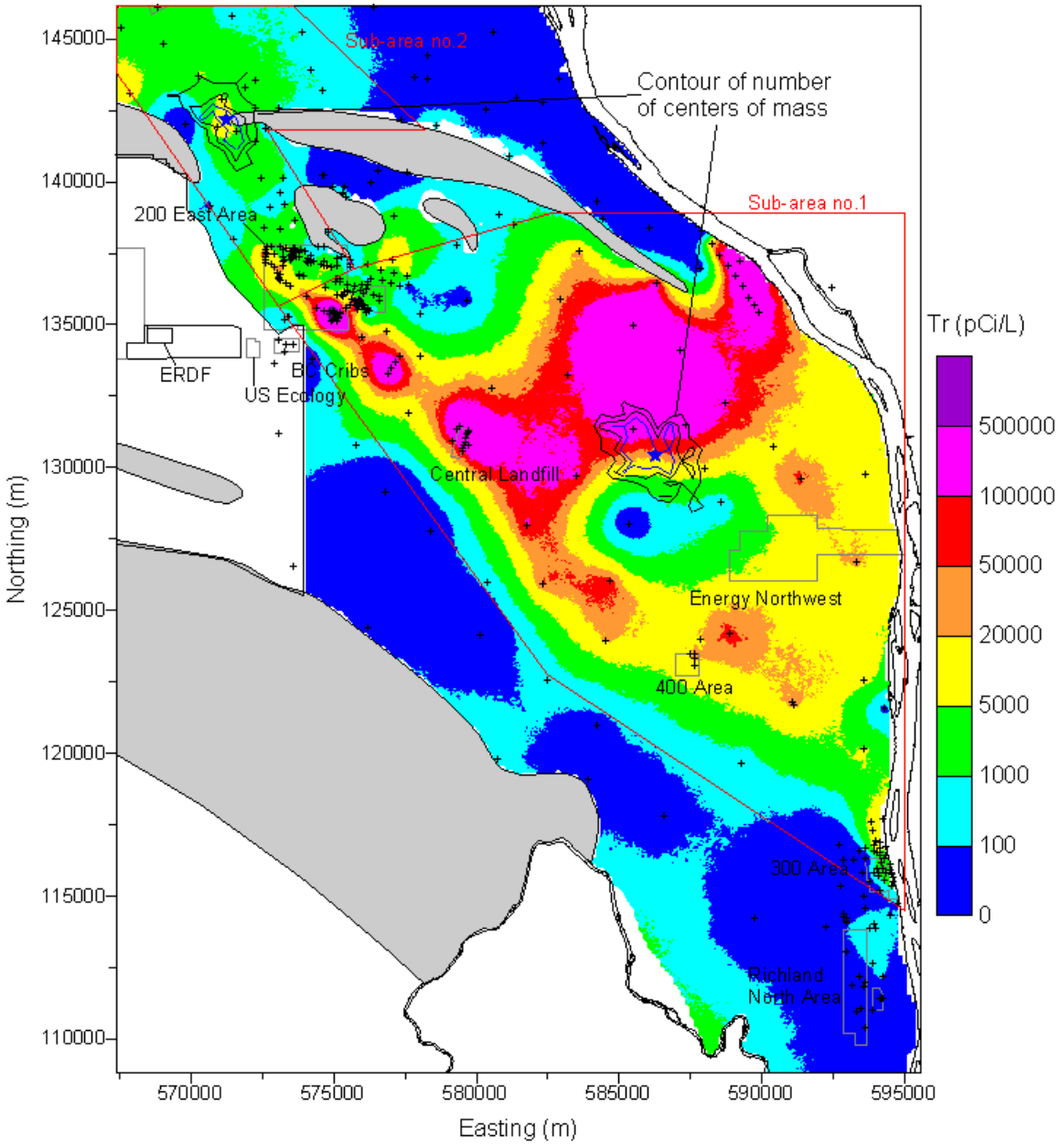

Figure B.12. Median of Simulated FY 1992 Tritium Concentrations in Grid 3 (200 East Area Plumes). Contours of the number of times that the center of mass within the sub-areas occurred within cells of an upscaled grid are shown with the average centers of mass shown by blue stars in each sub-area.

Table B.9. Coordinates for Sub-Area Boundaries for Grid 3 (200 East Area) of FY 1992 Tritium

Sub-Area 1		Sub-Area 2	
Easting (m)	Northing (m)	Easting (m)	Northing (m)
573050	135650	575750	136950
575750	136950	575453	137398
579634	138020	574753	137760
579609	137657	574263	137760
579790	137403	573593	139361
580020	137657	573671	139670
580074	138044	573852	139905
580045	138152	573827	139939
582650	138900	572657	141966
582909	138876	572501	142068
583780	138441	571487	142019
584838	137633	571409	142279
585773	137011	571722	142460
587393	136135	573593	142538
586272	137197	574557	142563
583966	138876	576868	142538
587109	138925	577416	142093
589685	137285	577910	142122
590620	136169	573600	146150
591192	134999	567400	146150
593273	133570	567400	143800
594184	131797	568320	142485
594497	130319	569201	142122
594521	128733	569769	141530
594732	127822	570156	140913
594913	126990	570283	140600
594575	124704	570259	140032
594521	123950	570102	139929
594521	121947	573050	135650
594472	118956	575750	136950
594262	117605		
594340	116694		
594810	114643		
582500	122750		
573050	135650		

Table B.10. Statistics of Locations of Center of Mass for Simulations of FY 1992 Tritium Calculated for a Depth of 5 m for Each Sub-Area of Grid 3 (200 East Area Plumes)

Coordinate (m)	Sub-Area 1		Sub-Area 2	
	Easting	Northing	Easting	Northing
Mean	586175.0	130186.6	571322.4	142135.7
Standard Error	49.6	49.2	36.0	42.3
Median	586114.3	130303.5	571393.6	142152.6
Standard Deviation	1052.9	1043.0	763.5	896.7
Kurtosis	-0.31	0.21	0.40	-0.16
Skewness	0.33	-0.50	-0.04	-0.17
Range	5620.3	6467.9	4578.5	4990.3
Minimum	583825.0	126248.5	569135.4	139448.3
Maximum	589445.4	132716.4	573713.9	144438.6
Count	450	450	450	450
97.5^{th} Percentile	588325.4	131929.4	572776.1	143774.2
2.5^{th} Percentile	584377.4	127935.5	569776.1	140339.5
Confidence Level of Mean (95.0%)	97.5	96.6	70.7	83.1

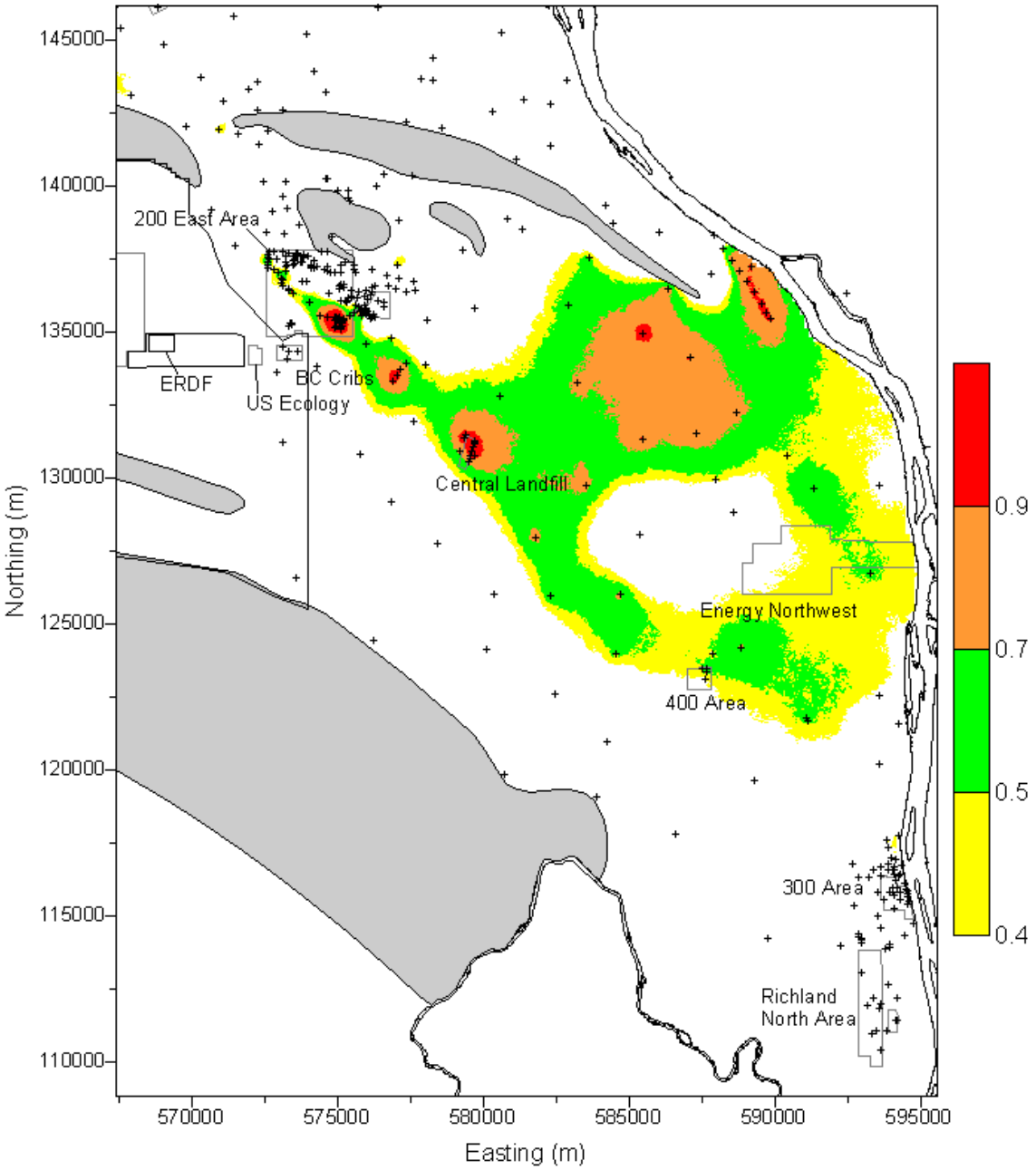

Figure B.13. Probability of Exceeding 20,000 pCi/L Based on Simulations of FY 1992 Tritium in Grid 3 (200 East Area Plumes)

Table B.11. Area Exceeding 20,000 pCi/L for FY 1992 Tritium for Each Simulation within Two Sub-Areas of Grid 3 (200 East Area Plumes)

Area (km^2)	Sub-Area 1	Sub-Area 2	Grid 3
Mean	117.24	6.70	133.82
Standard Error	0.60	0.09	0.63
Median	117.23	6.44	133.57
Standard Deviation	12.76	1.85	13.40
Kurtosis	0.09	0.19	0.21
Skewness	0.20	0.49	0.20
Range	78.34	11.19	85.00
Minimum	83.01	2.66	92.84
Maximum	161.35	13.85	177.84
Count	450	450	450
97.5^{th} Percentile	143.65	10.80	162.17
2.5^{th} Percentile	94.19	3.50	108.92
Confidence Level of Mean (95.0%)	1.18	0.17	1.24

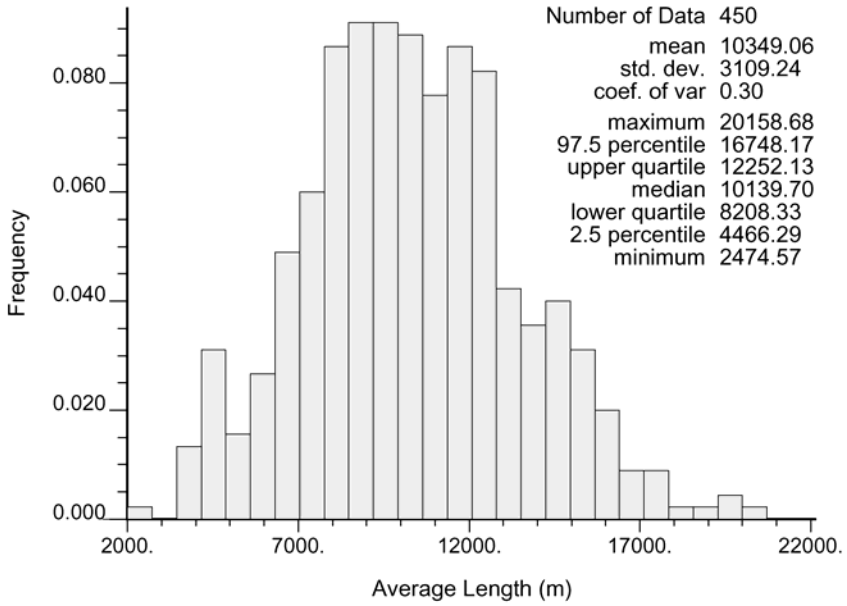

Figure B.14. Histogram of Average Length of Columbia River Shoreline Exceeding 20,000 pCi/L for FY 1992 Tritium in Grid 3

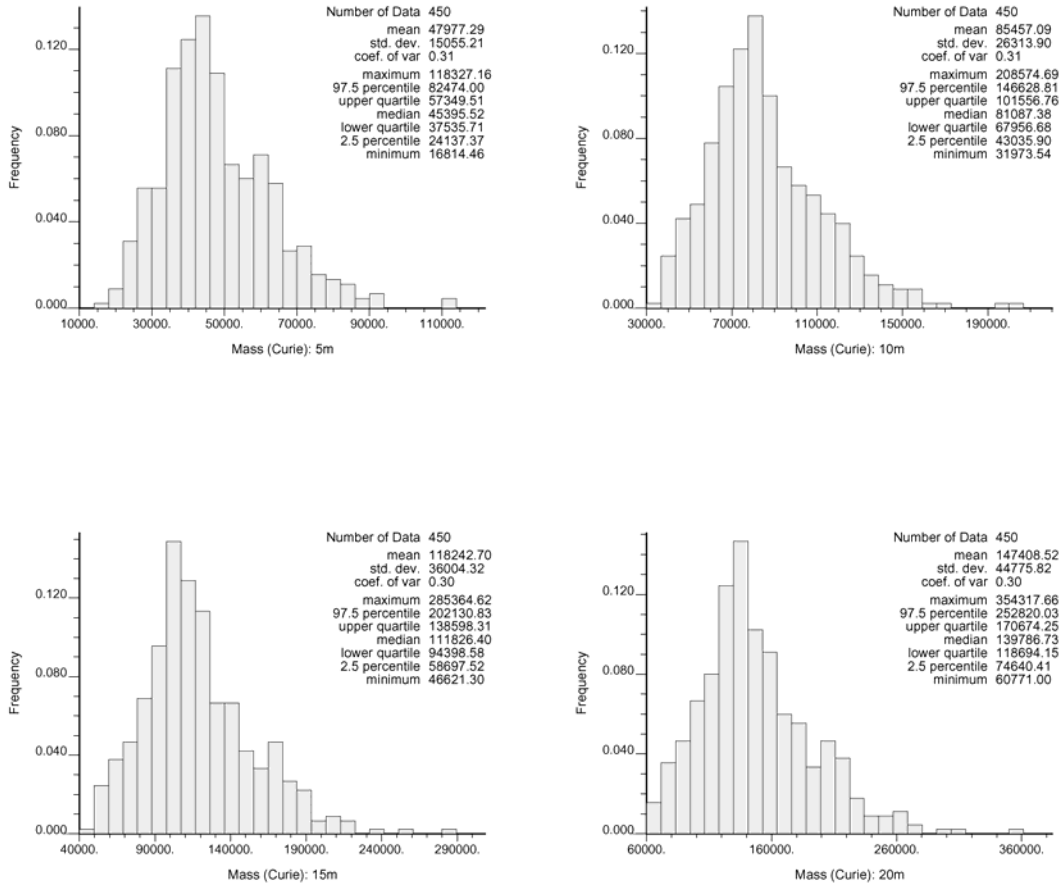

Figure B.15. Histograms of Total Activity in Simulations of FY 1992 Tritium within Sub-Area 1 of Grid 3 (200 East Area Plumes), Four Thickness Assumptions

Table B.12. Statistics of Total Activity of Simulations of FY 1992 Tritium within Sub-Area 1 of Grid 3 (200 East Area Plumes), Four Thickness Assumptions

Mass (Ci) in Depth	5 m	10 m	15 m	20 m
Mean	47,977.31	85,457.08	11,8242.70	147,408.47
Standard Error	710.50	1,241.83	1,699.15	2,113.10
Median	45,395.52	81,087.36	111,826.39	139,786.68
Standard Deviation	15,071.96	26,343.20	36,044.39	44,825.67
Kurtosis	1.42	1.33	1.24	1.18
Skewness	0.88	0.86	0.85	0.84
Range	101,512.70	176,601.14	238,743.31	293,546.67
Minimum	16,814.46	31,973.54	46,621.30	60,771.00
Maximum	118,327.16	208,574.68	285,364.61	354,317.67
Count	450	450	450	450
97.5^{th} Percentile	82,225.62	146,348.71	201,864.90	252,565.79
2.5^{th} Percentile	24,226.05	43,211.51	58,750.83	74,748.07
Confidence Level of Mean (95.0%)	1,396.32	2,440.52	3,339.28	4,152.80

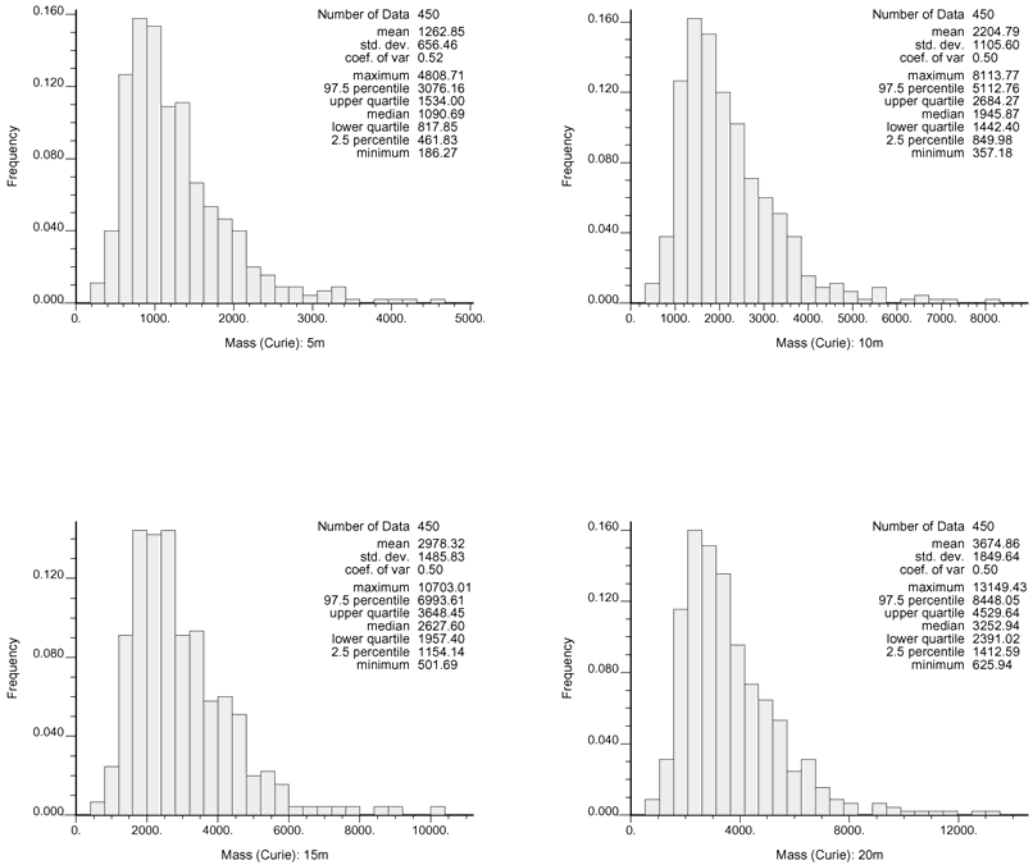

Figure B.16. Histograms of Total Activity in Simulations of FY 1992 Tritium within Sub-Area 2 of Grid 3 (200 East Area Plumes), Four Thickness Assumptions

Table B.13. Statistics of Total Activity of Simulations of FY 1992 Tritium within Sub-Area 2 of Grid 3 (200 East Area Plumes), Four Thickness Assumptions

Mass (Ci) in Depth	5 m	10 m	15 m	20 m
Mean	1,262.85	2,204.79	2,978.32	3,674.86
Standard Error	30.98	52.18	70.12	87.29
Median	1,090.69	1,945.86	2,627.59	3,252.94
Standard Deviation	657.19	1,106.83	1,487.48	1,851.70
Kurtosis	4.29	4.14	4.15	4.20
Skewness	1.69	1.63	1.63	1.64
Range	4,622.44	7,756.59	10,201.32	12,523.50
Minimum	186.27	357.18	501.69	625.94
Maximum	4,808.71	8,113.77	10,703.01	13,149.43
Count	450	450	450	450
97.5^{th} Percentile	3,065.12	5,067.22	6,972.57	8,292.36
2.5^{th} Percentile	467.39	865.78	1,169.19	1,422.89
Confidence Level of Mean (95.0%)	60.88	102.54	137.81	171.55

Appendix C

Figures and Data Tables for FY 2001 Technetium-99

Appendix C

Figures and Data Tables for FY 2001 Technetium-99

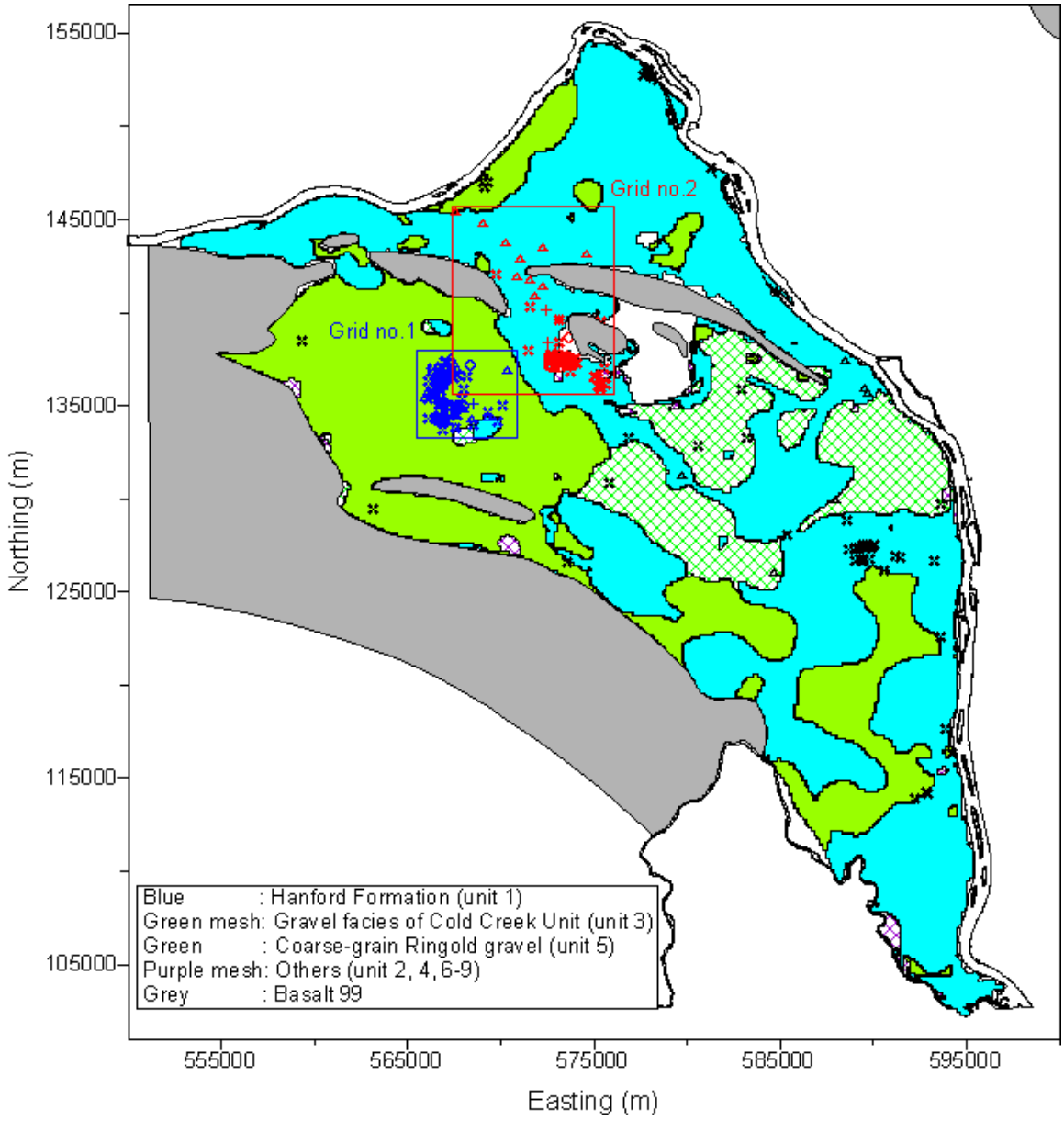

Figure C.1. Subsets of FY 2001 Technetium-99 Data and the Subcrop Formation Units at the FY 2001 Water Table

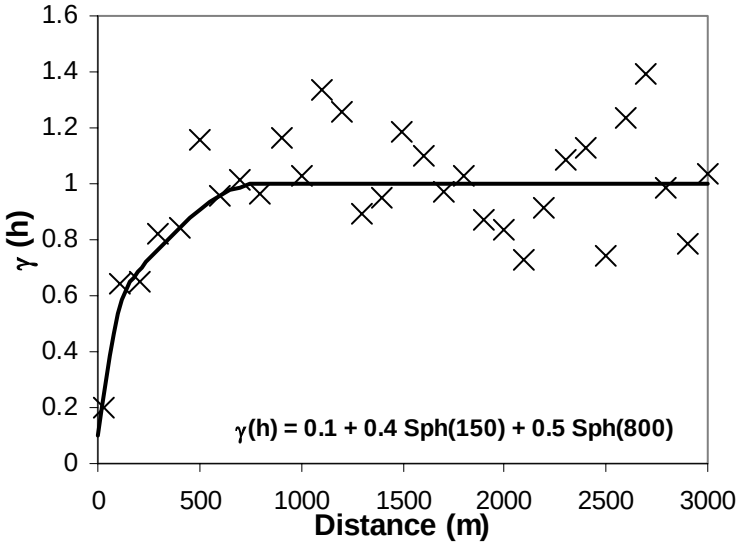

Figure C.2. Variograms and Models of Normal Scores of the FY 2001 Technetium-99 Data in Local Grid 1. Experimental variogram values designated by X, with the models fit to the data denoted by solid black lines.

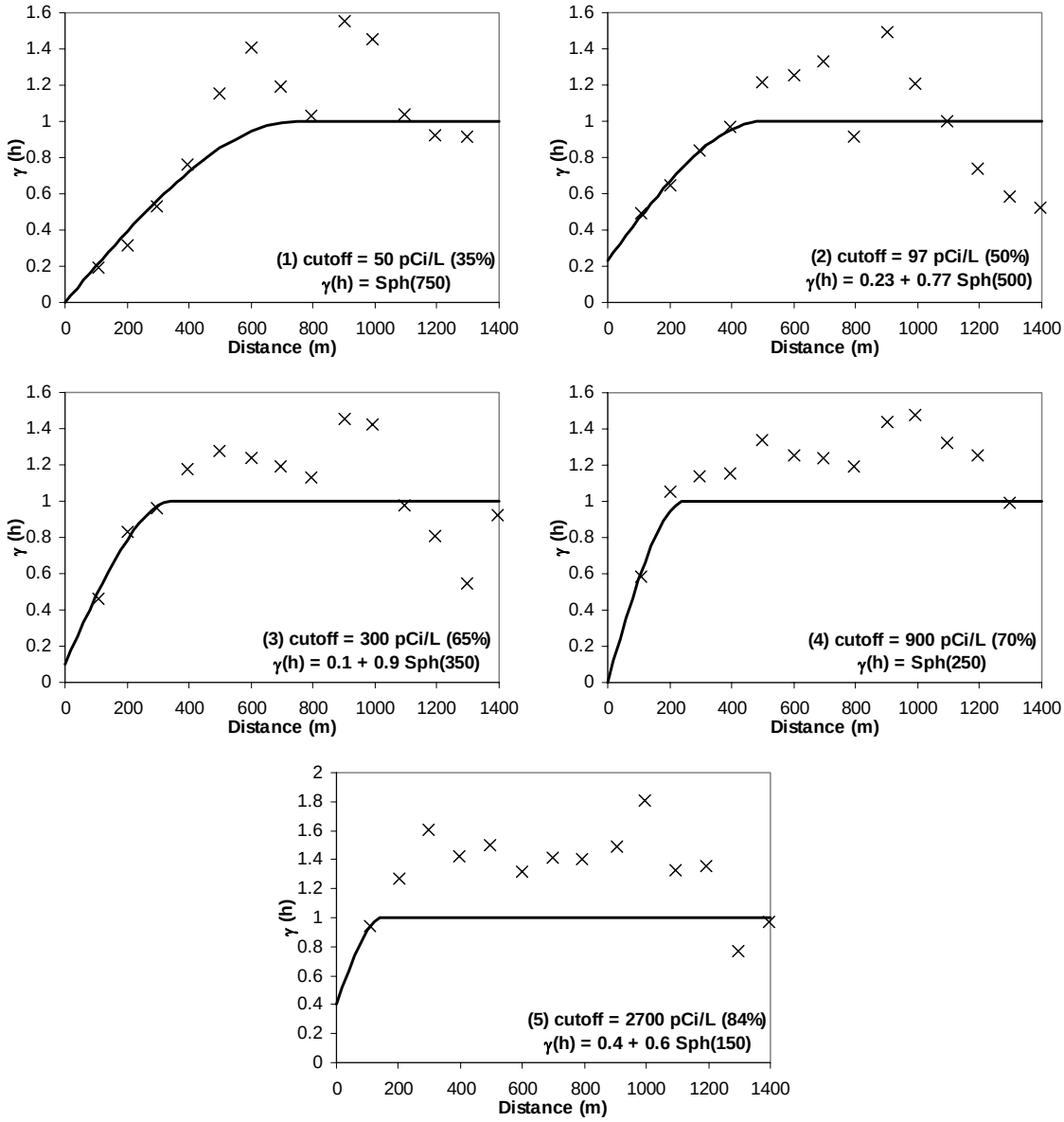

Figure C.3. Indicator Variograms and Models of the FY 2001 Technetium-99 Data in Local Grid 2. Experimental variogram values designated by X, with the models fit to the data denoted by olid black lines.

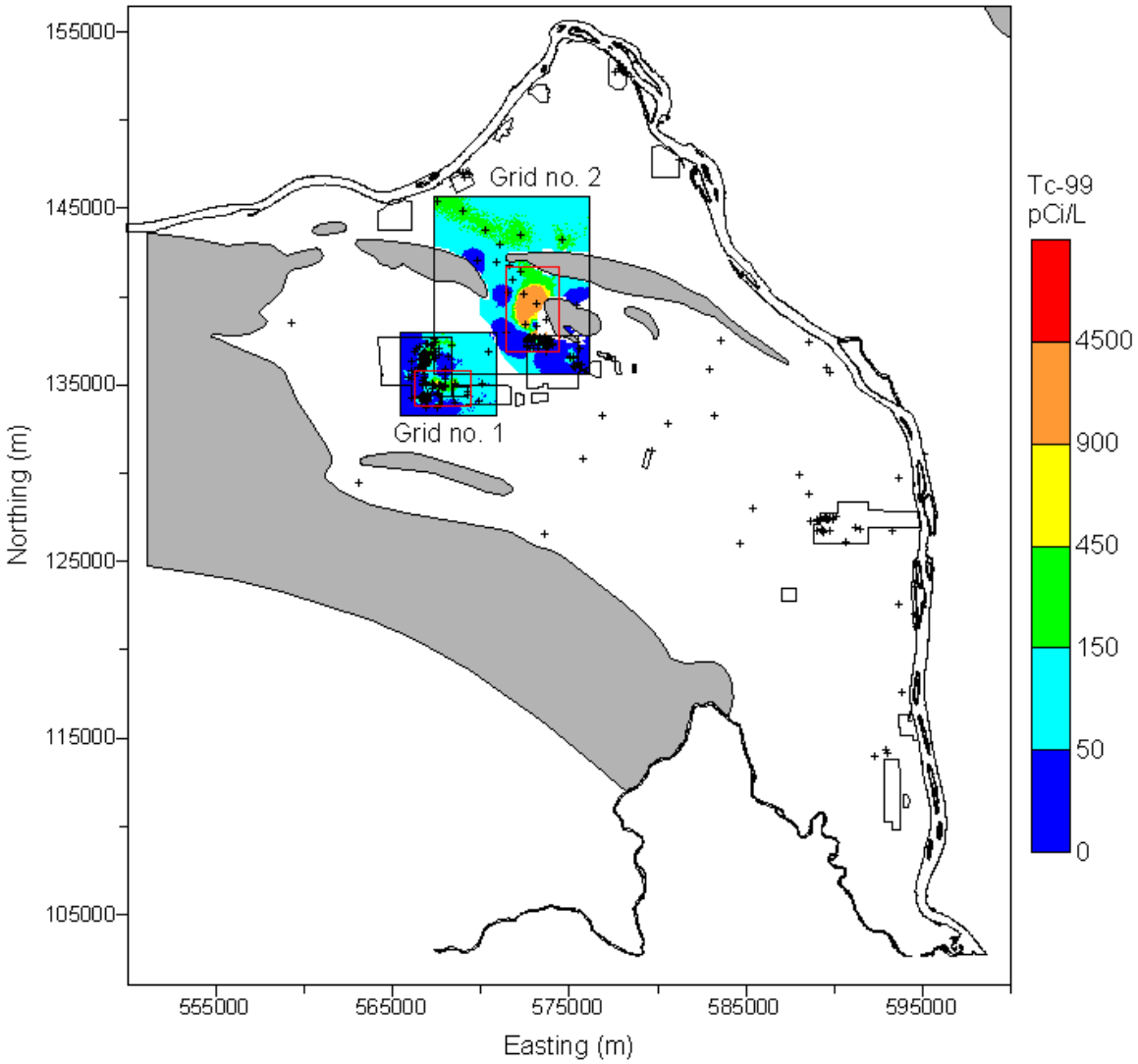

Figure C.4. Median of Simulations of FY 2001 Technetium-99 Concentrations for Grids 1 and 2

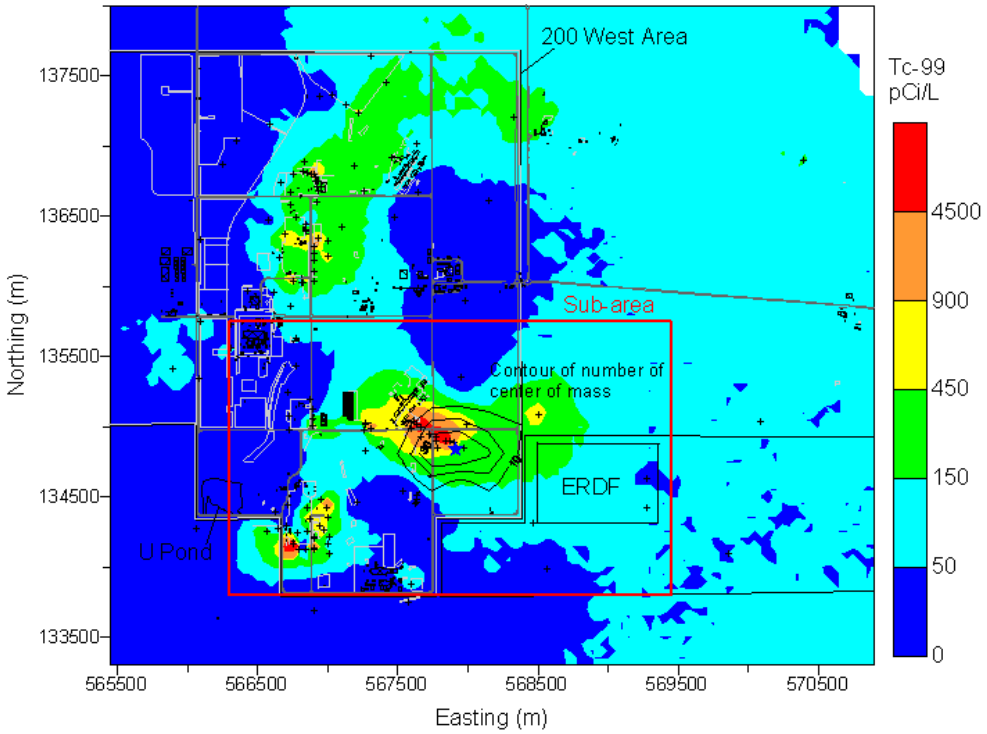

Figure C.5. **Median of Simulated FY 2001 Technetium-99 Concentrations in Grid 1 (200 West Area). Contours of the number of times that the center of mass within the sub-area occurred within cells of an upscaled grid are shown with the average centers of mass shown by blue star in the sub-area.**

Table C.1. **Coordinates for Sub-Area Boundary for Grid 1 (200 West Area) of FY 2001 Technetium-99**

Easting (m)	Northing (m)
566300	133800
569450	133800
569450	135750
566300	135750
566300	133800

Table C.2. Statistics of Centers of Mass of Individual Simulations of FY 2001 Technetium-99 Calculated for a Depth of 5 m for the Sub-Area of Grid 1 (200 West Area)

Coordinate (m)	Sub-Area	
	Easting	Northing
Mean	567987.9	134825.7
Standard Error	15.2	8.7
Median	567950.0	134826.9
Standard Deviation	263.2	151.2
Kurtosis	-0.29	-0.14
Skewness	0.40	-0.07
Range	1350.0	818.5
Minimum	567371.9	134398.8
Maximum	568721.8	135217.3
Count	300	300
97.5^{th} Percentile	568570.4	135117.1
2.5^{th} Percentile	567564.6	134515.1
Confidence Level of Mean (95.0%)	29.9	17.2

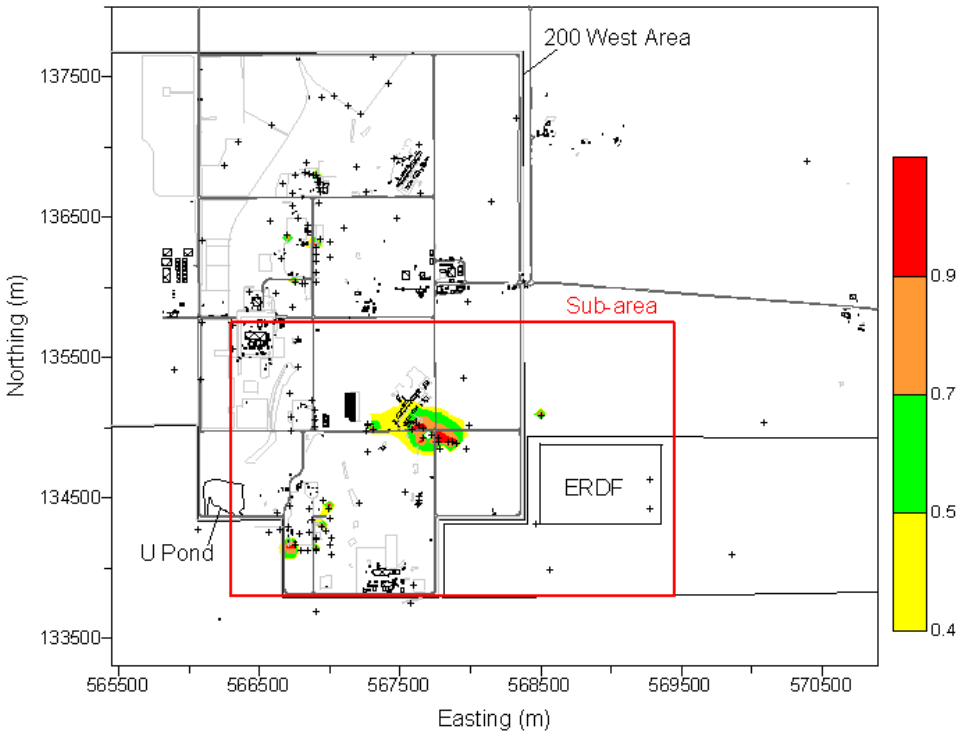

Figure C.6. Probability of Exceeding 900 pCi/L Based on Simulations of FY 2001 Technetium-99 in Grid 1 (200 West Area)

Table C.3. Area Exceeding 900 pCi/L for FY 2001 Technetium-99 for Each Simulation within Sub-Area of Grid 1 (200 West Area)

Area (km^2)	Sub-Area	Grid 1
Mean	0.71	2.71
Standard Error	0.01	0.05
Median	0.67	2.55
Standard Deviation	0.20	0.79
Kurtosis	0.16	0.31
Skewness	0.69	0.74
Range	1.07	4.05
Minimum	0.33	1.16
Maximum	1.40	5.21
Count	300	300
97.5^{th} Percentile	1.14	4.57
2.5^{th} Percentile	0.41	1.44
Confidence Level of Mean (95.0%)	0.02	0.09

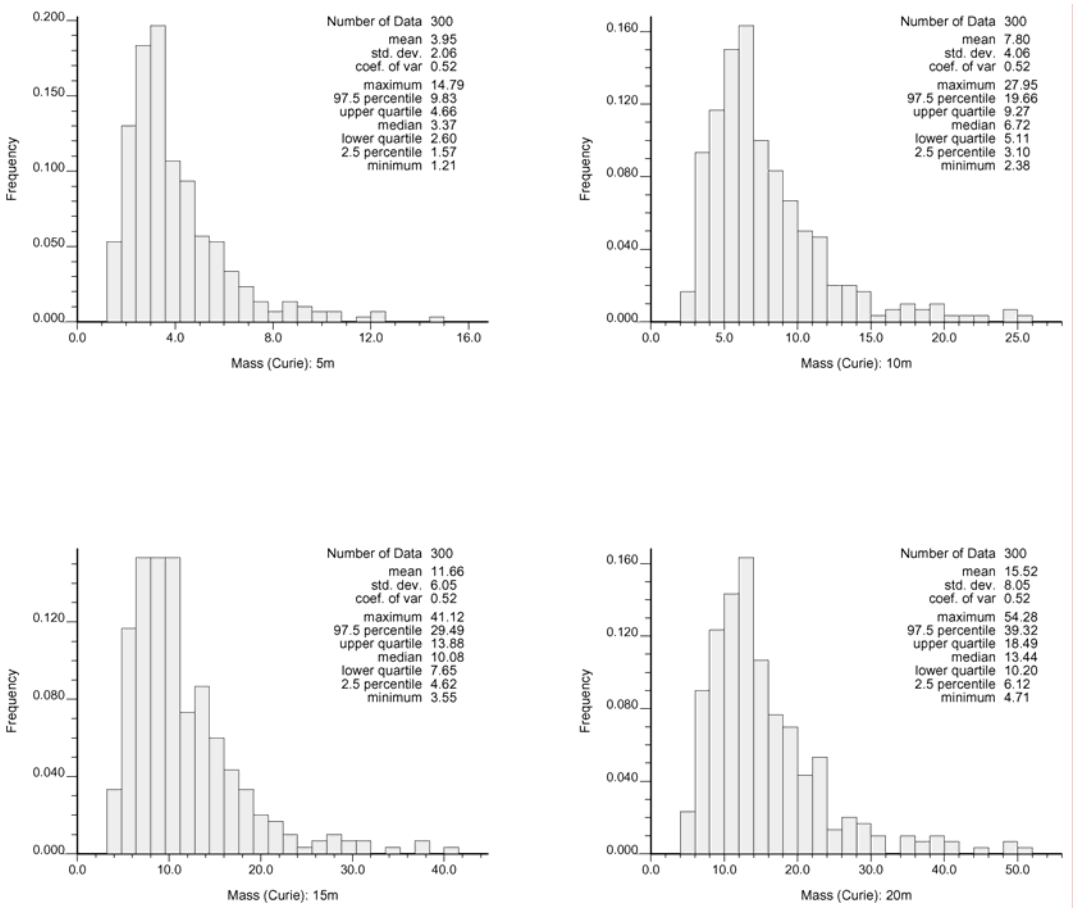

Figure C.7. Histograms of Total Activity in Simulations of FY 2001 Technetium-99 within Sub-Area of Grid 1 (200 West Area), Four Thickness Assumptions

Table C.4. Statistics of Total Activity of Simulations of FY 2001 Technetium-99 within Sub-Area of Grid 1 (200 West Area), Four Thickness Assumptions

Mass (Ci) in Depth	5 m	10 m	15 m	20 m
Mean	3.95	7.80	11.66	15.52
Standard Error	0.12	0.23	0.35	0.47
Median	3.37	6.72	10.08	13.44
Standard Deviation	2.07	4.06	6.06	8.06
Kurtosis	4.74	4.49	4.41	4.38
Skewness	1.86	1.84	1.83	1.83
Range	13.57	25.57	37.57	49.57
Minimum	1.21	2.38	3.55	4.71
Maximum	14.79	27.95	41.12	54.28
Count	300	300	300	300
97.5^{th} Percentile	9.83	19.66	29.49	39.32
2.5^{th} Percentile	1.57	3.10	4.62	6.12
Confidence Level of Mean (95.0%)	0.23	0.46	0.69	0.92

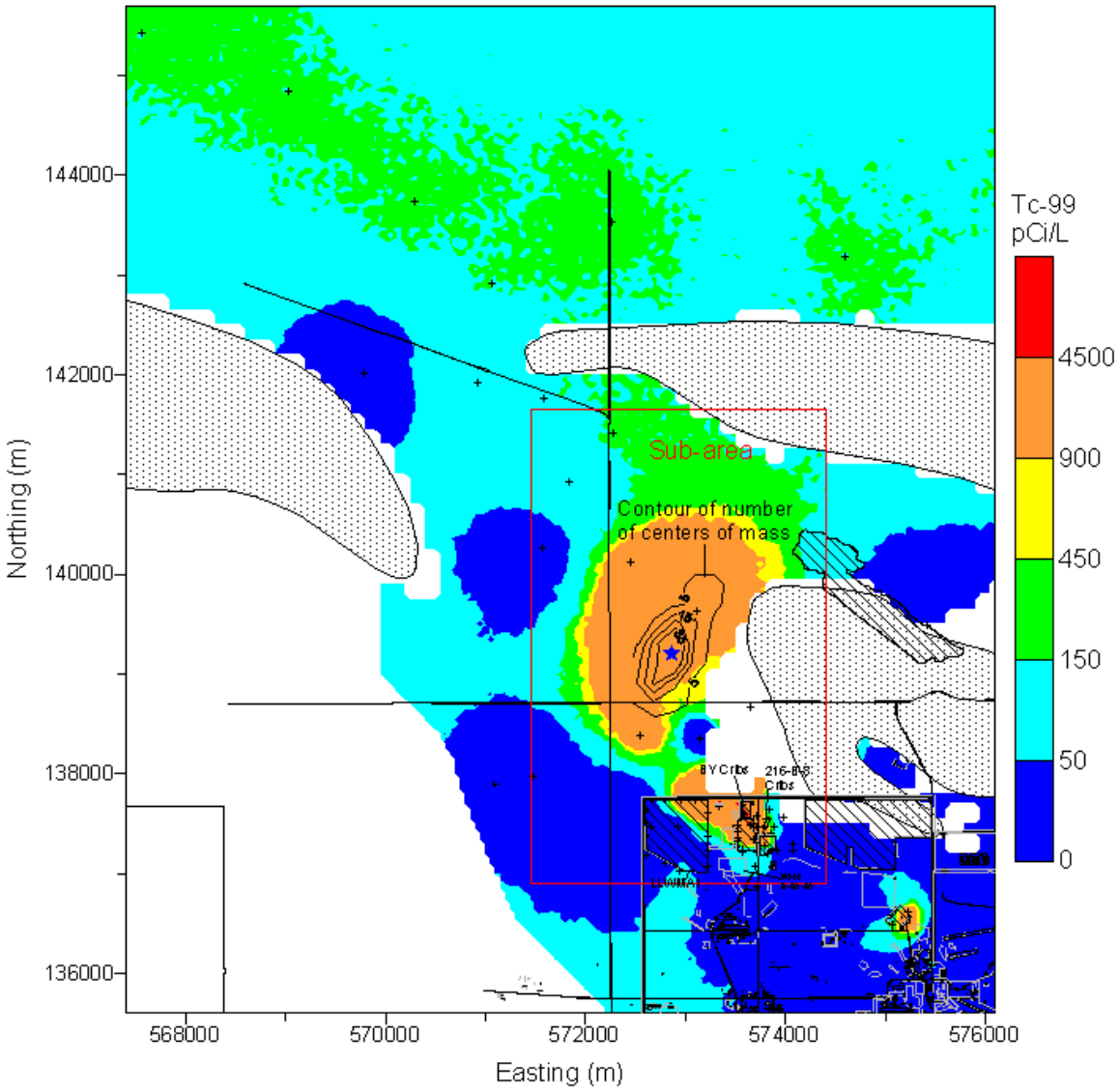

Figure C.8. Median of Simulated FY 2001 Technetium-99 Concentrations in Grid 2 (200 East Area Plume). Contours of the number of times that the center of mass within the sub-area occurred within cells of an upscaled grid are shown with the average centers of mass shown by blue star in the sub-area.

Table C.5. Coordinates for Sub-Area Boundary for Grid 2 (200 East Area) of FY 2001 Technetium-99

Easting (m)	Northing (m)
571450	141650
573143	141650
573780	141258
574149	141271
574400	141212
574400	139984
573913	139954
573706	139790
573632	139598
573617	139480
573558	139495
573499	139450
573483	139214
573364	139139
573379	139050
573217	139050
573202	138605
573350	138546
573350	138428
573215	138413
573215	137820
573676	137820
573706	137953
573795	137953
573795	137850
573928	137835
573987	137510
574400	137510
574400	136900
571450	136900
571450	141650

Table C.6. Statistics of Centers of Mass of Individual Simulations of FY 2001 Technetium-99 Calculated for a Depth of 5 m for the Sub-Area of Grid 2 (200 East Area Plume)

Coordinate (m)	Sub-Area	
	Easting	Northing
Mean	572769.0	139527.1
Standard Error	11.3	15.9
Median	572756.5	139521.3
Standard Deviation	226.9	318.7
Kurtosis	-0.12	0.17
Skewness	0.44	0.26
Range	1198.3	1930.8
Minimum	572294.6	138627.4
Maximum	573492.9	140558.1
Count	400	400
97.5^{th} Percentile	573289.7	140200.6
2.5^{th} Percentile	572373.2	138968.8
Confidence Level of Mean (95.0%)	22.3	31.3

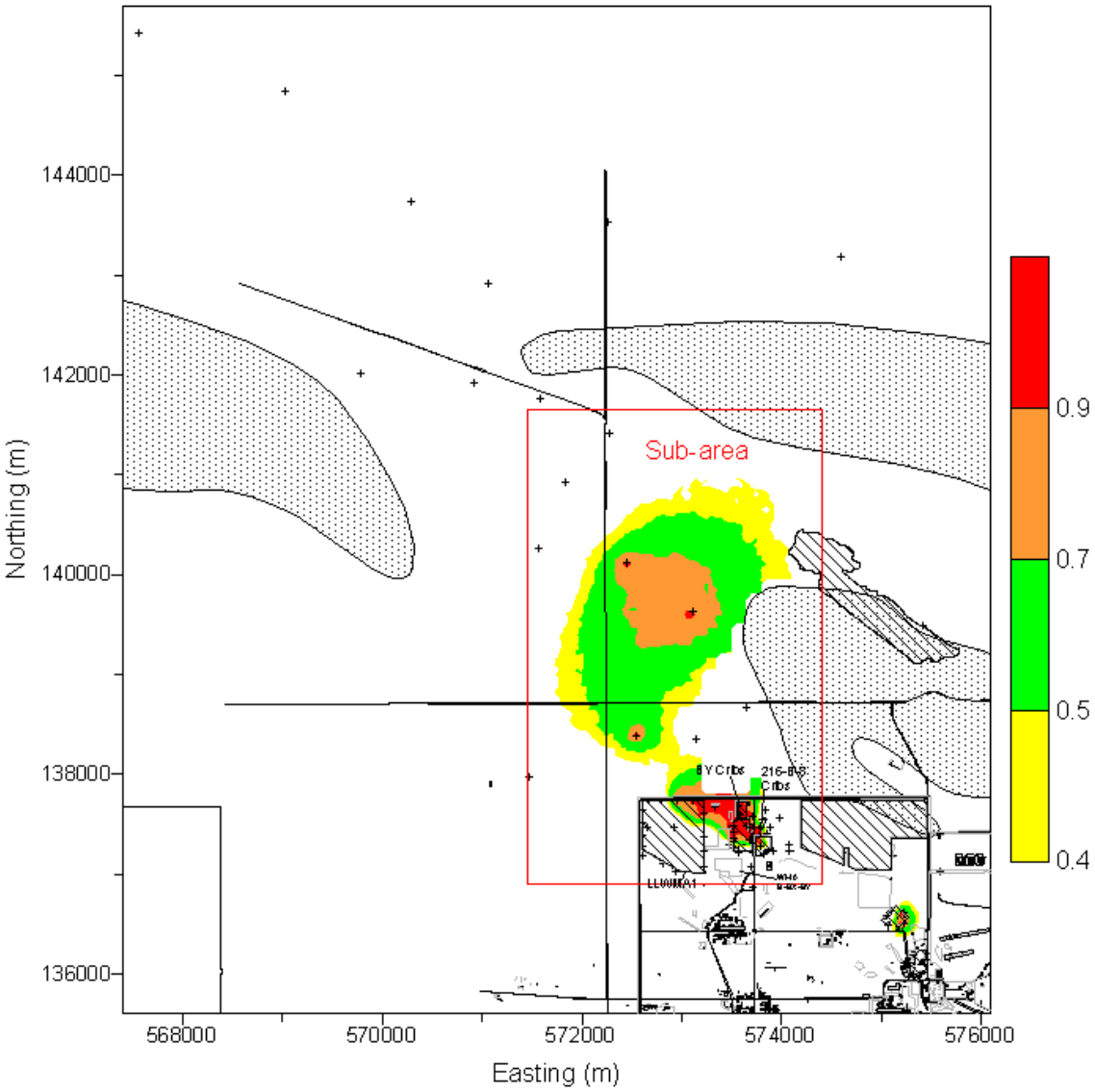

Figure C.9. Probability of Exceeding 900 pCi/L Based on Simulations of FY 2001 Technetium-99 in Grid 2 (200 East Area Plume)

Table C.7. Area Exceeding 900 pCi/L for FY 2001 Technetium-99 for Each Simulation within Sub-Area of Grid 2 (200 East Area Plume)

Area (km^2)	Sub-Area	Grid 2
Mean	3.89	10.59
Standard Error	0.05	0.16
Median	3.89	10.53
Standard Deviation	1.06	3.18
Kurtosis	-0.21	0.05
Skewness	0.07	0.41
Range	5.26	18.99
Minimum	1.34	3.27
Maximum	6.60	22.25
Count	400	400
97.5^{th} Percentile	6.17	17.24
2.5^{th} Percentile	1.81	5.09
Confidence Level of Mean (95.0%)	0.10	0.31

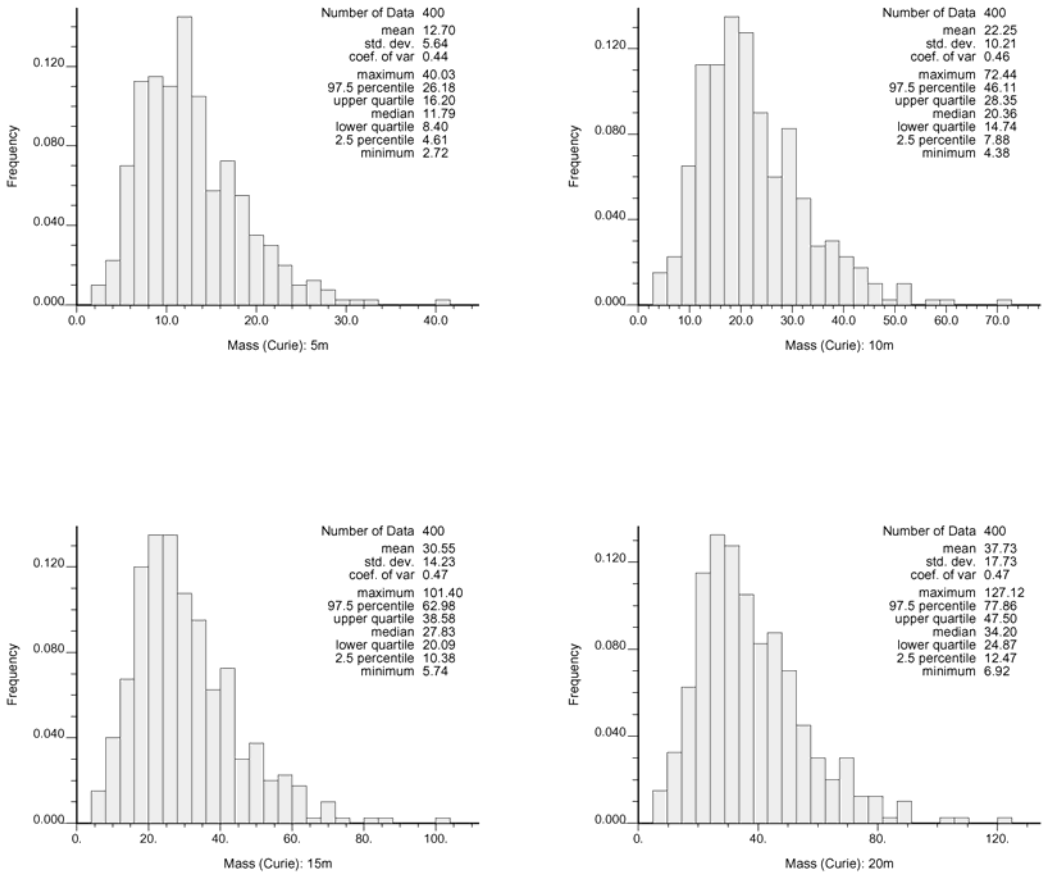

Figure C.10. Histograms of Total Activity in Simulations of FY 2001 Technetium-99 within Sub-Area of Grid 2 (200 East Area Plume), Four Thickness Assumptions

Table C.8. Statistics of Total Activity of Simulations of FY 2001 Technetium-99 within Sub-Area of Grid 2 (200 East Area Plume), Four Thickness Assumptions

Mass (Ci) in Depth	5 m	10 m	15 m	20 m
Mean	12.70	22.25	30.55	37.73
Standard Error	0.28	0.51	0.71	0.89
Median	11.79	20.36	27.82	34.20
Standard Deviation	5.65	10.22	14.25	17.75
Kurtosis	1.50	1.76	1.94	2.09
Skewness	0.99	1.06	1.10	1.13
Range	37.31	68.06	95.66	120.19
Minimum	2.72	4.38	5.74	6.92
Maximum	40.03	72.44	101.40	127.12
Count	400	400	400	400
97.5^{th} Percentile	26.48	46.47	63.05	78.51
2.5^{th} Percentile	4.60	7.87	9.90	12.41
Confidence Level of Mean (95.0%)	0.56	1.00	1.40	1.74

Appendix D

Figures and Data Tables for FY 1992 Technetium-99

Appendix D

Figures and Data Tables for FY 1992 Technetium-99

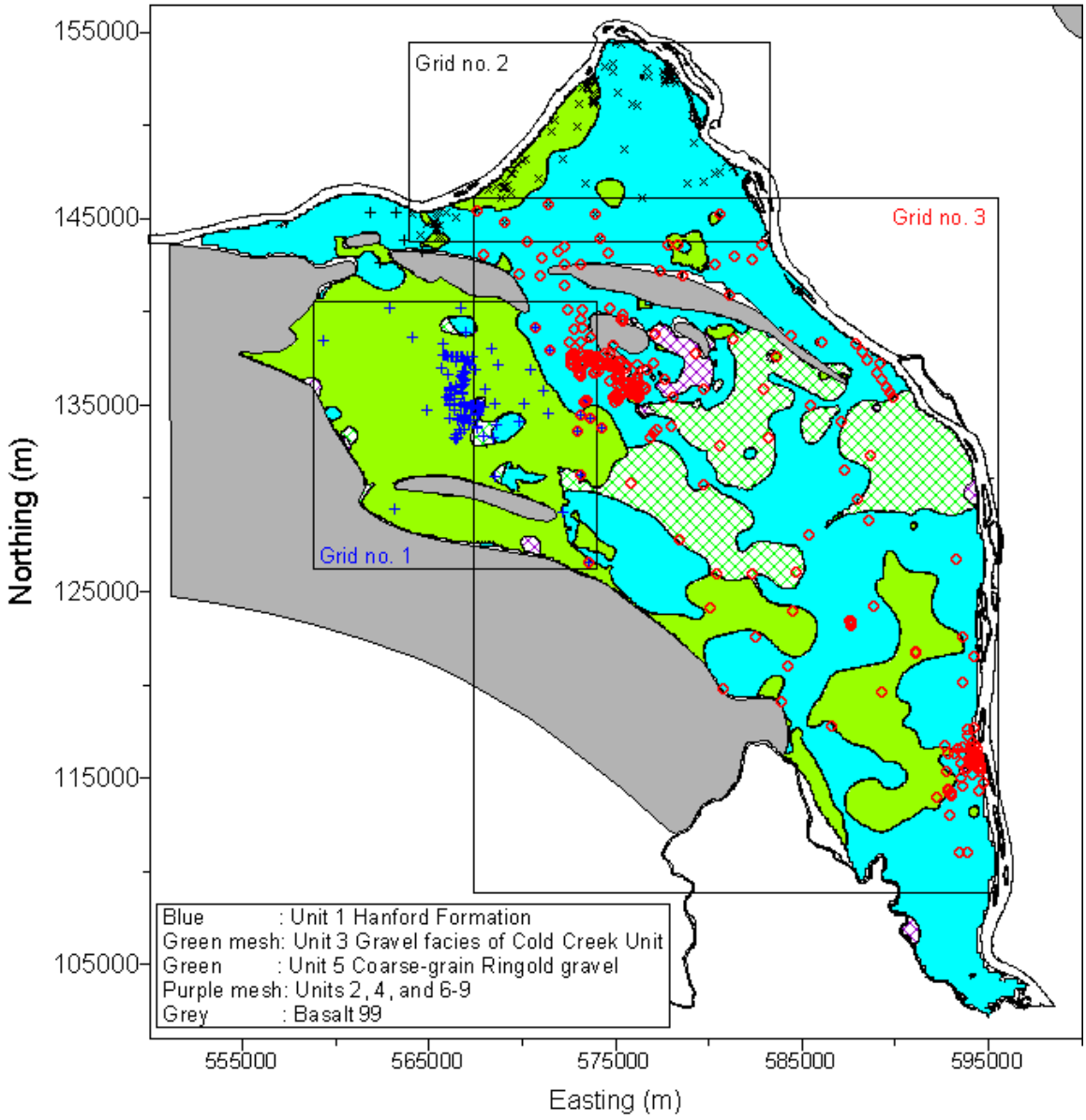

Figure D.1. Subsets of FY 1992 Technetium-99 Data and Subcrop Formation Units at the FY 1992 Water Table

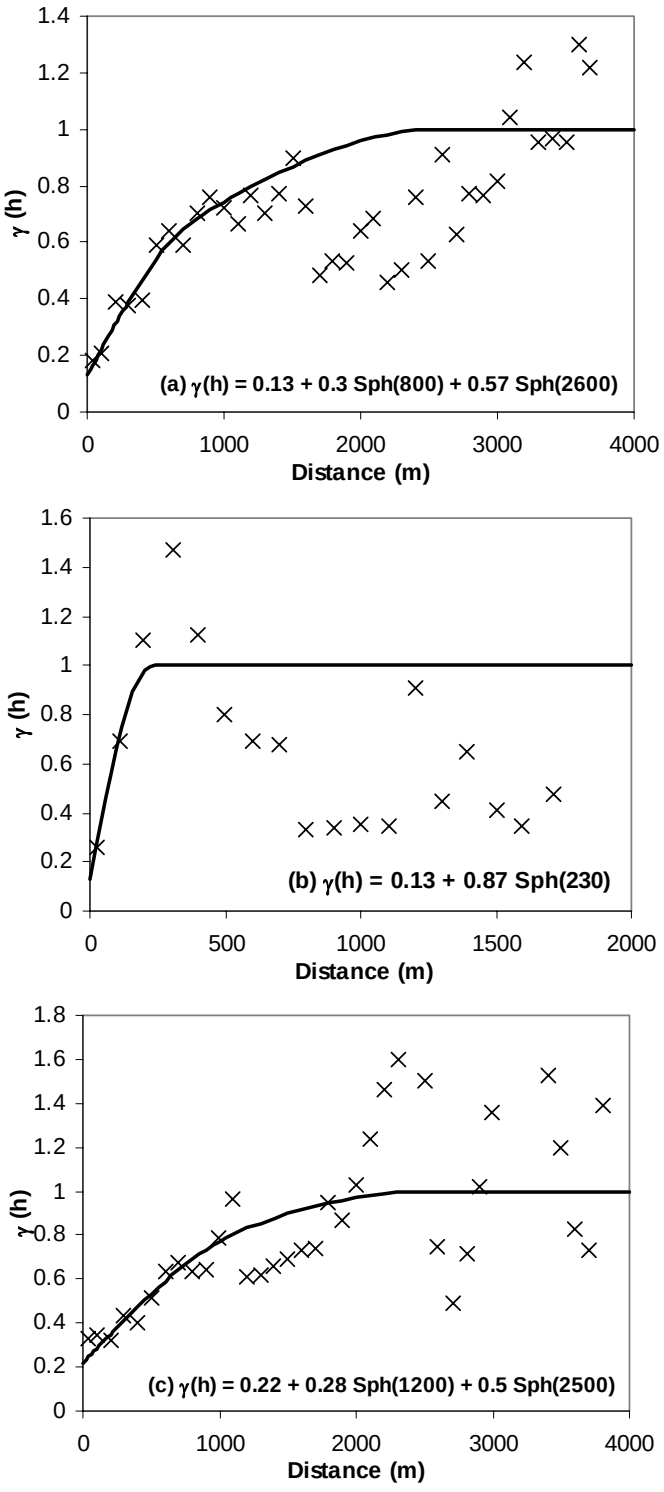

Figure D.2. Variograms and Models of Normal Scores of the FY 1992 Technetium-99 Data in Local Grid 1 (a), Grid 2 (b) and Grid 3 (c). Experimental variogram values designated by X, with the models fit to the data denoted by solid black lines.

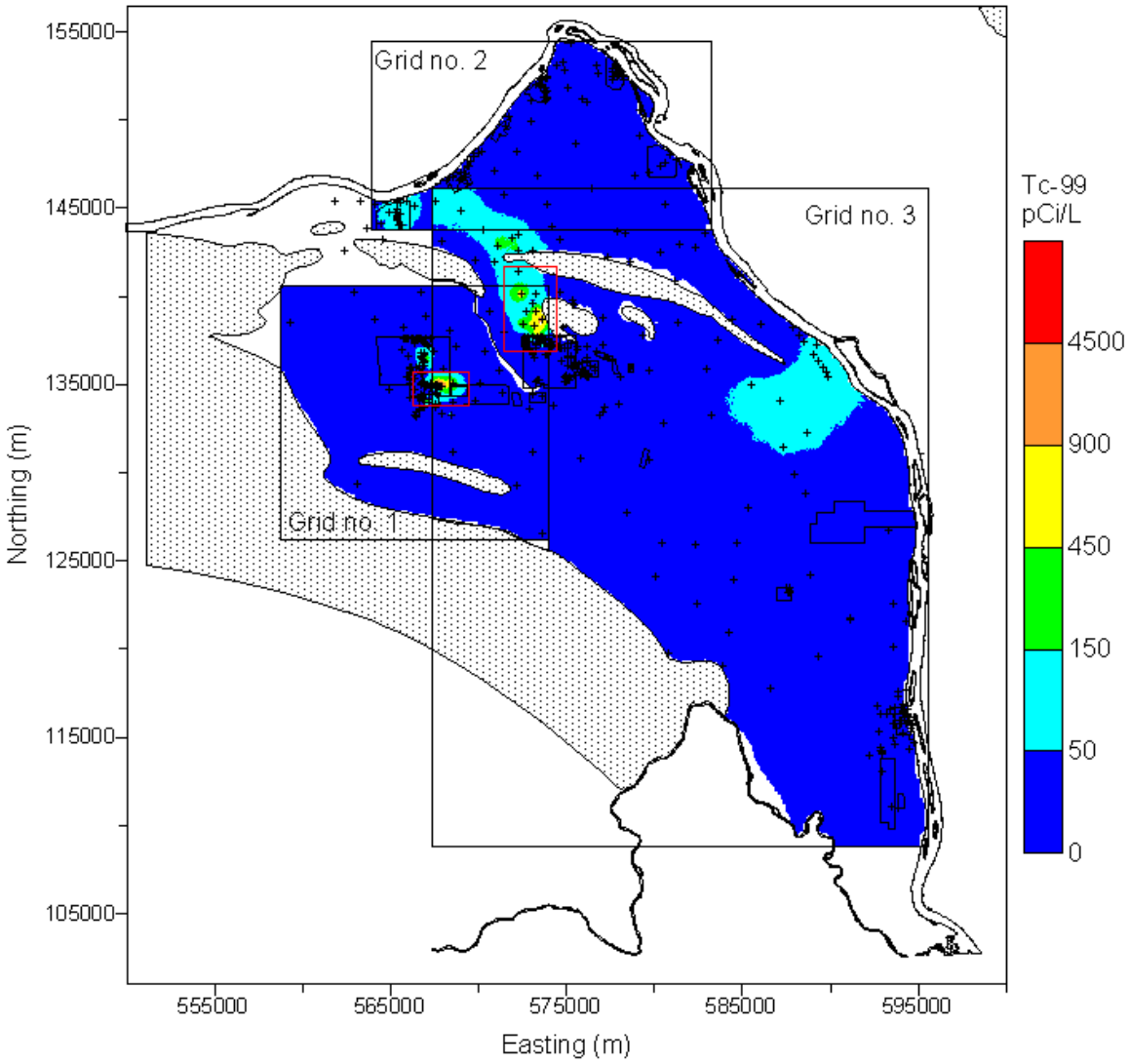

Figure D.3. Median of Simulations of FY 1992 Technetium-99 Concentrations for Grids 1, 2, and 3

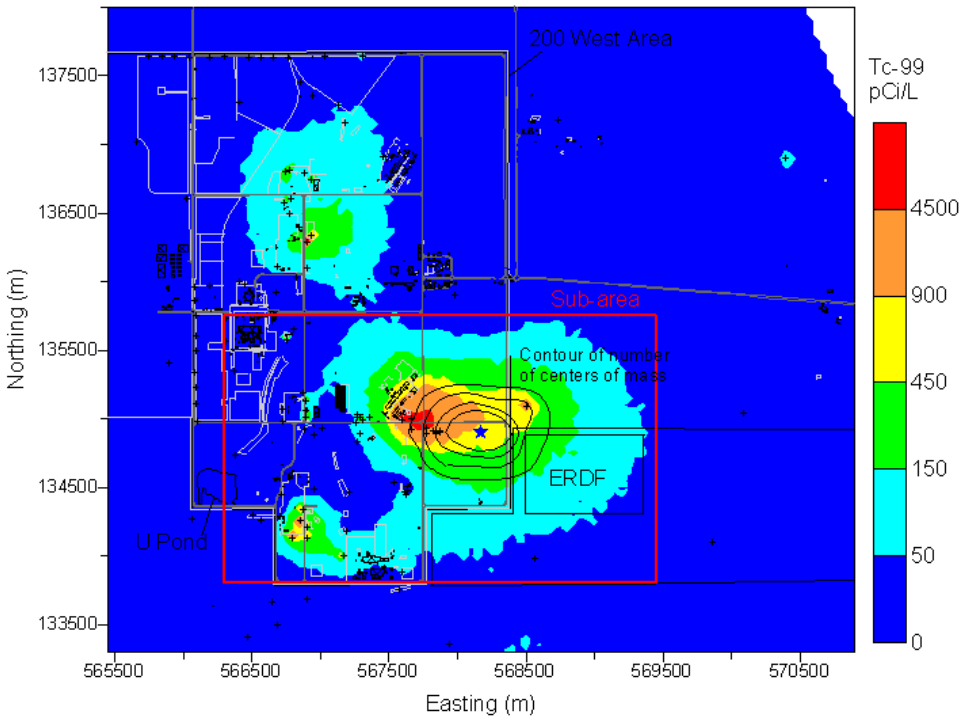

Figure D.4. **Median of Simulated FY 1992 Technetium-99 Concentrations in Grid 1 (200 West Area). Contours of the number of times that the center of mass within the sub-area occurred within cells of an upscaled grid are shown with the average centers of mass shown by blue star in the sub-area.**

Table D.1. **Coordinates for Sub-Area Boundary for Grid 1 (200 West Area) of FY 1992 Technetium-99**

Easting (m)	Northing (m)
566300	133800
569450	133800
569450	135750
566300	135750
566300	133800

Table D.2. Statistics of Centers of Mass of Individual Simulations of FY 1992 Technetium-99 Calculated for a Depth of 5 m for the Sub-Area of Grid 1 (200 West Area)

Coordinate (m)	Sub-Area	
	Easting	Northing
Mean	568227.8	134862.4
Standard Error	12.8	8.4
Median	568231.1	134854.6
Standard Deviation	270.9	179.0
Kurtosis	-0.46	-0.49
Skewness	-0.10	-0.08
Range	1361.2	870.2
Minimum	567534.6	134394.6
Maximum	568895.8	135264.8
Count	450	450
97.5^{th} Percentile	568723.9	135191.0
2.5^{th} Percentile	567689.8	134515.2
Confidence Level of Mean (95.0%)	25.1	16.6

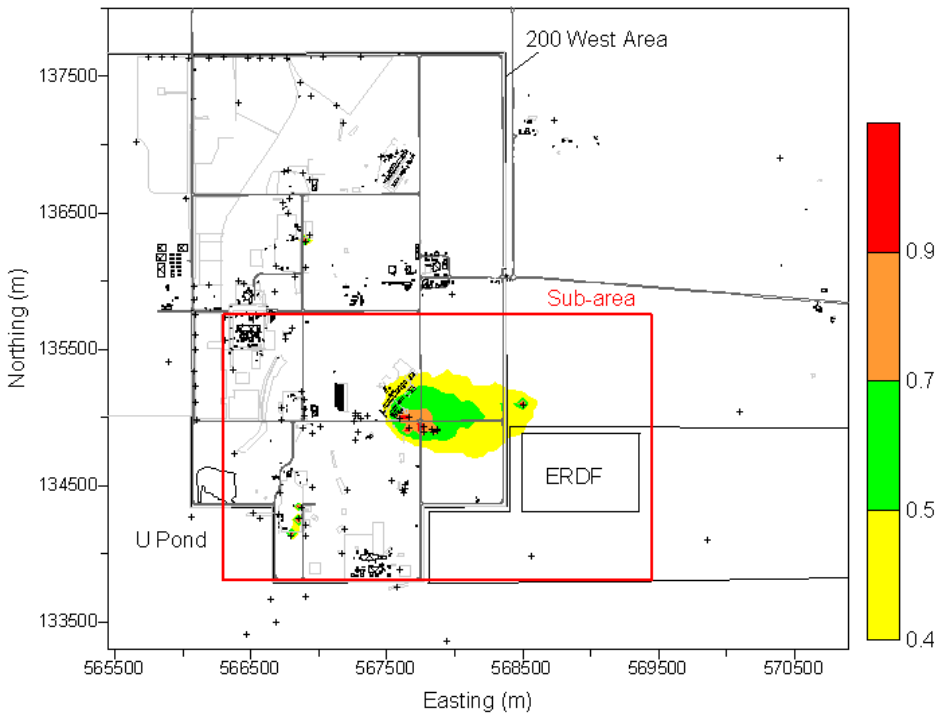

Figure D.5. Probability of Exceeding 900 pCi/L Based on Simulations of FY 1992 Technetium-99 in Grid 1 (200 West Area)

Table D.3. Area Exceeding 900 pCi/L for FY 1992 Technetium-99 for Each Simulation within Sub-Area of Grid 1 (200 West Area)

Area (km^2)	Sub-Area	Grid 1
Mean	1.01	6.55
Standard Error	0.02	0.14
Median	0.95	5.89
Standard Deviation	0.39	2.92
Kurtosis	-0.25	2.02
Skewness	0.56	1.19
Range	1.86	18.28
Minimum	0.27	1.55
Maximum	2.13	19.82
Count	450	450
97.5^{th} Percentile	1.92	13.67
2.5^{th} Percentile	0.41	2.64
Confidence Level of Mean (95.0%)	0.04	0.27

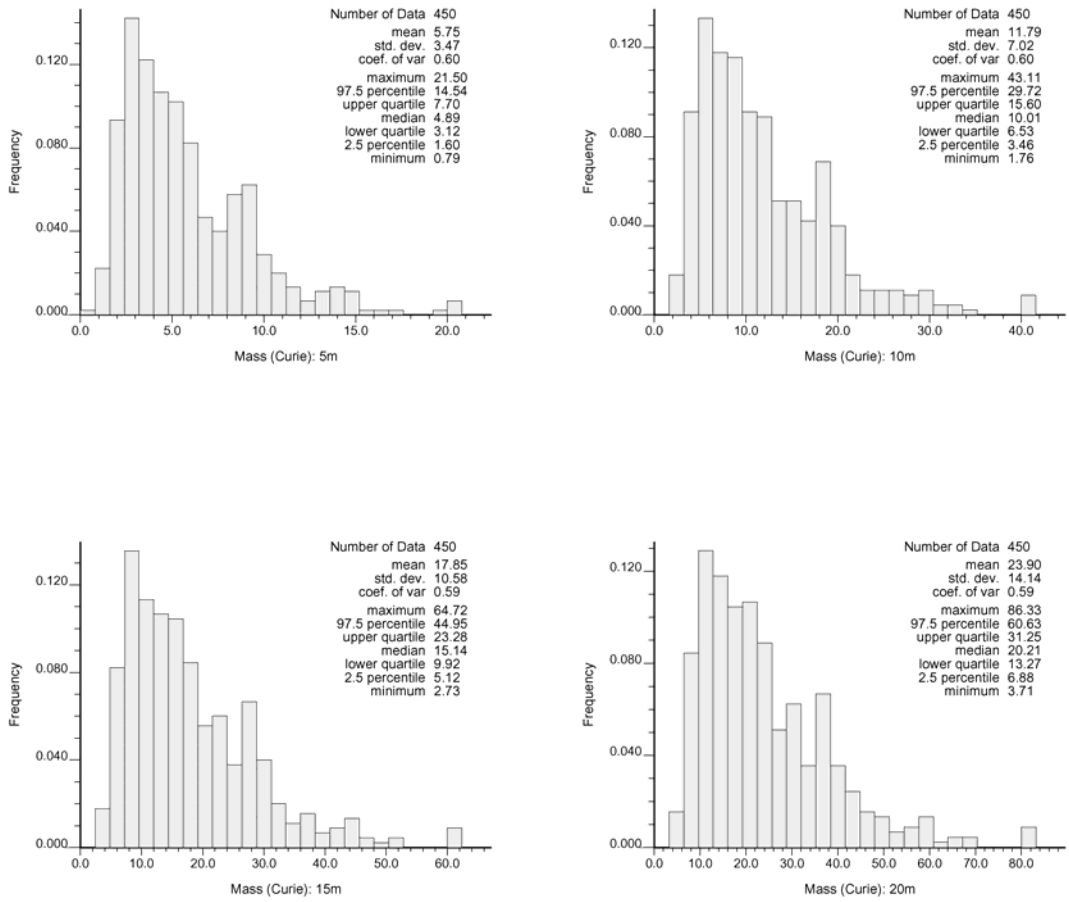

Figure D.6. Histograms of Total Activity in Simulations of FY 1992 Technetium-99 within the Sub-Area of Grid 1 (200 West Area), Four Thickness Assumptions

Table D.4. Statistics of Total Activity of Simulations of FY 1992 Technetium-99 within the Sub-Area of Grid 1 (200 West Area), Four Thickness Assumptions

Mass (Ci) in Depth	5 m	10 m	15 m	20 m
Mean	5.75	11.79	17.85	23.90
Standard Error	0.16	0.33	0.50	0.67
Median	4.89	10.01	15.14	20.21
Standard Deviation	3.48	7.03	10.59	14.16
Kurtosis	2.34	2.45	2.51	2.54
Skewness	1.36	1.37	1.38	1.39
Range	20.71	41.34	61.99	82.63
Minimum	0.79	1.76	2.74	3.71
Maximum	21.50	43.11	64.72	86.33
Count	450	450	450	450
97.5^{th} Percentile	14.54	29.59	44.79	60.63
2.5^{th} Percentile	1.62	3.50	5.12	6.92
Confidence Level of Mean (95.0%)	0.32	0.65	0.98	1.31

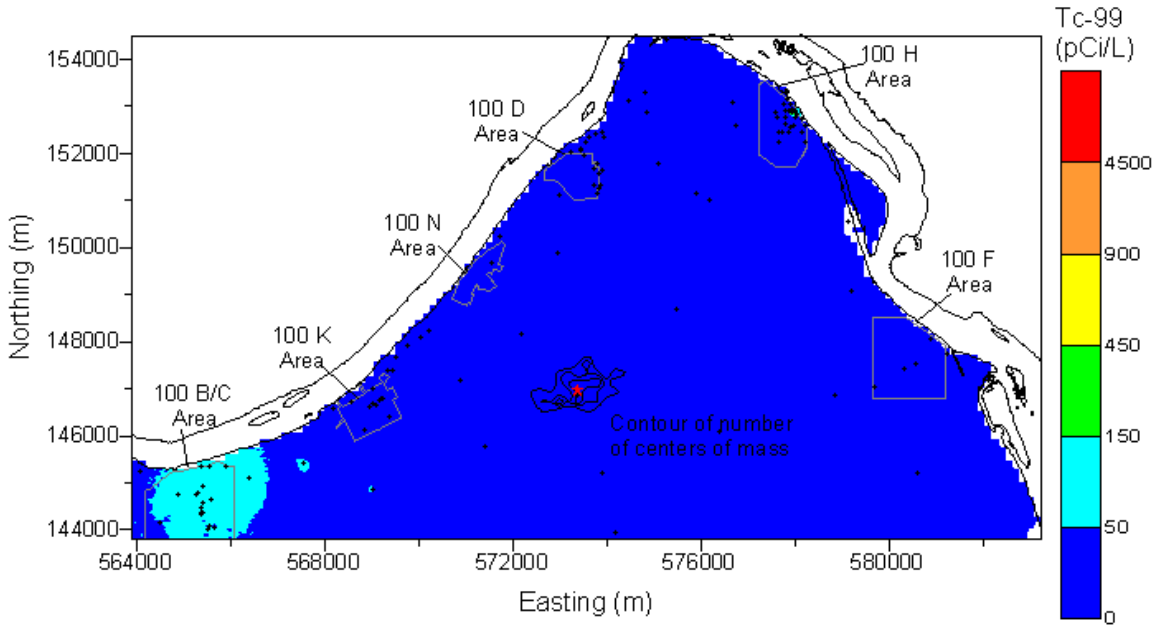

Figure D.7. Median of Simulated FY 1992 Technetium-99 Concentrations in Grid 2 (100 Areas). Contours of the number of times that the center of mass within the grid occurred within cells of an upscaled grid are shown with the average centers of mass shown by red star in the grid. The maximum technetium-99 activity in Grid 2 for FY 1992 is only 632 pCi/L. No values over the 900 pCi/L DWS were simulated in the grid, so several of the standard metrics do not apply to this grid, including the area above the drinking water standard and the length of the Columbia River shoreline above the drinking water standard.

Table D.5. Coordinates for Sub-Area Boundary for Grid 2 (100 Areas) of FY 1992 Technetium-99

Easting (m)	Northing (m)	Easting (m)	Northing (m)
563900	143800	574635	154500
563900	145566	575910	154500
564206	145277	577761	153410
564778	145277	578239	152710
565610	145502	579740	151371
566373	145754	579962	150987
566915	145882	579962	150573
567588	146172	579706	149806
567905	146522	579582	149614
568736	147033	579706	149200
569056	147447	580124	148787
569597	147959	580985	148211
570361	148692	581463	147764
570967	149392	582227	147350
572118	150987	581941	146902
572754	151785	582516	145724
573070	152199	582897	145118
573965	152744	583216	144129
573996	153030	583250	143800
574315	153828	563900	143800
574379	154144		

Table D.6. Statistics of the Locations of Centers of Mass for Simulations of FY 1992 Technetium-99 within Grid 2 (100 Areas)

Coordinate (m)	Easting	Northing
Mean	573369.1	146967.7
Standard Error	35.4	21.3
Median	573401.6	146950.4
Standard Deviation	613.8	369.4
Kurtosis	-0.14	0.07
Skewness	-0.24	0.14
Range	3427.1	2216.2
Minimum	571431.2	145937.8
Maximum	574858.3	148154.0
Count	300	300
97.5^{th} Percentile	574473.9	147716.8
2.5^{th} Percentile	572179.8	146234.4
Confidence Level (95.0%)	69.7	42.0

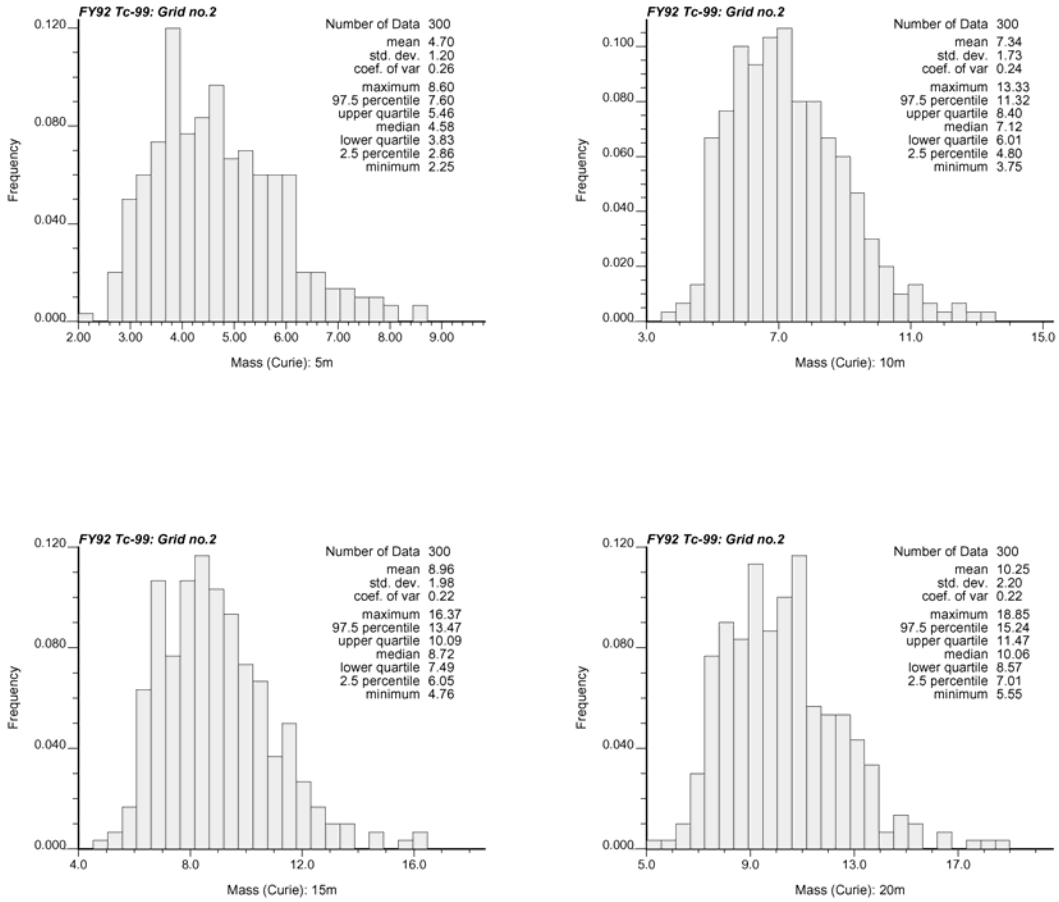

Figure D.8. Histograms of Total Activity in Simulations of FY 1992 Technetium-99 within Grid 2 (100 Areas), Four Thickness Assumptions

Table D.7. Statistics of Total Activity of Simulations of FY 1992 Technetium-99 within Grid 2 (100 Areas), Four Thickness Assumptions

Mass (Ci) in Depth	5 m	10 m	15 m	20 m
Mean	4.70	7.34	8.96	10.25
Standard Error	0.07	0.10	0.11	0.13
Median	4.58	7.12	8.72	10.06
Standard Deviation	1.21	1.73	1.98	2.21
Kurtosis	0.16	0.48	0.86	1.05
Skewness	0.64	0.72	0.79	0.81
Range	6.35	9.58	11.61	13.30
Minimum	2.25	3.75	4.76	5.55
Maximum	8.60	13.33	16.37	18.85
Count	300	300	300	300
97.5^{th} Percentile	7.60	11.32	13.47	15.24
2.5^{th} Percentile	2.86	4.80	6.05	7.01
Confidence Level of Mean (95.0%)	0.14	0.20	0.23	0.25

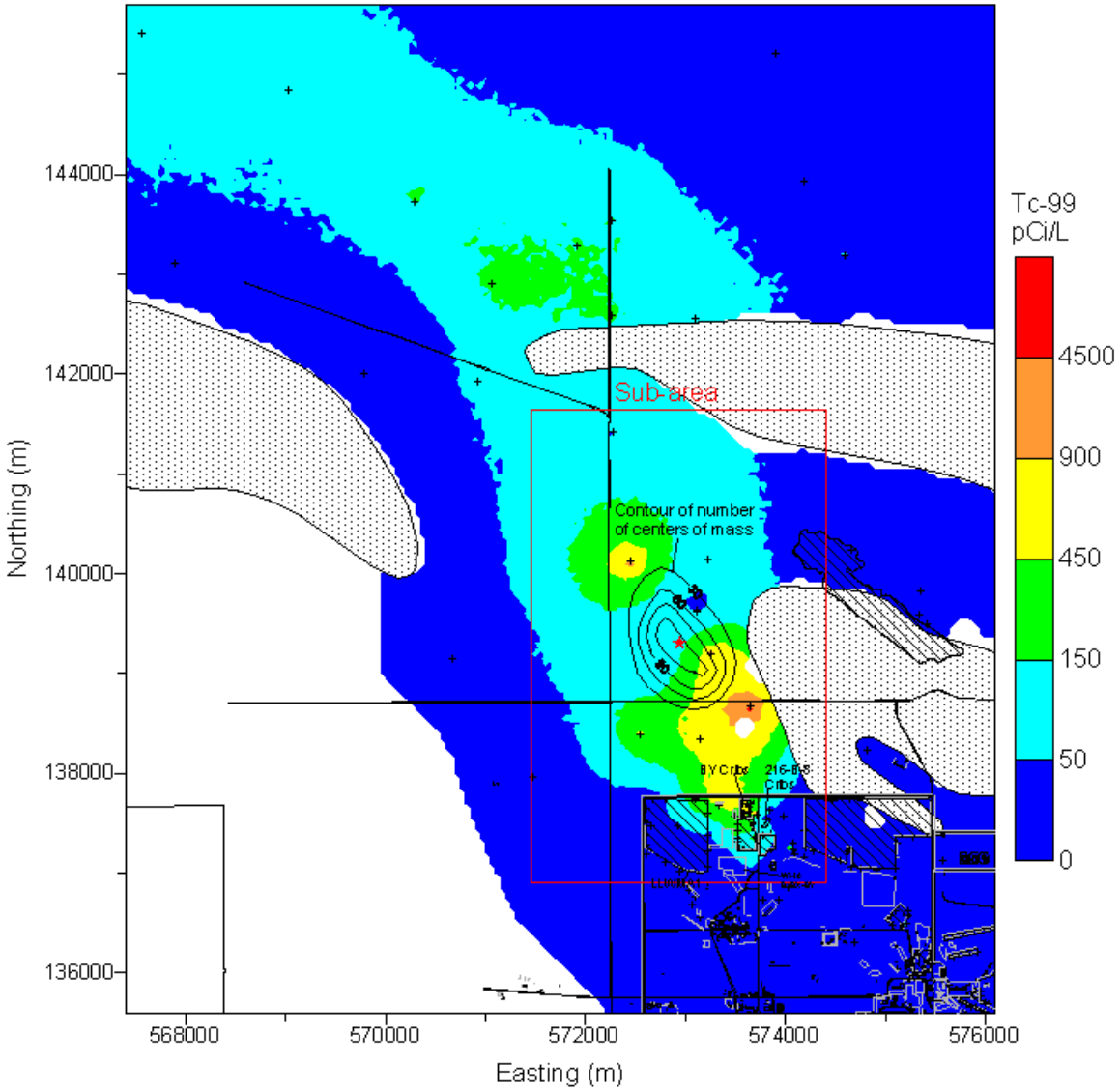

Figure D.9. **Median of Simulated FY 1992 Technetium-99 Concentrations in Grid 3 (200 East Area Plume). Contours of the number of times that the center of mass within the sub-area occurred within cells of an upscaled grid are shown with the average centers of mass shown by red star in the sub-area.**

Table D.8. Coordinates for Sub-Area Boundary for Grid 3 (200 East Area) of FY 1992 Technetium-99

Easting (m)	Northing (m)
571450	136900
574400	136900
574400	137731
574231	137856
573860	138723
573645	139197
573645	139612
573698	139739
573839	139834
573942	139879
574400	139864
574400	141205
574238	141212
574202	141256
574142	141256
574105	141205
573713	141205
573282	141568
573098	141650
571450	141650
571450	136900

Table D.9. Statistics of Centers of Mass of Individual Simulations of FY 1992 Technetium-99 Calculated for a Depth of 5 m for Sub-Area of Grid 3 (200 East Area Plume)

Coordinate (m)	Sub-Area	
	Easting	Northing
Mean	572723.3	139632.1
Standard Error	10.0	14.4
Median	572721.9	139628.1
Standard Deviation	243.9	351.6
Kurtosis	0.45	-0.59
Skewness	0.18	-0.01
Range	1592.2	1732.8
Minimum	572059.9	138739.3
Maximum	573652.1	140472.1
Count	600	600
97.5^{th} Percentile	573217.1	140310.3
2.5^{th} Percentile	572225.3	138948.4
Confidence Level of Mean (95.0%)	19.6	28.2

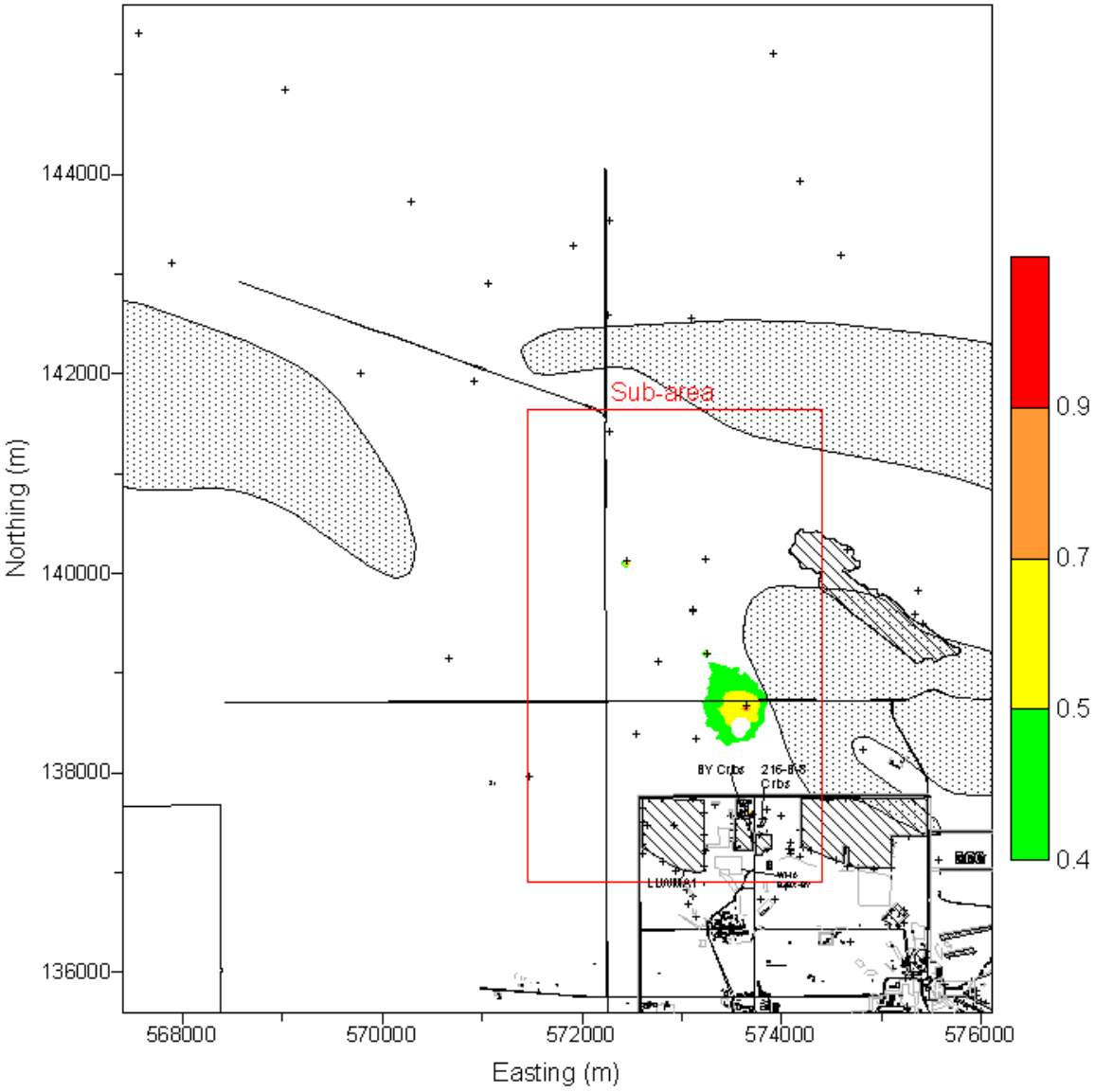

Figure D.10. Probability of Exceeding 900 pCi/L Based on Simulations of FY 1992 Technetium-99 in Grid 3 (200 East Area Plume)

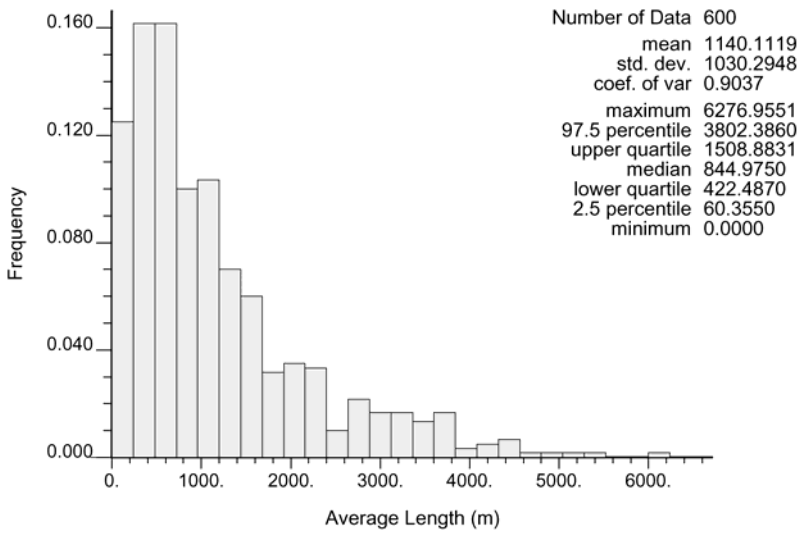

Figure D.11. Histogram of the Average Length of Columbia River Shoreline Exceeding 900 pCi/L for FY 1992 Technetium-99 in Grid 3 (200 East Area)

Table D.10. Area Exceeding 900 pCi/L for FY 1992 Technetium-99 for Each Simulation within Sub-Area of Grid 3 (200 East Area Plume)

Area (km^2)	Sub-Area	Grid 3
Mean	1.32	13.30
Standard Error	0.02	0.17
Median	1.25	12.96
Standard Deviation	0.48	4.18
Kurtosis	1.50	1.04
Skewness	0.98	0.72
Range	3.30	28.18
Minimum	0.36	4.34
Maximum	3.66	32.52
Count	600	600
97.5^{th} Percentile	2.48	22.66
2.5^{th} Percentile	0.61	6.86
Confidence Level of Mean (95.0%)	0.04	0.33

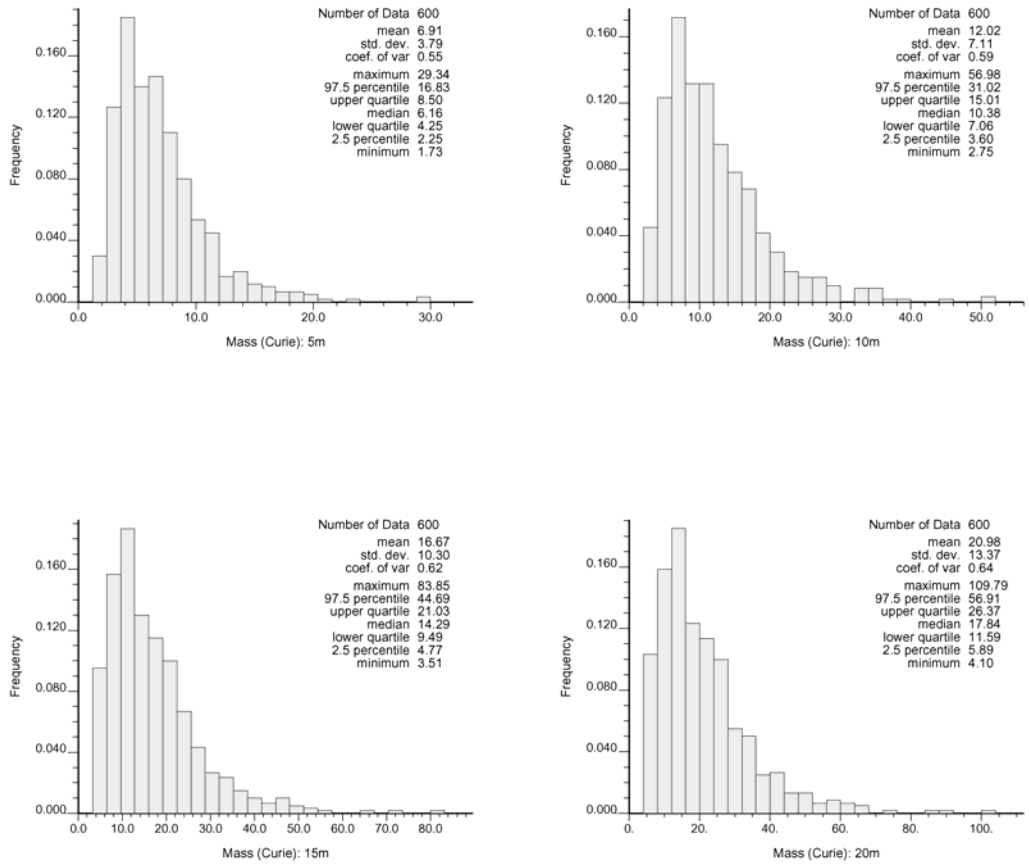

Figure D.12. Histograms of Total Activity in Simulations of FY 1992 Technetium-99 within the Sub-Area of Grid 3 (200 East Area Plume), Four Thickness Assumptions

Table D.11. Statistics of Total Activity of Simulations of FY 1992 Technetium-99 within the Sub-Area of Grid 3 (200 East Area Plume), Four Thickness Assumptions

Mass (Ci) in Depth	5 m	10 m	15 m	20 m
Mean	6.91	12.02	16.67	20.98
Standard Error	0.15	0.29	0.42	0.55
Median	6.16	10.38	14.29	17.84
Standard Deviation	3.79	7.11	10.31	13.38
Kurtosis	4.89	5.37	5.64	5.89
Skewness	1.71	1.80	1.85	1.89
Range	27.61	54.23	80.34	105.69
Minimum	1.73	2.75	3.51	4.10
Maximum	29.34	56.98	83.85	109.79
Count	600	600	600	600
97^{th} Percentile	17.07	32.07	45.88	57.37
2.5^{th} Percentile	2.24	3.58	4.76	5.86
Confidence Level of Mean (95.0%)	0.30	0.57	0.83	1.07

Appendix E

Figures and Data Tables for FY 2001 Iodine-129

Appendix E

Figures and Data Tables for FY 2001 Iodine-129

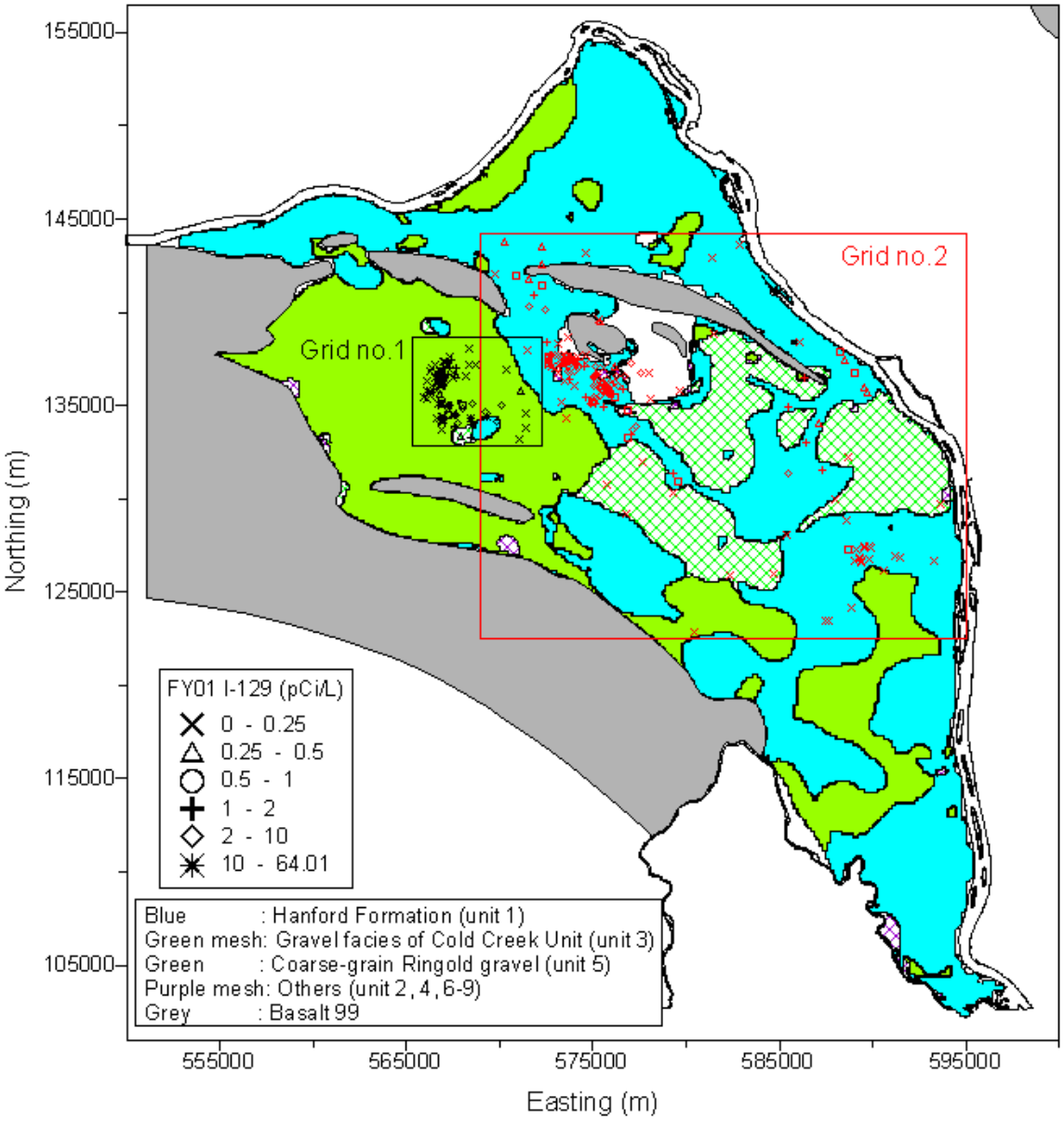

Figure E.1. Subsets of FY 2001 Iodine-129 Data and Subcrop Formation Units at the FY 2001 Water Table

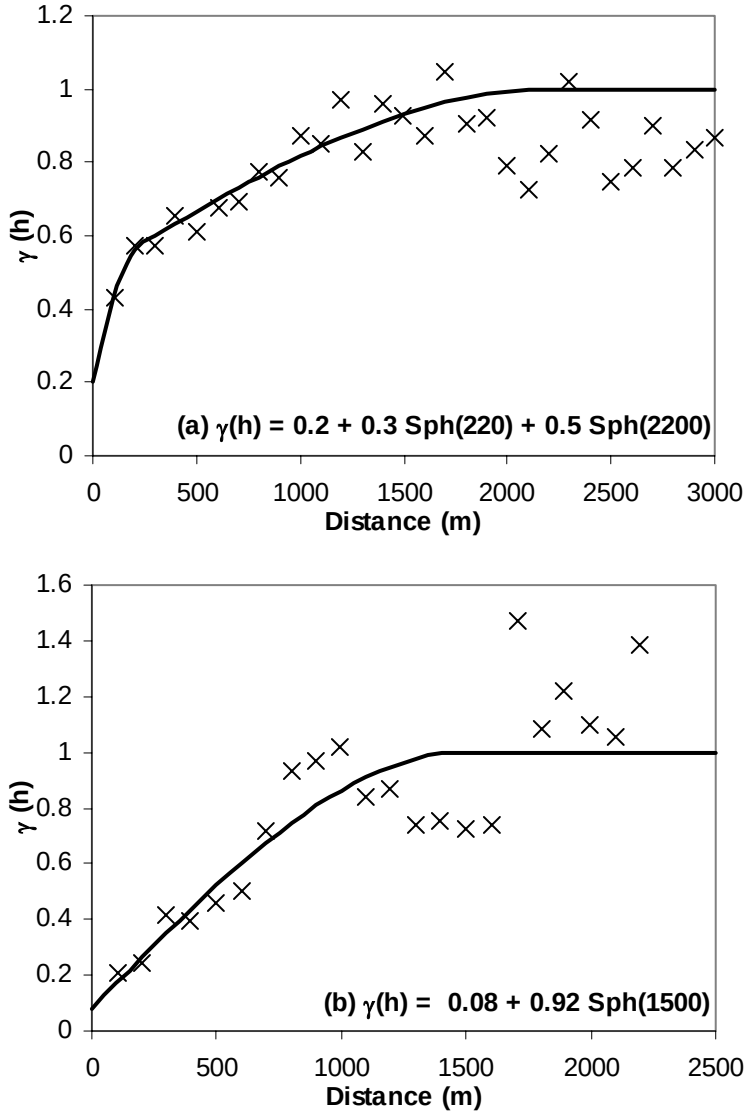

Figure E.2. Variograms and Models of Normal Scores of the FY 2001 Iodine-129 Data in Local Grid 1 (a) and Grid 2 (b). Experimental variogram values designated by X, with the models fit to the data denoted by solid black lines.

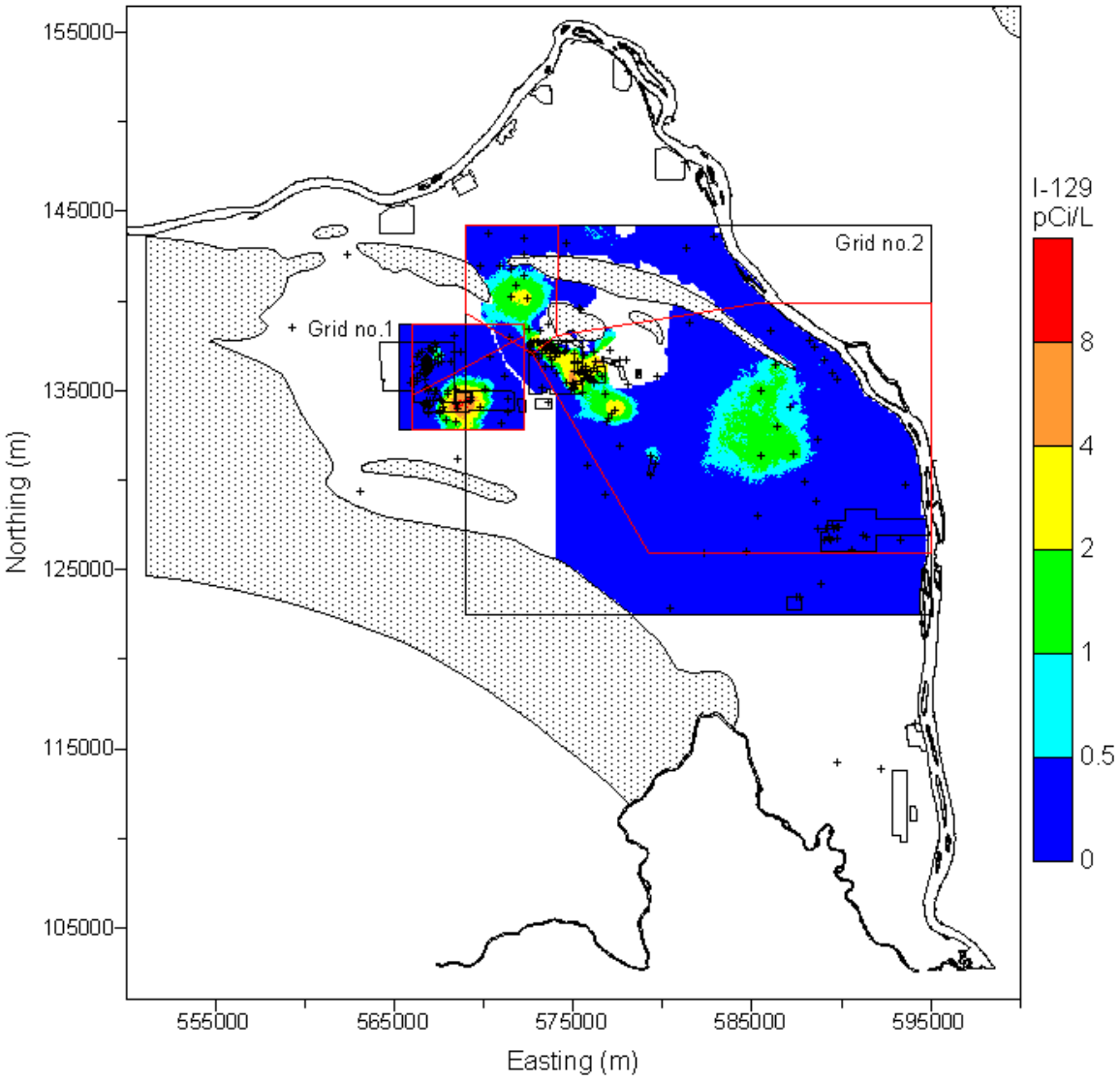

Figure E.3. Median of Simulations of FY 2001 Iodine-129 Concentrations for Grids 1 and 2

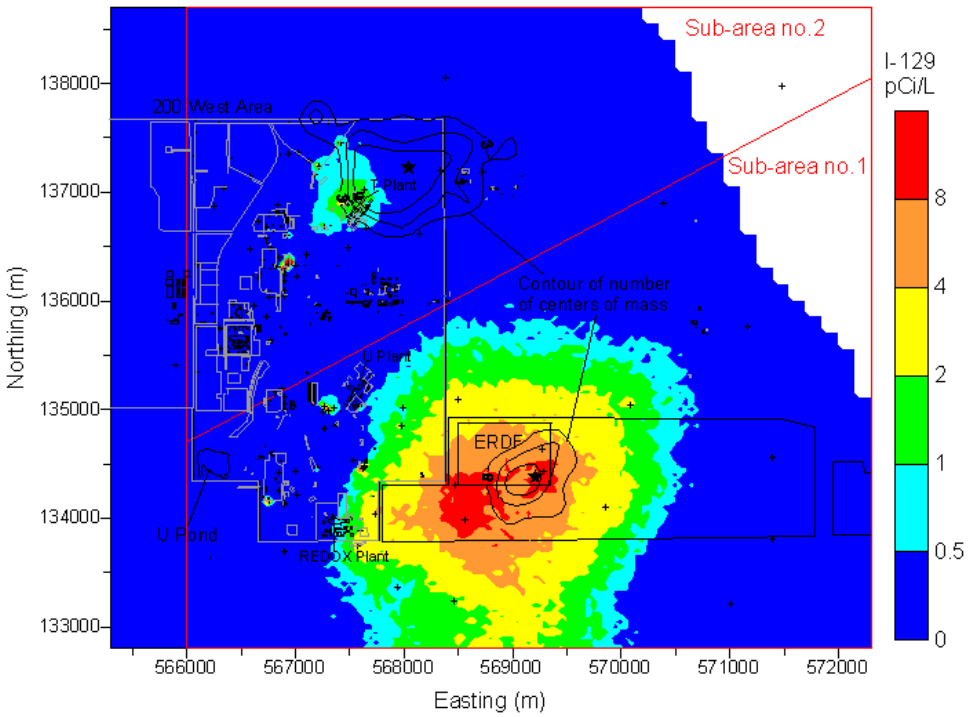

Figure E.4. **Median of Simulated FY 2001 Iodine-129 Concentrations in Grid 1 (200 West Area). Contours of the number of times that the center of mass within the sub-areas occurred within cells of an upscaled grid are shown with the average centers of mass shown by black star in the sub-areas.**

Table E.1. **Coordinates for Sub-Area Boundaries for Grid 1 (200 West Area) of FY 2001 Iodine-129**

Sub-Area 1		Sub-Area 2	
Easting (m)	Northing (m)	Easting (m)	Northing (m)
566000	132800	566000	134700
572300	132800	570952	137348
572300	135121	570791	137400
572146	135153	570813	137667
572146	135557	570674	137699
571261	136357	570663	138104
571261	136624	570515	138167
571113	136655	570536	138424
571102	137061	570365	138456
570963	137124	570365	138573
570952	137348	570217	138615
566000	134700	570195	138700
566000	132800	566000	138700
		566000	134700

Table E.2. Statistics of Centers of Mass of Individual Simulations of FY 2001 Iodine-129 Calculated for a Depth of 5 m for the Sub-Areas of Grid 1 (200 West Area)

Coordinate (m)	Sub-Area 1		Sub-Area 2	
	Easting	Northing	Easting	Northing
Mean	569213.8	134344.3	568037.5	137220.8
Standard Error	16.2	13.4	27.9	16.4
Median	569181.8	134340.0	567993.1	137222.7
Standard Deviation	281.2	232.5	483.3	284.6
Kurtosis	0.85	-0.10	0.27	-0.52
Skewness	0.50	0.30	0.43	-0.03
Range	1812.6	1177.7	2640.7	1453.4
Minimum	568534.8	133824.8	566905.4	136451.6
Maximum	570347.4	135002.5	569546.1	137905.0
Count	300	300	300	300
97.5^{th} Percentile	569877.8	134866.2	569178.5	137716.8
2.5^{th} Percentile	568689.5	133925.9	567171.7	136684.1
Confidence Level of Mean (95.0%)	31.9	26.4	54.9	32.3

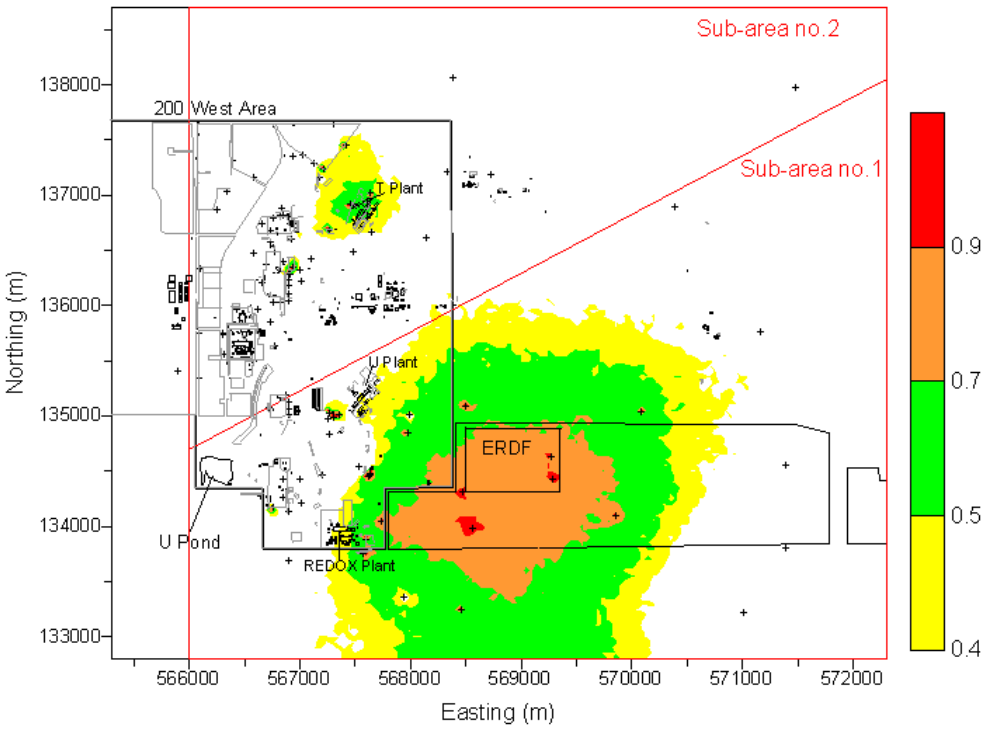

Figure E.5. Probability of Exceeding 1 pCi/L Based on Simulations of FY 2001 Iodine-129 in Grid 1 (200 West Area)

Table E.3. Area Exceeding 1 pCi/L for FY 2001 Iodine-129 for Each Simulation within Sub-Areas of Grid 1 (200 West Area)

Area (km^2)	Sub-Area 1	Sub-Area 2	Grid 1
Mean	8.08	2.32	11.17
Standard Error	0.08	0.04	0.10
Median	8.06	2.16	11.02
Standard Deviation	1.31	0.70	1.72
Kurtosis	0.22	1.14	-0.10
Skewness	0.29	1.01	0.17
Range	7.29	3.82	8.76
Minimum	4.74	1.16	7.13
Maximum	12.03	4.98	15.89
Count	300	300	300
97.5^{th} Percentile	10.85	3.96	14.87
2.5^{th} Percentile	5.76	1.29	7.87
Confidence Level of Mean (95.0%)	0.15	0.08	0.20

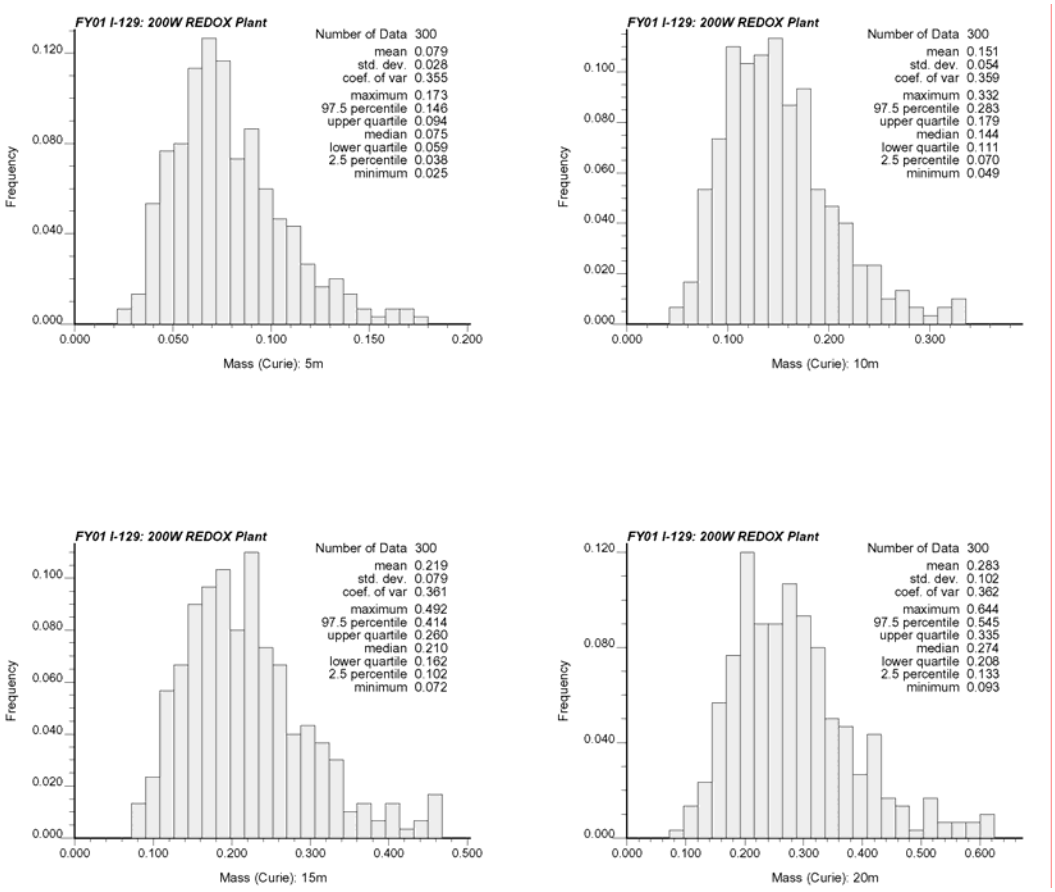

Figure E.6. Histograms of Total Activity in Simulations of FY 2001 Iodine-129 within Sub-Area 1 of Grid 1 (200 West Area), Four Thickness Assumptions

Table E.4. Statistics of Total Activity of Simulations of FY 2001 Iodine-129 within Sub-Area 1 of Grid 1 (200 West Area), Four Thickness Assumptions

Mass (Ci) in Depth	5 m	10 m	15 m	20 m
Mean	0.0788	0.1506	0.2187	0.2833
Standard Error	0.0016	0.0031	0.0046	0.0059
Median	0.0744	0.1443	0.2096	0.2732
Standard Deviation	0.0280	0.0541	0.0790	0.1026
Kurtosis	0.6636	0.7715	0.8586	0.9137
Skewness	0.8307	0.8590	0.8854	0.9032
Range	0.1475	0.2832	0.4201	0.5507
Minimum	0.0255	0.0492	0.0718	0.0935
Maximum	0.1729	0.3324	0.4920	0.6442
Count	300	300	300	300
97.5^{th} Percentile	0.1457	0.2828	0.4135	0.5446
2.5^{th} Percentile	0.0376	0.0700	0.1022	0.1329
Confidence Level of Mean (95.0%)	0.0032	0.0061	0.0090	0.0117

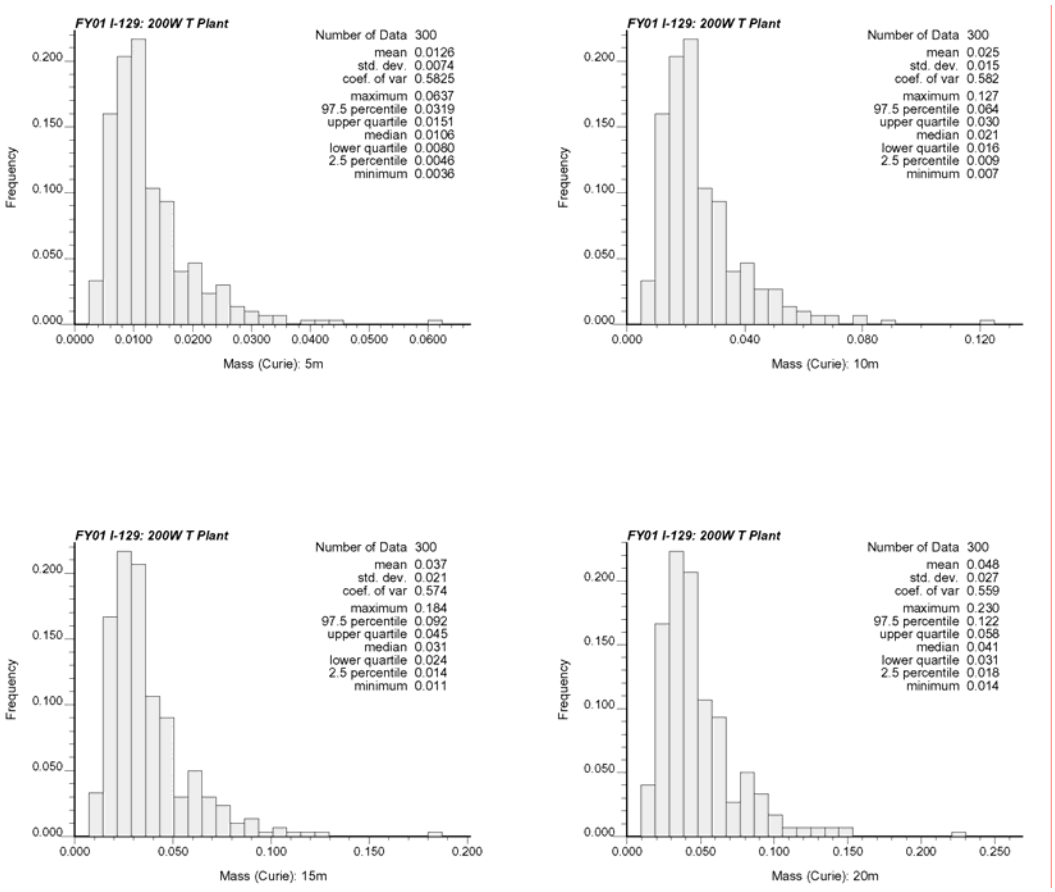

Figure E.7. Histograms of Total Activity in Simulations of FY 2001 Iodine-129 within Sub-Area 2 of Grid 1 (200 West Area), Four Thickness Assumptions

Table E.5. Statistics of Total Activity of Simulations of FY 2001 Iodine-129 within Sub-Area 2 of Grid 1 (200 West Area), Four Thickness Assumptions

Mass (Ci) in Depth	5 m	10 m	15 m	20 m
Mean	0.0126	0.0252	0.0373	0.0483
Standard Error	0.0004	0.0008	0.0012	0.0016
Median	0.0106	0.0211	0.0312	0.0407
Standard Deviation	0.0074	0.0147	0.0214	0.0271
Kurtosis	9.5127	9.5111	9.0143	8.1742
Skewness	2.3911	2.3902	2.3233	2.2051
Range	0.0601	0.1201	0.1734	0.2162
Minimum	0.0036	0.0072	0.0107	0.0140
Maximum	0.0637	0.1272	0.1841	0.2302
Count	300	300	300	300
97.5^{th} Percentile	0.0319	0.0637	0.0922	0.1222
2.5^{th} Percentile	0.0046	0.0093	0.0136	0.0179
Confidence Level of Mean (95.0%)	0.0008	0.0017	0.0024	0.0031

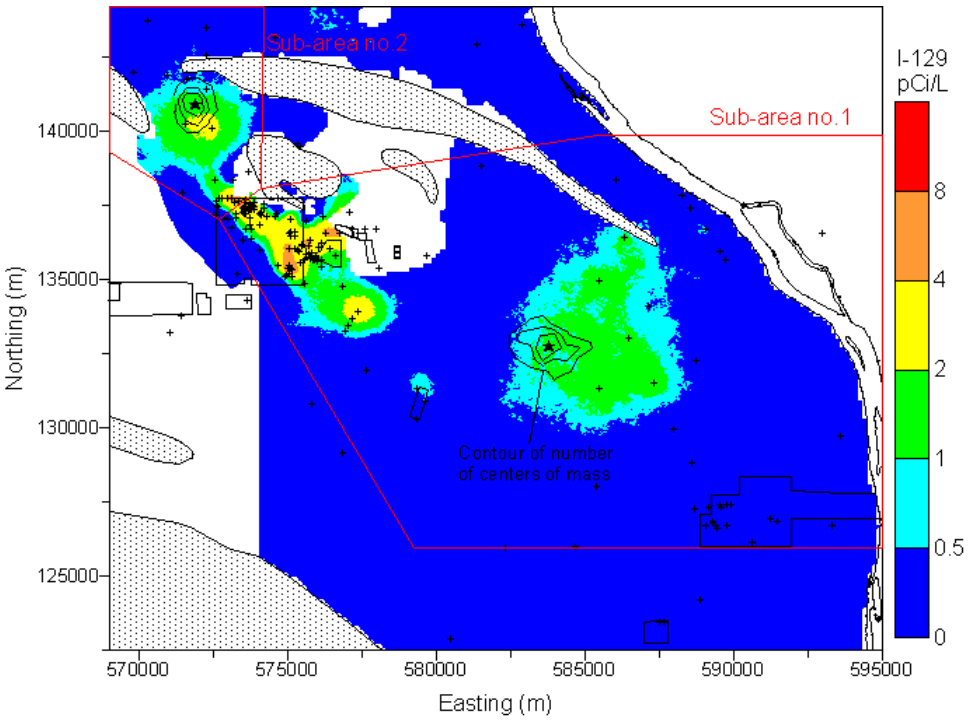

Figure E.8. **Median of Simulated FY 2001 Iodine-129 Concentrations in Grid 2 (200 East Area Plumes). Contours of the number of times that the center of mass within the sub-areas occurred within cells of an upscaled grid are shown with the average centers of mass shown by black stars in the sub-areas.**

Table E.6. Coordinates for Sub-Area Boundaries for Grid 2 (200 East Area) of FY 2001 Iodine-129

Sub-Area 1				Sub-Area 2	
Easting (m)	Northing (m)	Easting (m)	Northing (m)	Easting (m)	Northing (m)
572700	137050	580272	136063	572700	137050
573684	137815	580272	136890	573684	137815
573684	137971	580128	136953	573225	137815
573779	137971	580114	137351	573225	138979
573793	137812	580272	137415	573535	139485
573970	137826	580286	138427	573838	139938
573970	137540	580430	138477	574145	139942
574842	137540	580430	139128	574154	141260
574887	137365	581873	139332	573495	141260
575601	137365	582746	138984	573495	141425
575651	137207	583410	138730	572915	141805
575920	137207	584319	137984	572558	142015
575920	137781	585508	137161	571455	142015
576316	137826	587335	136130	571382	142253
576664	137826	587430	136257	571604	142505
576714	138079	586444	137017	572364	142505
576858	138509	585287	137889	573485	142565
577098	138572	584174	138699	573562	142655
577130	138414	583238	139571	574195	142664
577270	138427	585400	139900	574200	144200
577288	138287	585902	139900	569000	144200
577396	138287	587028	138920	569000	142212
577396	137844	588267	138129	569822	141466
576750	137225	589537	137365	570085	141226
576555	137225	590170	136637	570505	140209
576510	137066	590650	136176	570505	139775
576542	136777	591047	135511	570205	139775
576960	136447	591219	135000	570205	139924
576960	135764	591536	134652	569930	139924
577112	135714	593263	133539	569930	139006
577112	135289	593851	132554	570546	138346
577256	135289	594136	131744	572700	137050
577288	135127	594312	130903		
578287	135127	594457	130302		
578350	135289	594520	128100		
579033	135289	594805	127747		
579078	135440	594805	125950		
579526	135440	579250	125950		
579558	135574	572700	137050		
579811	135606				

Table E.7. Statistics of Centers of Mass of Individual Simulations of FY 2001 Iodine-129 Calculated for a Depth of 5 m for the Sub-Areas of Grid 2 (200 East Area Plumes)

Coordinate (m)	Sub-Area 1		Sub-Area 2	
	Easting	Northing	Easting	Northing
Mean	583567.1	132677.4	571816.0	141075.3
Standard Error	31.3	25.0	13.8	19.3
Median	583564.1	132701.4	571797.6	141082.2
Standard Deviation	700.4	558.5	309.0	430.9
Kurtosis	0.06	-0.06	-0.13	-0.02
Skewness	0.06	-0.24	0.21	0.02
Range	4406.1	3148.6	1768.9	2512.2
Minimum	581204.8	130762.6	570957.1	139849.6
Maximum	585610.9	133911.2	572726.1	142361.7
Count	500	500	500	500
97.5^{th} Percentile	584952.5	133743.2	572458.6	141906.6
2.5^{th} Percentile	582203.1	131489.9	571233.5	140212.6
Confidence Level of Mean (95.0%)	61.5	49.1	27.2	37.9

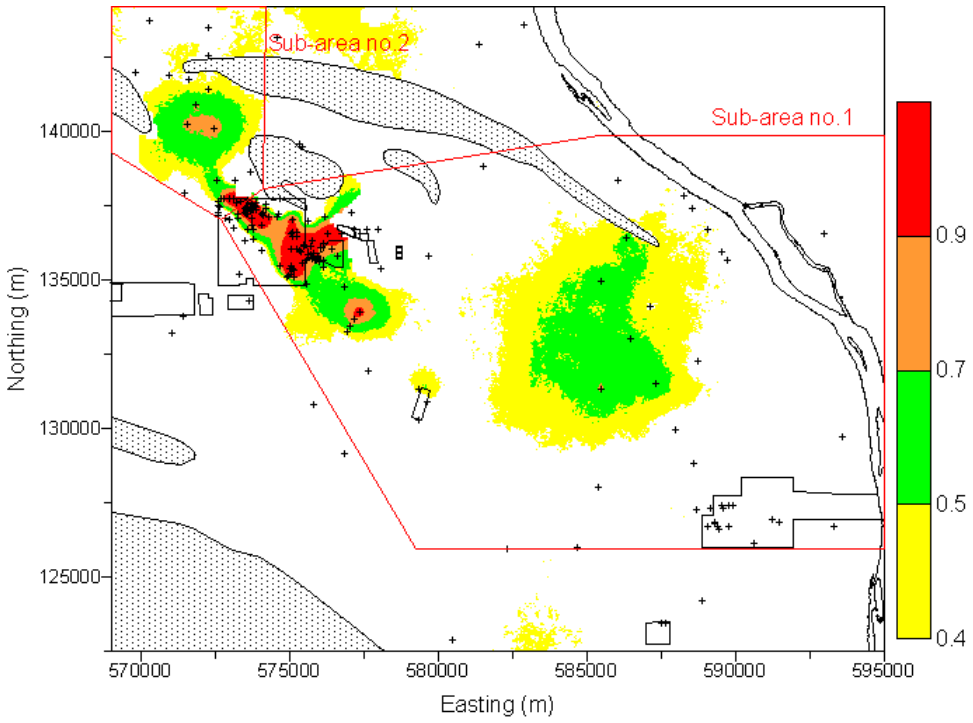

Figure E.9. Probability of Exceeding 1 pCi/L Based on Simulations of FY 2001 Iodine-129 in Grid 2 (200 East Area Plumes)

Table E.8. Area Exceeding 1 pCi/L for FY 2001 Iodine-129 for Each Simulation within Sub-Areas of Grid 2 (200 East Area Plumes)

Area (km^2)	Sub-Area 1	Sub-Area 2	Grid 2
Mean	71.30	10.83	114.32
Standard Error	0.55	0.10	0.670
Median	71.07	10.78	113.69
Standard Deviation	12.36	2.24	15.56
Kurtosis	-0.11	-0.06	-0.11
Skewness	0.11	-0.08	0.12
Range	69.70	12.65	89.93
Minimum	37.26	3.72	73.48
Maximum	106.96	16.37	163.41
Count	500	500	500
97.5^{th} Percentile	95.46	15.41	144.13
2.5^{th} Percentile	47.50	6.27	84.41
Confidence Level of Mean (95.0%)	1.09	0.20	1.37

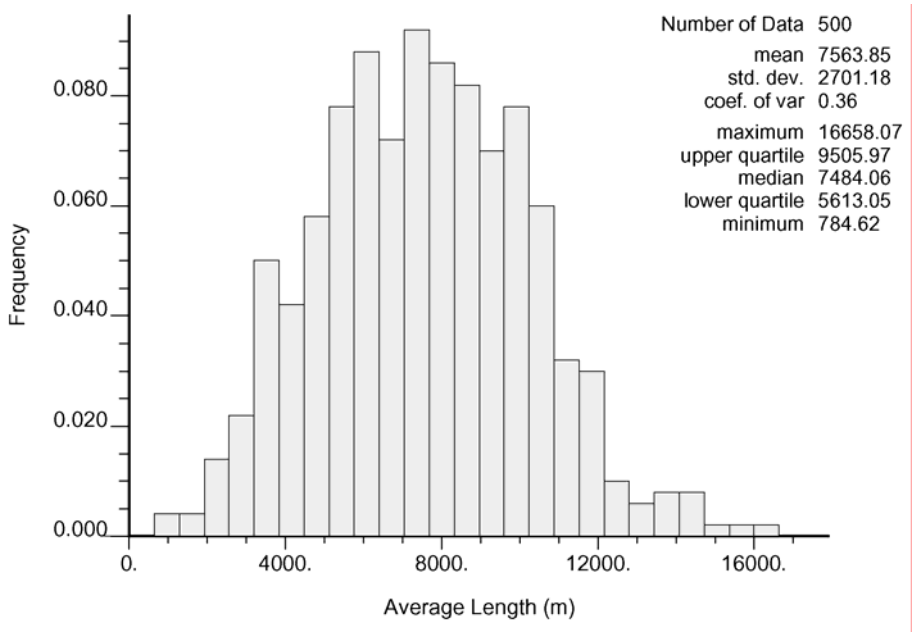

Figure E.10. Histogram of the Average Length of Columbia River Shoreline Exceeding 1 pCi/L for FY 2001 Iodine-129 in Grid 2 (200 East Area Plumes)

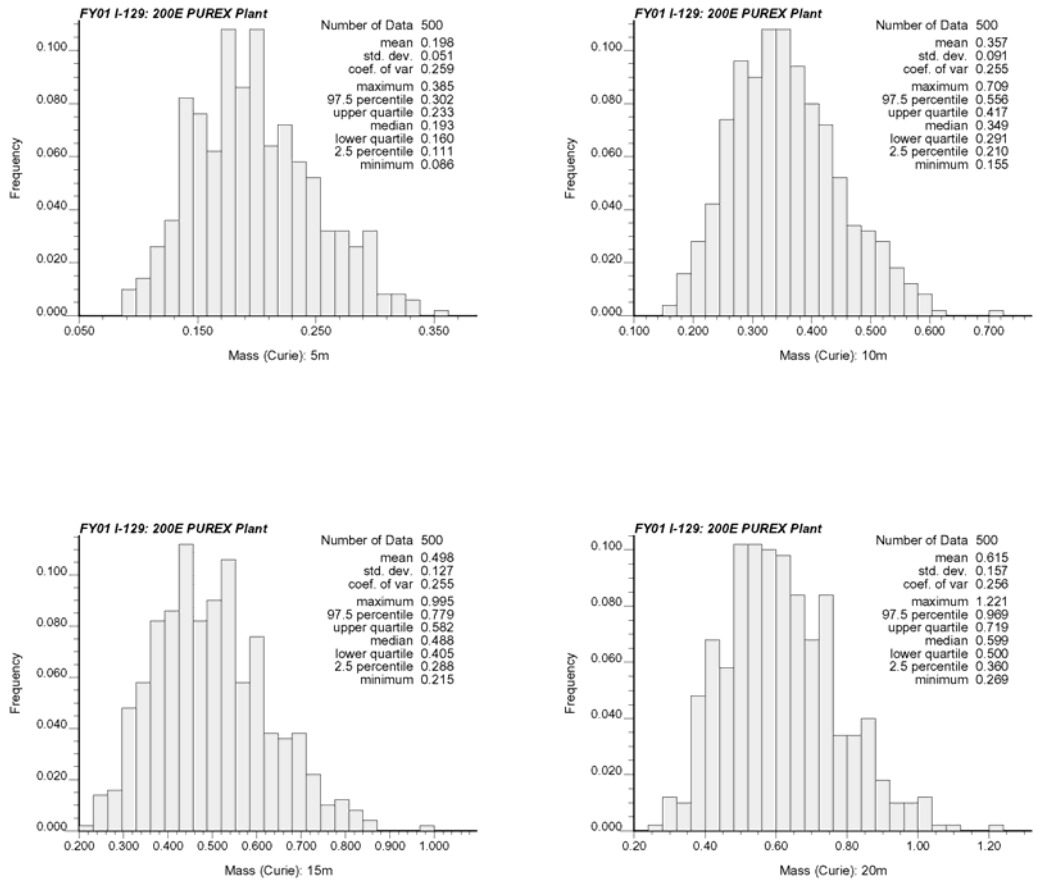

Figure E.11. Histograms of Total Activity in Simulations of FY 2001 Iodine-129 within Sub-Area 1 of Grid 2 (200 East Area), Four Thickness Assumptions

Table E.9. Statistics of Total Activity of Simulations of FY 2001 Iodine-129 within Sub-Area 1 of Grid 2 (200 East Area), Four Thickness Assumptions

Mass (Ci) in Depth	5 m	10 m	15 m	20 m
Mean	0.1979	0.3569	0.4976	0.6145
Standard Error	0.0023	0.0041	0.0057	0.0070
Median	0.1935	0.3495	0.4885	0.5992
Standard Deviation	0.0512	0.0911	0.1269	0.1573
Kurtosis	-0.1737	-0.0172	0.0752	0.1244
Skewness	0.4051	0.4483	0.4793	0.5102
Range	0.2991	0.5547	0.7797	0.9525
Minimum	0.0863	0.1546	0.2151	0.2687
Maximum	0.3854	0.7092	0.9948	1.2212
Count	500	500	500	500
97.5^{th} Percentile	0.3016	0.5558	0.7795	0.9685
2.5^{th} Percentile	0.1108	0.2098	0.2876	0.3604
Confidence Level of Mean (95.0%)	0.0045	0.0080	0.0111	0.0138

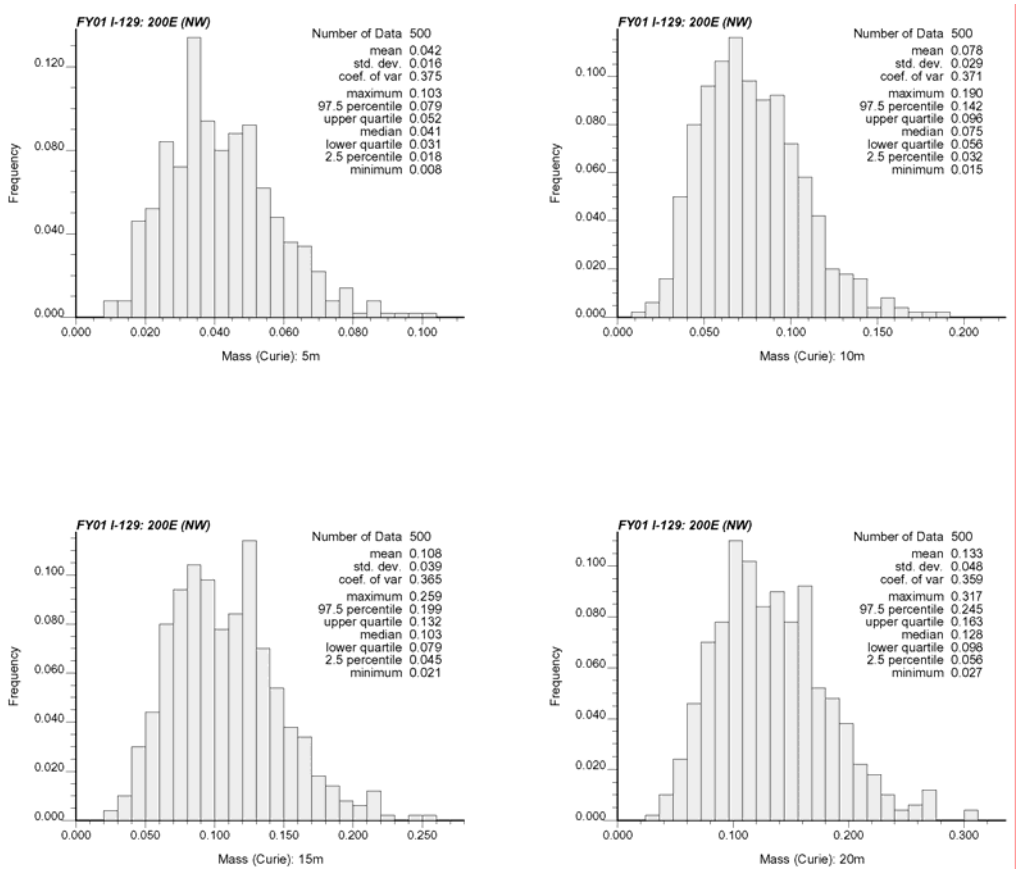

Figure E.12. Histograms of Total Activity in Simulations of FY 2001 Iodine-129 within Sub-Area 2 of Grid 2 (200 East Area), Four Thickness Assumptions

Table E.10. Statistics of Total Activity of Simulations of FY 2001 Iodine-129 within Sub-Area 2 of Grid 2 (200 East Area), Four Thickness Assumptions

Mass (Ci) in Depth	5 m	10 m	15 m	20 m
Mean	0.0424	0.0778	0.1076	0.1333
Standard Error	0.0007	0.0013	0.0018	0.0021
Median	0.0405	0.0746	0.1030	0.1281
Standard Deviation	0.0159	0.0289	0.0393	0.0479
Kurtosis	0.4067	0.4503	0.4432	0.4278
Skewness	0.6301	0.6339	0.6221	0.6116
Range	0.0941	0.1741	0.2378	0.2908
Minimum	0.0084	0.0155	0.0214	0.0266
Maximum	0.1025	0.1896	0.2592	0.3174
Count	500	500	500	500
97.5^{th} Percentile	0.0786	0.1422	0.1988	0.2448
2.5^{th} Percentile	0.0176	0.0321	0.0445	0.0557
Confidence Level of Mean (95.0%)	0.0014	0.0025	0.0034	0.0042

Appendix F

Figures and Data Tables for FY 1992 Iodine-129

Appendix F

Figures and Data Tables for FY 1992 Iodine-129

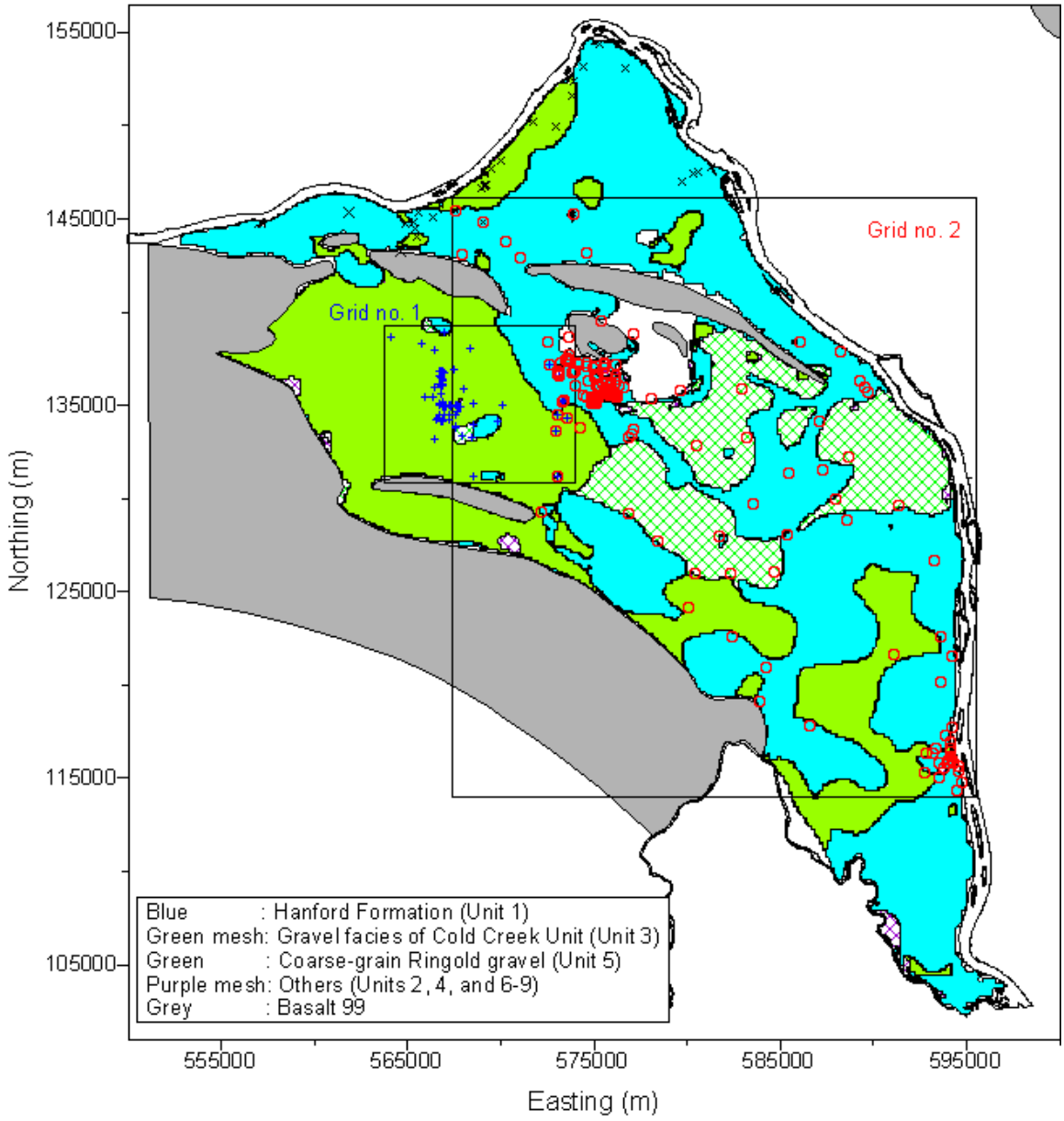

Figure F.1. Subsets of FY 1992 Iodine-129 Data and Subcrop Formation Units at the FY 1992 Water Table

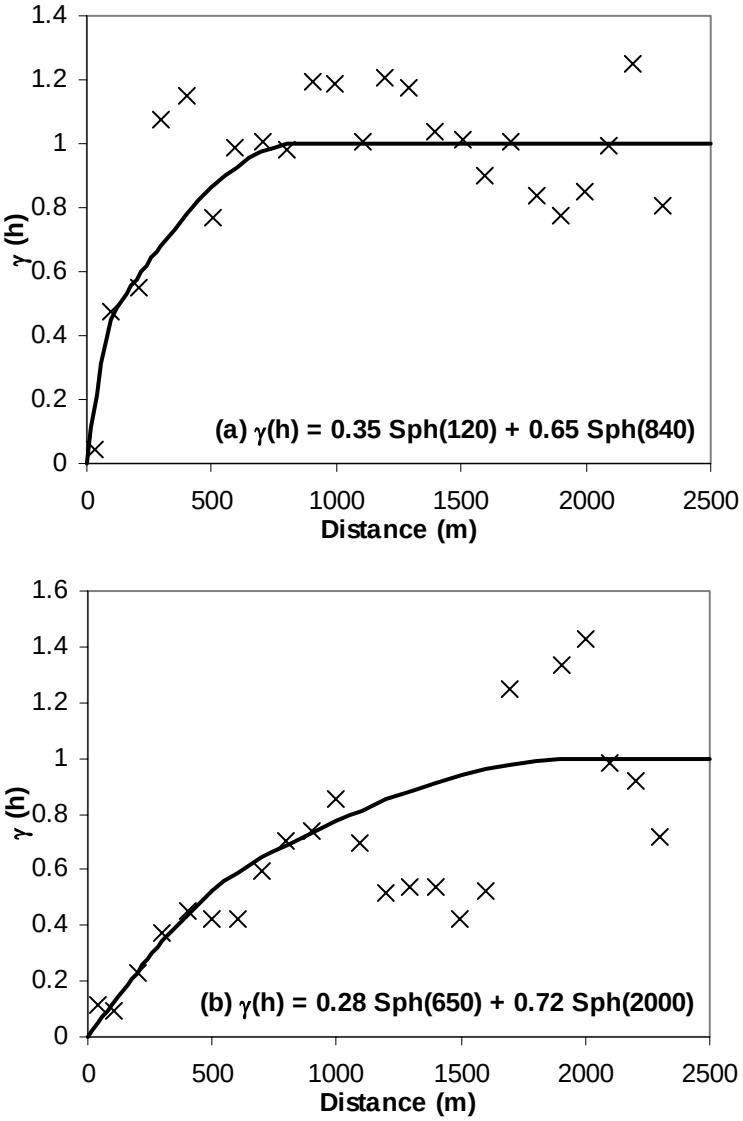

Figure F.2. Variograms and Models of Normal Scores of the FY 1992 Iodine-129 Data in Local Grid 1 (a) and Grid 2 (b). Experimental variogram values designated by x, with the models fit to the data denoted by solid black lines.

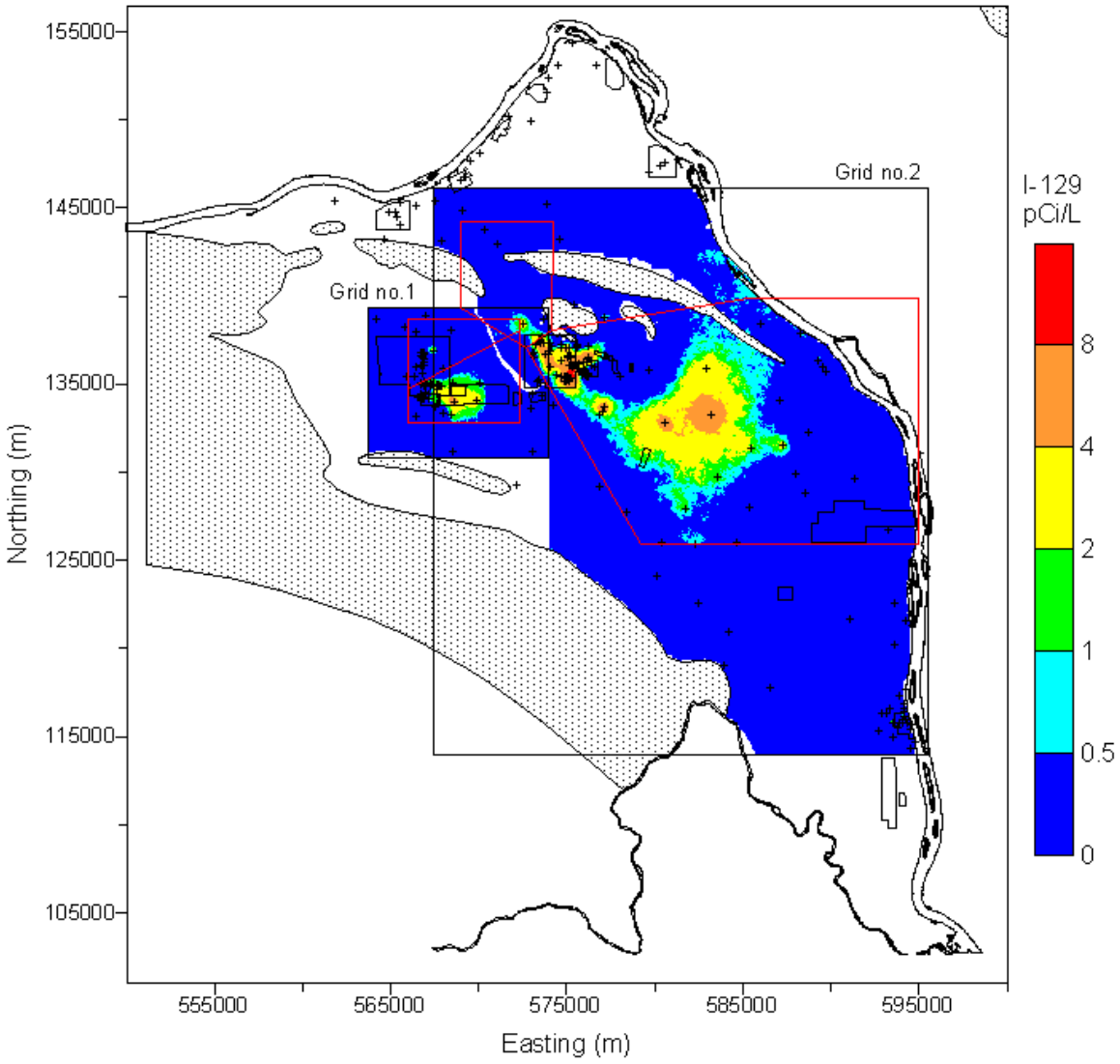

Figure F.3. **Median of Simulations of FY 1992 Iodine-129 Concentrations for Grids 1 and 2. There were only 27 iodine-129 data in the 100 Areas (all lower than the drinking water standard 1 pCi/L). No spatial structure was detected in the data from that area, so the geostatistical analysis and calculation of history matching metrics were not performed.**

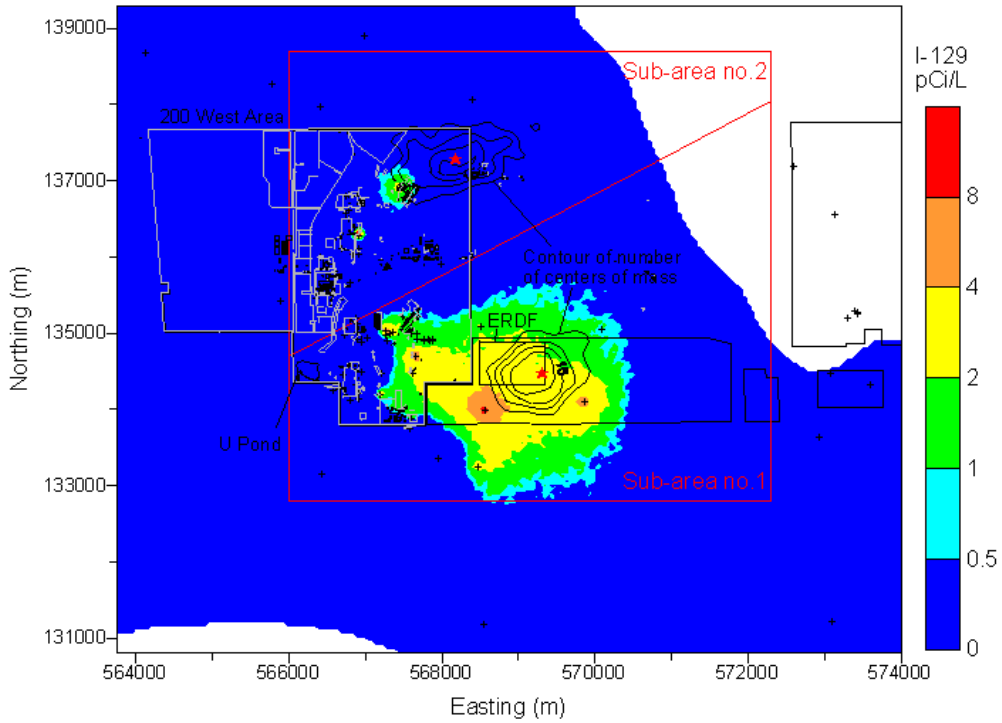

Figure F.4. **Median of Simulated FY 1992 Iodine-129 Concentrations in Grid 1 (200 West Area). Contours of the number of times that the center of mass within the sub-areas occurred within cells of an upscaled grid are shown with the average centers of mass shown by red stars in the sub-areas.**

Table F.1. **Coordinates for Sub-Area Boundaries for Grid 1 (200 West Area) of FY 1992 Iodine-129**

Sub-Area 1		Sub-Area 2	
Easting (m)	Northing (m)	Easting (m)	Northing (m)
566000	132800	566000	134700
572300	132800	570850	137280
572300	134916	570500	138209
571950	135569	570348	138514
571356	136148	570151	138700
570850	137280	566000	138700
566000	134700	566000	134700
566000	132800		

Table F.2. Statistics of Centers of Mass of Individual Simulations of FY 1992 Iodine-129 Calculated for a Depth of 5 m for Sub-Areas of Grid 1 (200 West Area)

Coordinate (m)	Sub-Area 1		Sub-Area 2	
	Easting	Northing	Easting	Northing
Mean	569301.4	134376.4	568181.8	137278.2
Standard Error	14.2	13.4	24.8	12.2
Median	569267.6	134342.5	568168.3	137287.9
Standard Deviation	302.0	283.6	526.9	259.7
Kurtosis	0.03	-0.15	0.00	-0.20
Skewness	0.38	0.39	0.23	-0.12
Range	1736.1	1623.1	3119.4	1541.5
Minimum	568543.8	133653.2	566667.1	136360.4
Maximum	570279.9	135276.3	569786.5	137901.8
Count	450	450	450	450
97.5^{th} Percentile	569928.6	134969.3	569333.4	137778.9
2.5^{th} Percentile	568775.8	133899.3	567167.3	136778.0
Confidence Level of Mean (95.0%)	28.0	26.3	48.8	24.1

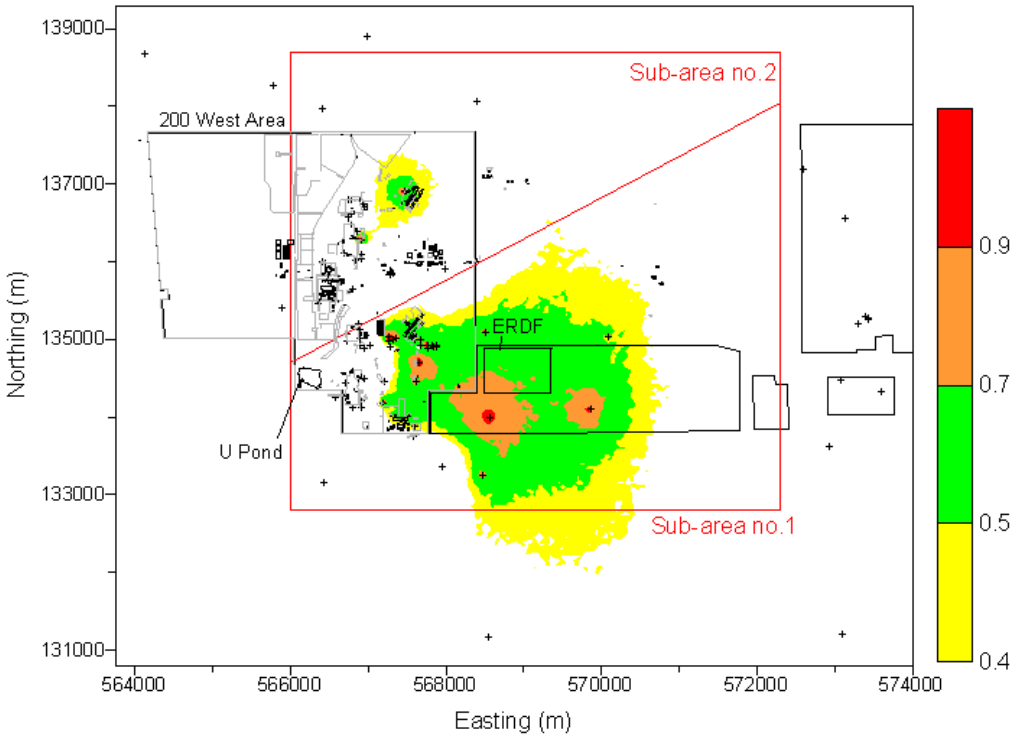

Figure F.5. Probability of Exceeding 1 pCi/L Based on Simulations of FY 1992 Iodine-129 in Grid 1 (200 West Area)

Table F.3. Area Exceeding 1 pCi/L for FY 1992 Iodine-129 for Each Simulation within Sub-Areas of Grid 1 (200 West Area)

Area (km^2)	Sub-Area 1	Sub-Area 2	Grid 1
Mean	7.23	2.89	17.08
Standard Error	0.07	0.05	0.16
Median	7.13	2.77	16.99
Standard Deviation	1.53	1.11	3.48
Kurtosis	-0.34	0.38	-0.34
Skewness	0.31	0.69	0.15
Range	8.50	5.77	19.52
Minimum	3.52	0.73	8.12
Maximum	12.01	6.50	27.63
Count	450	450	450
97.5^{th} Percentile	10.36	5.56	24.13
2.5^{th} Percentile	4.68	1.13	10.62
Confidence Level of Mean (95.0%)	0.14	0.10	0.32

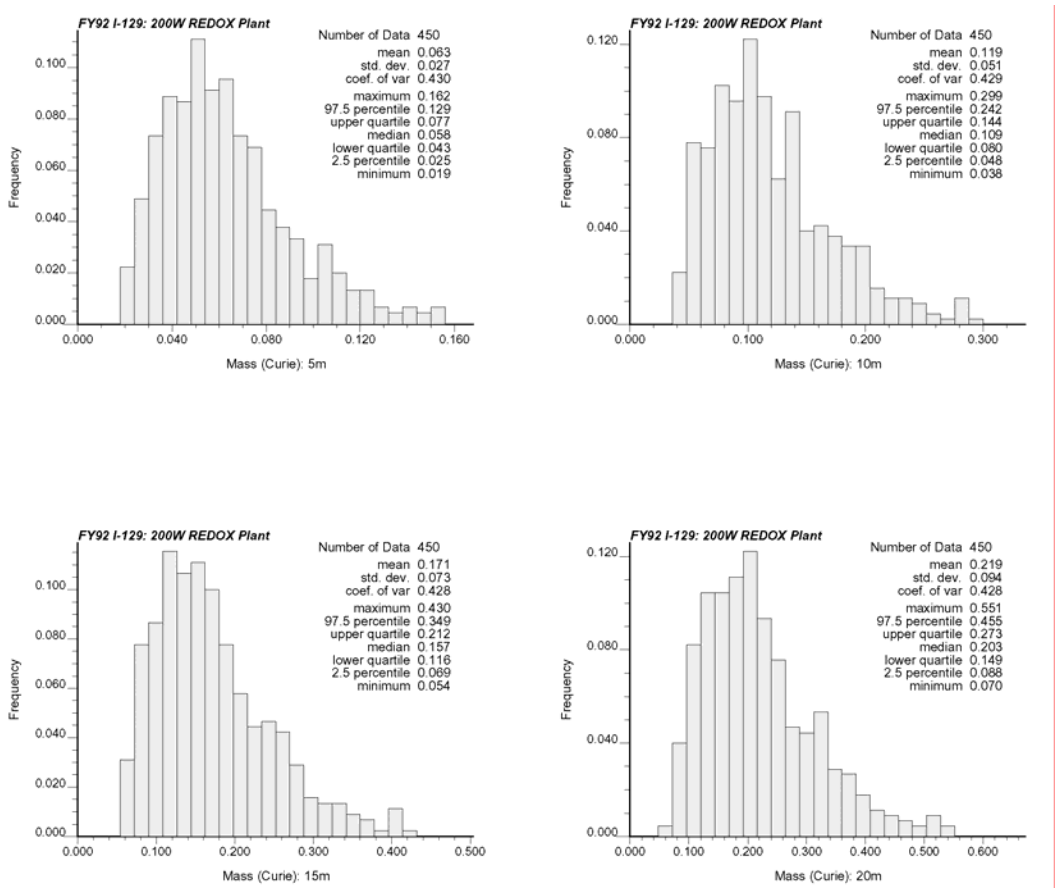

Figure F.6. Histograms of Total Activity in Simulations of FY 1992 Iodine-129 within Sub-Area 1 of Grid 1 (200 West Area), Four Thickness Assumptions

Table F.4. Statistics of Total Activity of Simulations of FY 1992 Iodine-129 within Sub-Area 1 of Grid 1 (200 West Area), Four Thickness Assumptions

Mass (Ci) in Depth	5 m	10 m	15 m	20 m
Mean	0.0633	0.1190	0.1708	0.2195
Standard Error	0.0013	0.0024	0.0035	0.0044
Median	0.0584	0.1092	0.1574	0.2029
Standard Deviation	0.0272	0.0511	0.0732	0.0941
Kurtosis	0.6970	0.6817	0.6776	0.6956
Skewness	0.9262	0.9266	0.9253	0.9273
Range	0.1434	0.2610	0.3754	0.4814
Minimum	0.0186	0.0376	0.0545	0.0700
Maximum	0.1620	0.2986	0.4299	0.5514
Count	450	450	450	450
97.5^{th} Percentile	0.1277	0.2419	0.3489	0.4529
2.5^{th} Percentile	0.0253	0.0484	0.0690	0.0877
Confidence Level of Mean (95.0%)	0.0025	0.0047	0.0068	0.0087

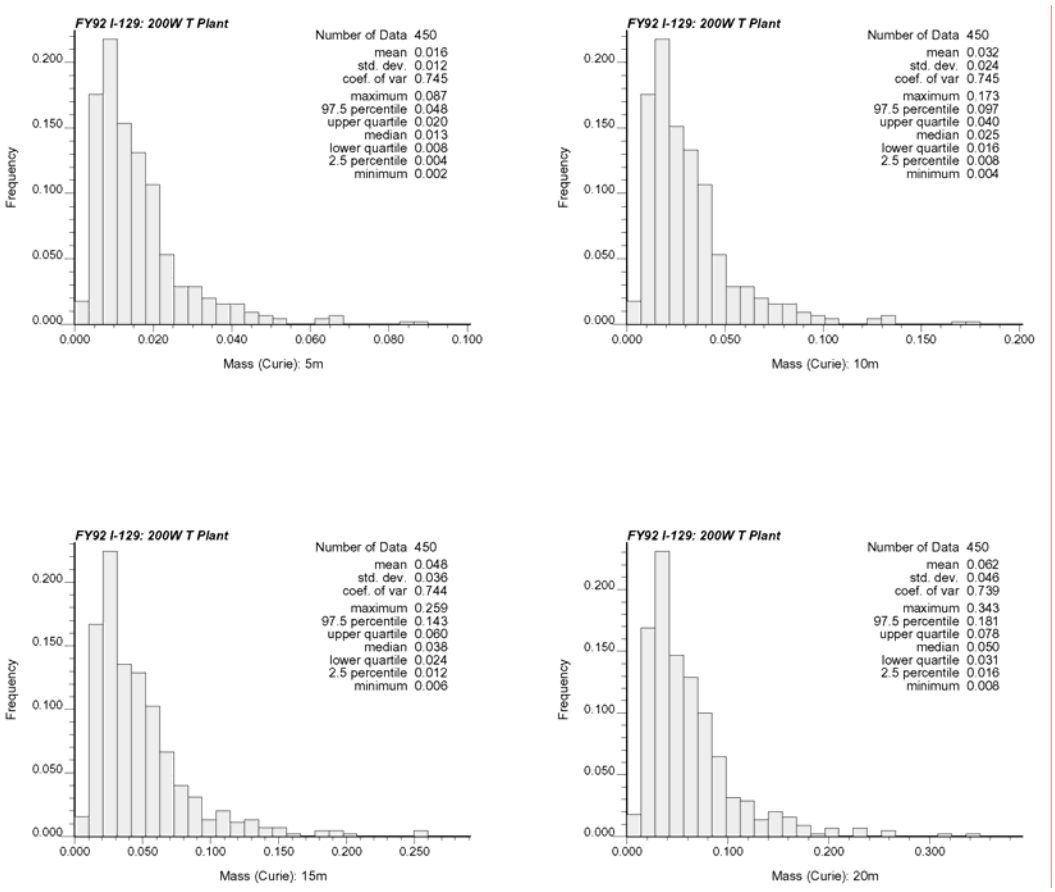

Figure F.7. Histograms of Total Activity in Simulations of FY 1992 Iodine-129 within Sub-Area 2 of Grid 1 (200 West Area), Four Thickness Assumptions

Table F.5. Statistics of Total Activity of Simulations of FY 1992 Iodine-129 within Sub-Area 2 of Grid 1 (200 West Area), Four Thickness Assumptions

Mass (Ci) in Depth	5 m	10 m	15 m	20 m
Mean	0.0160	0.0321	0.0478	0.0619
Standard Error	0.0006	0.0011	0.0017	0.0022
Median	0.0127	0.0255	0.0381	0.0499
Standard Deviation	0.0120	0.0239	0.0356	0.0458
Kurtosis	7.0938	7.0938	7.1390	7.2792
Skewness	2.2204	2.2204	2.2226	2.2300
Range	0.0845	0.1690	0.2531	0.3344
Minimum	0.0021	0.0042	0.0063	0.0081
Maximum	0.0866	0.1732	0.2593	0.3425
Count	450	450	450	450
97.5^{th} Percentile	0.0479	0.0959	0.1423	0.1794
2.5^{th} Percentile	0.0040	0.0080	0.0119	0.0158
Confidence Level of Mean (95.0%)	0.0011	0.0022	0.0033	0.0042

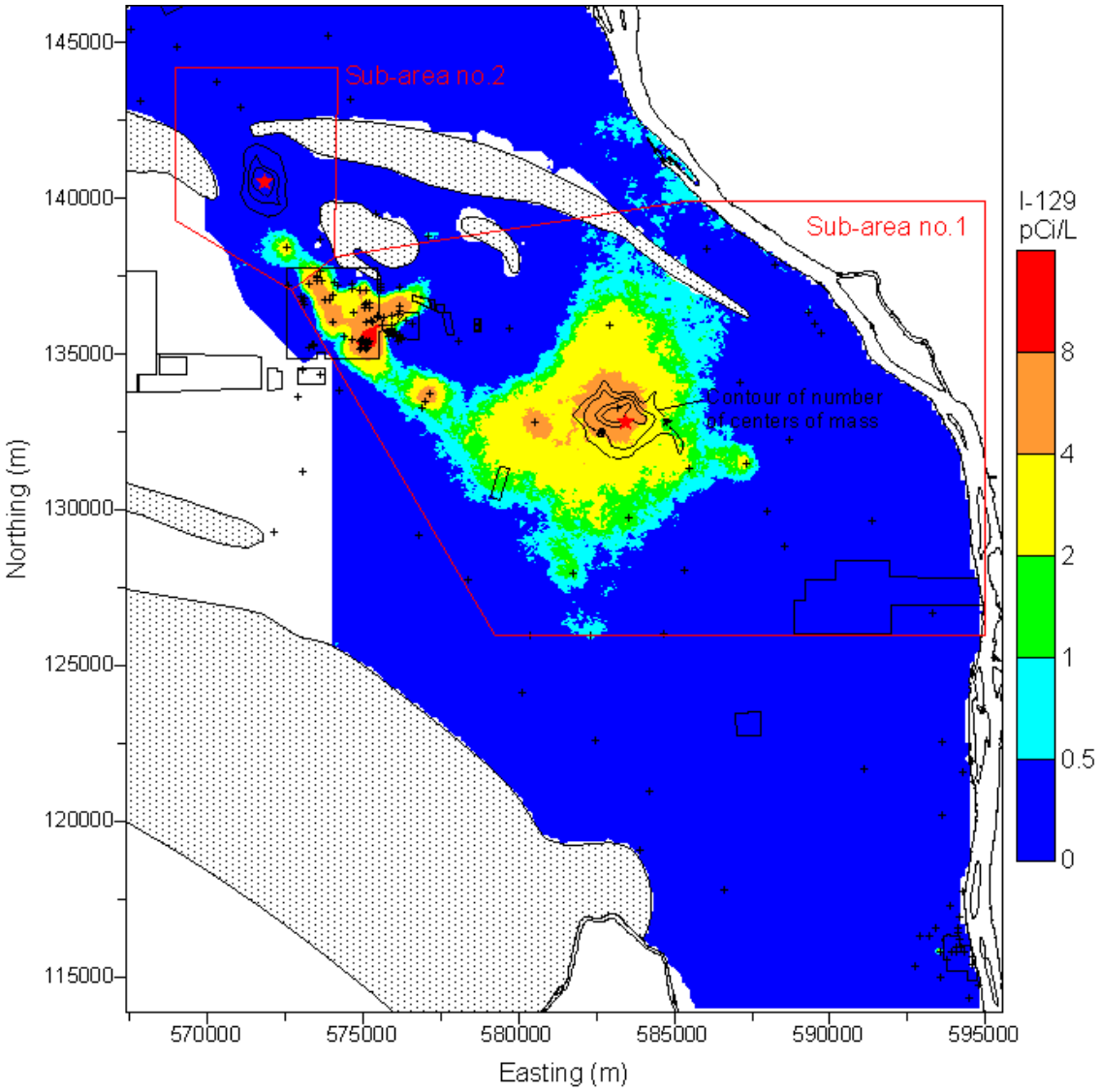

Figure F.8. Median of Simulated FY 2001 Iodine-129 Concentrations in Grid 2 (200 East Area Plumes). Contours of the number of times that the center of mass within the sub-area occurred within cells of an upscaled grid are shown with the average centers of mass shown by red stars in the sub-areas.

Table F.6. Coordinates for Sub-Area Boundaries for Grid 2 (200 East Area) of FY 1992 Iodine-129

Sub-Area 1				Sub-Area 2	
Easting (m)	Northing (m)	Easting (m)	Northing (m)	Easting (m)	Northing (m)
572700	137050	582746	138984	572700	137050
574100	138100	583410	138730	574100	138100
574114	138075	584319	137984	573955	138563
574285	137776	585508	137161	573675	139155
574417	137704	587335	136130	573634	139413
574665	137776	587430	136257	573698	139712
575466	137383	586444	137017	573946	139883
575565	137415	585287	137889	574145	139983
575542	137546	584174	138699	574136	141200
575163	137835	583238	139571	573698	141200
574733	138174	585400	139900	573164	141602
575113	138256	585902	139900	572536	142031
575556	137894	587028	138920	572332	142072
575764	137794	588267	138129	571627	141995
576103	137794	589537	137365	571505	142013
576424	137876	590170	136637	571387	142235
576650	138057	590650	136176	571753	142452
576790	138256	591047	135511	573512	142565
576781	138536	591219	135000	574186	142551
578192	138744	591536	134652	574200	144200
578464	138560	593263	133539	569000	144200
578870	138560	593851	132554	569000	142162
579513	138183	594136	131744	569628	141715
579553	137595	594312	130903	570279	140706
579702	137446	594457	130302	570388	140105
579861	137446	594520	128100	570125	139929
580042	137654	594805	127747	569936	140037
580033	138183	594805	125950	569936	139006
579870	138563	579250	125950	570537	138378
579531	138975	572700	137050	572700	137050
581865	139345				

Table F.7. Statistics of Centers of Mass of Individual Simulations of FY 1992 Iodine-129 Calculated for a Depth of 5 m for Sub-Areas of Grid 2 (200 East Area Plumes)

Coordinate (m)	Sub-Area 1		Sub-Area 2	
	Easting	Northing	Easting	Northing
Mean	583217.2	132781.1	571787.5	140646.9
Standard Error	44.3	35.3	21.5	34.6
Median	583138.7	132846.0	571801.2	140589.7
Standard Deviation	827.8	660.5	403.0	647.9
Kurtosis	0.67	-0.35	-0.16	-0.21
Skewness	0.44	-0.19	-0.16	0.23
Range	5607.9	3446.4	2155.3	3596.3
Minimum	581105.2	130923.3	570606.1	138927.2
Maximum	586713.2	134369.7	572761.4	142523.5
Count	350	350	350	350
97.5^{th} Percentile	585038.8	134011.8	572543.3	141989.9
2.5^{th} Percentile	581731.7	131396.6	570994.9	139469.1
Confidence Level of Mean (95.0%)	87.0	69.4	42.4	68.1

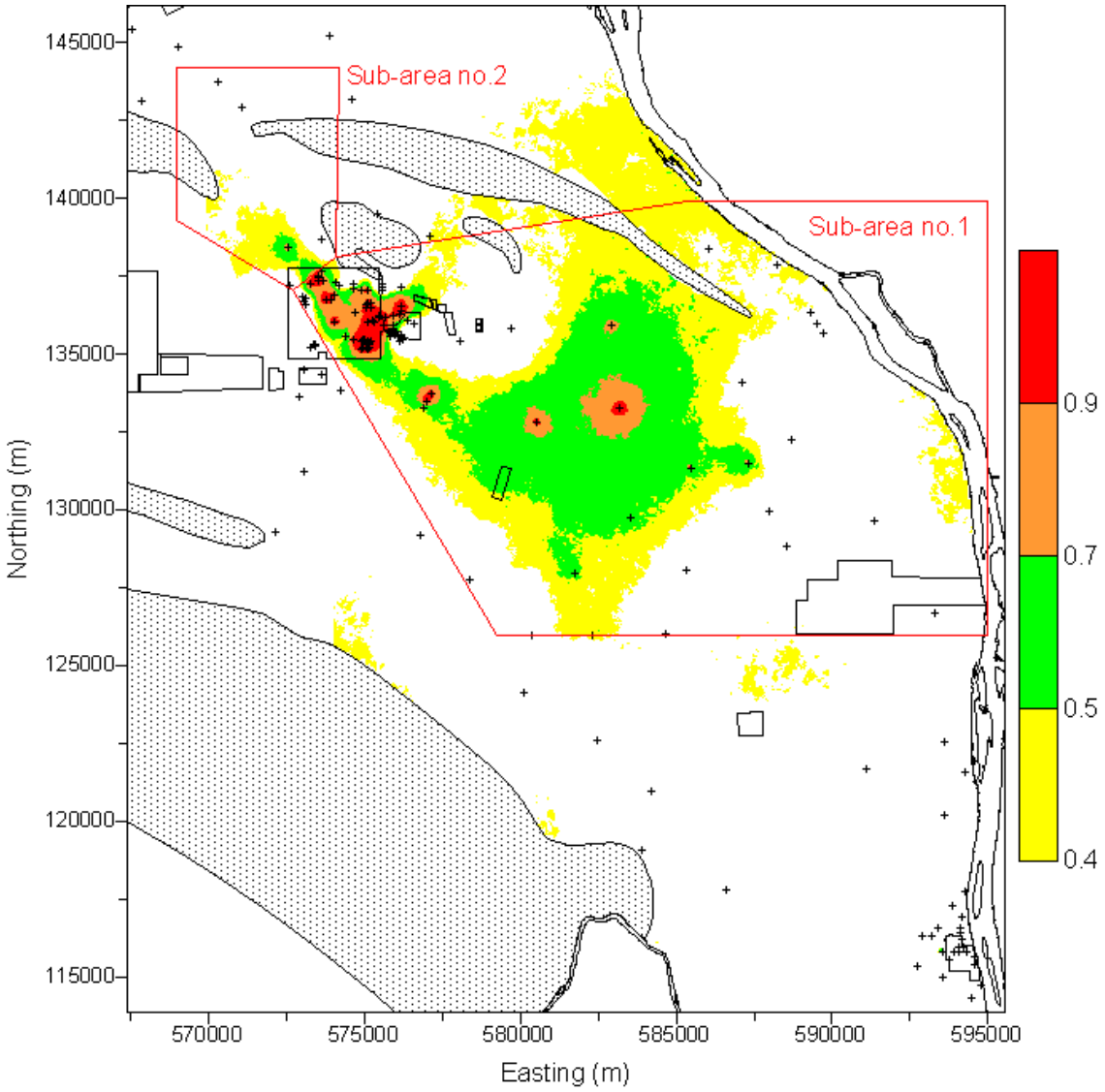

Figure F.9. Probability of Exceeding 1 pCi/L Based on Simulations of FY 1992 Iodine-129 in Grid 2 (200 East Area Plumes)

Table F.8. Area Exceeding 1 pCi/L for FY 1992 Iodine-129 for Each Simulation within Sub-Areas of Grid 2 (200 East Area Plumes)

Area (km^2)	Sub-Area 1	Sub-Area 2	Grid 3
Mean	88.08	7.82	165.92
Standard Error	0.65	0.19	1.06
Median	86.85	7.31	165.11
Standard Deviation	12.21	3.56	19.81
Kurtosis	-0.28	0.07	-0.23
Skewness	0.13	0.65	0.21
Range	67.47	17.66	119.97
Minimum	54.74	1.29	121.58
Maximum	122.21	18.94	241.54
Count	350	350	350
97.5^{th} Percentile	111.62	16.11	202.97
2.5^{th} Percentile	67.15	2.08	131.25
Confidence Level of Mean (95.0%)	1.28	0.37	2.08

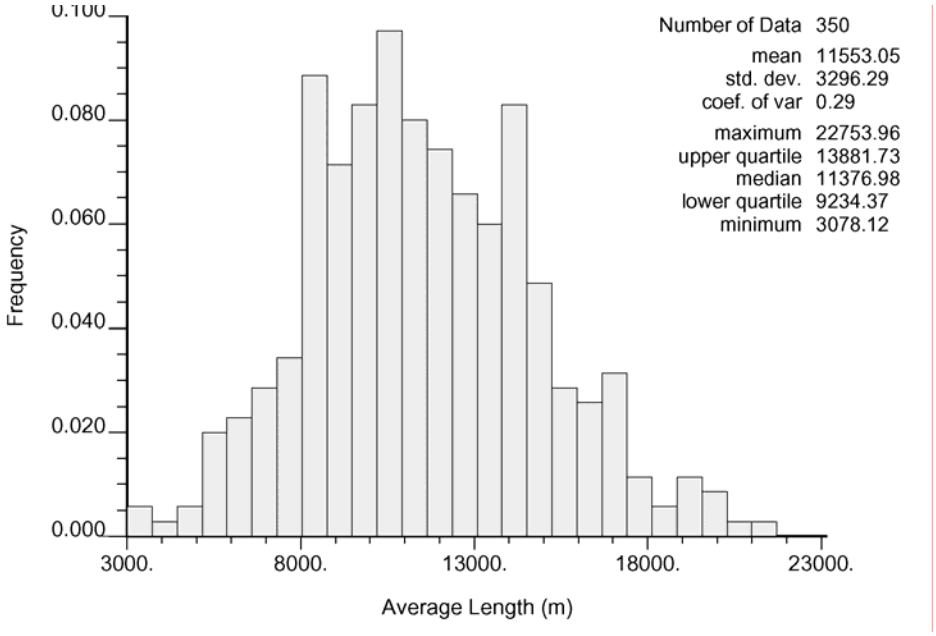

Figure F.10. Histogram of the Average Length of Columbia River Shoreline Exceeding 1 pCi/L for FY 1992 Iodine-129 in Grid 2 (200 East Area Plumes)

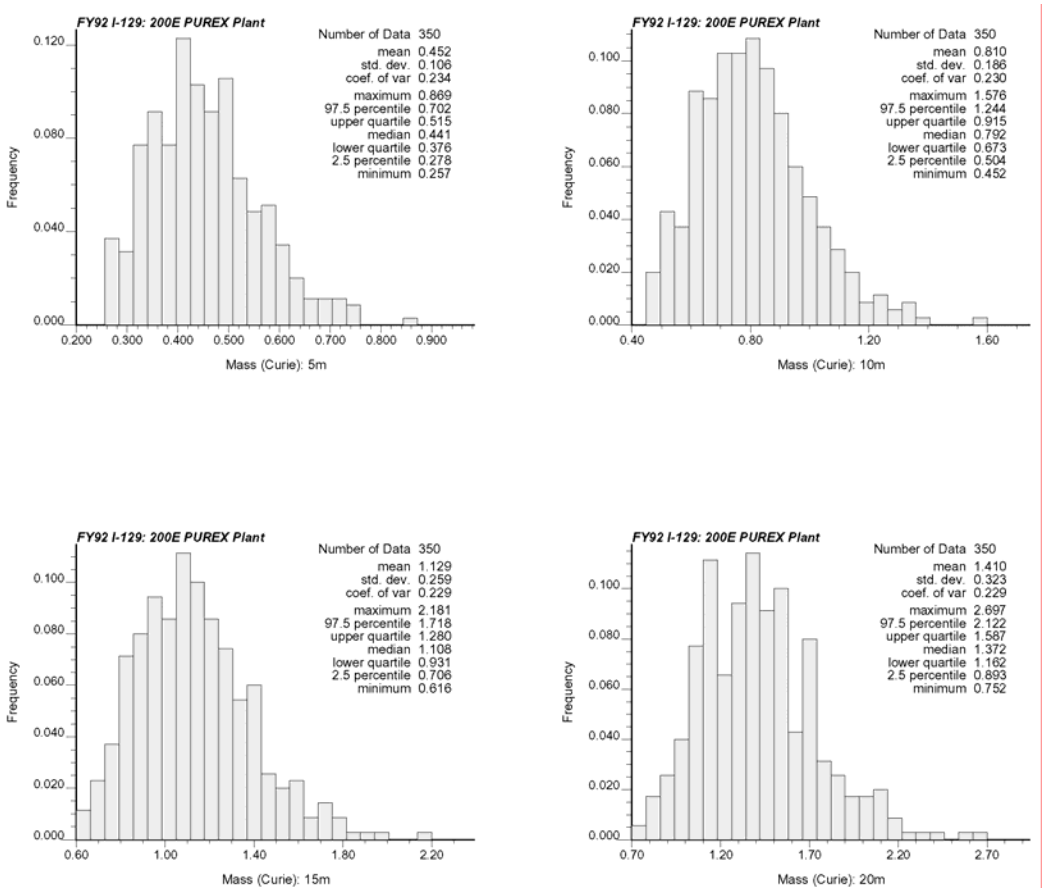

Figure F.11. Histograms of Total Activity in Simulations of FY 1992 Iodine-129 within Sub-Area 1 of Grid 2 (200 East Area), Four Thickness Assumptions

Table F.9. Statistics of Total Activity of Simulations of FY 1992 Iodine-129 within Sub-Area 1 of Grid 2 (200 East Area), Four Thickness Assumptions

Mass (Ci) in Depth	5 m	10 m	15 m	20 m
Mean	0.4518	0.8100	1.1292	1.4100
Standard Error	0.0057	0.0100	0.0139	0.0173
Median	0.4412	0.7917	1.1084	1.3718
Standard Deviation	0.1061	0.1866	0.2592	0.3237
Kurtosis	0.3687	0.6081	0.6523	0.6701
Skewness	0.6037	0.6636	0.6745	0.6759
Range	0.6121	1.1241	1.5650	1.9441
Minimum	0.2570	0.4520	0.6157	0.7525
Maximum	0.8692	1.5761	2.1807	2.6966
Count	350	350	350	350
97.5^{th} Percentile	0.7033	1.2459	1.7181	2.1220
2.5^{th} Percentile	0.2777	0.5023	0.7005	0.8910
Confidence Level of Mean (95.0%)	0.0112	0.0196	0.0273	0.0340

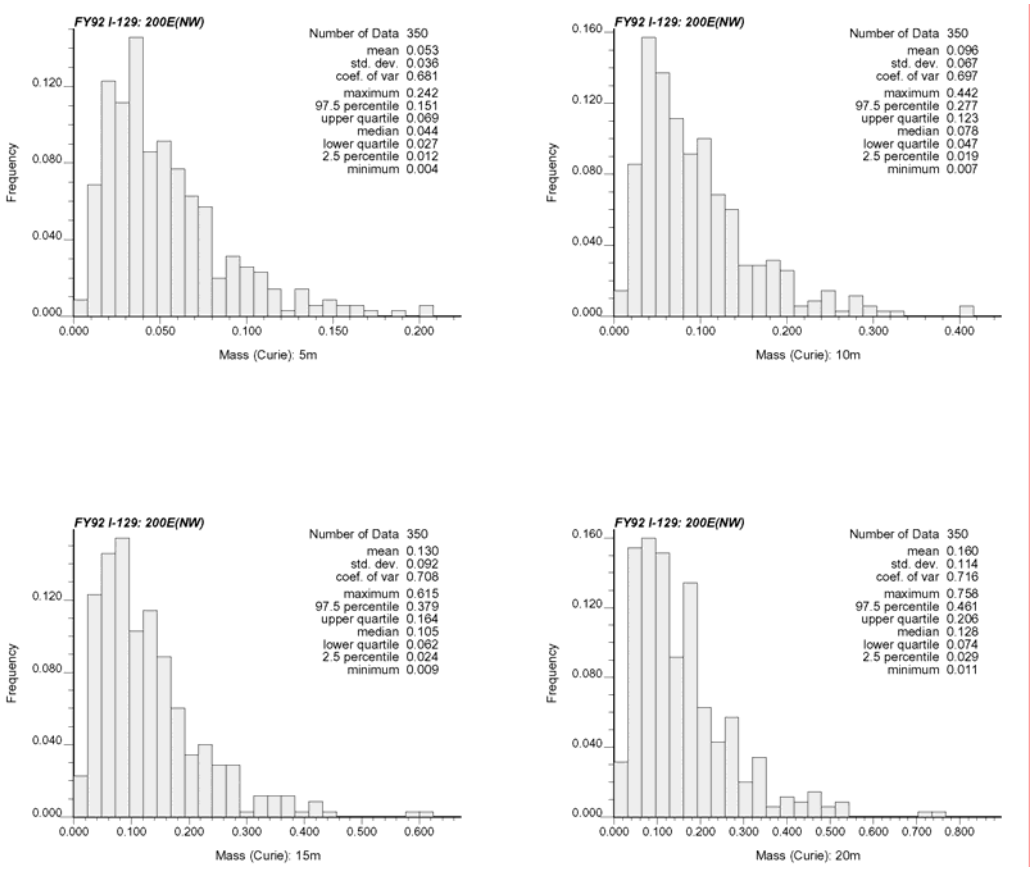

Figure F.12. Histograms of Total Activity in Simulations of FY 1992 Iodine-129 within Sub-Area 2 of Grid 2 (200 East Area), Four Thickness Assumptions

Table F.10. Statistics of Total Activity of Simulations of FY 1992 Iodine-129 within Sub-Area 2 of Grid 2 (200 East Area), Four Thickness Assumptions

Mass (Ci) in Depth	5 m	10 m	15 m	20 m
Mean	0.0534	0.0960	0.1305	0.1595
Standard Error	0.0019	0.0036	0.0049	0.0061
Median	0.0440	0.0783	0.1052	0.1285
Standard Deviation	0.0364	0.0670	0.0925	0.1144
Kurtosis	4.1850	4.2031	4.1345	4.0238
Skewness	1.6959	1.7015	1.6943	1.6849
Range	0.2373	0.4347	0.6055	0.7472
Minimum	0.0044	0.0071	0.0091	0.0110
Maximum	0.2417	0.4418	0.6147	0.7582
Count	350	350	350	350
97.5^{th} Percentile	0.1514	0.2781	0.3790	0.4614
2.5^{th} Percentile	0.0119	0.0188	0.0240	0.0290
Confidence Level of Mean (95.0%)	0.0038	0.0070	0.0097	0.0120

Appendix G

Figures and Data Tables for FY 2001 Uranium

Appendix G

Figures and Data Tables for FY 2001 Uranium

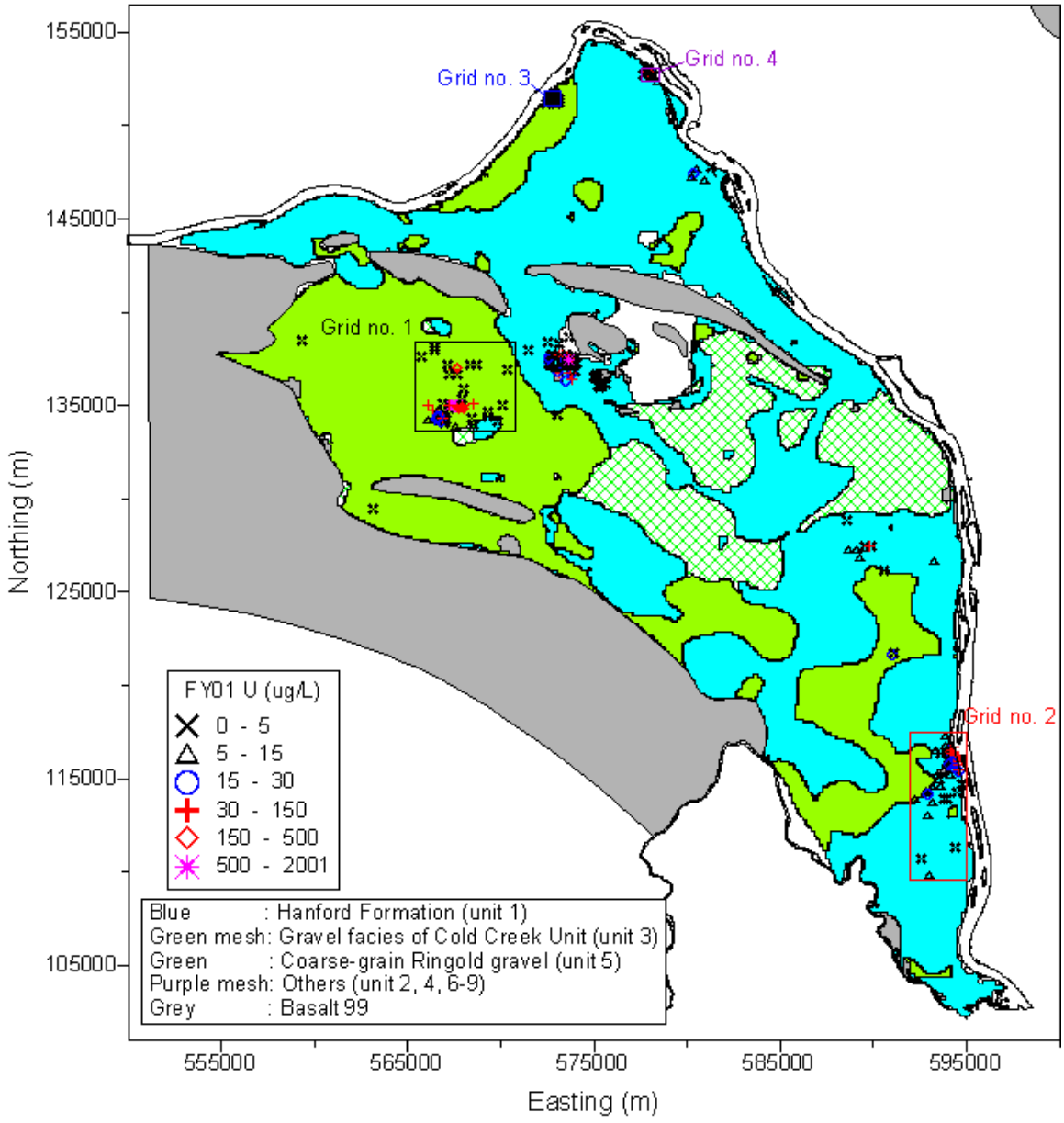

Figure G.1. Subsets of FY 2001 Uranium Data and Subcrop Formation Units at the FY 2001 Water Table. Although an area is highlighted for Grid 3, initial data analysis indicated that reliable results could not be obtained in that area.

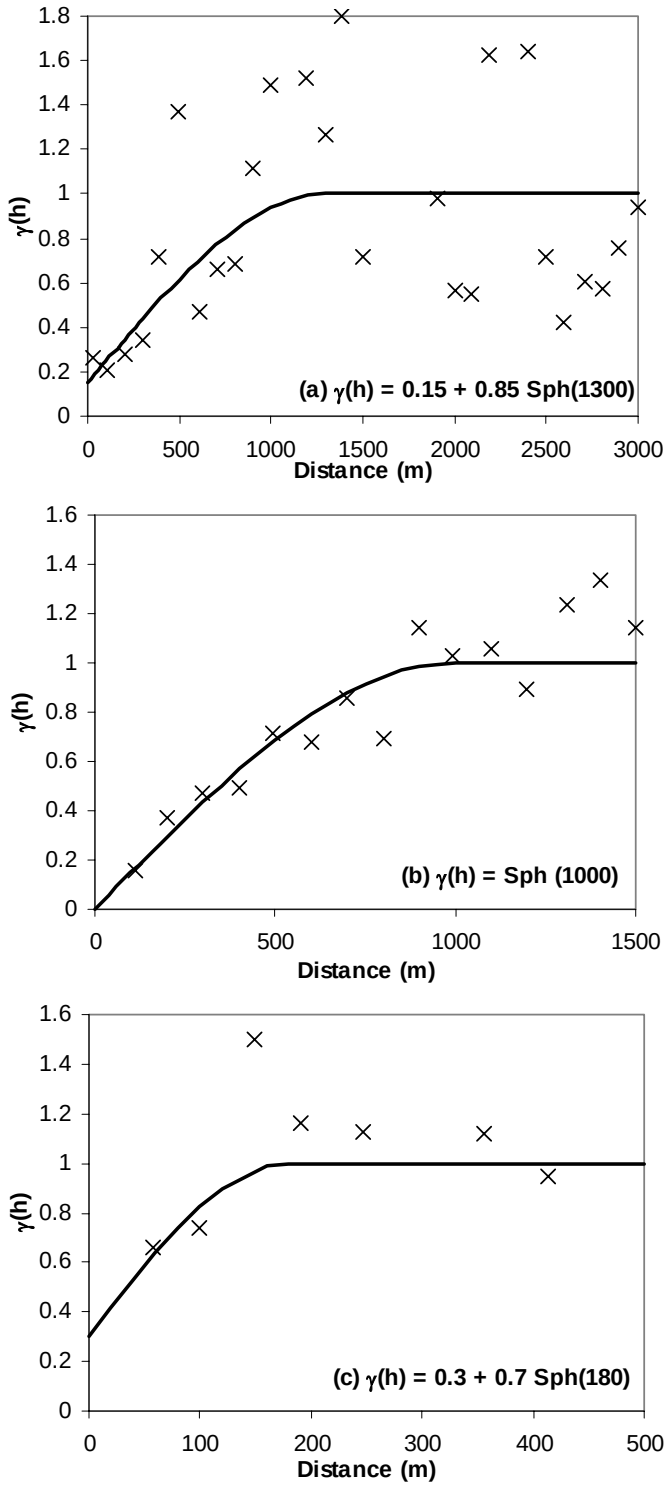

Figure G.2. Variograms and Models of Normal Scores of the FY 2001 Uranium Data in Local Grid 1 (a), Grid 2 (b), and Grid 4 (c). Experimental variogram values designated by X, with the models fit to the data denoted by the solid black lines.

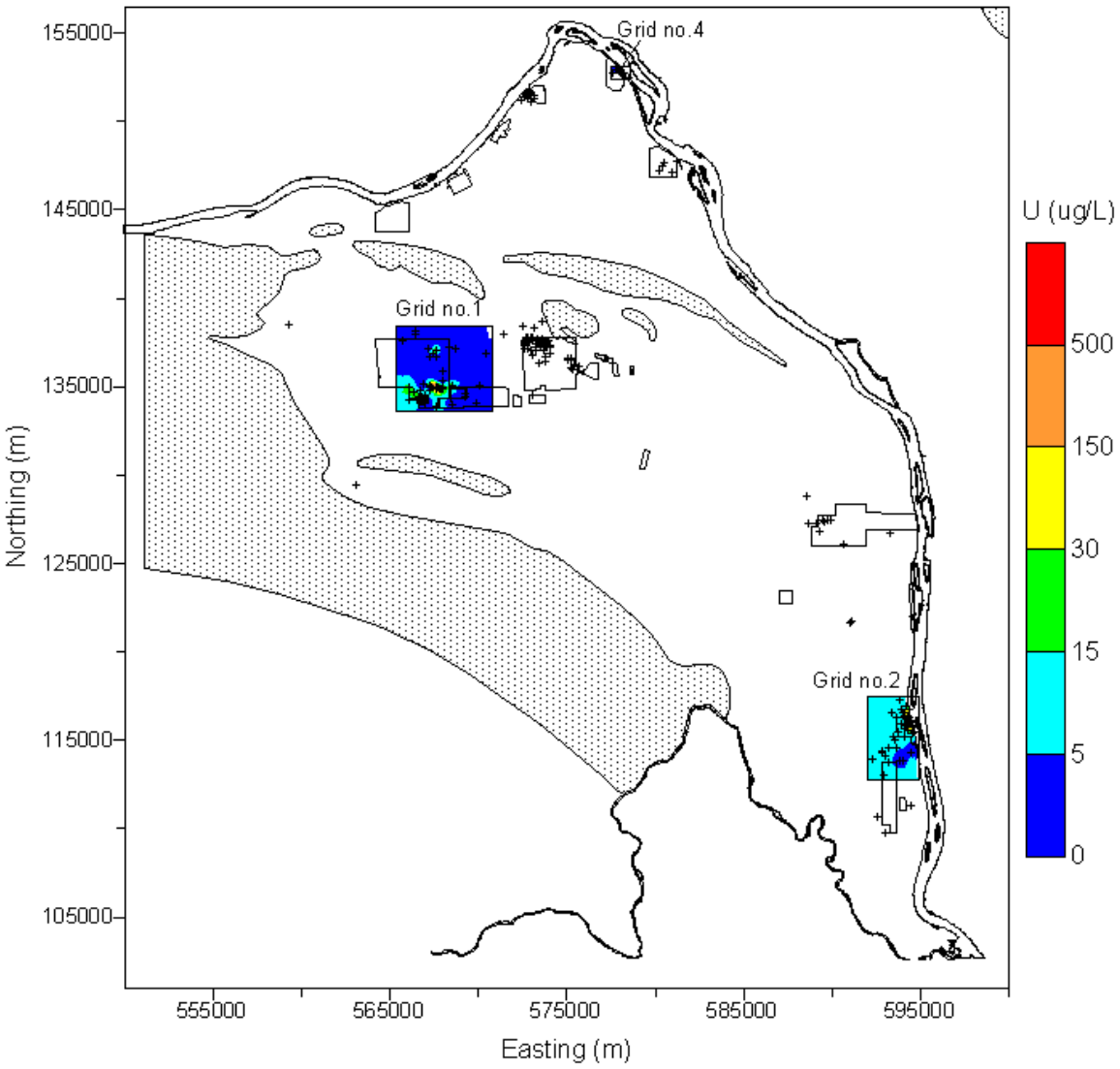

Figure G.3. Median of Simulations of FY 2001 Uranium Concentrations for Grids 1, 2, and 4. No spatial structure was detected in the data from the 200 East Area, so the geostatistical analysis and calculation of history matching metrics were not performed.

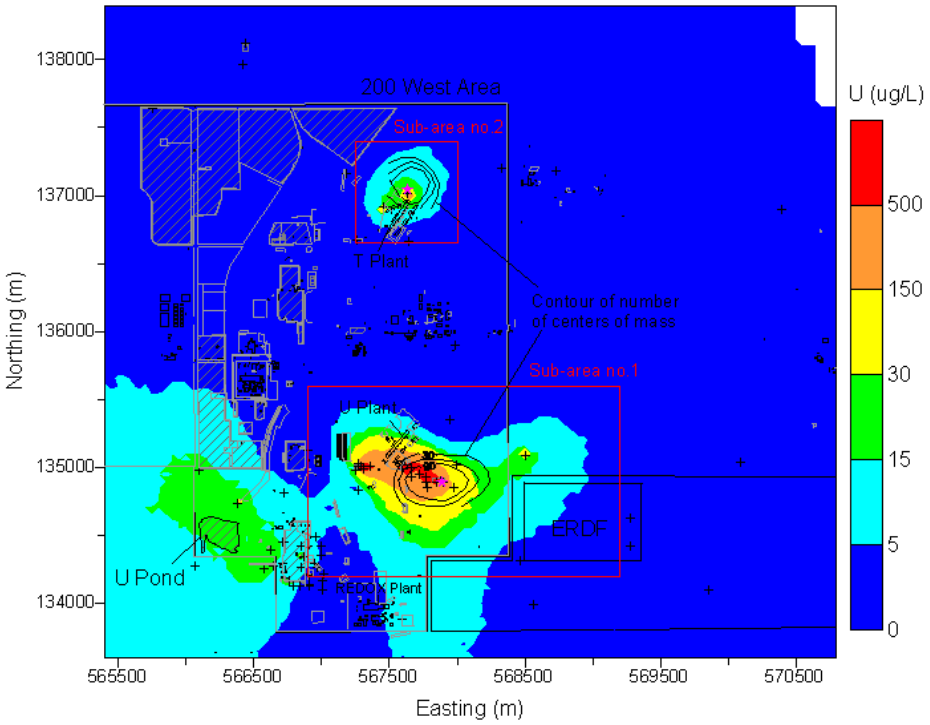

Figure G.4. Median of Simulated FY 2001 Uranium Concentrations in Grid 1 (200 West Area). Contours of the number of times that the center of mass within the sub-areas occurred within cells of an upscaled grid are shown with the average centers of mass shown by pink star in the sub-areas.

Table G.1. Coordinates for Sub-Area Boundaries for Grid 1 (200 West Area) of FY 2001 Uranium

Sub-Area 1		Sub-Area 2	
Easting (m)	Northing (m)	Easting (m)	Northing (m)
566900	134200	567250	136650
569200	134200	568000	136650
569200	135600	568000	137400
566900	135600	567250	137400
566900	134200	567250	136650

Table G.2. Statistics of Centers of Mass of Individual Simulations of FY 2001 Uranium Calculated for a Depth of 5 m for the Sub-Areas of Grid 1 (200 West Area)

Coordinate (m)	Sub-Area 1		Sub-Area 2	
	Easting	Northing	Easting	Northing
Mean	567883.9	134892.2	567634.4	137042.3
Standard Error	6.7	3.9	2.7	2.8
Median	567873.2	134888.5	567633.3	137038.4
Standard Deviation	171.7	98.7	69.6	70.4
Kurtosis	0.24	0.15	-0.42	-0.24
Skewness	0.54	0.21	0.17	0.26
Range	1009.9	615.3	378.0	424.0
Minimum	567470.6	134606.9	567454.3	136829.8
Maximum	568480.5	135222.2	567832.3	137253.8
Count	650	650	650	650
97.5^{th} Percentile	568258.2	135096.0	567777.5	137187.1
2.5^{th} Percentile	567605.6	134712.9	567506.9	136919.2
Confidence Level of Mean (95.0%)	13.2	7.6	5.4	5.4

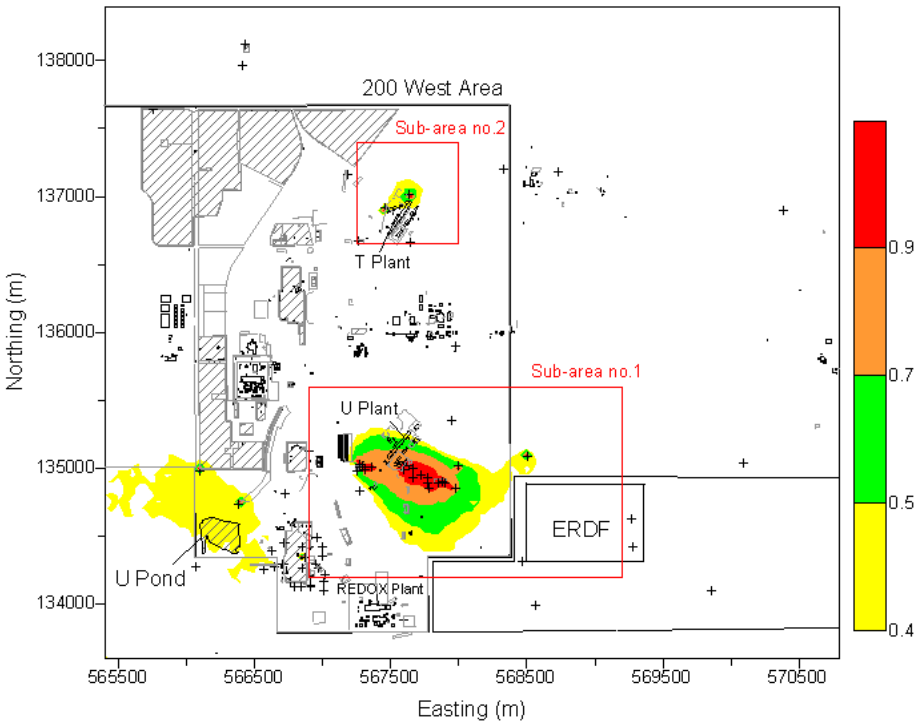

Figure G.5. Probability of Exceeding 30 µg/L Based on Simulations of FY 2001 Uranium in Grid 1 (200 West Area)

Table G.3. Area Exceeding 30 µg/L for FY 2001 Uranium for Each Simulation within Sub-Areas of Grid 1 (200 West Area)

Area (km^2)	Sub-Area 1	Sub-Area 2	Grid 1
Mean	0.834	0.104	33.19
Standard Error	0.008	0.002	0.36
Median	0.813	0.095	31.70
Standard Deviation	0.213	0.058	9.29
Kurtosis	0.316	0.340	0.30
Skewness	0.515	0.747	0.65
Range	1.310	0.330	57.70
Minimum	0.358	0.010	13.30
Maximum	1.668	0.340	71.00
Count	650	650	650
97.5^{th} Percentile	1.290	0.228	54.25
2.5^{th} Percentile	0.470	0.020	17.88
Confidence Level of Mean (95.0%)	0.016	0.004	0.72

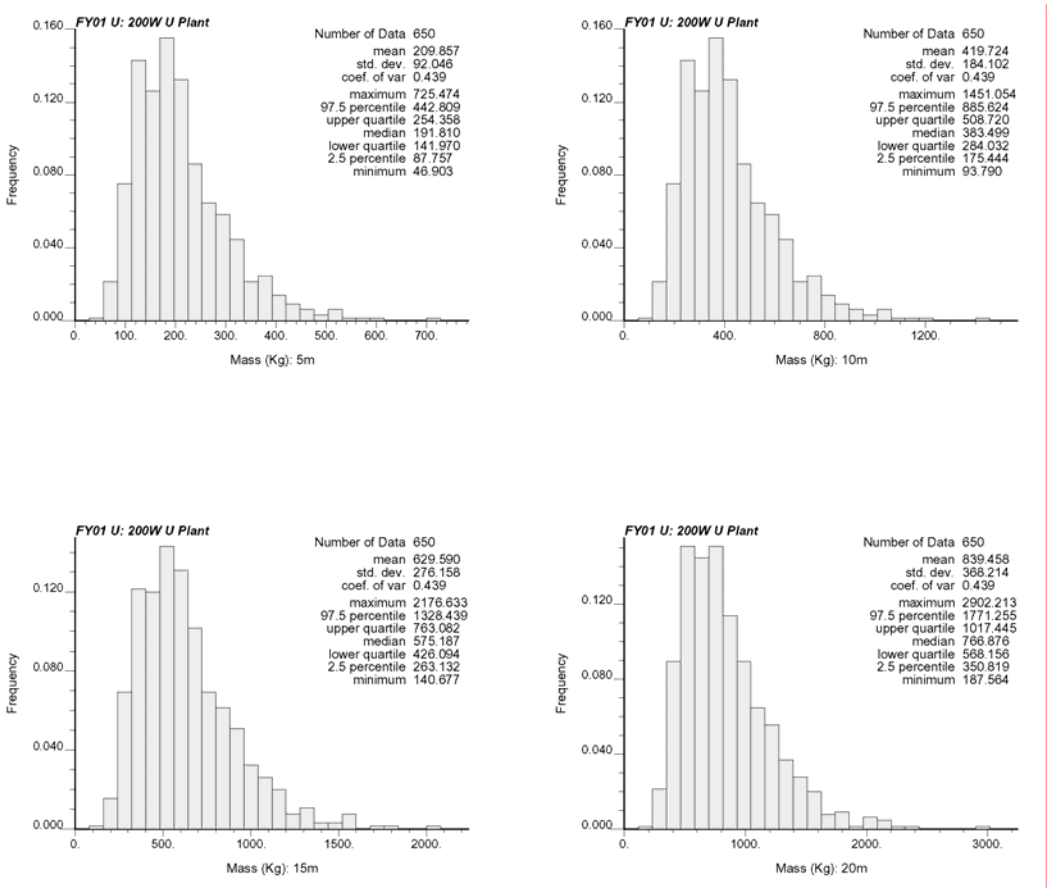

Figure G.6. Histograms of Total Activity in Simulations of FY 2001 Uranium within Sub-Area 1 of Grid 1 (200 West Area), Four Thickness Assumptions

Table G.4. Statistics of Total Activity of Simulations of FY 2001 Uranium within Sub-Area 1 of Grid 1 (200 West Area), Four Thickness Assumptions

Mass (kg) in Depth	5 m	10 m	15 m	20 m
Mean	209.86	419.72	629.59	839.46
Standard Error	3.61	7.23	10.84	14.45
Median	191.81	383.50	575.19	766.87
Standard Deviation	92.12	184.24	276.37	368.50
Kurtosis	2.63	2.63	2.62	2.62
Skewness	1.29	1.29	1.29	1.29
Range	678.57	1,357.26	2,035.96	2,714.65
Minimum	46.90	93.79	140.68	187.56
Maximum	725.47	1,451.05	2,176.63	2,902.21
Count	650	650	650	650
97.5^{th} Percentile	442.69	885.39	1,328.09	1,770.79
2.5^{th} Percentile	87.98	175.87	263.75	351.64
Confidence Level of Mean (95.0%)	7.09	14.19	21.29	28.38

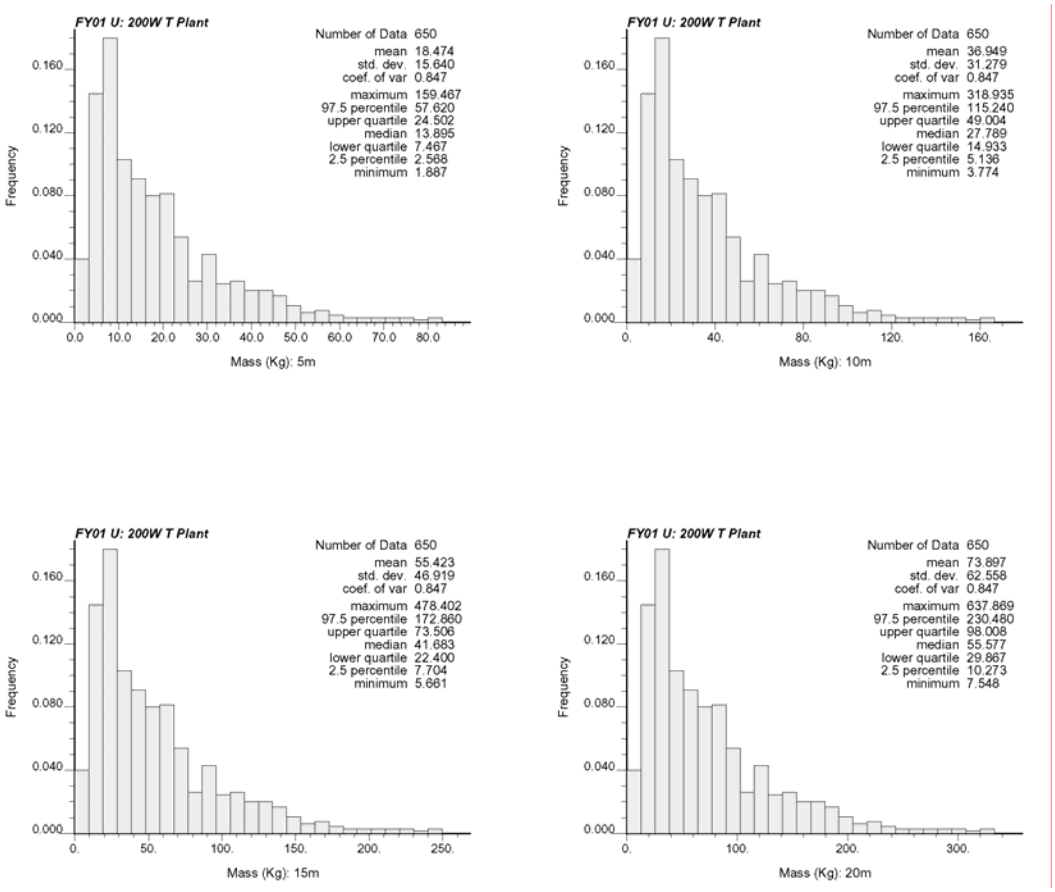

Figure G.7. Histograms of Total Mass in Simulations of FY 2001 Uranium within Sub-Area 2 of Grid 1 (200 West Area), Four Thickness Assumptions

Table G.5. Statistics of Total Mass of Simulations of FY 2001 Uranium within Sub-Area 2 of Grid 1 (200 West Area), Four Thickness Assumptions

Mass (kg) in Depth	5 m	10 m	15 m	20 m
Mean	18.47	36.95	55.42	73.90
Standard Error	0.61	1.23	1.84	2.46
Median	13.89	27.79	41.68	55.58
Standard Deviation	15.65	31.30	46.95	62.61
Kurtosis	11.87	11.87	11.87	11.87
Skewness	2.41	2.41	2.41	2.41
Range	157.58	315.16	472.74	630.32
Minimum	1.89	3.77	5.66	7.55
Maximum	159.47	318.93	478.40	637.87
Count	650	650	650	650
97.5^{th} Percentile	57.56	115.13	172.69	230.25
2.5^{th} Percentile	2.58	5.16	7.74	10.32
Confidence Level of Mean (95.0%)	1.21	2.41	3.62	4.82

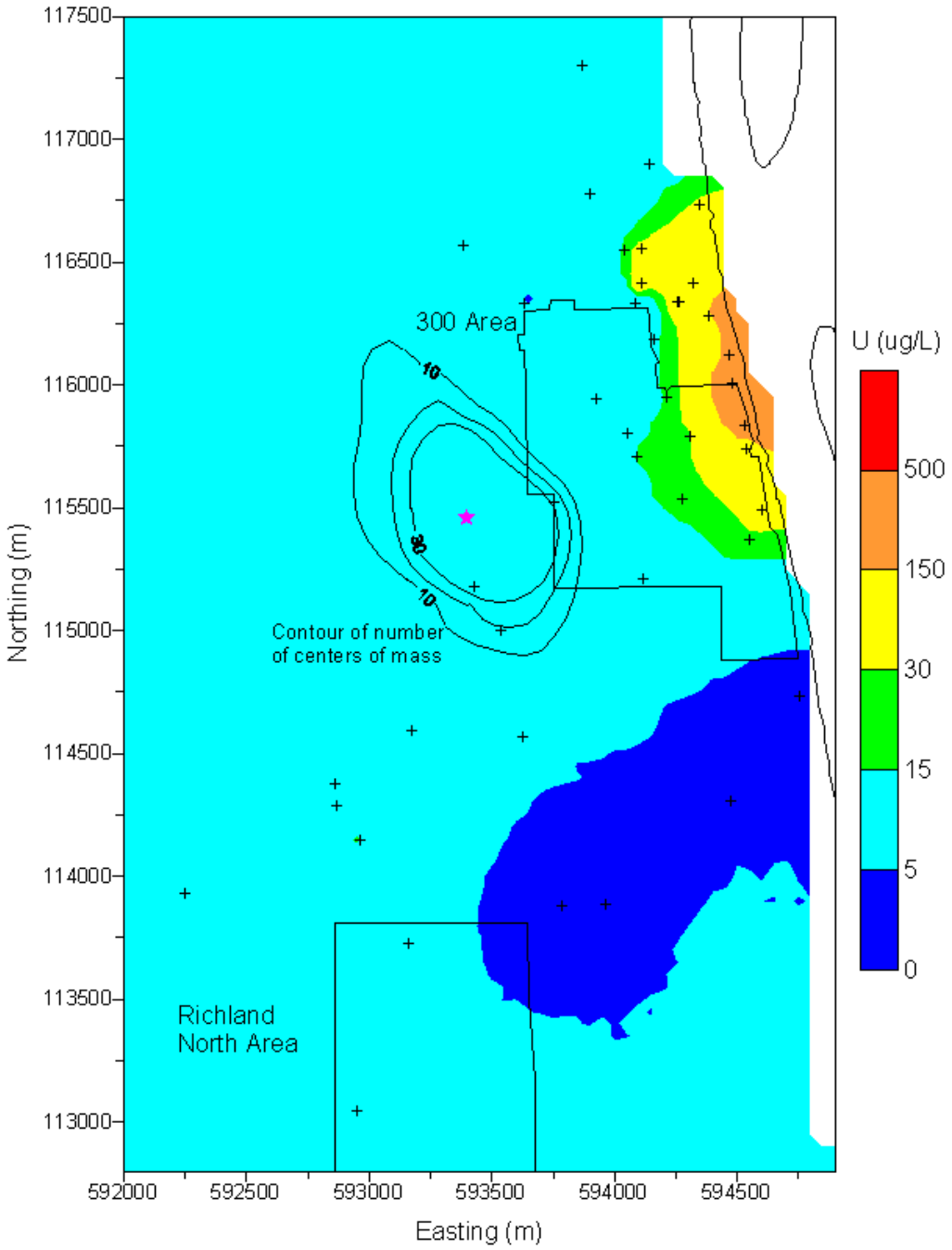

Figure G.8. Median of Simulated FY 2001 Uranium Concentrations in Grid 2 (300 Area). Contours of the number of times that the center of mass within the grid occurred within cells of an upscaled grid are shown with the average centers of mass shown by pink star in the grid.

Table G.6. Coordinates for Sub-Area Boundary for Grid 2 (300 Area) of FY 2001 Uranium

Easting (m)	Northing (m)
592000	117500
594196	117500
594196	116904
594254	116850
594450	116850
594450	116397
594551	116258
594551	116043
594659	115960
594659	115599
594700	115568
594700	115251
594800	115156
594800	112958
594900	112908
594900	112800
592000	112800
592000	117500

Table G.7. Statistics of the Area Exceeding 30 μg/L and Locations of Centers of Mass for Simulations of FY 2001 Uranium within Grid 2 (300 Area)

	Area (km^2)	Center of Mass (unit: m)	
		Easting	Northing
Mean	1.426	593475.2	115499.7
Standard Error	0.026	9.3	12.3
Median	1.261	593495.4	115492.9
Standard Deviation	0.652	237.4	313.9
Kurtosis	1.593	-0.54	0.15
Skewness	1.211	-0.33	-0.05
Range	3.928	1156.5	1784.0
Minimum	0.508	592821.6	114557.1
Maximum	4.435	593978.1	116341.1
Count	650	650	650
97.5^{th} Percentile	3.073	593864.5	116123.8
2.5^{th} Percentile	0.615	592975.2	114855.3
Confidence Level (95.0%)	0.050	18.3	24.2

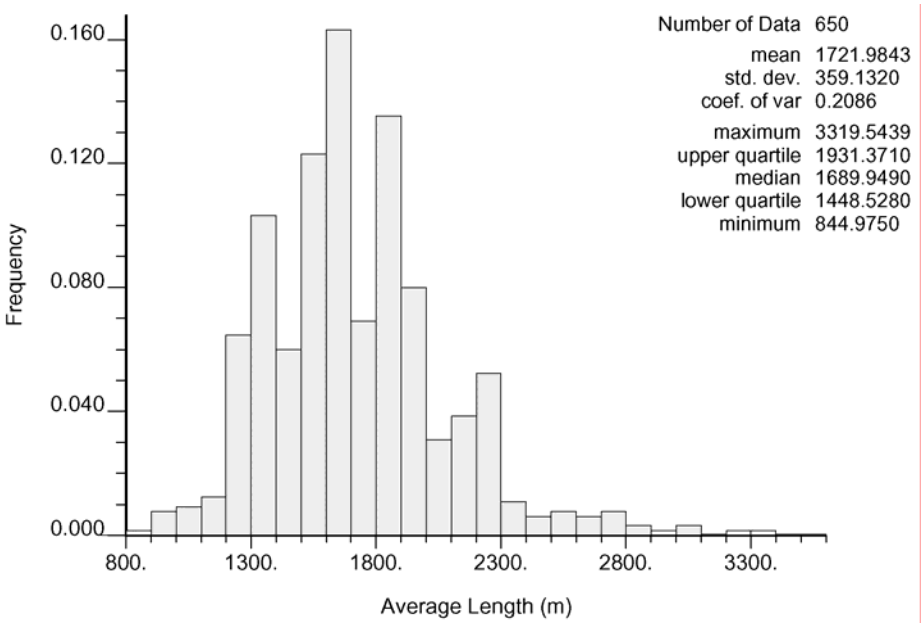

Figure G.9. Histogram of the Average Length of Columbia River Shoreline Exceeding 30 μg/L for FY 2001 Uranium in Grid 2 (300 Area)

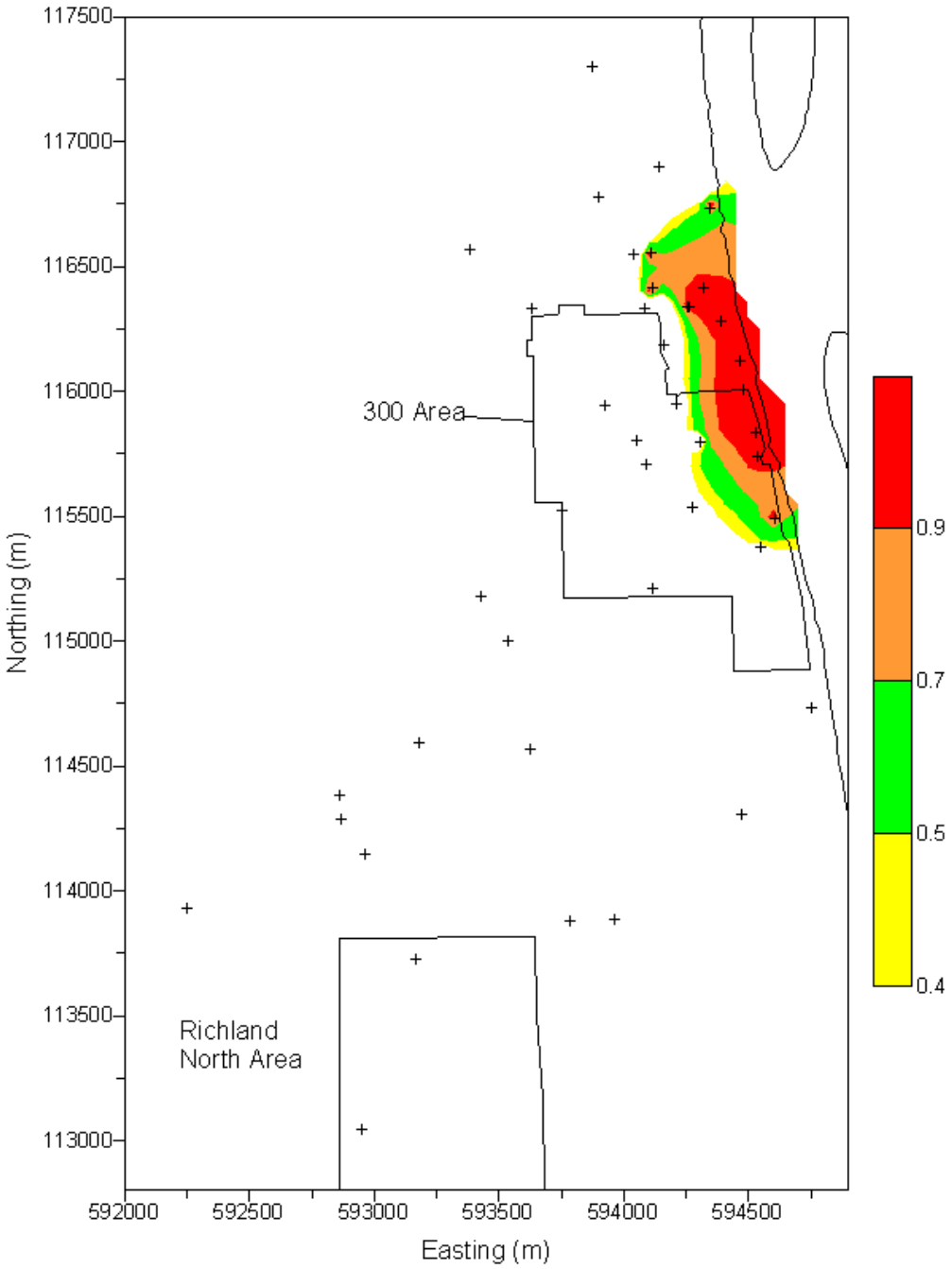

Figure G.10. Probability of Exceeding 30 μg/L Based on Simulations of FY 2001 Uranium in Grid 2 (300 Area)

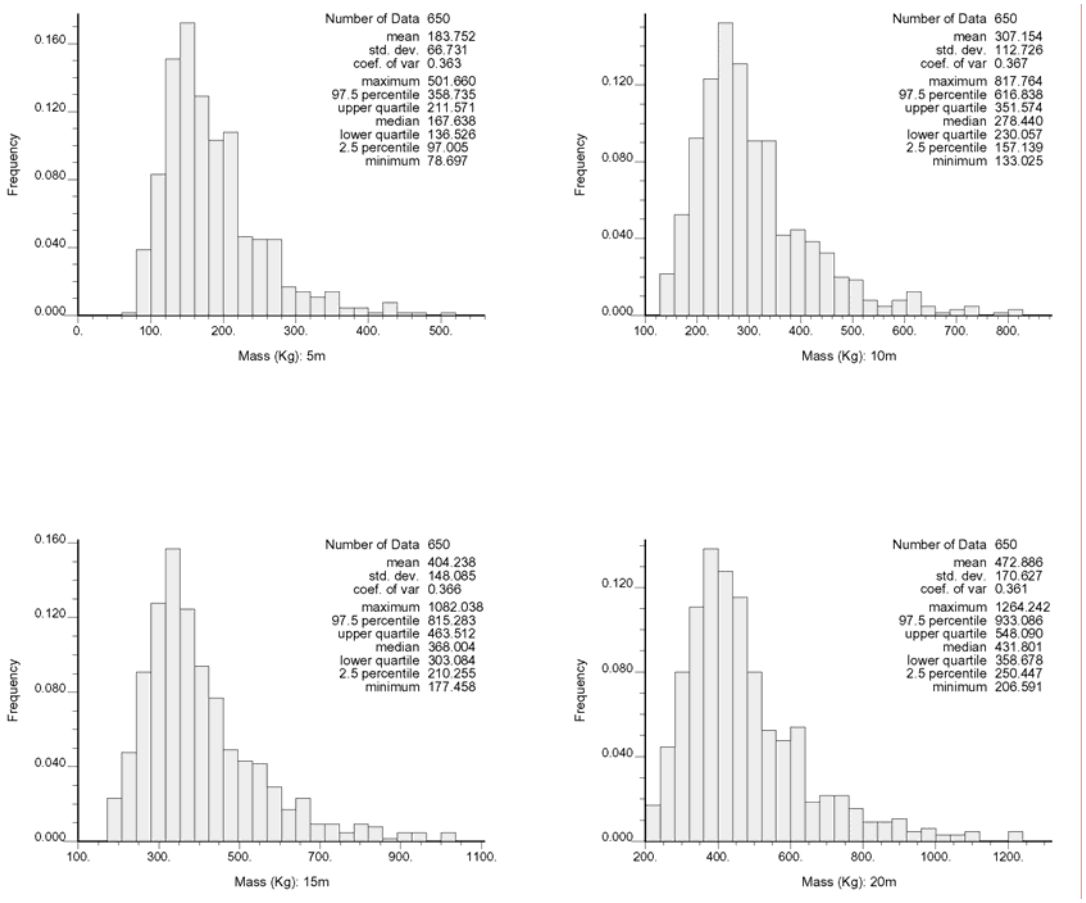

Figure G.11. Histograms of Total Mass in Simulations of FY 2001 Uranium within Grid 2 (300 Area), Four Thickness Assumptions

Table G.8. Statistics of Total Mass of Simulations of FY 2001 Uranium within Grid 2 (300 Area), Four Thickness Assumptions

Mass (kg) in Depth	5 m	10 m	15 m	20 m
Mean	183.75	307.15	404.24	472.89
Standard Error	2.62	4.42	5.81	6.70
Median	167.64	278.44	368.00	431.80
Standard Deviation	66.78	112.81	148.20	170.76
Kurtosis	2.65	2.71	2.71	2.76
Skewness	1.41	1.45	1.45	1.46
Range	422.96	684.74	904.58	1,057.65
Minimum	78.70	133.02	177.46	206.59
Maximum	501.66	817.76	1,082.04	1,264.24
Count	650	650	650	650
97.5^{th} Percentile	358.47	615.93	814.09	928.62
2.5^{th} Percentile	97.11	157.38	210.97	251.01
Confidence Level of Mean (95.0%)	5.14	8.69	11.41	13.15

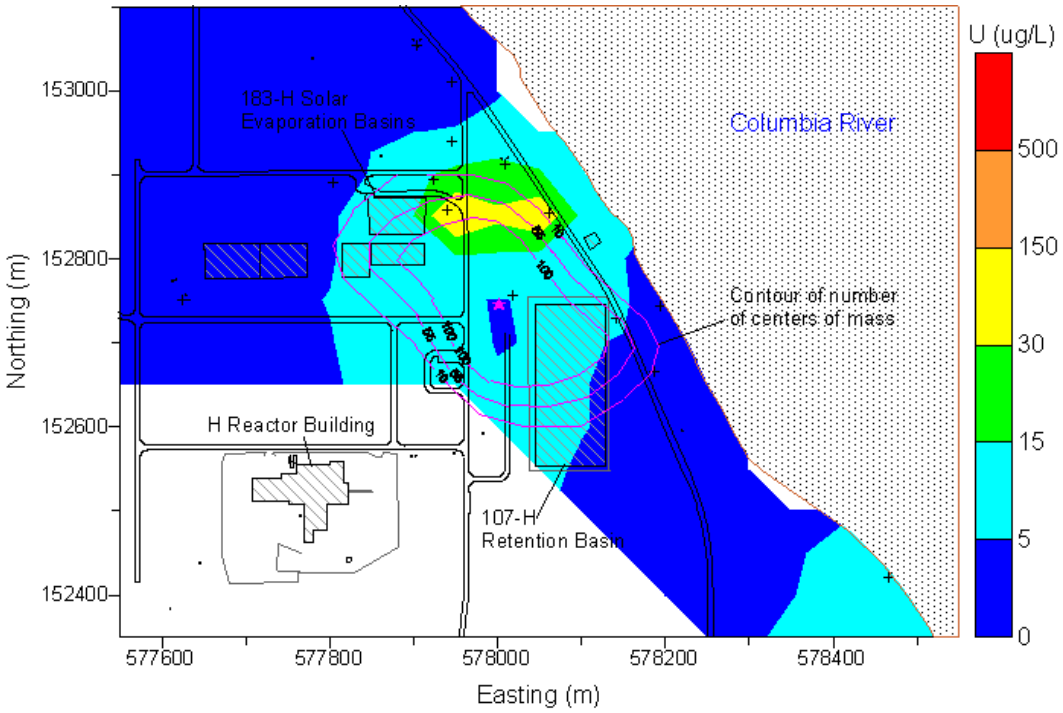

Figure G.12. Median of Simulated FY 2001 Uranium Concentrations in Grid 4 (100 H Area). Contours of the number of times that the center of mass within the grid occurred within cells of an upscaled grid are shown with the average centers of mass shown by pink star in the grid.

Table G.9. Coordinates for Sub-Area Boundary for Grid 4 (100 H Area) of FY 2001 Uranium

Easting (m)	Northing (m)
577550	153100
578000	153100
578000	153000
578050	152950
578150	152950
578150	152900
578200	152850
578200	152800
578250	152750
578250	152700
578300	152650
578300	152550
578350	152500
578450	152500
578500	152450
578550	152450
578550	152350
578250	152350
577950	152650
577550	152650
577550	153100

Table G.10. Statistics of the Area Exceeding 30 μg/L and Locations of Centers of Mass for Simulations of FY 2001 Uranium within Grid 4 (100 H Area)

	Area (km^2)	Center of Mass (unit: m)	
		Easting	Northing
Mean	0.062	578005.1	152742.3
Standard Error	0.001	2.6	2.0
Median	0.060	578004.9	152743.3
Standard Deviation	0.025	70.1	54.2
Kurtosis	0.097	-0.46	-0.16
Skewness	0.571	-0.11	0.11
Range	0.143	366.6	308.2
Minimum	0.010	577815.7	152600.3
Maximum	0.153	578182.3	152908.4
Count	700	700	700
97.5^{th} Percentile	0.118	578134.1	152854.1
2.5^{th} Percentile	0.023	577864.8	152637.6
Confidence Level (95.0%)	0.002	5.2	4.0

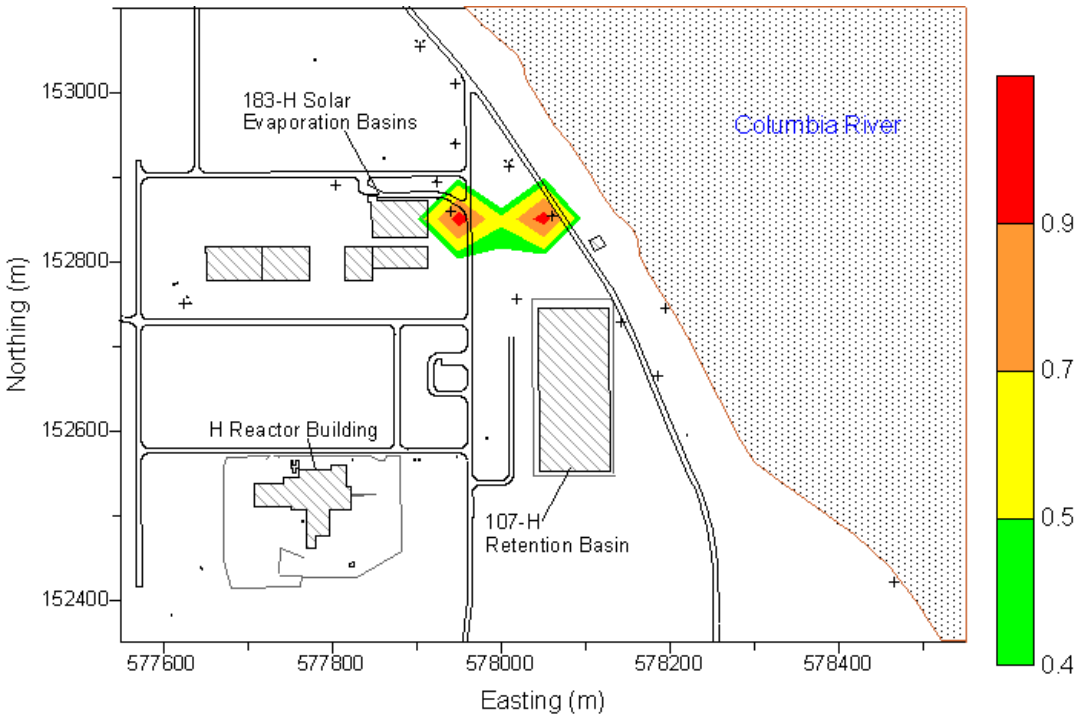

Figure G.13. Probability of Exceeding 30 µg/L Based on Simulations of FY 2001 Uranium in Grid 4 (100 H Area)

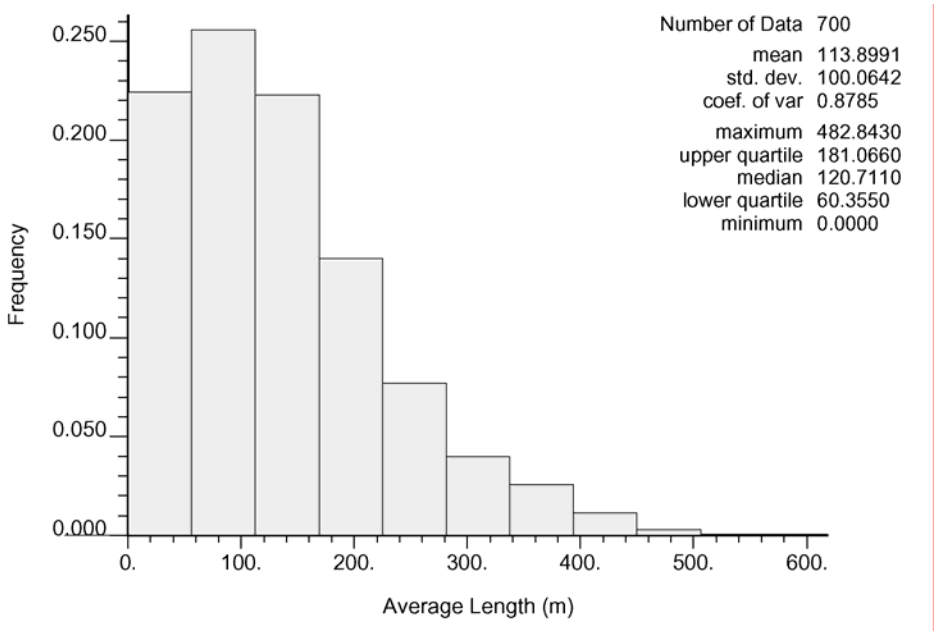

Figure G.14. Histogram of the Average Length of Columbia River Shoreline Exceeding 30 µg/L for FY 2001 Uranium in Grid 4 (100 H Area)

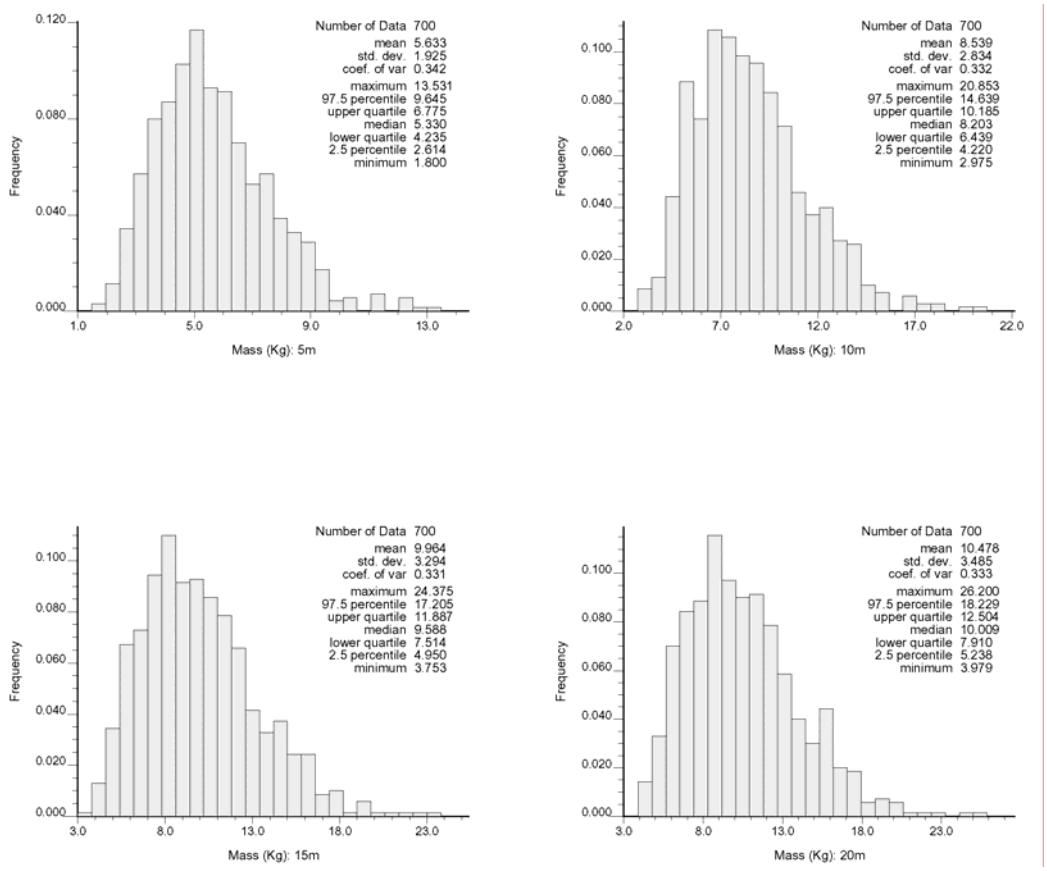

Figure G.15. Histograms of Total Mass in Simulations of FY 2001 Uranium within Grid 4 (100 H Area), Four Thickness Assumptions

Table G.11. Statistics of Total Mass of Simulations of FY 2001 Uranium within Grid 4 (100 H Area), Four Thickness Assumptions

Mass (kg) in Depth	5 m	10 m	15 m	20 m
Mean	5.633	8.539	9.964	10.478
Standard Error	0.073	0.107	0.125	0.132
Median	5.330	8.204	9.589	10.009
Standard Deviation	1.926	2.836	3.296	3.488
Kurtosis	0.759	0.744	0.641	0.713
Skewness	0.765	0.768	0.752	0.771
Range	11.731	17.879	20.622	22.221
Minimum	1.800	2.975	3.753	3.979
Maximum	13.531	20.853	24.375	26.200
Count	700	700	700	700
97.5^{th} Percentile	9.643	14.639	17.204	18.229
2.5^{th} Percentile	2.614	4.220	4.950	5.238
Confidence Level of Mean (95.0%)	0.143	0.210	0.245	0.259

Appendix H

Figures and Data Tables for FY 1992 Uranium

Appendix H

Figures and Data Tables for FY 1992 Uranium

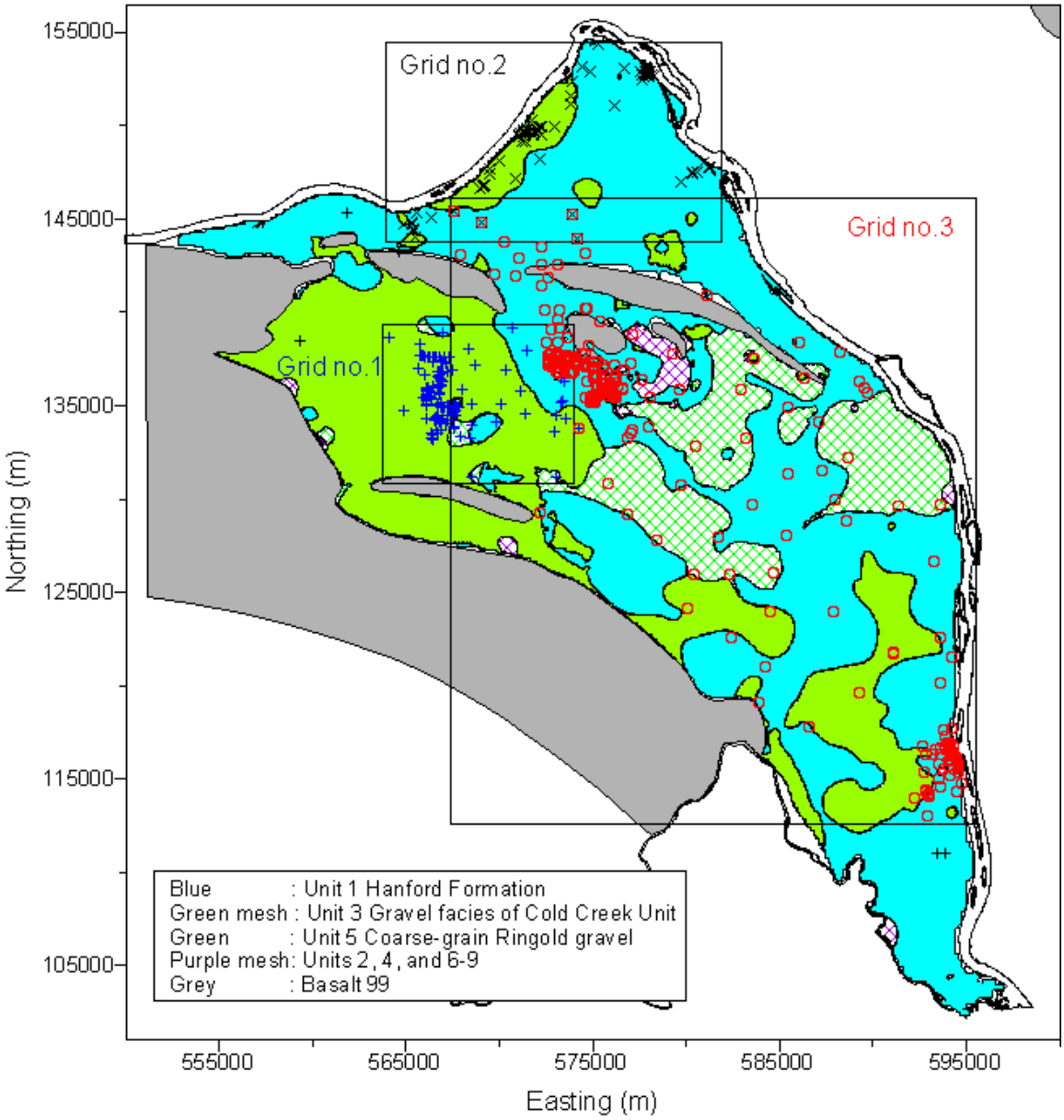

Figure H.1. Subsets of FY 1992 Uranium Data and Subcrop Formation Units at the FY 1992 Water Table

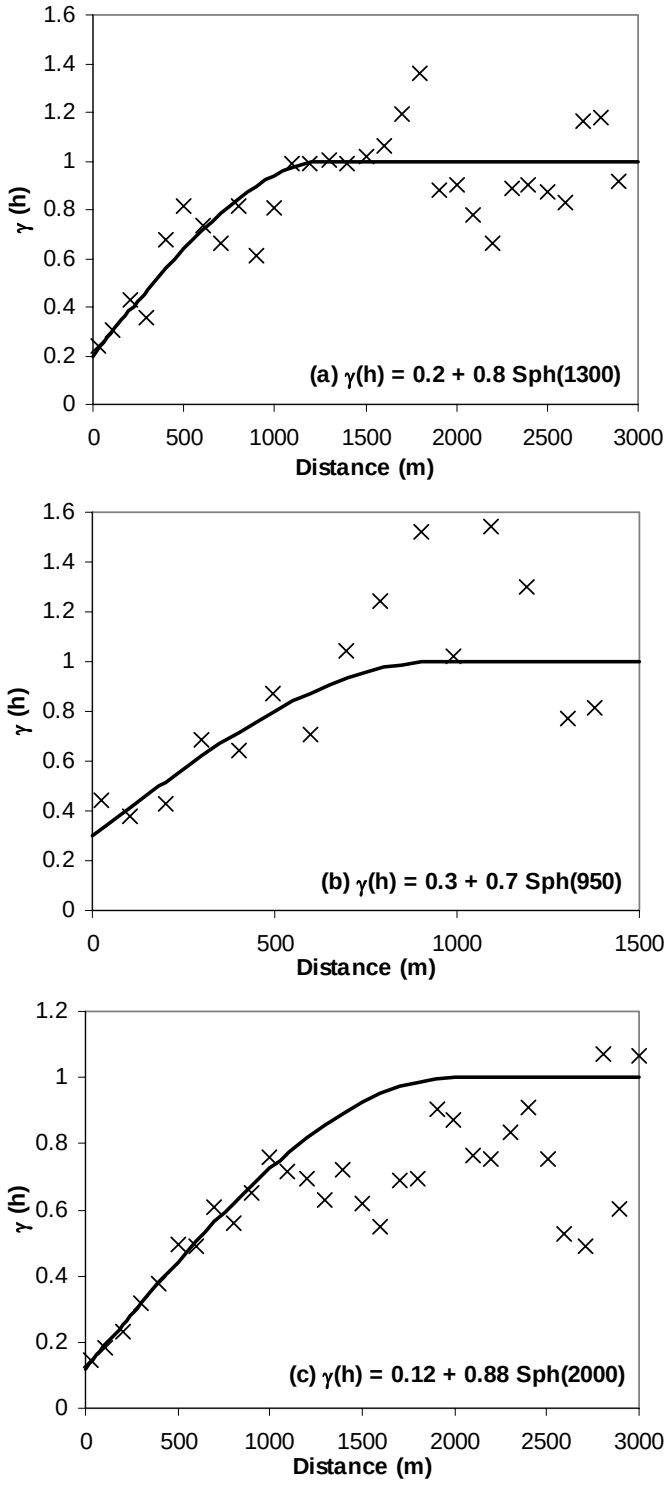

Figure H.2. Variograms and Models of Normal Scores of the FY 1992 Uranium Data in Local Grid 1 (a), Grid 2 (b), and Grid 3 (c). Experimental variogram values designated by X, with the models fit to the data denoted by the solid black lines.

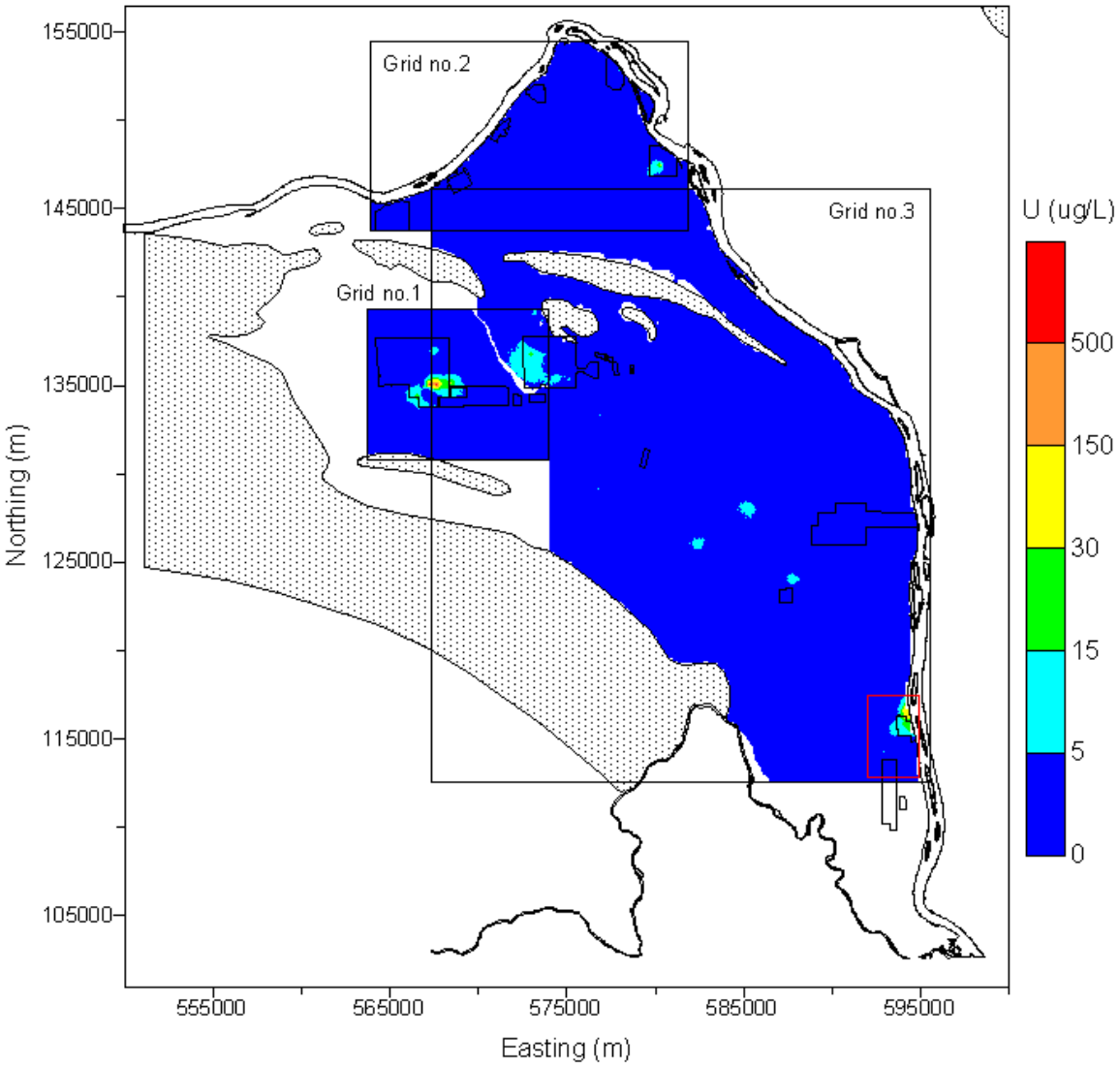

Figure H.3. Median of Simulations of FY 1992 Uranium Concentrations for Grids 1, 2, and 3

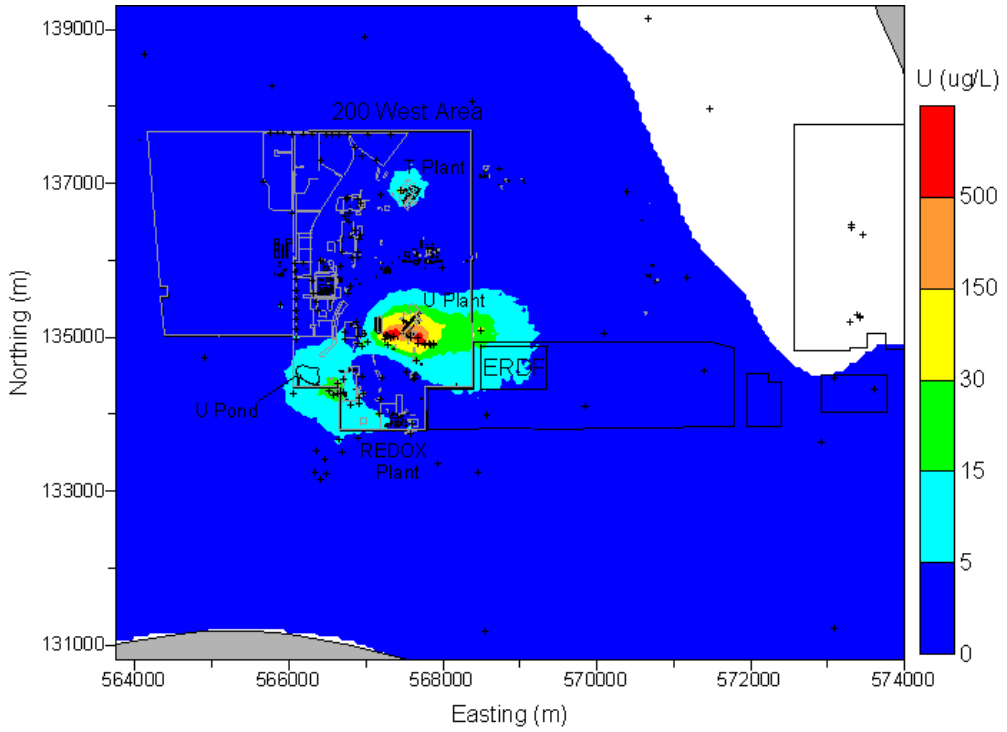

Figure H.4. Median of Simulated FY 1992 Uranium Concentrations in Grid 1 (200 West Area)

Table H.1. Coordinates for the Boundary of Grid 1 (200 West Area) of FY 1992 Uranium

Easting (m)	Northing (m)
563750	139300
569750	139300
569850	139000
570350	138450
571350	136150
571950	135550
572250	134950
572800	134500
573050	134500
573650	134900
574000	134900
574000	130800
567450	130800
566650	131100
566400	131100
566350	131150
566000	131150
565950	131200
564950	131200
564900	131150
564200	131150
564150	131100
564000	131100
563950	131050
563750	131050
563750	139300

Table H.2. Statistics of the Area Exceeding 30 µg/L and Locations of Centers of Mass for Simulations of FY 1992 Uranium within Grid 1 (200 West Area)

	Area (km^2)	Center of Mass (unit: m)	
		Easting	Northing
Mean	6.98	569192.6	133900.9
Standard Error	0.09	44.0	28.9
Median	6.79	569250.9	133900.8
Standard Deviation	2.18	1032.3	678.8
Kurtosis	0.38	0.24	-0.39
Skewness	0.58	-0.51	0.10
Range	12.89	6057.4	3853.1
Minimum	2.23	565613.5	132013.3
Maximum	15.11	571670.9	135866.4
Count	550	550	550
97.5th Percentile	11.67	570900.2	135201.5
2.5th Percentile	3.55	566803.9	132681.6
Confidence Level (95.0%)	0.18	86.5	56.9

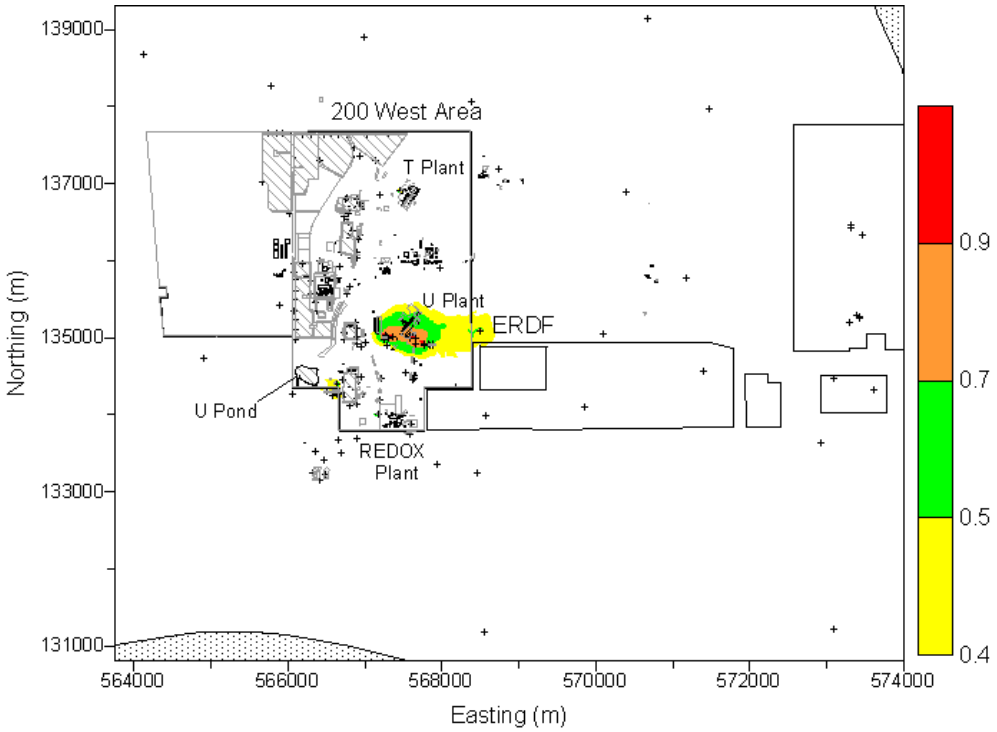

Figure H.5. Probability of Exceeding 30 µg/L Based on Simulations of FY 1992 Uranium in Grid 1 (200 West Area)

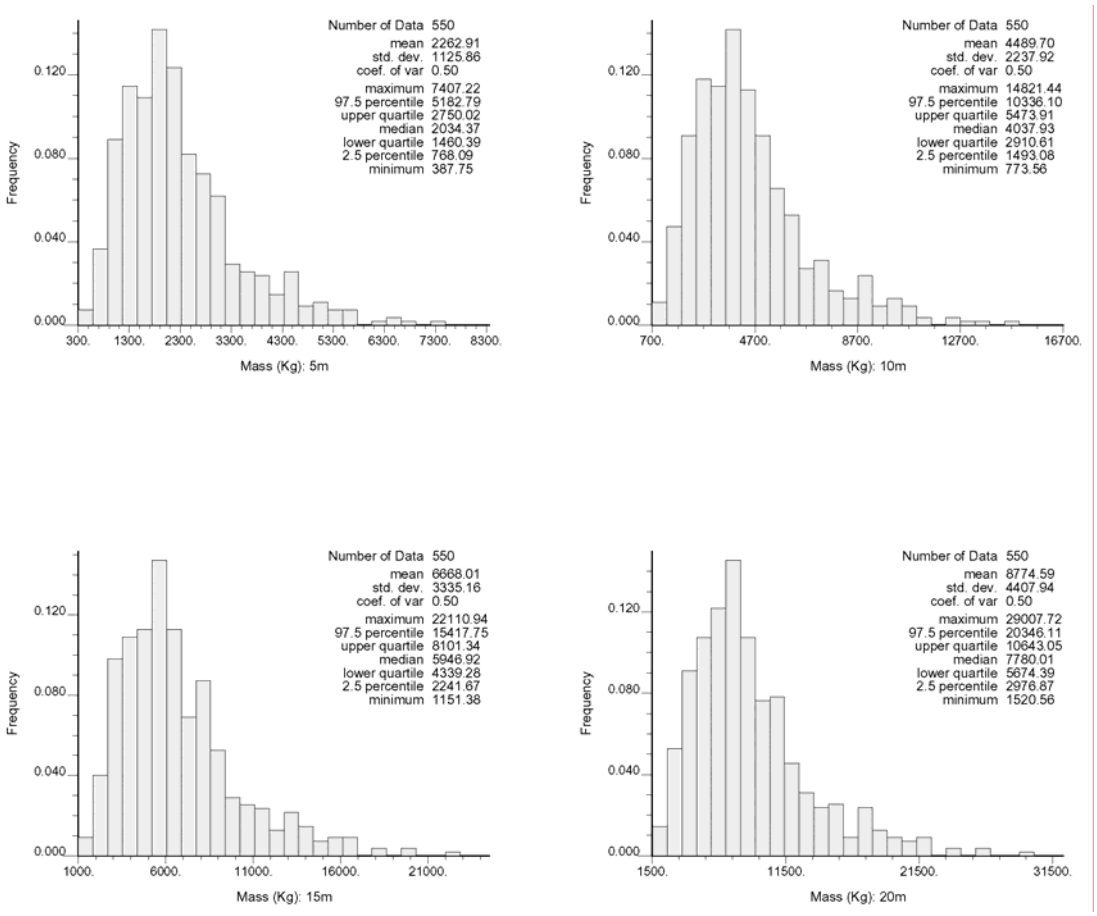

Figure H.6. Histograms of Total Mass in Simulations of FY 1992 Uranium within Grid 1 (200 West Area), Four Thickness Assumptions

Table H.3. Statistics of Total Mass of Simulations of FY 1992 Uranium within Grid 1 (200 West Area), Four Thickness Assumptions

Mass (kg) in Depth	5 m	10 m	15 m	20 m
Mean	2,262.90	4,489.69	6,668.01	8,774.60
Standard Error	48.05	95.51	142.34	188.13
Median	2,034.37	4,037.93	5,946.91	7,780.00
Standard Deviation	1,126.88	2,239.96	3,338.20	4,411.96
Kurtosis	2.08	2.10	2.10	2.09
Skewness	1.29	1.30	1.30	1.31
Range	7,019.47	14,047.89	20,959.56	27,487.17
Minimum	387.75	773.56	1,151.38	1,520.56
Maximum	7,407.22	14,821.44	22,110.94	29,007.72
Count	550	550	550	550
97.5^{th} Percentile	5,187.91	10,338.39	15,440.26	20,406.87
2.5^{th} Percentile	763.42	1,483.63	2,232.25	2,967.34
Confidence Level of Mean (95.0%)	94.39	187.61	279.60	369.54

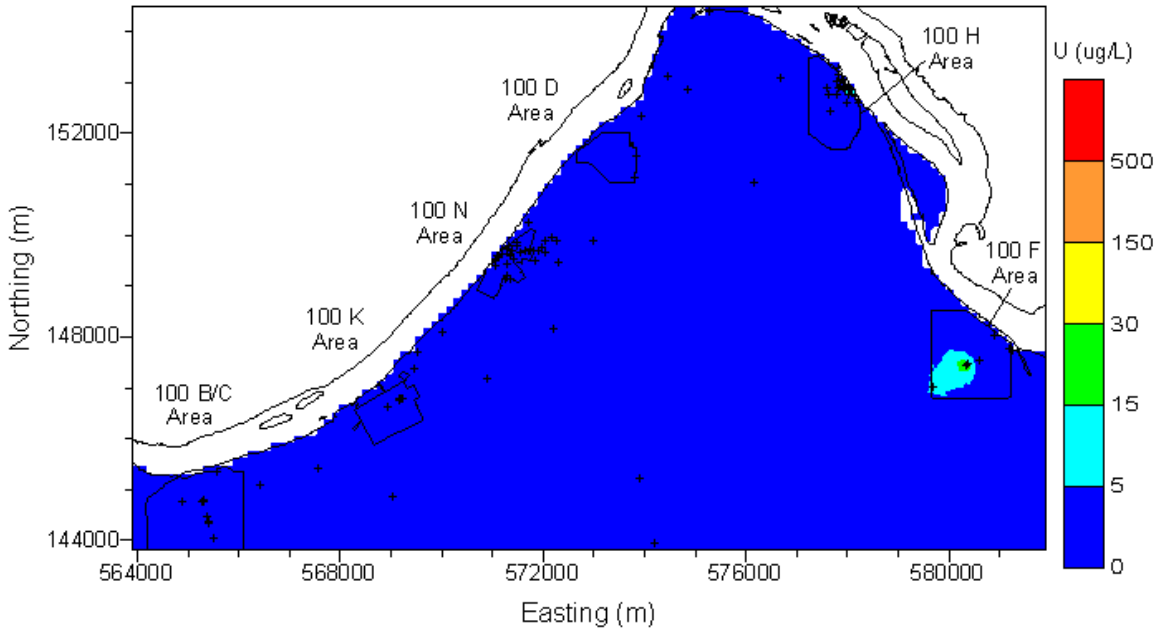

Figure H.7. Median of Simulated FY 1992 Uranium Concentrations in Grid 2 (100 Areas)

Table H.4. Coordinates for the Boundary of Grid 2 (100 Areas) of FY 1992 Uranium

Easting (m)	Northing (m)
563900	143800
563900	145566
564206	145277
564778	145277
565610	145502
566373	145754
566915	145882
567588	146172
567905	146522
568736	147033
569056	147447
569597	147959
570361	148692
570967	149392
572118	150987
572754	151785
573070	152199
573965	152744
573996	153030
574315	153828
574379	154144
574635	154500
575910	154500
577761	153410
578239	152710
579740	151371
579962	150987
579962	150573
579706	149806
579582	149614
579706	149200
580124	148787
580985	148211
581463	147764
581900	147700
581900	143800
563900	143800

Table H.5. Statistics of the Area Exceeding 30 μg/L and Locations of Centers of Mass for Simulations of FY 1992 Uranium within Grid 2 (100 Areas)

	Area (km^2)	Center of Mass (unit: m)	
		Easting	Northing
Mean	7.13	575292.6	147010.4
Standard Error	0.12	35.4	20.0
Median	6.64	575312.2	146986.3
Standard Deviation	3.06	936.3	529.9
Kurtosis	1.21	-0.17	-0.23
Skewness	0.99	-0.05	0.32
Range	19.57	5996.8	2888.2
Minimum	0.91	572180.9	145797.1
Maximum	20.48	578177.8	148685.3
Count	700	700	700
97.5^{th} Percentile	14.27	577016.1	148183.8
2.5^{th} Percentile	2.65	573596.9	146065.1
Confidence Level (95.0%)	0.23	69.5	39.3

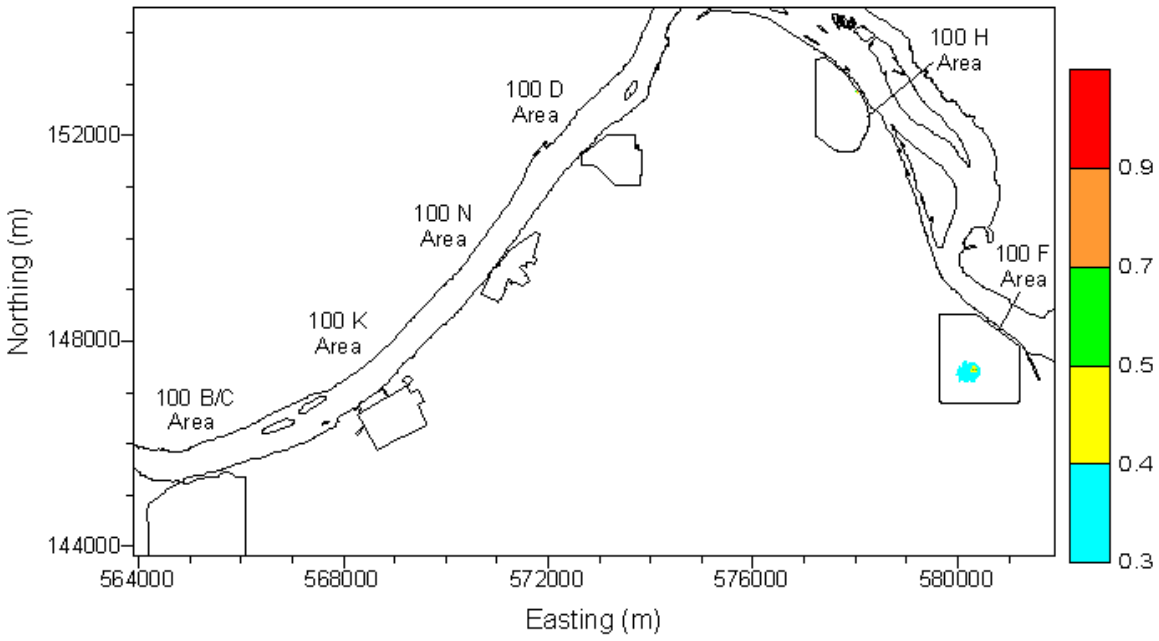

Figure H.8. Probability of Exceeding 30 µg/L Based on Simulations of FY 1992 Uranium in Grid 2 (100 Areas)

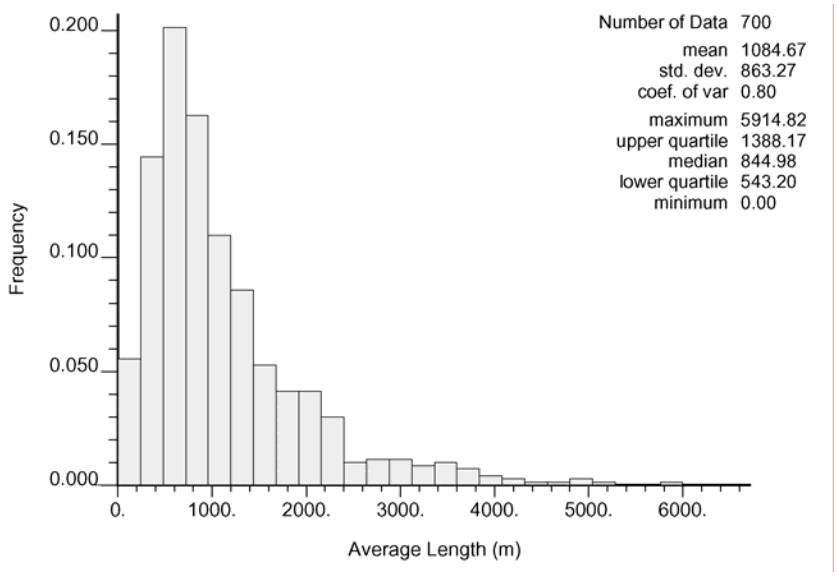

Figure H.9. Histogram of the Average Length of Columbia River Shoreline Exceeding 30 µg/L for FY 1992 Uranium in Grid 2 (100 Areas)

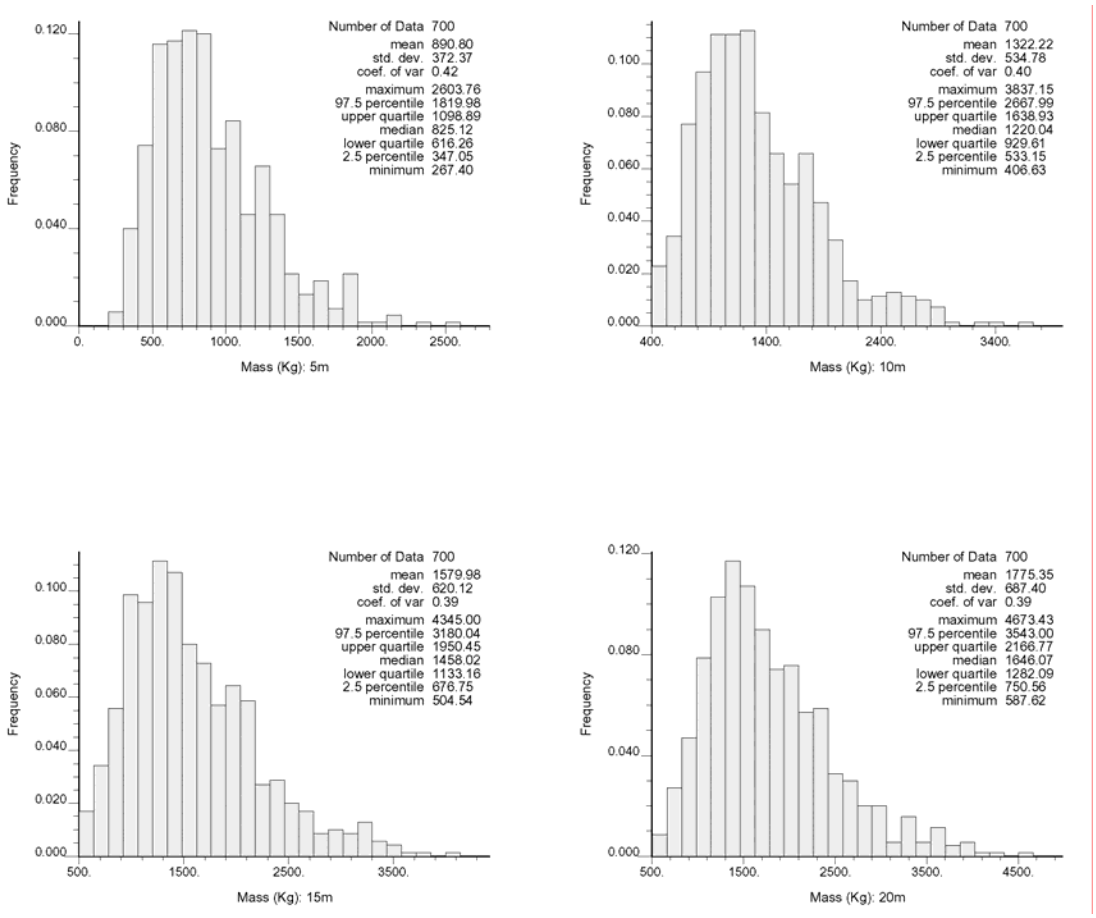

Figure H.10. Histograms of Total Mass in Simulations of FY 1992 Uranium within Grid 2 (100 Areas), Four Thickness Assumptions

Table H.6. Statistics of Total Mass of Simulations of FY 1992 Uranium within Grid 2 (100 Areas), Four Thickness Assumptions

Mass (kg) in Depth	5 m	10 m	15 m	20 m
Mean	890.80	1,322.22	1,579.98	1,775.35
Standard Error	14.08	20.23	23.45	26.00
Median	825.12	1,220.04	1,458.02	1,646.08
Standard Deviation	372.64	535.16	620.56	687.89
Kurtosis	1.10	1.22	1.05	0.96
Skewness	0.98	1.01	0.98	0.96
Range	2,336.36	3,430.52	3,840.46	4,085.82
Minimum	267.40	406.63	504.54	587.62
Maximum	2,603.76	3,837.15	4,345.00	4,673.43
Count	700	700	700	700
97.5^{th} Percentile	1,819.97	2,667.91	3,180.04	3,542.94
2.5^{th} Percentile	347.05	533.15	676.75	750.56
Confidence Level of Mean (95.0%)	27.65	39.71	46.05	51.05

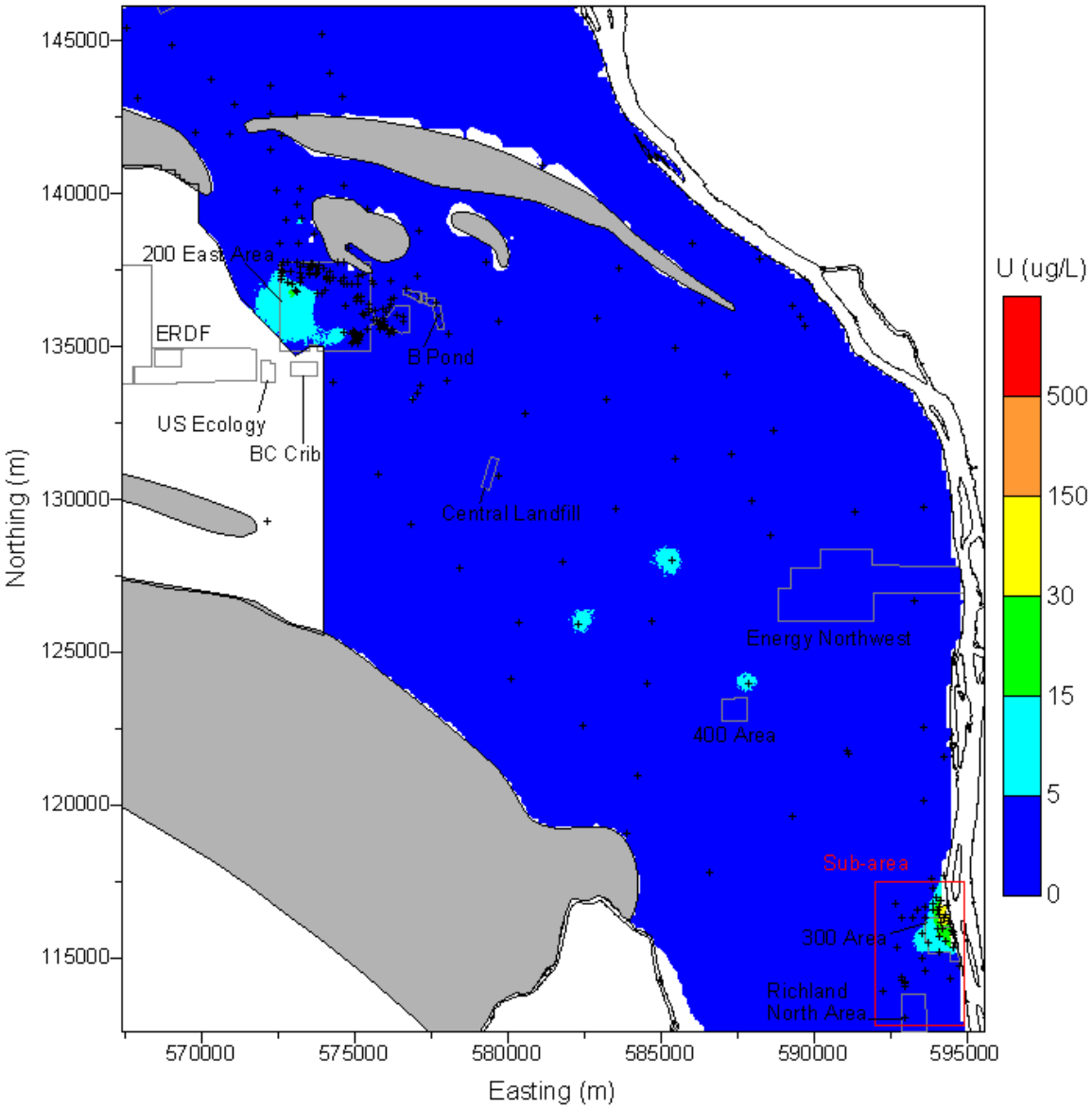

Figure H.11. Median of Simulated FY 1992 Uranium Concentrations in Grid 3

Table H.7. Coordinates for Sub-Area Boundary of Grid 3 of FY 1992 Uranium

Easting (m)	Northing (m)
592000	117500
594196	117500
594196	116904
594254	116850
594450	116850
594450	116397
594551	116258
594551	116043
594659	115960
594659	115599
594700	115568
594700	115251
594800	115156
594800	112958
594900	112908
594900	112800
592000	112800
592000	117500

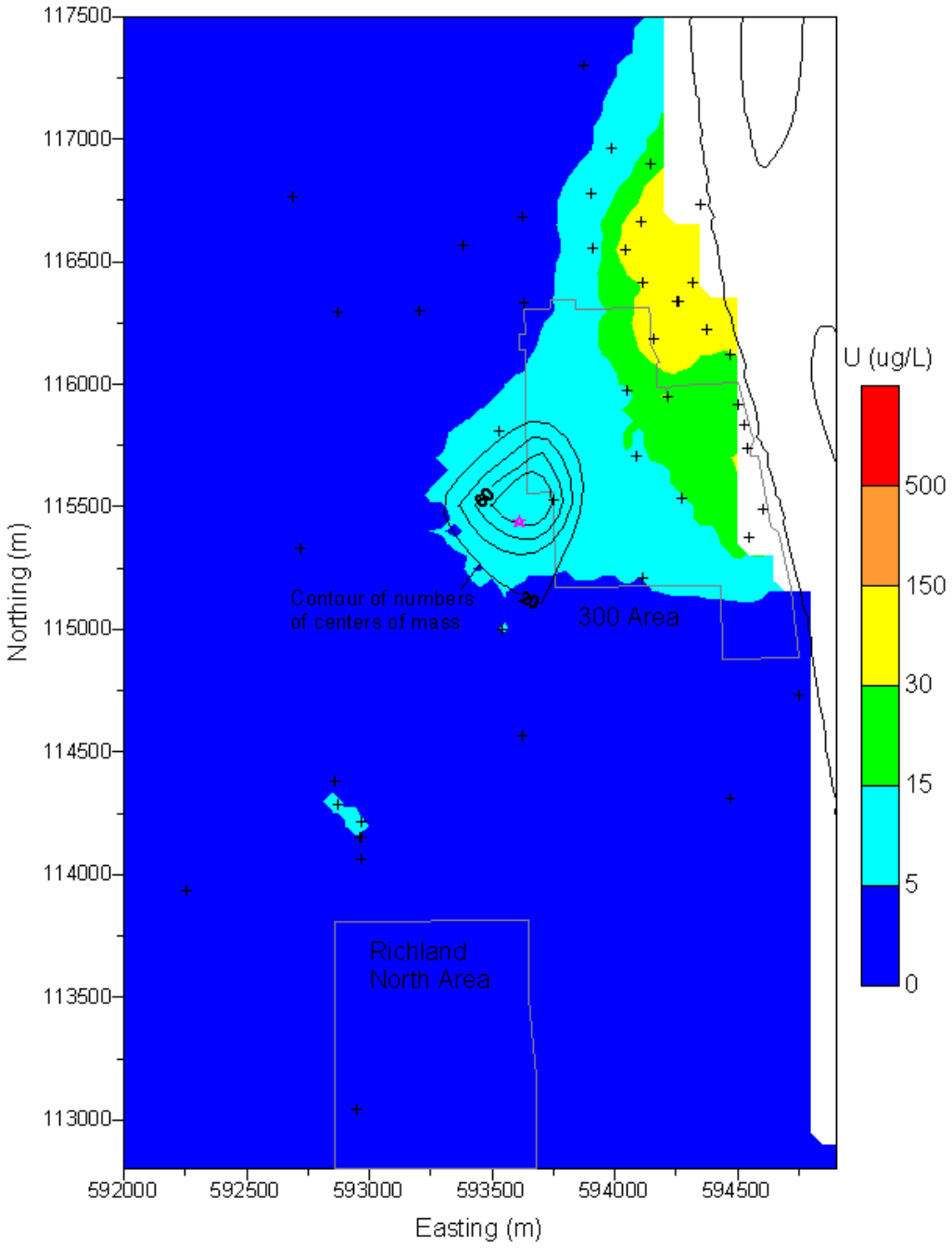

Figure H.12. Median of Simulated FY 1992 Uranium Concentrations in Sub-Area (300 Area Plume) of Grid 3. Contours of the number of times that the center of mass within the sub-area occurred within cells of an upscaled grid are shown with the average centers of mass shown by pink star in the sub-area.

Table H.8. Statistics of Centers of Mass of Individual Simulations of FY 1992 Uranium Calculated for a Depth of 5 m for Sub-Area (300 Area Plume) of Grid 3

Coordinate (m)	Sub-Area	
	Easting	Northing
Mean	593680.0	115464.8
Standard Error	6.5	11.5
Median	593687.9	115519.9
Standard Deviation	138.9	243.0
Kurtosis	0.62	1.90
Skewness	-0.49	-1.26
Range	900.2	1476.5
Minimum	593188.8	114557.4
Maximum	594089.0	116033.9
Count	450	450
97.5^{th} Percentile	593932.7	115779.4
2.5^{th} Percentile	593360.4	114807.4
Confidence Level of Mean (95.0%)	12.9	22.5

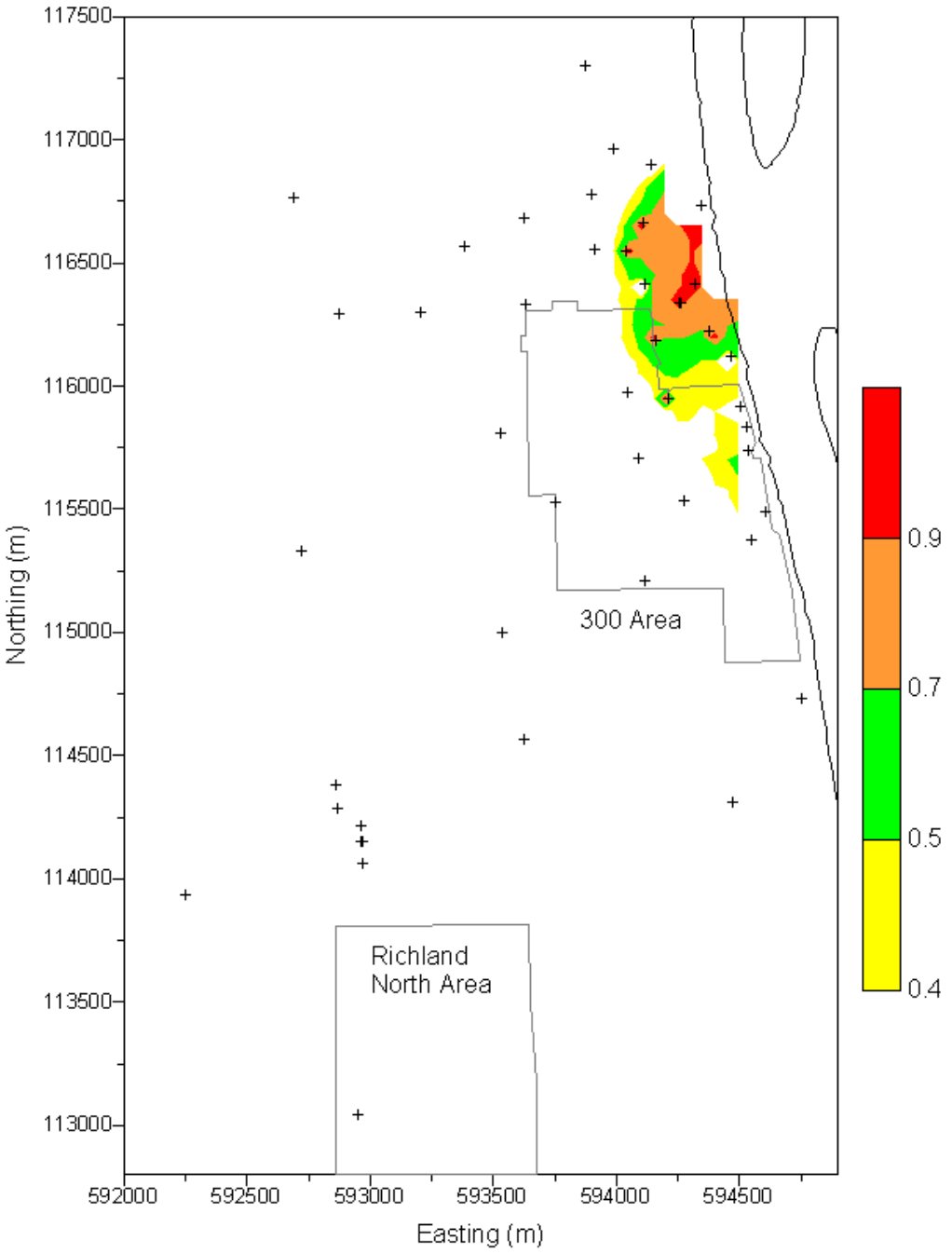

Figure H.13. Probability of Exceeding 30 µg/L Based on Simulations of FY 1992 Uranium in Sub-Area (300 Area Plume) of Grid 3

Table H.9. Statistics of the Area Exceeding 30 μg/L for Simulations of FY 1992 Uranium within Sub-Area (300 Area Plume) of Grid 3

Area (km^2)	Sub-Area	Grid 3
Mean	0.64	20.95
Standard Error	0.01	0.27
Median	0.60	20.46
Standard Deviation	0.19	6.61
Kurtosis	3.19	0.68
Skewness	1.37	0.66
Range	1.31	38.90
Minimum	0.26	8.02
Maximum	1.57	46.92
Count	450	600
97.5^{th} Percentile	1.06	35.69
2.5^{th} Percentile	0.38	9.99
Confidence Level of Mean (95.0%)	0.02	0.53

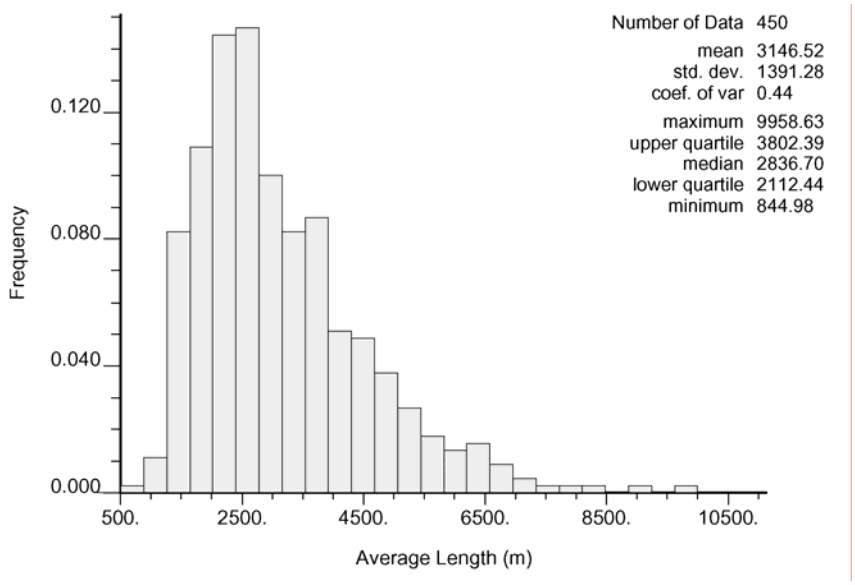

Figure H.14. Histogram of the Average Length of Columbia River Shoreline Exceeding 30 μg/L for FY 1992 Uranium in Grid 3

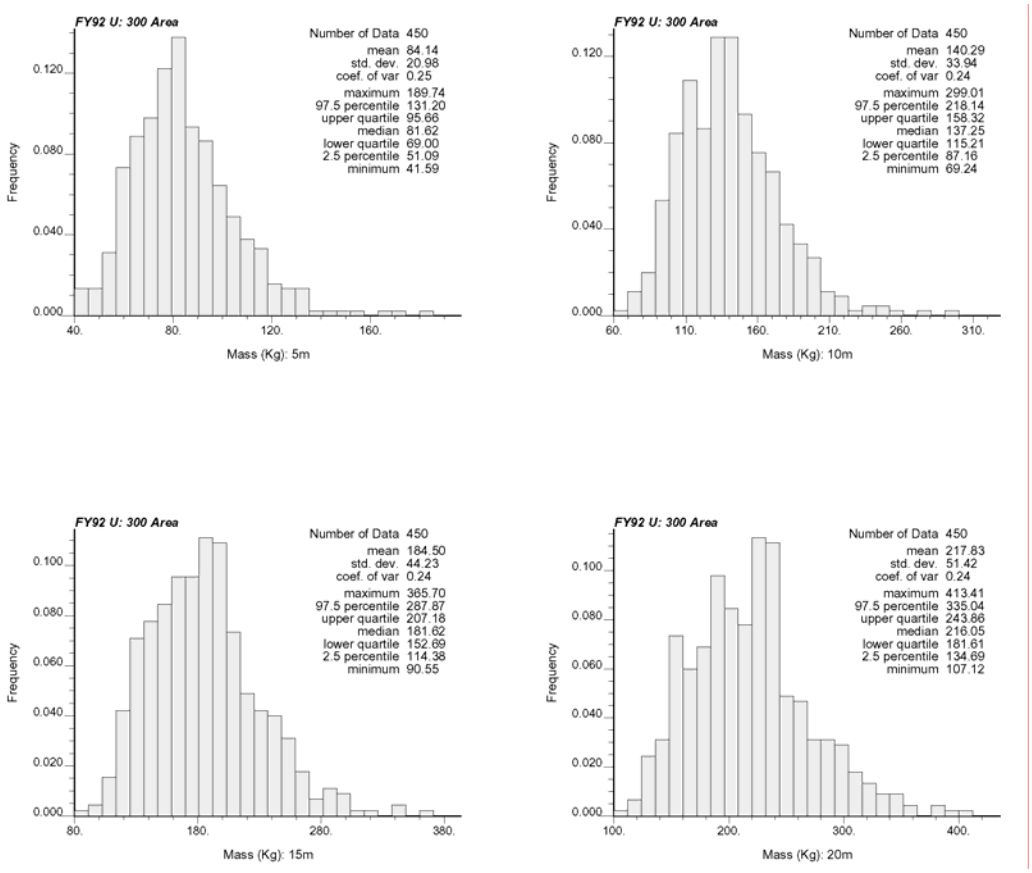

Figure H.15. Histograms of Total Mass in Simulations of FY 1992 Uranium within Sub-Area of Grid 3 (300 Area Plume), Four Thickness Assumptions

Table H.10. Statistics of Total Mass of Simulations of FY 1992 Uranium within Sub-Area of Grid 3 (300 Area Plume), Four Thickness Assumptions

Mass (kg) in Depth	5 m	10 m	15 m	20 m
Mean	84.14	140.29	184.50	217.83
Standard Error	0.99	1.60	2.09	2.43
Median	81.62	137.25	181.62	216.05
Standard Deviation	21.00	33.97	44.28	51.48
Kurtosis	2.12	1.41	0.82	0.56
Skewness	0.97	0.82	0.70	0.64
Range	148.15	229.77	275.16	306.29
Minimum	41.59	69.24	90.55	107.12
Maximum	189.74	299.01	365.70	413.41
Count	450	450	450	450
97.5^{th} Percentile	130.79	218.10	287.49	334.90
2.5^{th} Percentile	51.12	87.24	114.49	134.82
Confidence Level of Mean (95.0%)	1.95	3.15	4.10	4.77

Distribution

No. of Copies

ONSITE

2 **DOE Office of River Protection**

R. M. Yasek	H6-60
R. W. Lober	H6-60

9 **DOE Richland Operations Office**

B. L. Charboneau	A6-33
B. L. Foley	A6-38
J. P. Hanson	A5-13
R. D. Hildebrand	A6-38
J. G. Morse	A6-38
K. M. Thompson	A6-38
S. H. Wisness	A3-04
DOE Public Reading Room (2)	H2-53

5 **Bechtel Hanford Inc.**

P. G. Doctor	H9-01
K. R. Fecht	H9-04
K. A. Gano	H6-60
J. K. Linville	H0-23
S. G. Weiss	H0-23

9 **CH2M HILL Hanford Group, Inc.**

F. J. Anderson	E6-35
A. J. Knepp	H6-03
M. N. Jarayssi	H6-03
F. M. Mann	E6-35
W. J. McMahon	E6-35
C. W. Miller	H6-62
D. A. Myers	E6-35
C. D. Wittreich	H6-62
M. I. Wood	H8-44

2 **Fluor Federal Services**

R. Khaleel	E6-17
R. J. Puigh	E6-17

No. of Copies

8 **Fluor Hanford, Inc.**

J. V. Borghese	E6-35
F. M. Coony	E6-35
B. H. Ford	E6-35
T. W. Fogwell	E6-35
R. Jackson	E6-35
V. J. Rohay	E6-35
L. C. Swanson	E6-35
M. E. Todd-Robertson	E6-35

Stoller

R. G. McCain	B2-62

47 **Pacific Northwest National Laboratory**

R. L. Aaberg	K3-54
C. Arimescu	K6-04
M. P. Bergeron	K9-36
B. N. Bjornstad	K6-81
R. W. Bryce	E6-35
A. L. Bunn	K6-85
K. J. Cantrell	K6-81
Y. J. Chien	K6-81
R. L. Dirkes	K6-75
J. L. Downs	K6-85
D. W. Engle	K5-12
P. W. Eslinger	K6-04
M. J. Fayer	K9-33
E. J. Freeman	K9-36
M. D. Freshley	K9-33
G. W. Gee	K9-33
T. J. Gilmore	K6-81
D. G. Horton	K6-81
C. T. Kincaid	K9-33
G. V. Last (5)	K6-81
C. A. LoPresti	K5-12
W. J. Martin	K6-81
T. B. Miley	K6-04
C. J. Murray	K6-81
B. A. Napier	K3-54
W. E. Nichols	K9-33

No. of Copies		No. of Copies	
G. W. Patton	K6-75	M. B. Triplett	K6-04
J. V. Ramsdell, Jr.	K3-54	P. D. Thorne	K9-33
S. P. Reidel	K6-81	A. L. Ward	K9-33
M. C. Richmond	K9-33	M. D. White	K9-36
R. G. Riley	K6-96	M. D. Williams	K9-36
M. L. Rockhold	K9-36	S. K. Wurstner	K9-36
R. J. Serne	P7-22	S. B. Yabusaki	K9-36
D. L. Strenge	K3-54	Hanford Technical Library (2)	H2-53